

# **Plastic Foam Cutting Mechanics for Rapid Prototyping and Manufacturing Purposes**

Hadley Brooks

A thesis submitted in partial fulfilment of the requirements for the degree of Doctor of Philosophy in Mechanical Engineering at the University of Canterbury, Christchurch, New Zealand

March 2009



## Abstract

---

Development of foam cutting machines for rapid prototyping and manufacturing purposes began shortly after the first additive manufacturing machines became commercialised in the late 1980s. Increased computer power, the development and adoption of CAD/CAM software and rising demand for customisation has caused the rapid prototyping industry to grow swiftly in recent decades. While conventional rapid prototyping technologies are continuing to improve in speed and accuracy the ability to produce large ( $> 1\text{m}^3$ ) prototypes, moulds or parts it is still expensive, time consuming and often impossible. Foam cutting rapid prototyping and manufacturing machines are ideally suited to fulfil this niche because of their high speed, large working volumes and inexpensive working materials. Few foam cutting rapid prototyping machines have been commercialised to-date leaving significant opportunities for research and development in this area.

Thermal plastic foam cutting is the material removal process most commonly used in foam cutting rapid prototyping to shape or sculpt the plastic foam into desired shapes and sizes. The process is achieved by introducing a heat source (generally a wire or ribbon) which alters the physical properties of the plastic foam and allows low cutting forces to be achieved. In thermal plastic foam cutting the heat source is generated via Joule (electrical) heating. This study investigates the plastic foam cutting process using experimental cutting trials and finite element analysis.

The first part of this thesis presents an introduction to conventional foam cutting machines and rapid prototyping machines. It is suggested that a market opportunity lies out of reach of both of

these groups of machines. By combining attributes from each, foam cutting rapid prototyping machines can be developed to fill the gap.

The second part of this thesis introduces the state-of-the-art in foam cutting rapid prototyping and investigates previous research into plastic foam cutting mechanics.

The third part of this thesis describes cutting trials used to determine important factors which influence plastic foam cutting. Collectively over 800 individual cutting tests were made. The cutting trials included two main material sets, expanded polystyrene and extruded polystyrene, three different wire diameters, two hot-ribbon configurations and a wide range of feed rates and power inputs. For each cut the cutting force, wire temperature and kerf width was measured as well as observations of the surface texture. The data was then analysed and empirical relationships were identified. An excel spreadsheet is established which allows the calculation of important outcomes, such as kerf width, based on chosen inputs.

Quantitative measurements of the surface roughness and form, of cuts made with hot-tools, will not be addressed in this thesis. This body of work is currently under investigation by a colleague within the FAST group.

The fourth part of this thesis describes the formation of a nonlinear transient two-dimensional heat transfer finite element model, which is developed for plastic foam cutting simulations.

The conclusion is that the cutting trials contributed to a better understanding of plastic foam cutting mechanics. A new parameter was identified called the mass specific effective heat input, which is a function of the foam material and the cutting tool, it allows the prediction of cutting conditions with given cutting parameters and hence provides the necessary relationships needed for adaptive automated foam sculpting. Simulation results were validated by comparison with experimental data and provide a strong base for further developments including optimisation processes with adaptive control for kerf width (cut error) minimization.

This study has added considerably to the pool of knowledge for foam cutting with a hot-tool. In general, much of the work reported herein has not been previously published. This work provides the most advanced study of foam sculpting work available to date.



## Acknowledgements

---

It is a pleasure for me to record my appreciation to individuals who have helped me either directly or indirectly, in initiating and completing this thesis. First and foremost I am deeply grateful to Dr. David Aitchison for supervising this study. Dr. Aitchison's enthusiasm towards the project and words of encouragement made it easy for me to stay motivated. Whenever I felt a bit lost and lacking direction Dr. Aitchison knew what to say to get me back on track. I would also like to thank Dr Malcolm Taylor for providing valuable advice and helping to initiate the FAST project.

A special mention should be made to Dr. Mark Staiger, Dr. Susan Krumdieck and Dr. Timon Rubczuk who all contributed their unique skills and experiences to the project and helped me comprehend the wide range of topics covered in this thesis: materials, thermodynamics and finite element analysis. They helped make this project a truly multifaceted and interesting learning experience.

I would like to thank all of the technical staff for their support; in particular I would like to thank Eric Cox, Scott Amies, Ken Brown, Paul Wells, Mike Flaws, Julian Murphy, Adam Latham and Paul Southward.

I owe enormous appreciation to the students who came before me, especially Bernhard Kraus for setting such a high standard of work right from the beginning. I did my best to maintain his example. I would also like to thank the students who worked on the FAST project with me and made the experience so enjoyable: Anton Posthuma, Joe Bain, Ludovic Liotard and Delphine Biscaye.

To my girlfriend Madeline, thank you for putting up with my endless talking about robots and foam! Your support has been much appreciated.

Finally, I would like to thank my family who always supported me even though they were not really sure what it was I was doing! To my brothers Austin, Lance and Regan, it has been awesome having you in Christchurch and sharing all the good times to be had at the University of Canterbury. Together we are a force to be reckoned with (especially on the rugby field!). To Mum and Dad, although we have been separated by the Cook Strait for the last seven years I always felt you were close and I know you would be the first to help if I needed it. Thank you.

# Contents

---

<b>Abstract</b>	<b>i</b>
<b>Acknowledgements</b>	<b>iii</b>
<b>Contents</b>	<b>v</b>
<b>List of Figures</b>	<b>xii</b>
<b>List of Tables</b>	<b>xx</b>
<b>Abbreviations</b>	<b>xxi</b>
<b>Nomenclature</b>	<b>xxiii</b>
<b>1 Introduction</b>	<b>1</b>
1.1 Introduction	1
1.2 Rapid Prototyping and Manufacturing	2
1.2.1 Definition	3
1.2.2 Rapid Prototyping Methods	4

1.2.3	Summary of RP Technologies	15
1.3	Thermal Plastic Foam Cutting	16
1.3.1	Polystyrene Foams	17
1.3.2	Process Description	18
1.3.3	Commercial Machines and Tools	19
1.4	Motivation	25
1.5	Objectives and Scope	26
1.6	Outline of Thesis	26
<b>2</b>	<b>Literature Review</b>	<b>28</b>
2.1	Introduction	28
2.2	Foam Cutting RP Machines	29
2.2.1	Freeform Automated Sculpting Technology (FAST)	30
2.2.2	True Surface System (Trusurf)	34
2.2.3	Shapemaker I & II	35
2.2.4	ModelAngelo	36
2.2.5	Freeform Thick Layered Object Manufacturing (FF-TLOM)	38
2.2.6	Variable Lamination Manufacturing (VLM)	40
2.2.7	Rapid Heat Ablation (RHA)	42
2.2.8	Michelangelo	44

2.2.9	Stratoconcept HW Series	45
2.2.10	Summary of Foam cutting RP Machines	47
2.3	Empirical Studies of Factors in Foam Cutting	49
2.3.1	Energy Parameters	49
2.3.2	Material Properties	53
2.3.3	Tool Geometry	55
2.3.4	Summary of Empirical Studies	56
2.4	Numerical Simulations	58
2.4.1	Summary of Numerical Simulations	63
2.5	Summary of Literature Review	64
<b>3</b>	<b>Empirical Studies of Factors in Foam Cutting</b>	<b>66</b>
3.1	Introduction	66
3.2	Objectives	66
3.3	Materials	67
3.3.1	Polystyrene Foams	67
3.3.2	Cutting Tool Materials	73
3.4	Experimental Apparatus	75
3.4.1	Cutting Heads	75
3.4.2	Industrial Robot	81

3.4.3	Measurement Devices	81
3.4.4	Safety	87
3.5	General Experimental Method	88
3.6	Hot-wire Cutting Trials	90
3.6.1	Cutting Stages	90
3.6.2	Characteristic Cutting Force	90
3.6.3	Cutting Orientation	93
3.6.4	Surface Texture	95
3.6.5	Wire Temperature	99
3.6.6	Kerf width	105
3.6.7	Temperature Control	108
3.6.8	Effective Heat Input	112
3.6.9	Summary	120
3.7	Hot-ribbon Cutting Trials	122
3.7.1	Characteristic Cutting Force	123
3.7.2	Asymmetric Surface Effects	124
3.7.3	Transverse temperature profile	127
3.7.4	Kerf width	128
3.7.5	The Mass Specific Effective Heat Input	130

3.7.6	Summary	131
<b>4</b>	<b>Finite Element Method</b>	<b>132</b>
4.1	Introduction	132
4.2	Heat Diffusion Equation [55]	133
4.3	Finite Element Equation Formulation	134
4.4	Solving Nonlinear Transient Equations	138
4.4.1	Convergence	139
4.5	Summary	140
<b>5</b>	<b>Finite Element Analysis of Hot-tool Plastic Foam Cutting</b>	<b>141</b>
5.1	Introduction	141
5.2	Process Description	142
5.3	Heat Transfer Model	143
5.3.1	Assumptions	143
5.3.2	Elements Used	144
5.3.3	Material Properties	145
5.3.4	Mesh Management and Nodal Boundary Conditions	146
5.4	Simulation Results	148
5.4.1	Hot-wire Simulations	148
5.4.2	Hot-ribbon Simulations	152

5.5	Model limitations and Possible Improvements	157
5.6	Summary	157
<b>6</b>	<b>Conclusions</b>	<b>159</b>
6.1	Conclusions	160
6.1.1	Literature Review	160
6.1.2	Empirical Studies of Plastic Foam Cutting	161
6.1.3	Material Property Tests	162
6.1.4	Force Feedback Control System	162
6.1.5	Hot-tool Cutting Calculator	162
6.1.6	Numerical Model and Simulation	163
6.1.7	Summary	163
<b>7</b>	<b>Recommendations</b>	<b>164</b>
7.1.1	FAST Machine Technology	164
7.1.2	Further Experimental Studies	164
7.1.3	Tool path Generation and Optimisation	165
7.1.4	Numerical Simulations	165
7.1.5	Numerical Optimisation of Cutting tool Design	166
7.1.6	Design for Manufacturability (DFM) Rules	166
<b>8</b>	<b>References</b>	<b>167</b>



<b>Appendices</b>		<b>172</b>
Appendix A	Materials testing	173
Appendix B	Endothermic cooling effect calculations	176
Appendix C	Cutting head design	178
Appendix D	Thermocouple temperature measurement	182
Appendix E	Thermal imaging camera specifications	185
Appendix F	Surface texture tables	187
Appendix G	MasterCAM Brochure	190
Appendix H	ANSYS APDL code	198
Appendix I	FE Simulation screenshots	211
Appendix J	Associated published work	219
Appendix K	DVD contents page	220

## List of Figures

---

Figure 1.1 Common EPS objects cut with commercial foam cutting machines. Reproduced from [16].	2
Figure 1.2. Comparison between RP and conventional manufacturing processes.	4
Figure 1.3. Stereolithography process.	5
Figure 1.4. SLA machine and part.	6
Figure 1.5. EnvisionTecs' Perfactory and a part produced by it.	6
Figure 1.6. FDM process	7
Figure 1.7. FDM machine and parts.	8
Figure 1.8. Photopolymer phase change inkjet process.	9
Figure 1.9. Objet Eden 500V inkjet machine and parts produced by it.	9
Figure 1.10. 3D Printing process.	10
Figure 1.11. Z-Corp 3D printer with a coloured part and a flexible part.	11
Figure 1.12. SLS process.	12

Figure 1.13. Sinterstation® HiQ™ Series SLS® System with metal and plastic SLS parts.....	12
Figure 1.14. A LENS® based machine from Optomec and a metal bracket produced by it. ....	13
Figure 1.15. LOM process .....	14
Figure 1.16. Invision® LD 3D Modeller LOM machine and parts by 3D Systems. ....	14
Figure 1.17. Roland MDX-540 desktop mill and parts. ....	15
Figure 1.18. Cutting mechanisms. ....	19
Figure 1.19 Manually operated craft table cutter, combination cutter and CNC cutter from Demand Products. Reproduced from [27]. ....	20
Figure 1.20. Foam sculptures cut with MegaPlot foam cutting machines. Reproduced from [16].	21
Figure 1.21. Handheld foam cutting tools. Reproduced from [27]. ....	22
Figure 1.22. Standard blade profile shapes. Reproduced from [27]. ....	23
Figure 1.23. Foam sculptures created with hand tools. Reproduced from 3D Custom Foam Inc. [28]. ....	23
Figure 1.24. Comparison between PFC machines and PFC hand tools.....	24
Figure 1.25 Organisation of work in this thesis. ....	27
Figure 2.1. Research disciplines in plastic foam cutting.....	29
Figure 2.2. Comparison between conventional RP machines, foam cutting machines and foam cutting RP machines in terms of part complexity and part size. ....	30
Figure 2.3. FAST procedure summary. Reproduced from [32]. ....	32
Figure 2.4. IGES model of neck support created from scanned data and the sculpted part ready for use.....	33
Figure 2.5. IGES model and part sculpted from EPS showing complex 3D surfaces produced with the FAST system.....	33
Figure 2.6. Stepped versus ruled cuts.....	34
Figure 2.7. Life size dolphin and revolved shape created with the Trusurf system. ....	35

Figure 2.8. The JP-5 system and parts. ....	35
Figure 2.9. ModelAngelo apparatus. ....	37
Figure 2.10. Electrically heated cutting tool. ....	37
Figure 2.11. Parts sculpted using ModelAngelo. ....	38
Figure 2.12. Effects of different order surface approximations. ....	39
Figure 2.13. Prototype FF-TLOM cutting tool. ....	39
Figure 2.14. Examples of FF-TLOM multilayered stacked assemblies. ....	40
Figure 2.15 - Multi-piece layer concept ....	41
Figure 2.16. CAD representation of a human head and comparison of the fabricated parts. ....	41
Figure 2.17. The Rapid Shaper range from Menix Engineering Co. Ltd based on technology developed by the Korea Advanced Institute of Science and Technology. ....	42
Figure 2.18. Schematic of RHA process. ....	43
Figure 2.19. RHA tool and part. ....	43
Figure 2.20. Example of mesh simplification. ....	44
Figure 2.21. 8 axis setup and a test part produced by it. ....	45
Figure 2.22. Example of the Stratoconception® process for the Stratoconcept HWC. ....	46
Figure 2.23. Qualitative comparison of complexity and size of parts made with nine foam cutting RP machines. ....	47
Figure 2.24. Factors important in PFC ....	49
Figure 2.25. Kerf width under different cutting speed conditions. ....	51
Figure 2.26. Relationship between kerf width and effective heat input for RHA [10]. ....	52
Figure 2.27. Definition of cutting speed window defined by Broek et al [39]. ....	53
Figure 2.28. Microstructure of expandable polystyrene foam sheet. (a) 100x enlarged. (b) 400x enlarged [45]. ....	54

Figure 2.29. Relationship between weight loss and temperature [45].	55
Figure 2.30. RHA hot-tool.	56
Figure 2.31. Boundary conditions of local analysis. Reproduced from [42].	58
Figure 2.32. Schematic of thermal field showing heat affected region and maximum heat affected distance. Reproduced from [42].	59
Figure 2.33. Wire temperature for thick and thin cuts.	60
Figure 2.34. Comparison of experimental and analytical results with respect to melted width. Reproduced from [42].	61
Figure 2.35. Geometry and boundary conditions of local analysis. Reproduced from [9].	62
Figure 2.36. Comparison between analysis and experiment. a) Kerfwidth vs. heat input b) Cross-sectional shape of ablated groove. Reproduced from [9].	63
Figure 3.1. DMA storage and loss modulus for XPS foam.	70
Figure 3.2. Hot disk sensor.	70
Figure 3.3. SEM photograph showing effect of temperature on EPS cell structure. (a) 20 °C, (b) 110 °C, (c) 120 °C, (d) 160 °C. Reproduced from [50].	72
Figure 3.4. Typical TGA and DSC plots for EPS (0.024g/cm <sup>3</sup> ). Reproduced from [50].	73
Figure 3.5 Nikrothal N80 Ø 0.64 mm wire cutting XPS foam.	74
Figure 3.6. Schematic of plastic foam cutting system.	75
Figure 3.7. Hot-wire cutting head.	76
Figure 3.8. Hot-ribbon cutting head.	78
Figure 3.9. Hot-ribbon forming jig showing the profile selected for the cutting trials.	79
Figure 3.10. FE analysis of hot-ribbon cutting element. (a) Boundary conditions and loading (b) FOS (blue>1) (c) Von Mises stress (d) Displacement.	80
Figure 3.11. Hot-wire cutting trial experimental setup.	81
Figure 3.12 Load cell used in the cutting trials.	82

Figure 3.13. Calibration page.....	82
Figure 3.14. Comparing suppliers wire temperature data with experimental. ....	84
Figure 3.15. FLIR S65 thermal Imaging Camera. ....	85
Figure 3.16. Movement of data through various components of the data acquisition system.....	86
Figure 3.17. Data page of DAQ user interface. ....	87
Figure 3.18 Characteristic cutting force profile of a XPS sample (5A - 0.02 m/s) .....	91
Figure 3.19. Stage III cutting force vs. feed rate for various free air wire temperatures in XPS....	92
Figure 3.20. Cutting force vs. feed rate for different PS foams cut with 6A.....	93
Figure 3.21. Effect of cutting orientation on the cutting force (5A, 0.0167 m/s, XPS).....	95
Figure 3.22. Cutting force/surface finish relationship for S-grade EPS (5A – 0.0283m/s). ....	97
Figure 3.23. Cutting force/surface finish relationship for XPS (7A - 0.0267m/s). ....	98
Figure 3.24. Position of the thermocouple on the hot-wire during cutting. ....	100
Figure 3.25. 3D image of wire temperature during the cutting process (XPS, 1100mm/min, 7A). .....	101
Figure 3.26. Thin slice of foam sample showing the cross-sectional surface form (XPS, 7A, 1100mm/min). ....	101
Figure 3.27. S65 thermal camera image of hot-wire cutting (XPS, 8A, F0.0150).....	102
Figure 3.28. Wire temperature profiles recorded with the thermal imaging camera (XPS, 8A, F0.0150). ....	103
Figure 3.29. Thermal image of the hot-wire and thermocouple in free air.....	104
Figure 3.30. Comparison of the different temperature readings from the thermal imaging camera and the thermocouple.....	105
Figure 3.31. Longitudinal and transverse kerf variations.....	106
Figure 3.32. Measurement strategy for determining kerfwidth of hotwire cutting. ....	106

Figure 3.33. Kerfwidth vs. current for XPS cut at 0.0150m/s at two different positions along the sample length.....	107
Figure 3.34. Kerfwidth vs. wire temperature for EPS foam cut with a 0.64 mm diameter Nichrome wire. ....	108
Figure 3.35. Shows the wire temperature in the cut with and without temperature control (XPS, 0.0183m/s). ....	109
Figure 3.36. Part of the DAQ user form used to adjust the force feed-back wire temperature control. ....	109
Figure 3.37. Force profiles of constant and modulated current cuts (XPS, 0.0150m/s). ....	110
Figure 3.38. Kerf width of hot-wire with and without force feedback temperature control (XPS, 0.0150m/s). ....	111
Figure 3.39. Force and kerfwidth vs. effective heat input for VH Grade EPS.....	113
Figure 3.40. Volumetric effective heat input for XPS cuts with different wire diameters. ....	115
Figure 3.41. Summary of relationships between foam cutting parameters. ....	117
Figure 3.42. Hot-wire cutting calculator and necessary data.....	118
Figure 3.43. Hot-wire calculator results vs. the experimental line of best fit. ....	119
Figure 3.44. Tool path generation and optimisation within the FAST system. ....	120
Figure 3.45. Shaped and flat hot-ribbon configurations. ....	122
Figure 3.46. Characteristic force profiles for hot-ribbon cutting of XPS at 0.052m/s using various currents.....	124
Figure 3.47. Longitudinal hot-ribbon surface effects. ....	125
Figure 3.48. The weather board effect created by asymmetric cutting conditions.....	125
Figure 3.49. Temperature at different parts of the shaped hot-ribbon cutting tool (EPS, 16A, F0.050). ....	126
Figure 3.50. Geometric temperature compensation for asymmetrical cutting with a hot-ribbon. ....	126

Figure 3.51. Picture of the ribbon while cutting from underneath through a small slot (EPS, 18A, 0.062 m/s).....	127
Figure 3.52. Centreline temperature plot of the small area shown in the preceding thermal image. ....	128
Figure 3.53. Cutting force and kerfwidth against area specific effective heat input for XPS for hot-ribbon cutting.....	129
Figure 3.54. Cutting force and kerfwidth against area specific effective heat input for XPS for hot-wire cutting.....	129
Figure 3.55. Simplified representation of heat flows for hot-tools with different efficiency.....	130
Figure 3.56. Volume specific effective heat input for EPS cuts made with a hot-ribbon.....	130
Figure 4.1. Various modes of heat transfer in a two-dimensional solid.....	135
Figure 4.2. Incremental Newton-Raphson Procedure.....	139
Figure 5.1. Graphical representation of the hot-tool cutting process. ....	143
Figure 5.2. Element PLANE55 geometry. ....	145
Figure 5.3. Thermal material properties of EPS. a) Conductivity b) Specific Heat. ....	146
Figure 5.4. Thermal material properties of XPS. a) Conductivity b) Specific Heat. ....	146
Figure 5.5. Nodal boundary conditions applied at nodes relative to the local coordinates for two successive time steps.....	147
Figure 5.6. FEA temperature distribution for a hot-wire cut (EPS, 0.64 mm wire, F0.030).....	149
Figure 5.7. Comparison between FEA and experimental kerfwidths (XPS, 0.64 mm wire). ....	150
Figure 5.8. Comparison between FEA and experimental kerfwidths (EPS, 0.64 mm wire). ....	150
Figure 5.9. Comparison between FEA and experimental kerfwidths (XPS, 0.036 mm wire). ....	151
Figure 5.10. Comparison between FEA and experimental Kerfwidths (XPS, 0.91 mm wire).....	151
Figure 5.11. FEA temperature distribution for a hot-wire cut (EPS, ribbon, 281 °C, F0.038).....	152
Figure 5.12. Comparison between FEA and experimental kerf widths (EPS, ribbon). ....	153



Figure 5.13. Comparison between FEA and experimental kerf widths (XPS, ribbon). .....	153
Figure 5.14. The effect of curve radius on kerf widths cut with a hot-ribbon. ....	154
Figure 5.15. Curved cut with a hot-ribbon in EPS (315°C, 0.050) .....	155
Figure 5.16. Kerf width versus radius of curve for hot-ribbon cuts (EPS, 315°C, 0.050m/s). ....	156

## List of Tables

---

Table 1.1. Comparison of current RP technologies [19, 20, 23, 24].	16
Table 2.1. Comparison between VLM and LOM.	42
Table 2.2. Comparison of foam cutting RP machines.	48
Table 3.1. Technical Information of Expanded Polystyrene (Bondor: S-grade & VH-grade)	68
Table 3.2. Technical Information of Extruded Polystyrene (Styrofoam, DOW).	69
Table 3.3. Chemical, mechanical and physical properties of Nikrothal N80 hotwire.	74
Table 3.4. Experimental range of parameters.	89
Table 3.5. Diagrammatic representation of the three cutting stages with a hot-wire.	90
Table 3.6. Qualitative summary of XPS surface textures for a range of feed rates and currents cut with a 0.64 mm diameter Nichrome wire.	99
Table 3.7. Diagrammatic representation of the three cutting stages with a hot-ribbon.	123
Table 5.1. Parameters and values used for simulations.	142

# Abbreviations

---

AMT	Additive Manufacturing Technologies
APDL	ANSYS Parametric Design Language
CAD	Computer Aided Design
CAM	Computer Aided Manufacturing
CNC	Computer Numerical Control
DFM	Design for Manufacture
DMA	Dynamic Mechanical Analysis
DOF	Degree of Freedom
DSC	Differential Scanning Calorimeter
EPS	Expanded Polystyrene
FAST	Free-form Automated Sculpting Technology
FDM	Fused Deposition Modelling
FE	Finite Element
FEA	Finite Element Analysis

FEM	Finite Element Method
FF-TLOM	Free Form Thick Layered Object Manufacturing
HCC	Hot-tool Cutting Calculator
HDA	Hot Disk Analyser
LOM	Laminated Object Manufacturing
RHA	Rapid Heat Ablation
RP	Rapid Prototyping
RP&M	Rapid Prototyping and Manufacturing
RM	Rapid Manufacturing
RT	Rapid Tooling
SEM	Scanning Electron Microscope
SLA	Stereolithography Apparatus
SLS	Selective Laser Sintering
SRP	Subtractive Rapid Prototyping
.STL	<b>S</b> tereolithography file format
TGA	Thermo-gravimetric Analysis
TPFC	Thermal Plastic Foam Cutting
PF	Plastic Foam
PFC	Plastic Foam Cutting
PS	Polystyrene
PFC	Plastic Foam Cutting
VLM	Variable Layer Manufacturing
XPS	Extruded Polystyrene

## Nomenclature

---

$C_p$	Constant pressure specific heat
$h$	Convective heat transfer coefficient
$i$	Iteration or time step number
$I$	Electrical current
$K$	Conductivity
$N$	Node
$Q, q$	Electrical power
$T$	Temperature
$V_c$	Feed rate
$\alpha$	Surface absorbability
$\varepsilon$	Stefan-Boltzmann constant
$\rho$	Density

$\rho_f$	Foam density
$\lambda$ and $\eta$	Kerf width
$\dot{q}$	Rate of heat generation per unit volume
$Q_{eff}$	Area specific effective heat input
$^{Vol}Q_{eff}$	Volume specific effective heat input
$^{Mass}Q_{eff}$	Mass specific effective heat input

# 1 Introduction

---

## 1.1 Introduction

Since the accidental discovery of polystyrene in 1839 plastics and plastic foams have pervaded society and today plastic products are an integral part of everyday life. Plastic foams such as expanded polystyrene (EPS) and extruded polystyrene (XPS) are manufactured using casting and extruding processes [1]. Casting is used to manufacture net shape objects which require little or no post processing, however the costs associated with manufacturing the rigid moulds restricts the use of casting to high volume applications. Extruding processes create rectilinear shapes which often need to be cut in order to achieve a shape suitable for the final purpose.

Thermal plastic foam cutting (TPFC) is the material removal process most commonly used in low volume manufacturing to shape or sculpt the polystyrene into desired shapes and sizes. The process is achieved by introducing a heat source (generally a wire) which alters the physical properties of the plastic foam and allows low cutting forces to be achieved [2]. In TPFC the heat source is generated by passing an electrical current through a cutting element or 'hot-wire'. The kerf width and surface finish of a cut are determined by the feed rate, the electrical power input and the material properties of the cutting element and the foam. Plastic foam (PF) may also be cut with unheated conventional blades such as those found in craft knives. Such blades can produce smooth surface finishes if the cuts are straight and shallow in depth; however, blades fail to allow sharp curves and wide cuts to be made due to the blade geometry and high cutting forces associated with cold cutting. Conversely TPFC allows cuts of almost any length to be made with low cutting forces and high feed rates. Also hot-wires can be used to cut almost any

2D profile while hot-ribbons can be used to sculpt complex 3D surfaces. Thus TPFC improves process flexibility over cold cutting techniques while reducing manufacturing costs and time.

While the majority of current TPFC involves cutting with wires, recent research effort has seen the development of novel rapid prototyping machines which use a wide variety of cutting elements [3-15]. Promising potential applications for plastic foam cutting machines can be found in the building, aerospace, sports, arts and medical sectors. Figure 1.1 shows the wide range of objects able to be cut using commercial TPFC machines available from MegaPlot [16].



**Figure 1.1 Common EPS objects cut with commercial foam cutting machines. Reproduced from [16].**

The aims of this research include: an empirical study of the factors in thermal plastic foam cutting; developing a finite element model to simulate the process; and verifying the results of the simulations with experimental data. ‘Cold cutting’ or cutting without a heat source will not be discussed within this work. Hence for the rest of the thesis, plastic foam cutting is synonymous with thermal plastic foam cutting.

The next section of this chapter will provide a brief overview of the main rapid prototyping and manufacturing (RP & M) technologies currently available. The sections thereafter describe the PFC process, commercial foam cutting machines, the motivation behind the experimental research and the objectives and scope of the study. The final section outlines the structure of the thesis.

## **1.2 Rapid Prototyping and Manufacturing**

Today many technologies address the rapid creation of models, prototypes, casting patterns and low volume manufactured parts. These technologies are capable of producing complex freeform solid objects directly from a computer model without the need for part-specific tooling or knowledge. They are, for the most part, additive processes and have been given many names, the most common being rapid prototyping (RP). Other names include; additive manufacturing



technologies (AMT), solid freeform fabrication (SFF), desktop manufacturing (DTM) and 3D printing (3DP) [17]. Rapid prototyping machines can, in some cases, be used to manufacture objects for final application or to make tooling for low volume production. These processes are most commonly referred to as rapid manufacturing (RM) and rapid tooling (RT) respectively. This chapter will introduce the main RP & M technologies currently available and will describe some of the limitations associated with this developing industry.

### 1.2.1 Definition

There are many definitions of Rapid Prototyping however the following definition will be adopted for this dissertation:

*“RP is the process of generating an object directly from its digital representation in a CAD/CAM system.” [18]*

This definition allows the inclusion of subtractive, net-shape and hybrid manufacturing methods which are sometimes neglected due to their links with conventional manufacturing. CNC milling machines are gaining acceptance as a RP technology with the advent of personal or desktop milling machines that provide prototypes in a plethora of materials with superior speed and precision than many additive manufacturing systems [19].

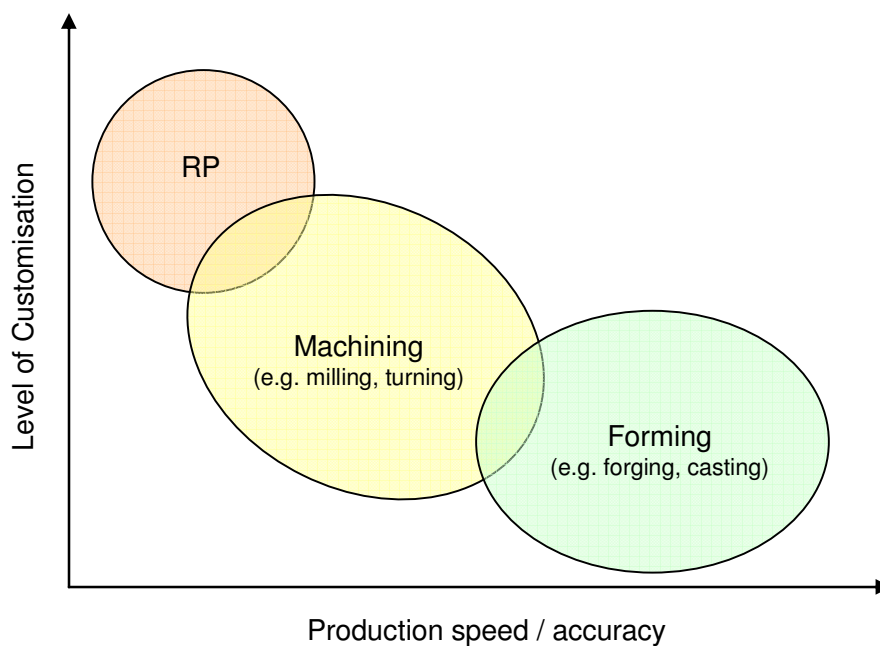
Four basic steps are required for any AMT process:

1. Development of a digital model of the part in a CAD system. This model may be built entirely in the CAD environment or may be built from scanned data. This model is then saved as a **STereoLithography** (.STL) file which is a triangulated approximation of the original CAD surface model. The number of triangles used to form the surface should be high enough to provide a suitably smooth and accurate surface representation.
2. The .STL file must then be read into a RP pre-processor. While some RP systems can accept .STL files directly most require pre-processing to ‘slice’ the model into cross-sections, optimise build parameters and verify the build sequence. ‘Slicing’ is performed by a simple mathematical algorithm, which finds the intersection points of the slicing plane and the triangular facets which are described in the .STL file. These cross-sections are saved into a file specific to the RP machine being used.
3. The RP machine then builds the part. Additive RP processes build the part one layer at a time from the bottom up while SRP processes remove excess material from the top down. The part will take anywhere from a few hours to a couple of days to build depending on the part and process. Often additive process will require the building of

supports along with the structure to ensure that any overhangs or fragile cross-sections are supported.

4. Finally the part is removed from the RP machine and post processed. RP parts often require supports to be removed and/or manual finishing (sanding, painting, curing etc) to obtain the desired result.

Figure 1.2 below shows where RP & M technologies fit in relation to conventional manufacturing processes in terms of production volumes and level of customisation. The high level of customisation achievable with RP makes it well suited for biomedical applications and the production of one-of-a-kind objects.



**Figure 1.2. Comparison between RP and conventional manufacturing processes.**

### 1.2.2 Rapid Prototyping Methods

The main recognised RP technologies can be categorised into seven groups that use similar processes. These groups are:

- Photopolymer-based systems including Stereolithography Apparatus (SLA)
- Fused Deposition Modelling (FDM)
- Inkjet and Jetted-Polymer (J-P) Systems
- 3D Printing (3DP)

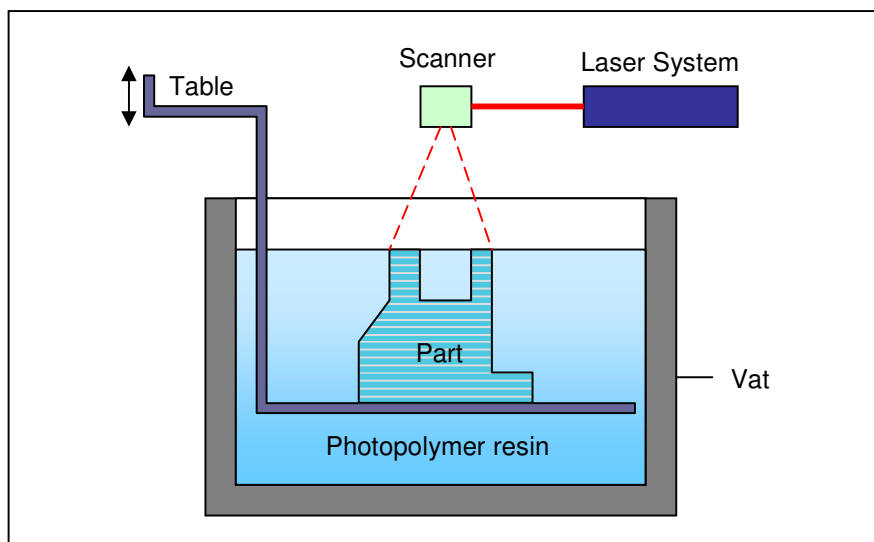
- Selective Laser Sintering (SLS)
- Laminated Object Manufacturing (LOM)
- Subtractive Rapid Prototyping (SRP)

A brief description of each of these processes follows, accompanied with photos of associated machines and example prototype parts.

### 1.2.2.1 Photopolymer-based Systems including Stereolithography Apparatus (SLA)

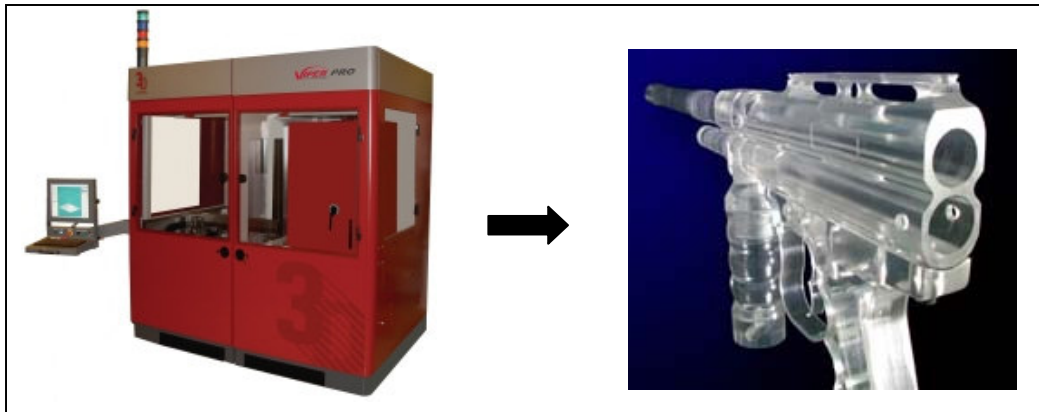
Photopolymer-based systems work by curing photopolymers with UV light one layer at a time. The most common system that uses this method of fabrication is called Stereolithography (SL). SL machines were the first commercial RP machines, commercialised by 3D Systems in 1986 and are still manufactured and distributed today. SLA machines are still expensive between 180,000 and 800,000 USD [20].

The SL process is essentially as follows; first the build table, which is situated at the top of the vat, is lowered by one layer thickness so that there is an even layer of resin covering the table. A laser is then used to cure the first layer by scanning the required cross section. Once the first layer has been scanned the table is lowered and the process is repeated. In this way the part gets built up, as seen in figure 1.3. Typical layer thicknesses range from (0.13 to 0.30 mm).



**Figure 1.3. Stereolithography process.**

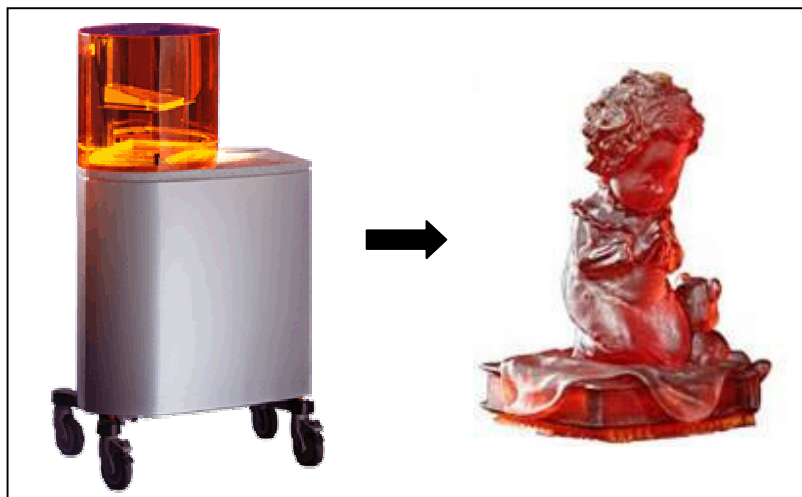
Objects which have overhangs or undercuts must be supported during the fabrication process by support structures. These are both manually or automatically designed and fabricated along with the object. Upon completion of the fabrication process, the object is elevated from the vat and the supports are broken off. Figure 1.4 shows a typical SLA machine and part.



**Figure 1.4. SLA machine and part.**

Until recently stereolithography was the bench mark for surface finish and accuracy within the AMT industry. The technology is also notable for the relatively large object sizes that are possible (508 x 508 x 610 mm for the SLA<sup>®</sup> 7000). On the negative side, working with liquid materials can be messy and parts often require a post-curing operation in a separate oven-like apparatus for complete cure and stability.

Recent developments in photopolymer technology have witnessed the introduction of several new machines capable of achieving SLA accuracy or better within shorter production time frames. One such technology is the Perfactory<sup>®</sup> system by EnvisionTec with accuracies as high as 25 microns. Unlike SLA which uses a laser to trace cross-sections of the part, the Perfactory<sup>®</sup> system cures each cross-section in a single flash by projecting a negative bitmap image of each layer. Figure 1.5 shows the Perfactory<sup>®</sup> Standard and a part produced with it.



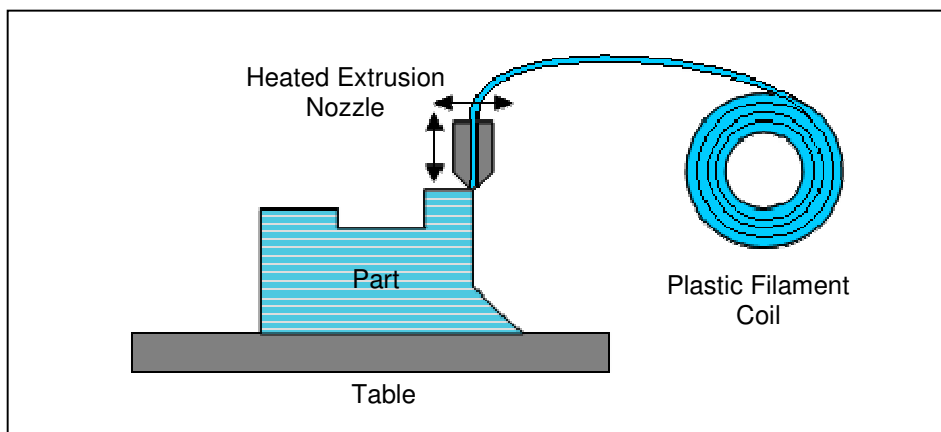
**Figure 1.5. EnvisionTecs' Perfactory and a part produced by it.**

The EnvisionTec system is compatible with several materials. The main material used is an orange coloured thermoset as shown in figure 1.5. The hardness of the material can be varied by controlling the degree of curing. This allows the creation of hard or fully flexible models.

As with other precision AMT technologies small build volumes and long build times prevent this technology from being used to produce large parts.

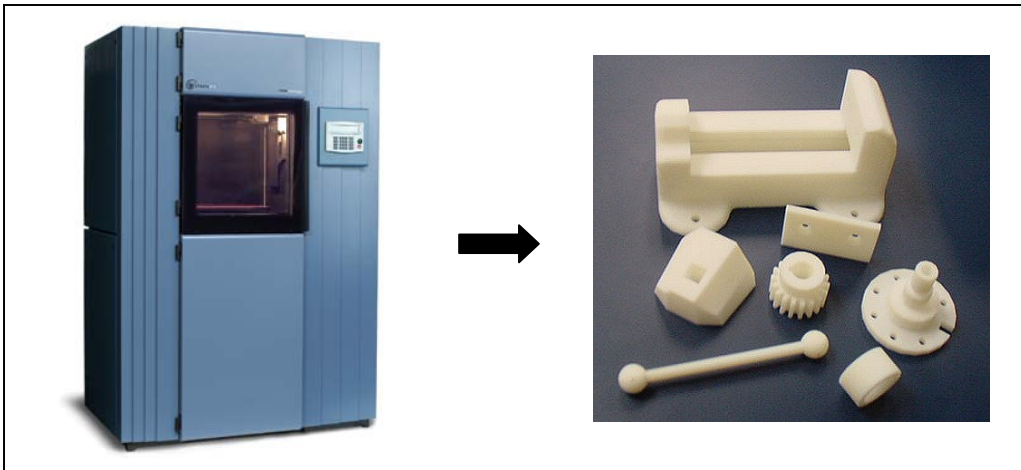
### 1.2.2.2 Fused Deposition Modelling (FDM)

FDM is one of the most widely used rapid prototyping technologies today and cost between 30,000 and 250,000 USD [20]. The durable parts produced by FDM can be used for functional tests and final use. A plastic filament is unwound from a coil and feed to a heated chamber where it melts. The molten plastic is then extruded out of the nozzle where it is deposited as a thin bead on the part being formed. The nozzle is close enough to the lower surface of the part to shear the plastic as it is deposited, leaving a flat surface for the next layer to be built on. The plastic hardens immediately after being extruded from the nozzle and bonds to the layer below. Nozzle diameters are approximately 0.3 mm at the opening and layer thicknesses can be as low as 0.178 mm. Figure 1.6 shows a schematic of the FDM system, revealing its basic features. Like SLA parts, FDM parts may require the construction of supports. These supports are built in the same way as the main part but with a separate nozzle and (in some cases) a different material. The support material may vary from that of the main part to allow easy removal when the part is complete. The recent development of water soluble supports mean little finishing is required.



**Figure 1.6. FDM process**

FDM machines can produce parts with engineering materials such as ABS and polycarbonate. This makes the parts durable and often fit for end use. The surface finish of FDM parts is not as good as SLA and the process is slow for parts with large volumes. The Titan FDM machine from STRATASYS has a build volume of 406 x 355 x 406 mm. Figure 1.7 shows a typical FDM machine from STRATASYS and the parts it builds.



**Figure 1.7. FDM machine and parts.**

### **1.2.2.3 Inkjet and Jetted-Polymer (J-P) Systems**

Inkjet systems work by depositing liquid polymers through jet heads. Two main variations exist; thermal phase change inkjets in which the liquids solidify due to a temperature drop and photopolymer phase change inkjets in which the liquid is cured with UV light.

#### **Thermal phase change inkjets:**

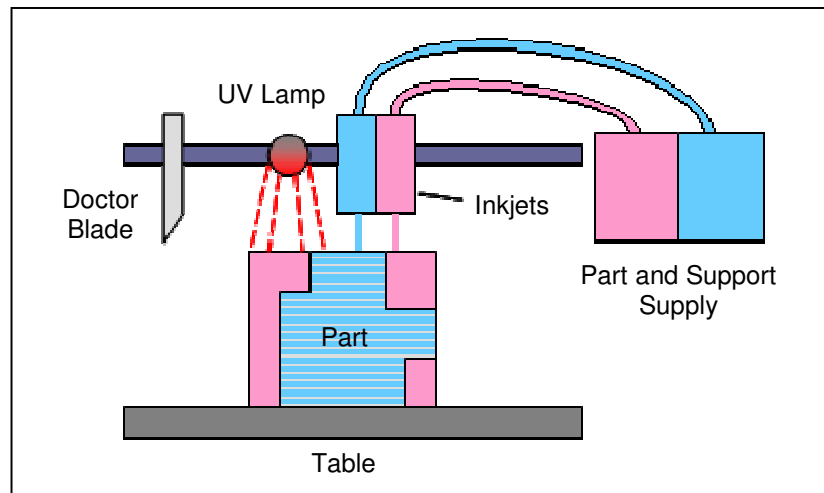
SolidScape Inc.'s machine uses two jets to deposit plastic build material and a wax-like support material which are held in a liquid state in a heated chamber. The jetting heads squirt tiny droplets of the materials as they are moved in the X-Y plane to form a layer of the object. The materials harden by rapidly dropping in temperature as they are deposited.

After an entire layer of the object is formed by jetting, a milling head is passed over the layer to make it a uniform thickness. After the object is completed, the wax support material is either melted or dissolved away.

The most outstanding characteristic of the SolidScape system is the ability to produce extremely fine resolution and surface finishes, essentially equivalent to CNC machines. However, the technique is very slow for large objects, making it suitable for applications in the jewellery industry, for example.

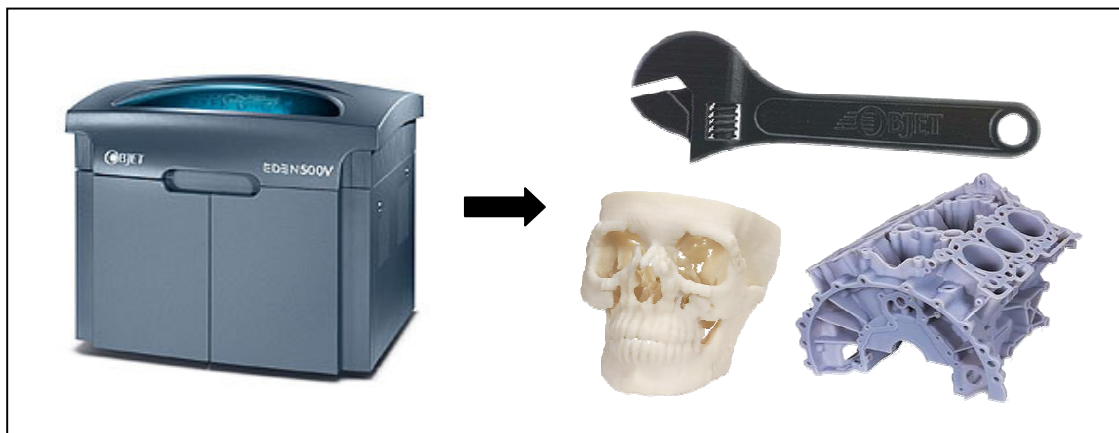
#### **Photopolymer phase change inkjets:**

Photopolymer inkjet machines such as the Objet Eden 500V use wide area inkjet heads to deposit both build and support materials layer by layer. It subsequently completely cures each layer after it is deposited with a UV flood lamp mounted on the print head. The support material, which is also a photopolymer, is removed by washing it away with pressurized water in a secondary operation. Figure 1.8 shows the photopolymer inkjet process.



**Figure 1.8. Photopolymer phase change inkjet process.**

Objet systems are capable of producing parts with sections as thin as 0.6 mm. A number of different propriety materials are available with different hardness's, flexibility and colour. Objet are renowned for producing systems that are exceptionally office/user friendly. 3D Systems produce similar machines in their Invision® product range. Figure 1.9 below shows the Objet Eden 500V system and parts produced by it.

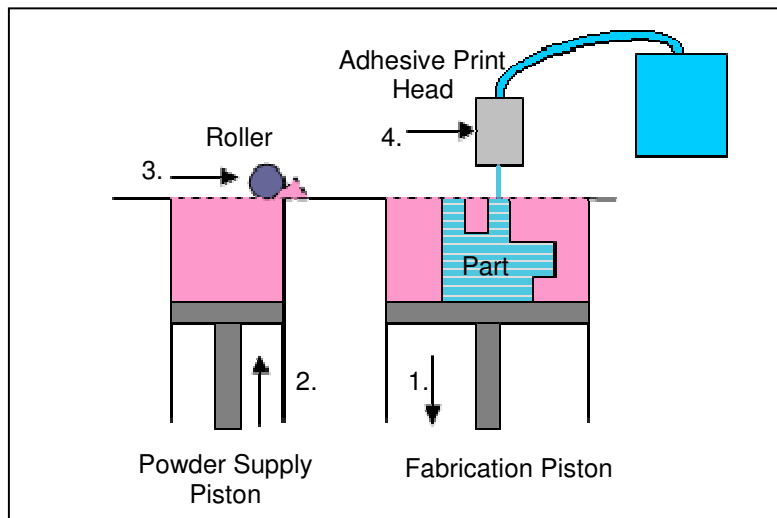


**Figure 1.9. Objet Eden 500V inkjet machine and parts produced by it.**

#### 1.2.2.4 3D Printing

3D printing is a term often used interchangeably with low cost AMT systems, especially by people new to the industry. It is however only truly applicable to one type of AMT. The main provider of 3D printing machines is Z-Corporation with machines in the \$15,000 – \$20,000 price range. IdeaLabs recently released a low-cost 3D Printer called Desktop Factory for under \$5,000 however the build size is small and the quality is not as good as that from Z-Corporation machines. The process starts by depositing a layer of powdered material on the surface of the

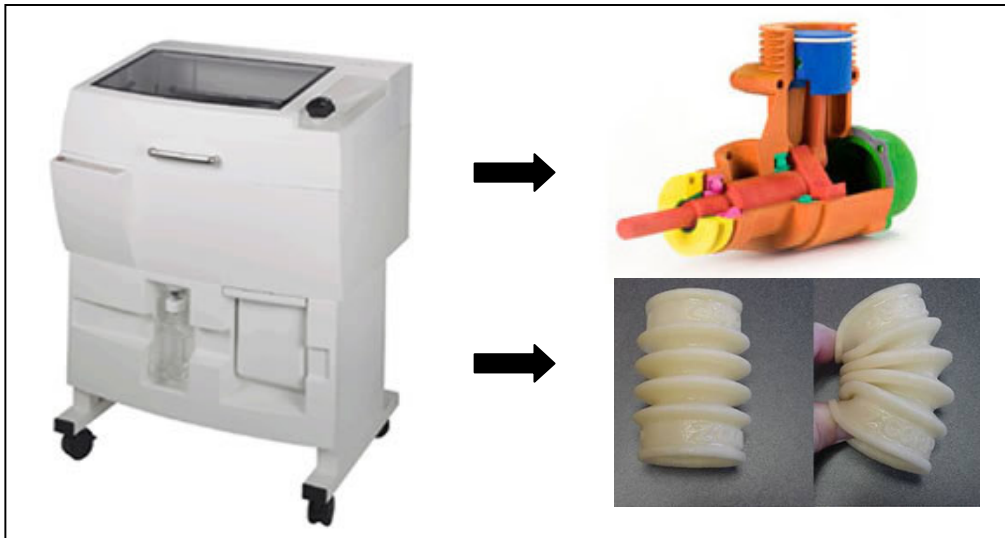
fabrication piston which is situated at the top of the fabrication chamber. Typical layer thicknesses range from 0.089 – 0.178 mm. The three main material powders used are plaster, starch and Z-Cast. A roller distributes and compresses the powder at the top of the fabrication chamber. The multi-channel jetting head subsequently deposits a liquid adhesive in a two dimensional pattern onto the powder layer binding the powder and forming a layer of the object. Once a layer is completed, the fabrication piston moves down by the thickness of a layer, and the process is repeated until the entire object is formed within the powder bed. No external supports are required during fabrication since the powder bed supports overhangs. The Z<sup>®</sup> 810 machine has a build volume of 508 x 610 x 406 mm [20]. Figure 1.10 shows the 3D printing process.



**Figure 1.10. 3D Printing process**

Parts built with plaster or starch powders are porous and can be infiltrated to improve their physical properties. Infiltrating plaster parts with epoxy provides hard machinable parts while infiltrating starch with wax or elastomers produces investment castings or flexible parts respectively. Z-Cast parts do not need to be infiltrated and can be directly used for investment casting. 3D printed parts can also be produced in colour by printing coloured inks as the parts are built. Figure 1.11 shows a Z-Corp 3D printer and two parts with different material properties.



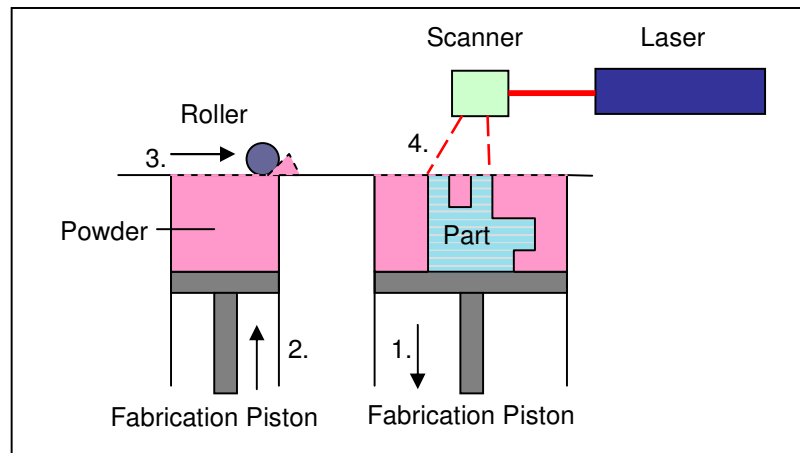


**Figure 1.11. Z-Corp 3D printer with a coloured part and a flexible part.**

3D printers have poor accuracy and surface finish compared with expensive SLA machines, however low cost, fast build times and ease of use means 3D printing is currently the fastest growing technology within the AMT industry [21].

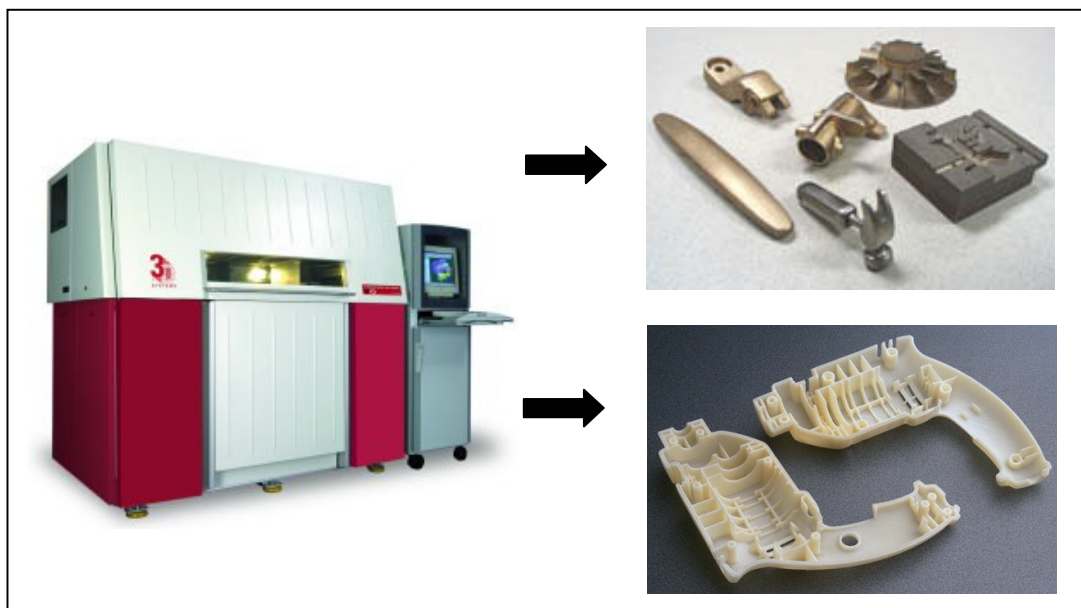
#### **1.2.2.5 Selective Laser Sintering (SLS)**

SLS can be used to produce polymer, metal and ceramic parts. A laser beam is traced over the surface of compacted powder to selectively melt and bond it to form a layer of the object. Layer thicknesses range from 0.10 to 0.015 mm. The fabrication chamber is maintained at a temperature just below the melting point of the powder so that heat from the laser need only elevate the temperature slightly to cause sintering. The process is repeated until the entire object is fabricated. After the object is fully formed, the piston is raised to elevate it. Excess powder is simply brushed away and final manual finishing may be carried out. No supports are required with this method since overhangs and undercuts are supported by the lightly compacted powder bed. Figure 1.12 shows the SLS process. The two main producers of SLS type machines are 3D Systems from the USA and Electro Optical Systems (EOS) from Germany.



**Figure 1.12. SLS process.**

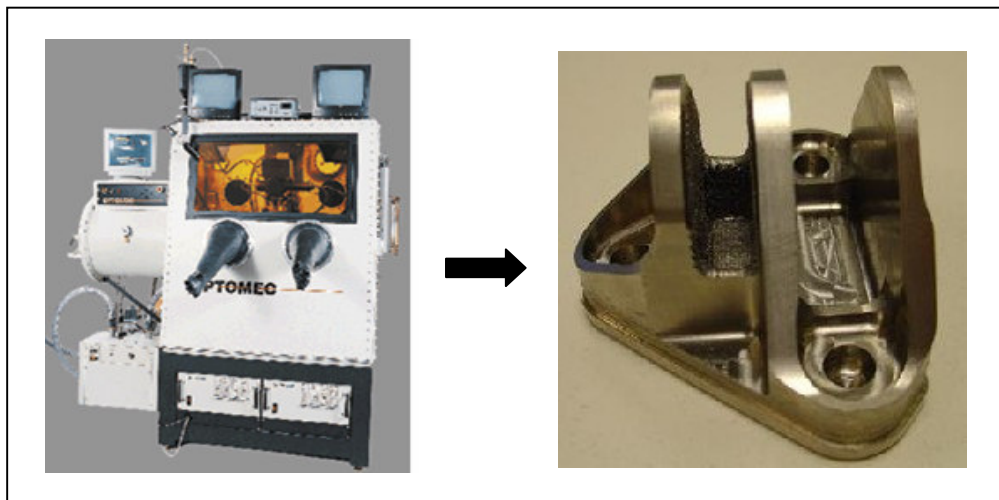
SLS parts can serve a number of different applications from casting to functional prototypes to rapid tooling depending on the material that is used. Polymers such as polycarbonate are used for investment casting patterns while sands are used for sand casting. Thermoset plastics such as glass filled nylon and polyamides can be used for functional prototypes where concept verification and fit analysis are important. A wide range of metal powders are used including copper amide, titanium alloys and carbon steel powder which can be used to produce soft tooling, injection mould dies or tool inserts for limited production runs. Additionally small batches of final use parts can be built simultaneously by filling the entire build volume with parts. Increasing the number of parts being built at one time greatly decreases the build time per part. The Vanguard Si2™ by 3D systems has a build volume of 330 x 381 x 432 mm.



**Figure 1.13. Sinterstation® HiQ™ Series SLS® System with metal and plastic SLS parts.**

SLS offers the advantage of making functional parts in final materials. The surface finish isn't as good as SLA and the equipment is expensive due to the complexity of the machinery. The Vanguard Si2™ costs around 300,000 USD [20]. SLS metal parts are often porous and may require infiltration with a secondary metal to improve mechanical characteristics.

Other techniques similar to SLS exist which aim to melt the metal powder as it is deposited instead of sinter it. One main technique known as LENS® (Laser Engineered Net Shaping) was developed by Sandia National Laboratory and Sandia Corporation. The strength of the technology lies in the ability to fabricate fully-dense metal parts with good metallurgical properties at reasonable speeds. Objects fabricated are near net shape, but generally require finishing. They have good grain structure, and have properties similar to, or even better than the intrinsic materials. Laser powder forming methods have fewer material limitations than SLS, don't require secondary firing operations as some of those processes do, and can also be used to repair parts as well as fabricate them.



**Figure 1.14. A LENS® based machine from Optomec and a metal bracket produced by it.**

#### **1.2.2.6 Laminated Object Manufacturing (LOM)**

LOM is the process of constructing objects by laminating successive cross-sections of material. Paper or plastic is unwound from a feed roll onto the stack and is bonded to the previous layer. Profiles are then cut by a laser or a knife that is mounted to an X-Y stage. Waste material is wound on a take-up roll. The method is self-supporting for overhangs and undercuts. Figure 1.15 shows a laser based LOM process.

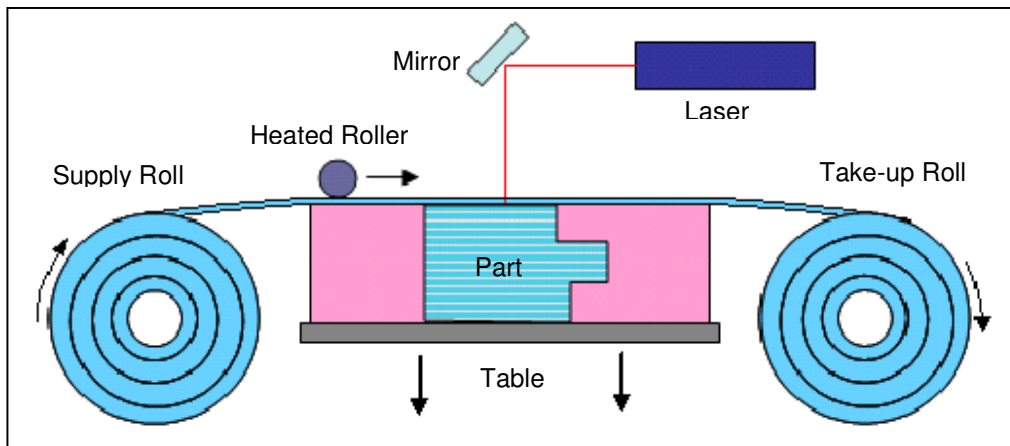


Figure 1.15. LOM process

The first commercial provider of laser based LOM machines, Helisys, ceased operation in 2000 however multiple new machines have been developed that produce paper, plastic and plastic foam laminated objects. The Invision® LD 3D modeller is a plastic film based LOM machine designed for desktop use which costs less than \$15,000 US. Figure 1.16 shows the Invision® LD 3D modelling machine by 3D Systems and some plastic parts produced by it.

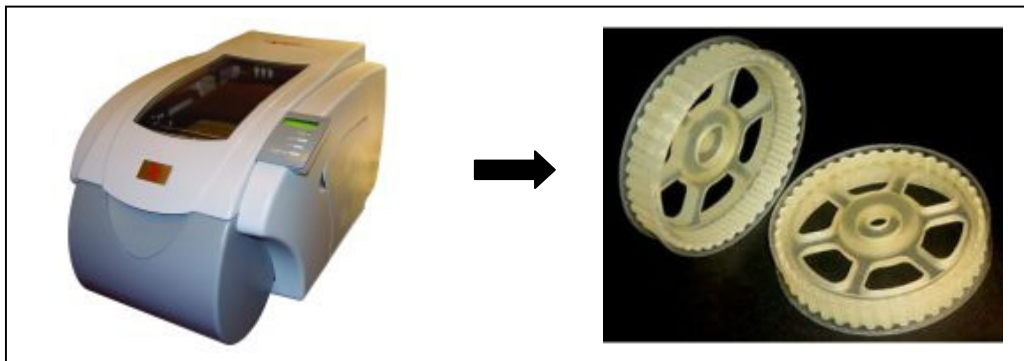


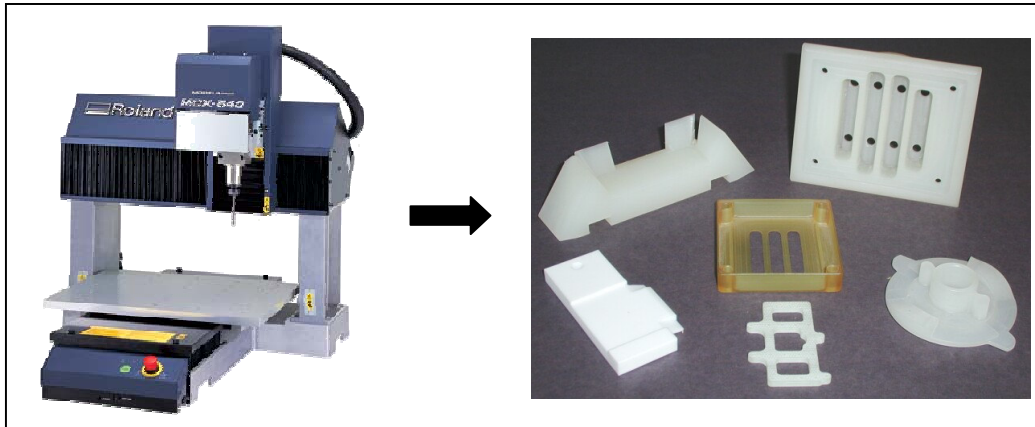
Figure 1.16. Invision® LD 3D Modeller LOM machine and parts by 3D Systems.

### 1.2.2.7 CNC Machining

Subtractive rapid prototyping (SRP) systems such as desktop milling machines are becoming increasingly user friendly and provide suitable solutions for many RP applications. SRP systems can cost less than half the cost of most additive systems while producing prototypes out of a wider variety of non-proprietary materials with greater precision and better surface finish. The dimensional accuracies that can be expected for AMT processes ranges from 0.13 to 0.76 mm while CNC machines achieve accuracies of 0.03 to 0.13 mm [20].

Complex geometries such as internal features and overhangs provide limitations to SRP systems however this is not always a disadvantage as manufacturability is often a property of interest.

Figure 1.17 shows a desktop SRP machine and some parts produced by a similar milling machine.



**Figure 1.17. Roland MDX-540 desktop mill and parts.**

CNC machining of a part requires the generation of tool paths which is often a complex procedure. Computer aided manufacturing (CAM) software provides a way to automate the tool path generation process. This software greatly increases the efficiency of machining processes and improves the ease of use of machining technology [22]. CAM software is discussed further in chapter 3.

### 1.2.3 Summary of RP Technologies

All additive RP processes are based on a layer by layer building process and use the .STL file format, which is a triangulated representation of the surface of the solid model. Subtractive RP technologies use machining operations to create prototypes using a variety of file formats including .STL files.

The majority of RP machines require little user experience, and are capable of producing complex parts which are difficult or even impossible to make using conventional methods. The variety and functionality of RP materials are continually evolving making RP systems suitable for short manufacturing runs for certain applications.

The major disadvantages of most commercial RP systems lie in the following areas:

- Build size - Most machines can only produce relatively small components (average build envelope is around 400 x 400 x 400 mm or 0.064 m<sup>3</sup>).
- Initial system cost is generally high (although some low end RP machines now cost under \$15,000 USD).

- Proprietary build materials are generally provided by the manufacturer of the machine only. The lack of competition means the material costs are often inflated.
- The strength of RP parts are generally weaker than if they were machined from a blank of the same material.

Table 1.1 shows a summary of the different RP technologies and the relative strengths and weaknesses of each.

**Table 1.1. Comparison of current RP technologies [19, 20, 23, 24].**

Property	RP Process						
	SLA	FDM	Inkjet	3DP	SLS	LOM	SRP
Speed	Average	Poor	Good	Very good	Average	Very good	Excellent
Build Size	Excellent	Excellent	Good	Poor	Excellent	Poor	Excellent
Cost	Very high	High	Moderate	Low	Very high	Low	Low
Accuracy	Excellent	Fair	Very good	Fair	Good	Fair	Excellent
Complexity	Excellent	Fair	Very good	Fair	Good	Fair	Poor
Build Material	Photopolymers	Plastics	Photopolymers	Plaster, Starch	Plastic, Metal	Paper, Plastic	Wood, Plastic, Metal

Most current RP machines provide accurate models with complex freeform geometries, however they are limited to build volumes no bigger than 0.2 m<sup>3</sup> with machine size and build times being the limiting factors. A number of RP technologies are currently being developed with build volumes greater than 0.5 m<sup>3</sup> to address this issue. In particular, plastic foam sculpting RP machines currently under development have the potential to build large inexpensive prototypes, moulds and concept models faster than conventional RP technologies. A detailed overview of novel foam sculpting RP machines is contained in chapter 2.

The next section of this chapter provides a brief overview of the plastic foam cutting process which is the focus of this research.

### 1.3 Thermal Plastic Foam Cutting

This section provides an overview of plastic foam cutting (PFC). It begins with information about polystyrene foams and their manufacture, followed by the PFC process and a brief description of

the thermomechanical mechanisms involved in the process. Then common commercial PFC machines and tools are discussed and compared with conventional rapid prototyping machines.

### **1.3.1 Polystyrene Foams**

Polystyrene (PS) foams are currently the most common material used in the foam cutting industry. PS foams are inexpensive and are widely available, the low density and rigid cell structure of PS foams mean they are well-suited for a wide range of applications and the physical properties make it ideal for thermal plastic foam cutting.

PS foam comes in a wide range of cell structures and densities however the chemical composition of each material is very similar (differing only by the blowing agents and molecular weights). Most can be placed in two groups: expanded polystyrene (EPS) and extruded polystyrene (XPS). These two foams will be explained further in the following sections.

#### **1.3.1.1 Expanded Polystyrene (EPS)**

Expanded polystyrene is a rigid, closed cell, thermoplastic foam material and produced from solid beads of polystyrene. Expanded polystyrene is made up of approximately 2% polystyrene and 98% air. It is manufactured by heating polystyrene pellets with steam so they expand rapidly within a mold and form a large block of low density foam. The expanded beads remain as air filled closed cells that resist the conduction of heat. This foam is light, usually 16-32 kg/m<sup>3</sup>, and very inexpensive.

EPS is manufactured from styrene monomer using a polymerisation process which produces translucent spherical beads of polystyrene, about the size of sugar granules. During this process a low boiling point hydrocarbon, usually pentane gas, is added to the material to assist expansion during subsequent processing. EPS is produced in a three stage process. In the first stage, polystyrene beads are expanded to between 40 and 50 times their original volume by heating to about 100 °C with steam in an enclosed vessel called a pre-expander. During this process the beads are stirred continuously. In this process the final density of the EPS is determined. After pre-expansion, the expanded beads are cooled and dried in a fluidised bed drier, before being pneumatically conveyed to storage silos for maturing.

During maturing, the second stage of processing, the expanded beads containing up to 90% air are stabilised over a period of typically 24 hours. Following pre-expansion the beads have a partial vacuum which must be equalised before final processing by allowing air to diffuse into the beads until equilibrium is reached.

In the third stage of processing, known as the molding stage, beads are conveyed into a mould, and once in the mould are heated again by the introduction of steam. Under the influence of

steam, the beads soften and start to expand again. However, as they are contained in a mould they cannot expand freely, and therefore create an internal pressure within the mould. Under this pressure the softened beads fuse together when the correct temperature is reached within the mould. Following fusion the mould is cooled, usually under the influence of a vacuum to remove moisture. The moulded product is ejected from the mould at the completion of the cycle. During processing the pentane gas is expanded, so that the finished products contain little residual gas.

#### **1.3.1.2 Extruded Polystyrene (XPS)**

Extruded polystyrene foam is the same chemical product as the expanded foam, but it is manufactured using a different process which extrudes the foam, resulting in a denser, more homogenous product with much smaller air pockets. XPS foam begins as solid polystyrene resin granules. The granules, along with special additives and a blowing agent are fed into an extruder. Within the extruder the mixture is combined and melted, under controlled conditions of high temperature and pressure, into a viscous plastic fluid. Then, a blowing agent is injected to make the mixture foamable. The hot, thick liquid is then forced in a continuous process through a die, at which time foaming and shaping occurs. As it emerges from the die it expands to foam, is shaped, cooled, and trimmed to dimension.

This continuous process produces a consistent quality foam product with a closed-cell structure that looks like a mass of uniform bubbles with common walls between them. Close inspection reveals that there are few, if any, voids between the cells and that a continuous smooth skin, top and bottom, has been formed.

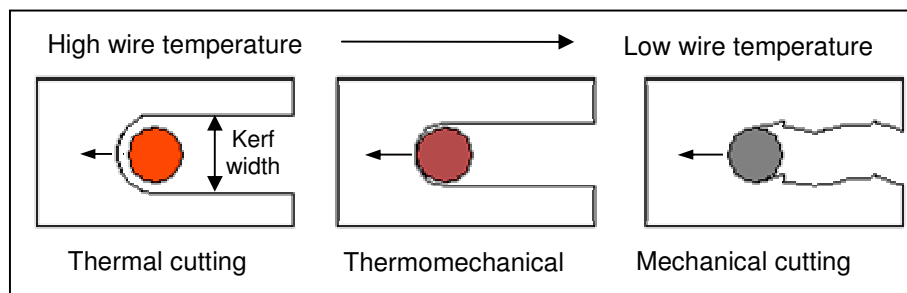
Extruded polystyrene has excellent resistance to moisture, is impervious to rot, mildew and corrosion. The closed-cell structure and lack of voids in XPS helps the foam to resist moisture penetration better than other materials.

### **1.3.2 Process Description**

Plastic foams are most commonly cut with hot-wires which are held straight to produce ruled surfaces and 2D profile cuts; and hot-ribbons which can be bent into any profile and used to cut revolved sections and complex surfaces [25]. Figure 1.19 shows both cutting elements being used in commercial cutting machines. While almost any plastic foam can be cut with hot-wires the most commonly cut materials are rigid foams such as EPS, XPS, polyurethane (PU), polyvinylchloride (PVC) and Polyethylene (PE) foams. Ideally the temperature of the cutting element should be adequate to 'melt' or sufficiently soften the foam immediately ahead of the wire/ribbon. Obtaining the correct wire or ribbon temperature and maintaining it throughout a cut will be discussed in detail in chapter 3.



The thermomechanical mechanisms present in PFC can be separated into three main cutting modes and the transitions between them. These modes are: Thermal cutting in which the foam is melted or 'vaporised' ahead of the advancing heat source; thermo-mechanical cutting in which the cutting element comes into contact with the foam and thus cuts via a combination of melting and shearing; and mechanical cutting which occurs when the temperature of the wire is too low relative to the feed rate or vice versa. Kerf is a common manufacturing term and is defined as the slot or groove made by a cutting tool. In PFC the kerf width depends on the cutting mode present as shown in figure 1.18 below.



**Figure 1.18. Cutting mechanisms.**

Mechanical cutting results in ripped or torn surfaces which, are often unacceptable for manufacturing purposes and is therefore only included for completeness. Often as a cut progresses with time the cutting mode will change from thermal cutting to thermo-mechanical or mechanical cutting with a transitional zone in between. Depending on the cutting conditions the transitional zone may be short ( $\approx 20$  mm) or it could run the entire length of the cut.

Under the correct cutting conditions thermo-mechanical cutting provides the smoothest surface finish while maintaining small kerf width, however, high cutting forces may be a limiting factor to obtaining high feed rates. Thermal cutting produces textured surfaces with large kerf widths. The maximum feed rate achievable with thermal cutting depends on the material properties of the cutting tool which is usually a metal alloy. Low yield strength at elevated temperatures often cause hot-wires to creep before failing while hot-ribbons yield and can undergo significant plastic deformation.

### 1.3.3 Commercial Machines and Tools

Due to the wide availability and low cost of plastic foams, these materials have become a popular sculpting material for artists, craftsmen, hobbyists and machinists. There is a wide variety of machines and tools currently being used to cut foam, however the majority fall into one of two categories; handheld tools, and stationary (floor or desk mounted) machines. The stationary machines may be manually operated or automated. Novel foam sculpting rapid prototyping machines will be discussed in chapter 2.

### 1.3.3.1 Stationary Machines

Stationary machines range in size from 300 mm to 3 m wide and the level of automation is equally varied [26]. There are a number of CNC foam cutting machine manufacturers situated around the globe, common names include; Croma of France, MegaPlot of Poland, Tekoa, Demand Foam Cutting and Hotwire Direct of the USA. The smaller machines are manually fed with jigs used to increase accuracy, while the mid size machines often have turn tables. Larger foam cutting machines are CNC controlled with multiple hot-wires. Depending on the size and level of automation machine prices typically range from \$300 to \$30,000 USD. Stationary machines have the ability to produce relatively accurate parts, however they are unable to create highly detailed part features. Figure 1.19 shows three different commercially available cutting machines made by Demand Foam Cutting [27].



**Figure 1.19 Manually operated craft table cutter, combination cutter and CNC cutter from Demand Products. Reproduced from [27].**

The Craft table cutter acts similar to a band saw however the blade is replaced with a hot-wire. Cutting is done manually and straight edges are possible with the aid of jigs. The key features of this machine are its quick and easy operation for cropping foam blanks and creating 2D profiles.

Stand-alone combination cutter uses a custom profile hot-ribbon created by the user to carve base revolves or arches. Excellent for revolved shapes with constant profiles. This process is semi-automated as once the profile is set the machine will rotate the foam blank into the hot ribbon with a motor driven turntable.

Computerised foam cutters provide fast, accurate sculptures that can be precisely duplicated. Extra skill is required to programme and operate the expensive machinery. As with the other stationary machines internal features such as double concave surfaces or hollow sections are not

possible. While most machines use springs to tension the wire, larger machines can also use pneumatic cylinders which provide more uniform tensioning loads.

Some examples of shapes cut with stationary foam cutting machines are shown in figure 1.20. Some of the complex objects shown (such as the column) were produced by assembling several geometrically simpler parts. The sculptures below would have required many different hot ribbon and hot wire machine configurations, however the dimensional accuracy and repeatability of the parts are high compared to parts made with handheld tools.



**Figure 1.20. Foam sculptures cut with MegaPlot foam cutting machines. Reproduced from [16].**

Below is a list of the advantages and disadvantages associated with commercial stationary foam cutting machines when compared to handheld cutting tools.

*Advantages:*

- Parts can be produced with good geometrical form
- Sculptures are repeatable
- Capable of high feed rates
- Low degree of sculpting skill required
- Wide range of machines ideally suited for specific tasks

*Disadvantages:*

- Expensive (compared with handheld tools)
- Single machines are often limited in functionality
- Intricate details and internal features often not possible
- CNC machines require additional training

- Large floor or table space required
- Machines generally have part size limitations

### 1.3.3.2 Handheld Tools

Hot knives and bow cutters are popular handheld devices as they are inexpensive (\$70-\$800 USD), simple to operate and can be used to create highly detailed parts. Figure 1.21 below shows some commercial handheld tools currently available.

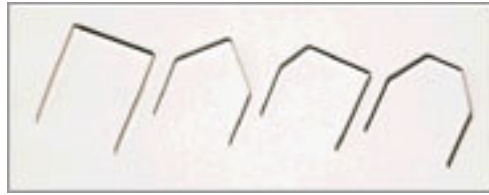


**Figure 1.21. Handheld foam cutting tools. Reproduced from [27].**

Bow cutters are excellent for straight cuts or 2D profiles. The large clearance between the wire and the arch allows for deep cuts. Blades or wires can be used allowing for extremely thin clean cuts.

Hot knives with a single blade are highly manoeuvrable. The finite length of the blade allows internal features to be cut. The accuracy of a single blade is less than that of a wire due to the width of the blade and its larger turning radius in the foam.

Hot knives with looped blades are the most common handheld tool. The blades are made with flat wire to provide strength in the cutting direction while providing a cleaner cut than a single blade. A range of standard shapes can be bought (figure 1.22) or flat wire can be bent into custom profiles to create almost any shape.



**Figure 1.22. Standard blade profile shapes. Reproduced from [27].**

Some examples of foam sculptures made with a range of handheld tools are shown below. As can be seen, extremely detailed sculptures of all sizes are possible. However, the outcome of such sculptures depends greatly on the skill of the artist or craftsman.



**Figure 1.23. Foam sculptures created with hand tools. Reproduced from 3D Custom Foam Inc. [28].**

Below is a list summarising the advantages and disadvantages of hand held foam cutting tools compared with floor or desk mounted foam cutting machines.

*Advantages:*

- Low cost
- No computer equipment or programming skills needed
- Controlled by dexterous human arm
- High level of detail possible
- Can use blades of any shape (customised profiles)
- Easy to quickly and efficiently change tools for different cuts
- No size limits

*Disadvantages:*

- Very difficult to make dimensionally accurate duplicates or prototypes
- Sculptor needs to be highly skilled
- Very time consuming (compared to automated methods)

**1.3.3.3 Summary of Machines and Tools**

The variety of PFC machines and tools available allow objects of all sizes and complexity to be cut, however often multiple machines or skilled craftsmen are required. Stationary machines excel at simple geometric profiles and revolved shapes while handheld tools are most suited to parts with intricate detail. Important to note is the inability of taut hot-wires to cut double concave surfaces, this is why ribbon profiles and blades are used for detailed features and pockets. Figure 1.24 summarises the properties of PFC machines and hand tools in terms of part complexity and sculpting speed/accuracy.

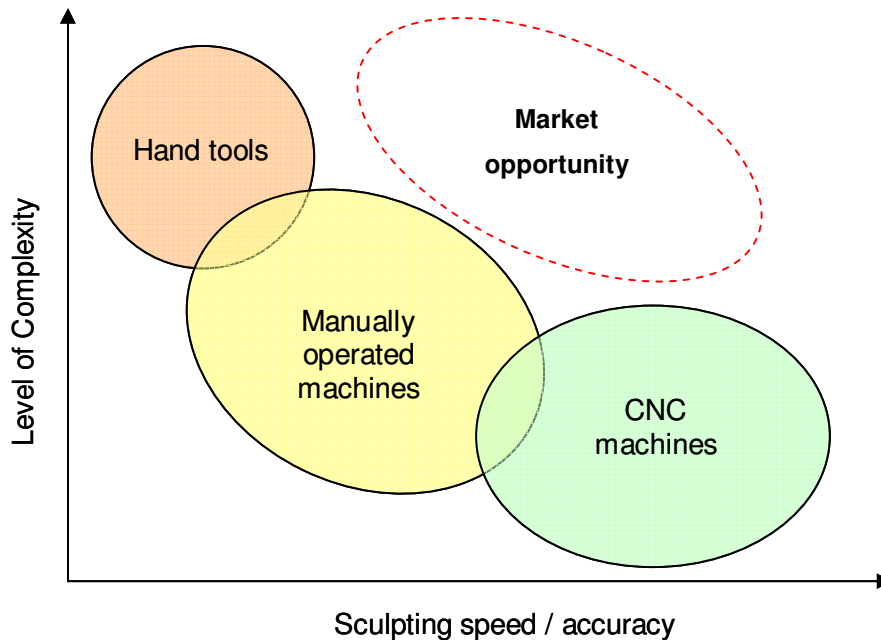


Figure 1.24. Comparison between PFC machines and PFC hand tools.

As can be seen in figure 1.24 there lies an opportunity to develop a method of foam sculpting that increases the complexity of parts made by CNC foam cutting machines. Ideally a machine will be developed that can sculpt complex objects with the dexterity of a human arm while maintaining the speed and repeatability of a CNC hot wire machine. Foam cutting rapid prototyping machines are one solution currently being developed to address this issue. These will be discussed in detail in chapter 2.

It is interesting to note that although PFC with hot wires and ribbons is wide spread in certain industries, and many commercial machines and tools have been developed, research into foam cutting mechanics is rare. The research contained in this thesis, on foam cutting mechanics, aims to elevate foam cutting from an estimated process to a highly accurate process optimised by science. The following sections describe more fully the motivations and objectives of this research.

## 1.4 Motivation

Plastic foam cutting is a widely adopted method of material removal for plastic foam, however little work has been reported on the mechanics of hot-tool foam cutting. The work reported which follows aims to address this imbalance. This section outlines the motivation for the investigation into PFC including the experimental cutting trials and the finite element simulations.

Firstly, experimental research to-date on PFC has been sparse with experimental data often presented in a qualitative fashion. Most of the published results focus on the relationship between feed rate, cutting force and kerf width while factors influencing wire temperature and surface finish have been largely overlooked [29]. In order to fully describe the factors influencing cutting behaviour a large body of empirical data is needed from which analytical and numerical models can be built. Also by examining the interactions between the cutting tool and the foam it is hoped a form of feedback control can be found to regulate the cutting element temperature.

Secondly, while experimental work is extremely useful for repeatable operations it has limited potential for expanding results into the general case. By using the insights gained by the early experimental work a numerical model can be developed for the steady state case that has the advantage of having predictive capabilities.

Thirdly, to fully exploit the advantages of PFC it is necessary to develop a method for determining the optimum condition of the cutting parameters necessary to satisfy cutting requirements. The finite element method provides a means to simulate the foam cutting process with the purpose of

verifying the theoretical model and ultimately providing a predictive tool. Simulations may also be used to optimise tool design to improve cutting characteristics.

## 1.5 Objectives and Scope

The objectives and scope of this research are as follows:

### 1. *Empirical Study:*

To quantitatively measure the cutting conditions present in PFC. This includes the effects of feed rate, materials, electrical power, cutting element geometry and cutting tool temperature on cutting force, surface texture and kerf width. To verify the finite element models and to obtain empirical formulae and values for force feedback temperature control.

### 2. *Numerical Model:*

Develop transient finite element models of the PFC process – the straight line cutting path case for both hot-wires and hot-ribbons and the curved cutting path case for hot-ribbons. Correct simulation will provide a means of predicting the results of future cuts and could lead to improved cutting tool design.

### 3. *Future Work:*

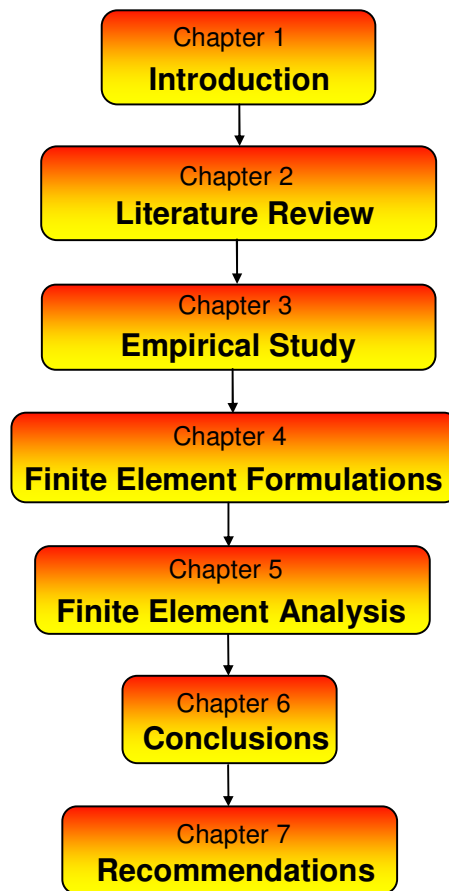
Propose improvements to current cutting tools and machining strategies.

## 1.6 Outline of Thesis

This section provides an outline of the organisation and contents of the remainder of the thesis.

The organisation of the work in this thesis is presented in figure 1.25. Work began with cutting trials, followed by the development of empirical formulae relating the various parameters present in PFC. Then finite element equations are formulated and a two dimensional transient thermal model is developed. The results from the finite element analysis are compared with the experimental data gained from the cutting trials and the effectiveness of the model is discussed. Each chapter, starting with the introductory chapter is outlined as follows:





**Figure 1.25 Organisation of work in this thesis.**

Chapter 2 gives a review of literature related to PFC theory and includes an overview of novel plastic foam rapid prototyping and manufacturing machines.

Chapter 3 provides details of the experimental work including experimental apparatus, experimental method, results and discussions.

Chapter 4 introduces the heat diffusion equation and formulates the finite element equations.

Chapter 5 provides details of the two dimensional transient thermal model for PFC, including geometry, elements used and temperature boundary conditions. The FEA results are then compared with experimental data.

Chapter 6 summaries the results and the conclusions.

Chapter 7 provides recommendations for further experimental work and potential improvements to the FEA.

## 2 Literature Review

---

### 2.1 Introduction

This chapter provides background information relating to plastic foam cutting mechanics. The literature review is divided into two sections; novel foam cutting machines for rapid prototyping and manufacturing purposes, and research into foam cutting mechanics. The two are intrinsically linked as the design and operation of foam cutting machines dictate the design of the cutting tool and the cutting mechanics that prevail. Research into foam cutting mechanics can be split further into two sub-categories, experimental work and numerical simulation – as shown in Figure 2.1.

Development of foam cutting machines for RP purposes began shortly after the first additive manufacturing machines became commercialised in the late 1980s. Increased computer power, the development and adoption of CAD/CAM software and rising demand for customisation has caused the RP industry to grow rapidly in recent decades. While conventional RP technologies are continuing to improve in speed and accuracy the ability to produce large ( $> 1 \text{ m}^3$ ) prototypes, moulds or parts it is still expensive, time consuming and often impossible [30]. Foam cutting machines have many attributes suited to large scale rapid prototyping and manufacturing (RP & M) such as fast build times and low cost materials [31]. Few RP foam cutting machines have been commercialised to-date leaving significant opportunities for research and development in this area. The following section will describe novel foam cutting RP machines that have been developed or are currently being developed at institutions around the world.

Several of the researchers developing foam cutting RP machines have carried out research into foam cutting mechanics with the purpose of improving the quality of their sculpted parts. Empirical work has concentrated on investigating the effects of process parameters on surface texture, kerf width and accuracy. Next, theoretical research into PFC mechanics is described. Analytical models have been developed, however most suffer from inaccuracies or a narrow range of application. Finite element simulations have successfully been carried out, the limitations of which will be discussed with recommended improvements. At the end of this chapter, concluding remarks are made concerning the recent development of PFC techniques and the issues that still remain.

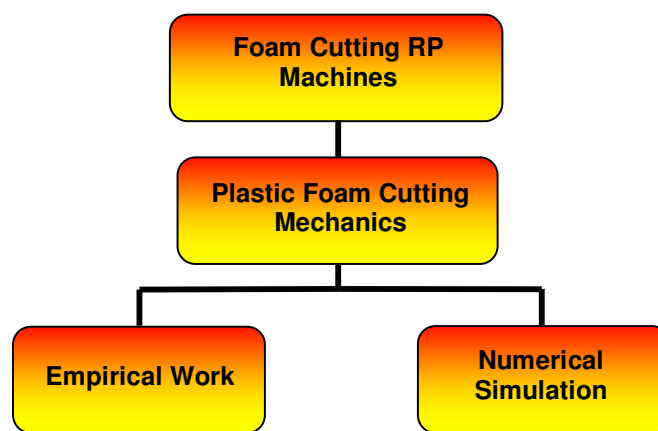


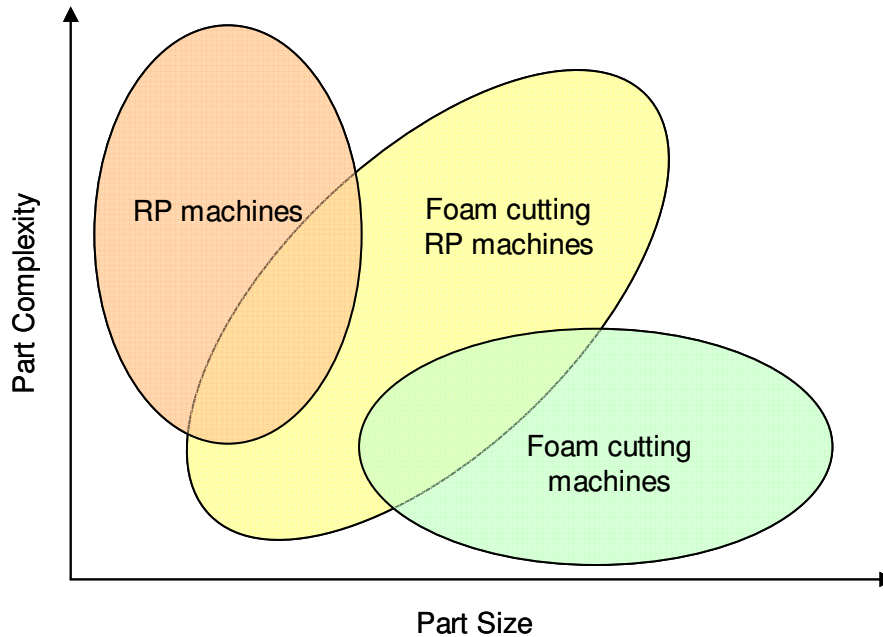
Figure 2.1. Research disciplines in plastic foam cutting.

## 2.2 Foam Cutting RP Machines

Foam cutting RP machines use a range of methods to produce plastic foam objects from CAD data. The criteria used to identify foam cutting RP systems in this thesis are as follows:

- The build material must be a plastic foam such as expanded polystyrene.
- The tool path and machining strategy should be determined directly from a 3D digital representation of the prototype.
- The system should be able to create complex freeform shapes.
- The system should have a software based user interface for efficient transfer of information between the operator and the RP system.

The main benefit of foam cutting RP machines when compared to conventional RP machines is the use of inexpensive materials and the possibility of producing large parts with rapid build times. Likewise, conventional foam cutting machines have the ability to cut large parts however the level of complexity able to be achieved is low. Foam cutting RP machines bridge the gap between conventional RP machines and conventional foam cutting machines as shown in figure 2.2.



**Figure 2.2. Comparison between conventional RP machines, foam cutting machines and foam cutting RP machines in terms of part complexity and part size.**

The following sections describe different foam cutting RP machines developed or currently under development around the world. The most common method of fabrication is layered manufacturing, in which the part is built up by assembling individual layers, however direct sculpting and heat ablation methods are also used.

### **2.2.1 Freeform Automated Sculpting Technology (FAST)**

FAST is a RP&M system currently under development within the Department of Mechanical Engineering, University of Canterbury, New Zealand and is the motivation for this thesis. The system currently consists of:

- A laser scanner for obtaining digital surface information.
- CAD/CAM software to prepare 3D models and produce cutting paths for the robot.

- A six axis Kuka KR6 industrial robot used to manipulate the cutting tool along the cutting paths.
- An electrically heated cutting tool used to cut the plastic foam.

This system is a form of robotic machining similar to that developed by Tangelder [30]. The main difference is the use of a hot-ribbon as the cutting tool and the method of producing the cutting paths.

The cutting elements used to date are 1/8" x 0.018" Nichrome ribbons which can be bent into any desired profile. In practice a jig is used to form ribbons with known dimensions. Ribbons with large profiles are used for roughing while ribbons with smaller profiles are used for detailed features and surfaces with high curvature. This combination of tools greatly reduces cutting times when compared to standard milling operations. A pneumatic gripper allows for automated tool changes, allowing many different ribbon profiles to be used in a short time. Hot-wires can also be used for profile cuts and objects with ruled surfaces.

A method of producing the robot control program was developed by Posthuma [32] in fulfilment of a Masters degree at the University of Canterbury. The process starts with an IGES model which is loaded into CAM software Mastercam™. Mastercam™ is then used to create roughing and finishing tool paths which are processed using a modified generic 5-axis post processor. The tool path data is then exported into an Excel spreadsheet where it is transformed into x y z A B C coordinates which can be read by another proprietary software package called RobotWorks™. RobotWorks™ is used to simulate the robot motion and carry out collision and joint limit checks. RobotWorks™ then converts the tool path data into Kuka language. The control program is subsequently loaded onto the robot PC and the program is executed. Figure 2.3 summarises the FAST Process.

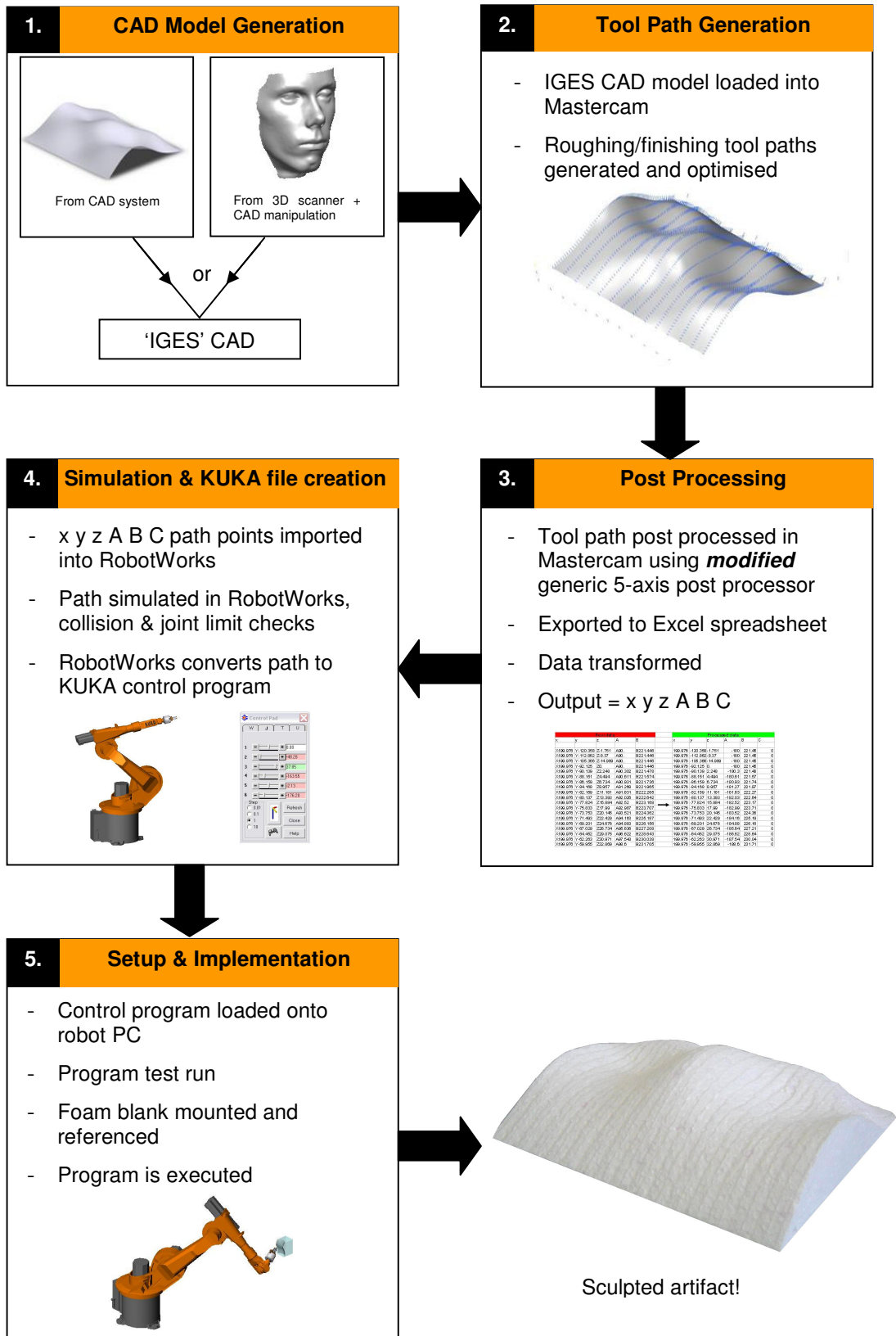
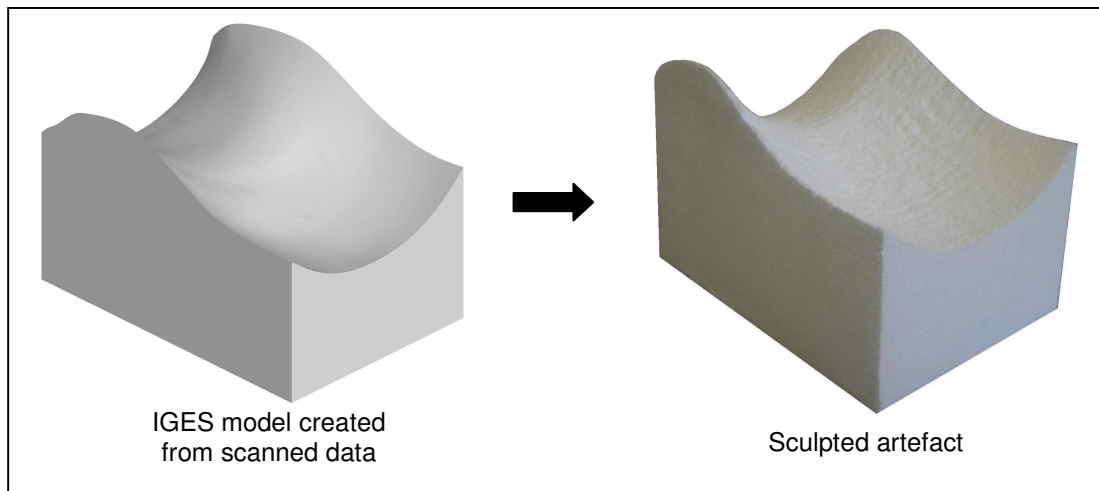


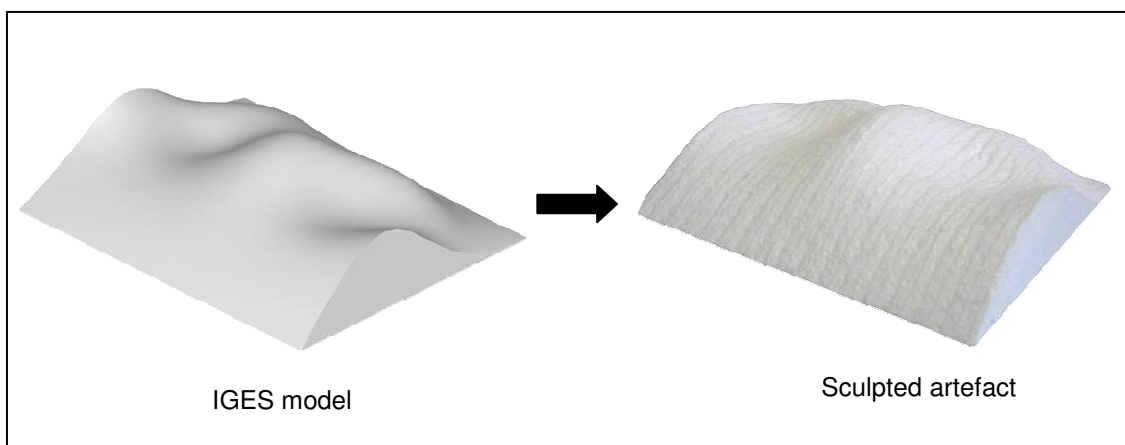
Figure 2.3. FAST procedure summary. Reproduced from [32].

The FAST system has successfully sculpted a number of arbitrarily chosen freeform surfaces out of EPS and XPS as well as custom fit supports trialled for medical purposes. Figures 2.4 & 2.5 show some examples of parts sculpted with the FAST system and relevant CAD models.



**Figure 2.4. IGES model of neck support created from scanned data and the sculpted part ready for use.**

The IGES model shown below was generated by lofting between 5 arbitrary profiles. These profiles were spaced 50 mm apart to generate a surface with both concave and convex features. Generating and processing the roughing and finishing tool paths took approximately 40 minutes. The size of the foam blank was 160 mm x 190 mm x 50 mm. The roughing pass was carried out using a 25 mm wide square profile Nichrome cutting blade in 1.7 minutes. The finishing pass was carried out using an 8 mm wide flat ended Nichrome blade in 2.2 minutes. The total process time required to make the part was 49 minutes.

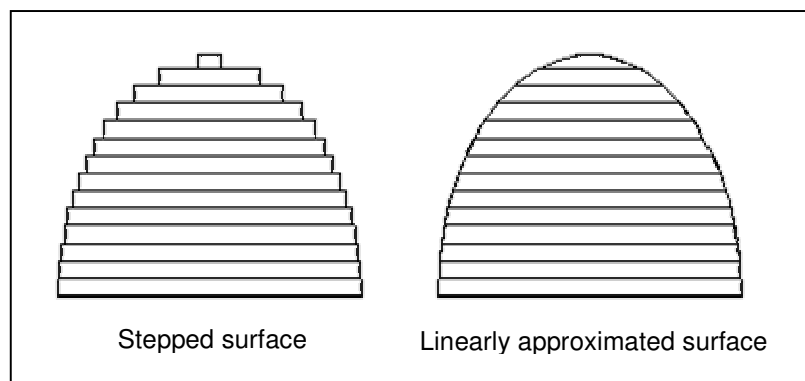


**Figure 2.5. IGES model and part sculpted from EPS showing complex 3D surfaces produced with the FAST system.**

Research on the FAST project is still ongoing and a number of improvements are envisaged for the future which will dramatically increase the size, speed and accuracy of the system.

### 2.2.2 True Surface System (Trusurf)

Trusurf is a layered manufacturing method developed by Hope et al at the Department of Mechanical Engineering, University of Queensland, Australia [33]. The system was developed primarily to produce large ( $> 1 \text{ m}^3$ ) free-form models out of polystyrene foam. It uses a high-pressure, 5-axis water-jet cutter to cut the model's cross-sections from layers of polystyrene (10, 20 and 30 mm stock sizes). The 5-axis cutter cuts the cross-sections with sloping edges (as opposed to vertical cuts) to eliminate the stepped surface finish common to many LOM systems (see figure 2.6).



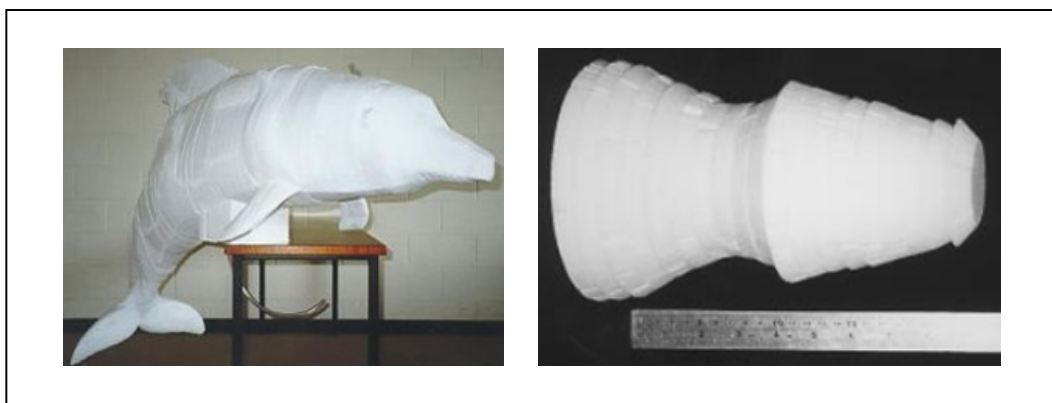
**Figure 2.6. Stepped versus ruled cuts.**

Once the thick cross-sections have been cut, they are assembled and bonded by hand to produce the finished model. The advantage of the Trusurf system lies in the fact that it can produce models with relatively thick layers as the linearly approximated sides reduce the number of layers required for a given model.

The Trusurf system generates B-splines directly from CAD models (as opposed to .STL files which are approximations of the CAD model) so the splines are exact, hence the name Trusurf.

Figure 2.7 below shows two objects made with the Trusurf system. Because the water cutter only produces linear approximations the surface finish is not ideal and discontinuities are visible between the layers. The errors can be minimised by decreasing the layer thicknesses although this also increases the build time.

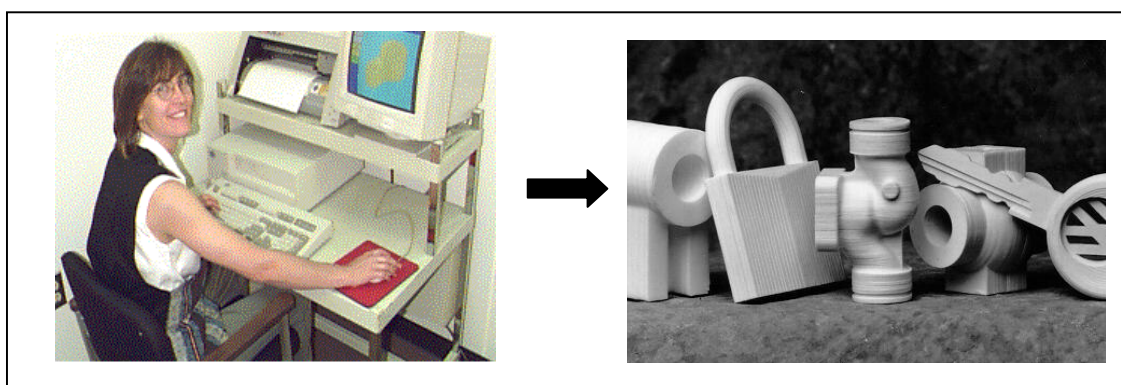




**Figure 2.7.** Life size dolphin and revolved shape created with the Trusurf system.

### 2.2.3 Shapemaker I & II

Shapemaker I and II are layer based manufacturing systems developed by the Manufacturing Processes Laboratory at the University of Utah [2, 34]. Shapemaker I is a simple LOM based system in which section profiles are cut using a plotter and manually stacked using a construction table and registration pins. After each individual layer is stacked, the backing layer is peeled off, thus exposing the adhesive and providing a bonding surface for the next layer. Materials used are paper, plastic foam and vinyl sheet attached to a backing layer. Shapemaker I is now commercialised as JP System 5 Desktop Rapid Prototyping by Schroff Development Corporation, and is primarily used as an education tool introducing university students to RP technologies. Figure 2.8 shows the JP System 5 and some paper models made from it.



**Figure 2.8.** The JP-5 system and parts.

Shapemaker II (SMII) differs from its predecessor in that it is aimed at producing large (>1 m<sup>3</sup>) full scale prototypes from polystyrene foam. The foam is cut using hot-wires which are attached to two plotting heads. The plotting heads move independently to create linear approximations of each section surface similar to the Trusurf system (in fact both were developed around the same time in 1996-1997).

Suggested applications of this technology include cores for large aerospace structures which would then be finished and covered in a composite material. SMII was successfully used to create a number of example objects including a wind turbine blade and a tail rudder. The turbine blade measured 1.2 m x 0.18 m x 2.1 m and the fabrication time was approximately 11 hours excluding CAD modelling.

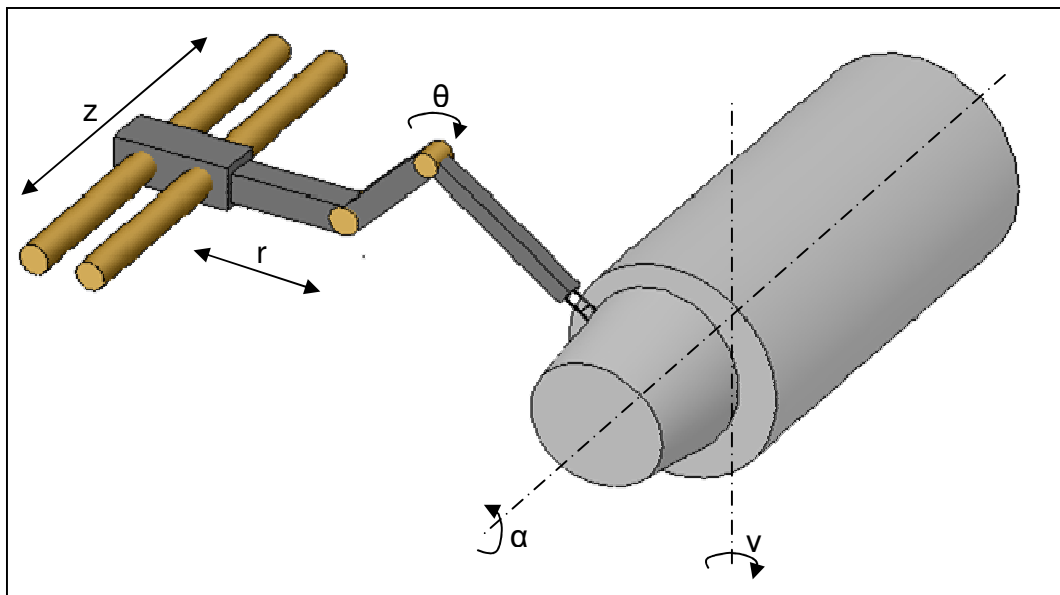
There are a number of limitations associated with SMII including:

- The cutting wire can not be tilted more than 45° limiting the accuracy for layers that require a larger slope.
- Models that have features less than 1" can not be reproducing using the required 1" thick foam.
- The individual layers have to be assembled by hand using registration holes and pins which could be cumbersome and time consuming.

#### **2.2.4 ModelAngelo**

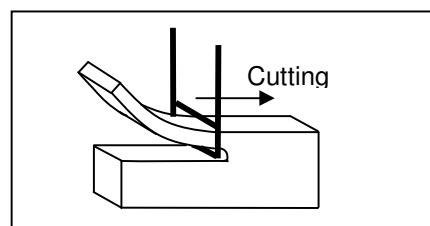
This system was developed by the Department of Mechanical Engineering at the American University of Beirut in Lebanon [8]. It consists of unique foam cutting RP equipment and software collectively called "ModelAngelo". ModelAngelo utilises a combination of linear and rotational axis to cut foam with a heated cutting tool.

The foam blank is held in a lathe like fixture the motion of which is synchronised with the cutting tool. Figure 2.9 shows the cutting tool, a part being sculpted and the available degrees of freedom (for clarity the foam holding fixtures have been omitted). The 'y' axis is used to rotate the foam part through a possible 90° to allow the ends to be sculpted, however one end of the part must remain flat so it can be held with the clamping pins.



**Figure 2.9. ModelAngelo apparatus.**

The tool consists of two short stainless steel wires, which are electrically heated above the melting point of the plastic foam used. The cutting tool is schematically illustrated in figure 2.10. The outer loop is used to cut the foam while the inner loop is used to manage the swarf. The inner loop is hotter than the outer loop because it does not contact the foam. This causes the foam nearest the inner loop to melt and contract curling the swarf upward. If the swarf is not removed from the cut surface it risks sticking back to the model and would then need to be removed by hand.



**Figure 2.10. Electrically heated cutting tool.**

The authors suggest a number of applications such as art sculpting, prototypes for fit and form evaluation, and casting processes for biomedical and engineering applications. Several finished products sculpted by ModelAngelo are shown in figure 2.11.



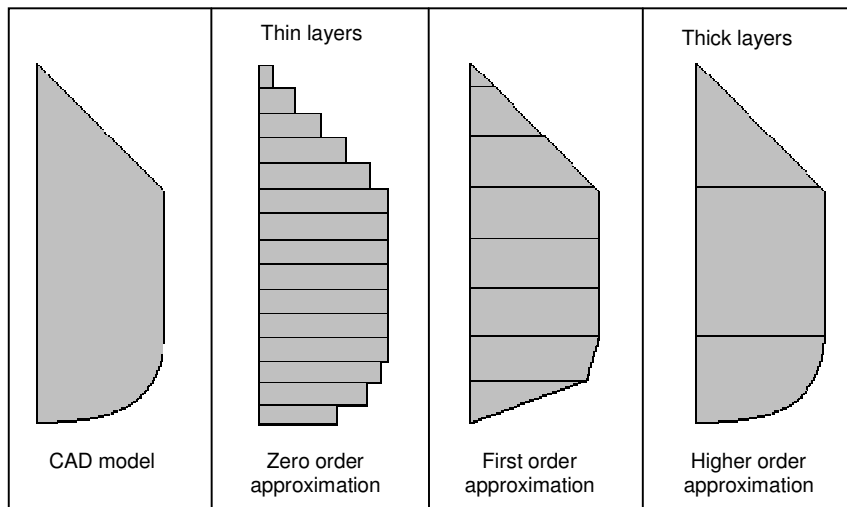
**Figure 2.11. Parts sculpted using ModelAngelo.**

### **2.2.5 Freeform Thick Layered Object Manufacturing (FF-TLOM)**

This process is currently under development within the Faculty of Design, Delft University of Technology in the Netherlands [6, 31, 35-40]. The proposed system builds models from XPS foam using a layered manufacturing method similar to the Trusurf system. FF-TLOM utilises an electrically heated Nichrome blade to cut section profiles which are then assembled manually.

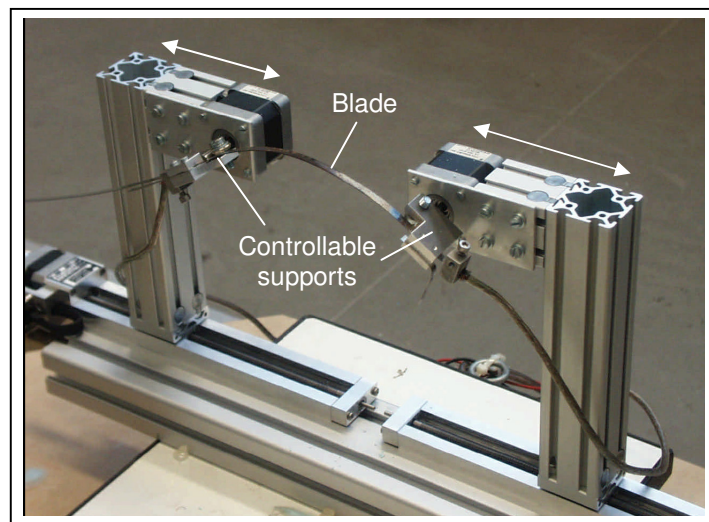
The unique feature of this process is the flexible cutting tool which changes shape to provide high order approximations of the desired surface as shown in figure 2.12. By using higher order approximations it is possible to achieve far more accurate models while using thicker layers. The cutting tool is a flexible Nichrome ribbon which is held between two supports. The supports are accurately rotated with stepper motors to change the shape of the ribbon to match the surface geometry. The ribbon shape for any given support orientation is calculated using minimum strain energy theory.

A prototype of the flexible cutting tool is shown in figure 2.13 [41]. The device has three degrees of freedom, the linear distance between the connection points and the rotational orientation of the supports. The length of the ribbon between the connection points is constant. A six axis Manutec R15 industrial robot was used to manipulate the foam slab while the tool remained in a fixed position this is because the prototype tool is rather large and heavy.



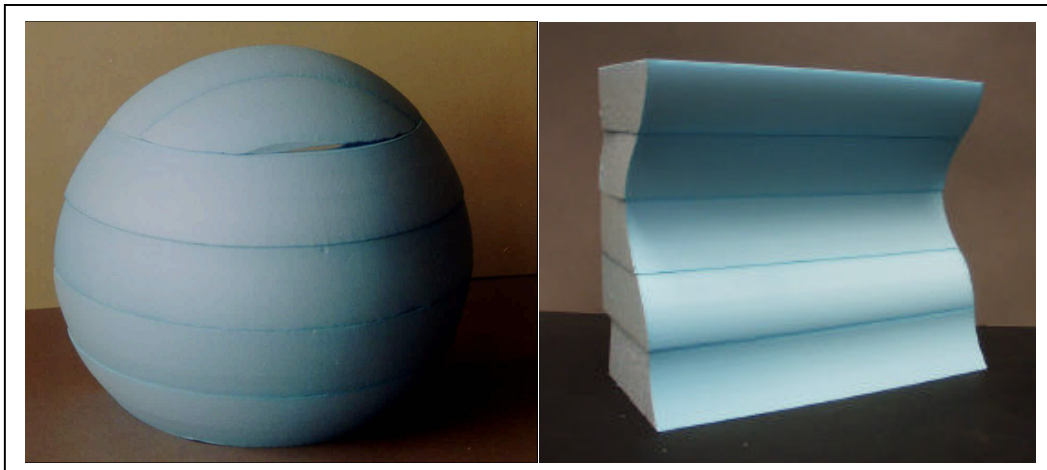
**Figure 2.12. Effects of different order surface approximations.**

The finite width of the blade provides limitations to the maximum rate at which curvature can change. While the ribbon is most suited to tangential cutting, rapidly changing surface curvature will require the ribbon to move with a transverse component. Any transverse movement of the ribbon will greatly reduce the maximum cutting speed of the ribbon and may negatively impact the surface finish and accuracy. For this reason FF-TLOM is most suited for revolved shapes or objects with slow changes in curvature.



**Figure 2.13. Prototype FF-TLOM cutting tool.**

The prototype FF-TLOM system has been used to produce a number of multilayered examples with constant layer thicknesses. Figure 2.14 shows a Styrofoam sphere and a surface with convex and concave curves cut using FF-TLOM.



**Figure 2.14. Examples of FF-TLOM multilayered stacked assemblies.**

A number of papers have been published by De Smit et al from the Delft University of Technology investigating the influential parameters of plastic foam cutting with a hot blade [35, 37, 40]. This work is largely experimental and will be discussed in detail in section 2.3.

## **2.2.6 Variable Lamination Manufacturing (VLM)**

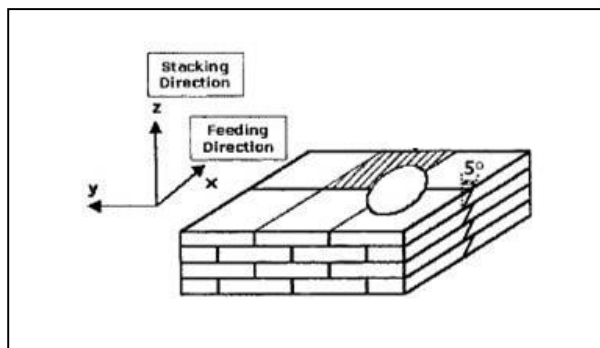
This system is currently being developed by Ahn et al at the Department of Mechanical Engineering, Korean Advanced Institute of Science and Technology (KAIST) in Taejeon, Korea for which a number of papers have been published [5, 42-45]. The published work details a number of investigations into hot-wire plastic foam cutting mechanics based on both experimental and theoretical work. A detailed review of this work is featured in section 2.3.

The VLM system uses a hot-wire to cut out 'thick' EPS cross-sections, which are consequently bonded together to form the finished object. The hotwire cutter is controlled within a four axis machine to cut sections with sloped edges similar to Shapemaker II.

The main advantages of VLM over the Shapemaker II system is the material handling process and VLM can use foam layers of varying thicknesses. The process consists of the following three main steps:

1. ***Material feeding and storing:*** EPS sheets (3.7-10 mm) are stored in a large roll and fed into the cutting area via several sets of rollers. Rollers acts to both apply the bonding agent to the underside of the layer and to control the thickness of the layer by exerting pressure. Controlled suction part holders then hold the dimensionally accurate stock layer in place from above.
2. ***Shape generation:*** The next step involves cutting out the required shapes. As can be seen from figure 2.15, the layers consist of several individual pieces, which are

assembled together like a jigsaw. The joining edges in the feeding direction are cut with opposite  $5^\circ$  angles and are staggered like brickwork in the transverse direction to improve the strength of the finished object.

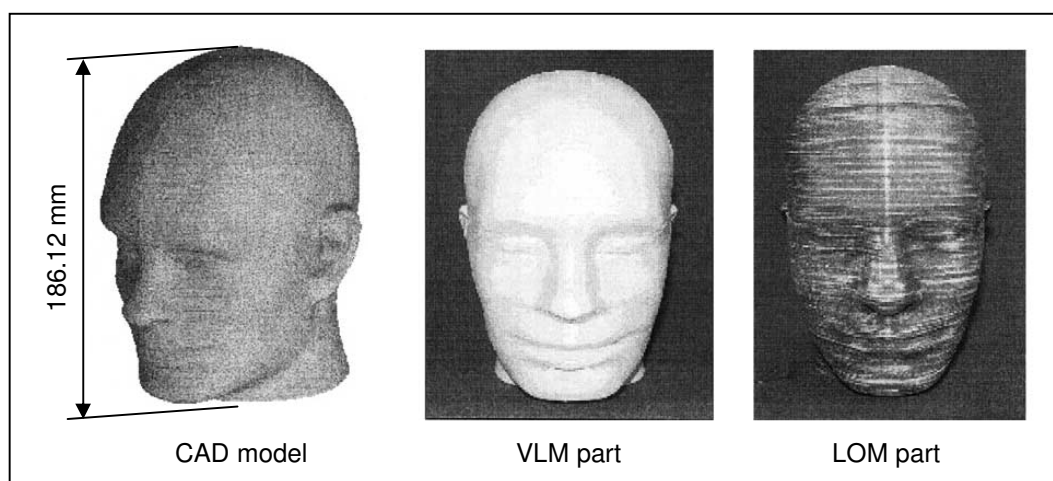


**Figure 2.15 - Multi-piece layer concept [5].**

3. ***Stacking and bonding:*** Once the individual pieces have been cut out, they are stacked on a controllable x-y table. After a layer has been assembled the table is moved below a pressing mechanism which is used to press the bonded layers in order to enhance the bonded strength of the finished model.

The un-cut material is then cut off and removed by gravity and the steps are repeated until the object is fully built.

Figure 2.16 shows an example of a VLM produced part and a LOM reference part used to evaluate the process.



**Figure 2.16. CAD representation of a human head and comparison of the fabricated parts [43].**

The authors conducted a comparison between their system and a conventional LOM RP system using the human head shape. The following results are shown in table 2.1 below.

**Table 2.1. Comparison between VLM and LOM.**

Process	Building Time (min)				Building Cost (USD)	Dimensional Accuracy %	
	Set-up	Building	Decubing	Total		In Plane	Z-dir
LOM	80	2125	120	2325	720	0.7	1.8
VLM	-	35	5	40	8	0.8	1.1

The VLM process has been commercialised by Menix Engineering Co., Ltd under the Rapid Shaper product line. The VLM 300 produces parts using 3.7 mm thick A4 sheets of EPS while the VLM 400 uses 3.7, 5 and 10 mm thick A3 EPS sheets.



**Figure 2.17. The Rapid Shaper range from Menix Engineering Co. Ltd based on technology developed by the Korea Advanced Institute of Science and Technology.**

### 2.2.7 Rapid Heat Ablation (RHA)

Researchers at KAIST (Kim et al) have also published a number of papers describing a novel hot tool used to ablate plastic foams [9, 10, 46]. The process, which the authors call rapid heat ablation (RHA), involves the use of a specially designed hot tool shaped similarly to a ball-end mill to create new surfaces by ablating foam. The process has been used for creating fine detail on VLM parts which is impossible to create with straight hot-wires and as a stand alone manufacturing method. Figure 2.18 provides a schematic of the tool.



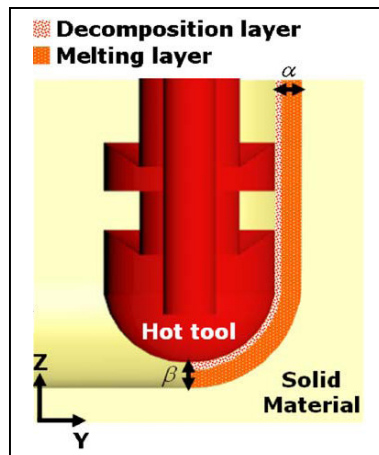


Figure 2.18. Schematic of RHA process [10].

The geometry of the RHA tool allows the tool path to be generated using conventional CAM software for a ball-end mill. Also because the entire length of the tool can be used to ‘machine’ the material it is possible to carry out the finishing cuts without the need for prior material removal. In a test carried out by the authors a large part was shaped in 55 minutes compared to 430 minutes by a commercial milling machine. This demonstrates a significant advantage can be gained by using RHA over conventional machining when shaping plastic foams. Other advantages include:

- Little to no swarf.
- Better surface finish and accuracy ( $R_a$  values  $1/10^{\text{th}}$  that of equivalent machined parts).
- Reduced machine time.

Figure 2.19 shows the RHA tool in action and a part produced by it.

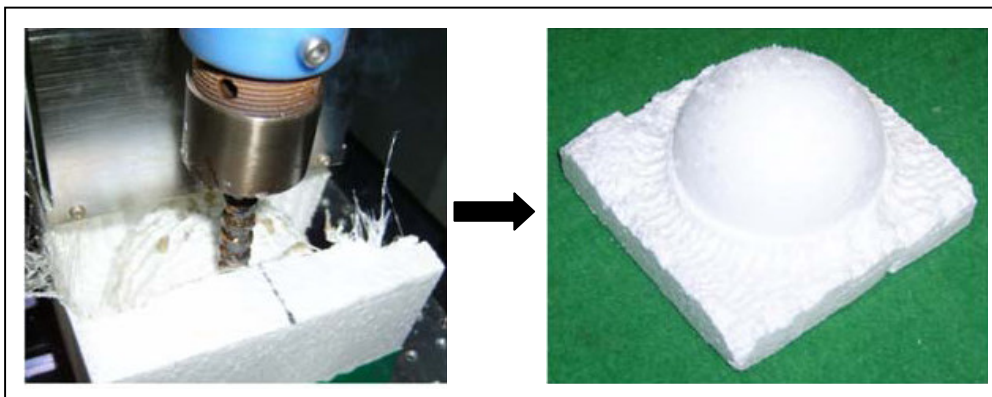


Figure 2.19. RHA tool and part [10].

One aspect of the RHA process that needs to be understood in order to achieve acceptable accuracies is the kerf width/effective power input relationship. The hotter the tool the greater the kerf width will be. It is therefore important to control the heat generated by the tool to minimise the kerf width and provide the greatest accuracy. Once the kerf width/power relationship is understood an appropriate offset can be made for the tool to obtain accurate surface geometry. Experimental and theoretical work exploring the cutting mechanics of the RHA process are discussed in detail in section 2.3.

### 2.2.8 Michelangelo

Michelangelo is an eight axis foam sculpting system developed by Zhu et al from the Tokyo Institute of Technology [11, 47]. It is composed of a six axis Motoman industrial robot and a two axis worktable. It carves simplified EPS models that consist of large flat faces with a hot-wire cutting tool.

A unique mesh simplification algorithm was created to reduce the complexity of the model by reducing the number of facets used to define the surface. Figure 2.20 shows an example of a model simplified using the mesh simplification algorithm. When the mesh is simplified to the desired resolution a tool path generation algorithm is used to create the tool path. A virtual reality simulation of the sculpting is run to ensure all faces can be cut without robot/work piece interference.

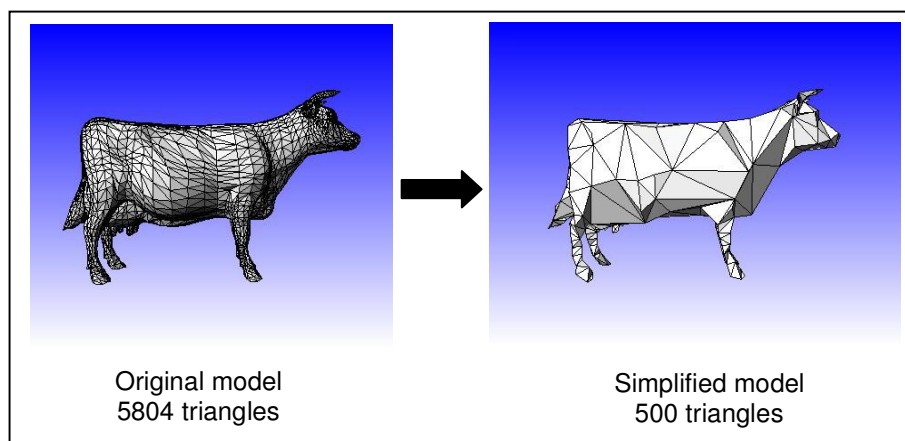
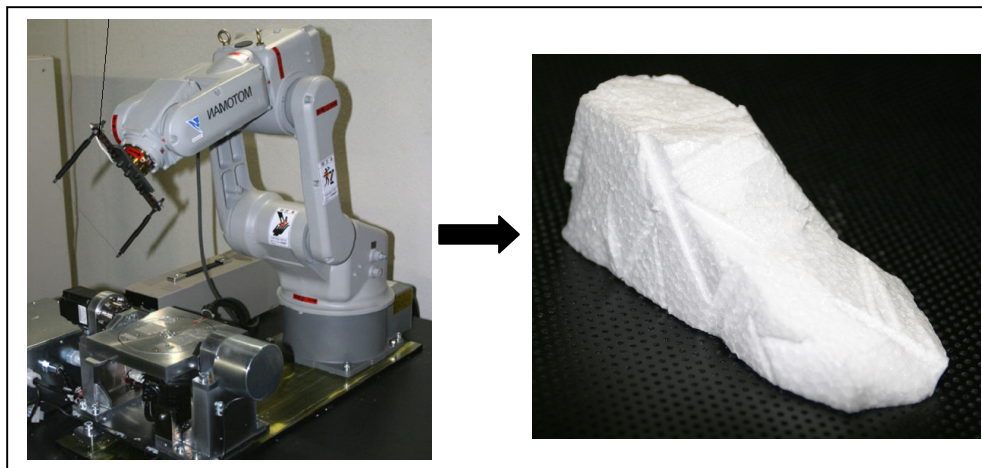


Figure 2.20. Example of mesh simplification [47].

By utilising a work table with an extra two degrees of freedom Michelangelo can sculpt relatively large models with a small machine as reaching behind the part is not an issue. Also, because a hot-wire is used as the cutting tool the cutting process is much faster than conventional machining practices. Figure 2.21 shows the robot and worktable setup and a test part produced by it.



**Figure 2.21. 8 axis setup and a test part produced by it [11].**

In summary Michelangelo is an effective sculpting system for the generation of rough objects. The unique mesh simplification algorithm and eight axis robot system means large objects can be sculpted quickly and to a user specified accuracy. However, a number of disadvantages exist when applying this technology for more accurate models. The system cannot sculpt features with fine detail, double concave surfaces or pockets because of the straight hot-wire cutting tool and the tool path generation scheme.

### **2.2.9 Stratoconcept HW Series**

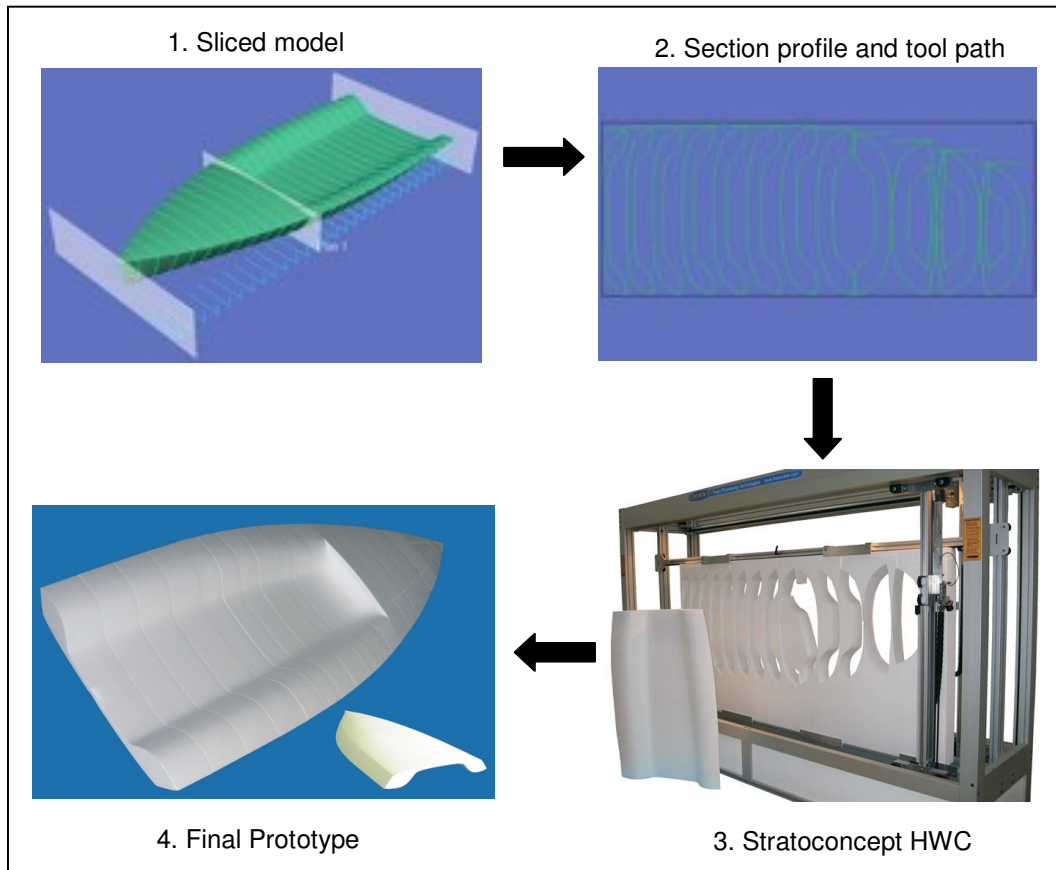
The Stratoconcept HW series was developed through a collaborative effort between Cromax, a French based manufacturer of hot-wire foam cutting systems, and Cirtes, the European centre of Rapid Prototyping and Tooling. This system uses a layer based manufacturing method to manufacture high volume parts at high speed. The foam parts include both interior and exterior details which allows for lightweight full scale prototypes [48].

Cromax adapted a cutting machine for the rapid manufacturing of foam products so that it could implement Cirtes' software for layer based design and construction. Cirtes' adapted its patented software based Stratoconception® rapid prototyping and tooling process to be compatible with Cromax's machine technology. The combined process operates as follows:

1. A CAD model is imported in .STL or DXF 3DFace format and is decomposed into 3D layers.
2. The system then automatically calculates the tool path for the four axis hot-wire cutter and the 'Strata' are cut out. The surface of the layers are linear approximations similar to that of the VLM process.

3. The final prototype is then manually assembled by stacking the layers and aligning the inserts.

Figure 2.22 demonstrates the Stratoconception® process associated with the Stratoconcept HWC and shows an example of an assembled full scale boat hull.



**Figure 2.22. Example of the Stratoconception® process for the Stratoconcept HWC [49].**

The Stratoconcept HWC series RP systems are ideally suited for manufacturing full scale large prototypes from polystyrene foams. The largest machine in the series is capable of producing parts with cross sections up to 5 m wide and 2.5 m tall with an infinite length. The prototypes can be made hollow for lightweight manufacturing. Inserts are used to align and strengthen the prototypes to withstand handling.

Disadvantages of the system include:

- The final prototype must be assembled manually and glued.
- Detail in the z direction must be larger than the standard thickness of the foam stock.

- The surface is a linear approximation of the input model meaning some post processing may be needed.
- Some 'expert' knowledge is required in placing the inserts and choosing the 'strata' orientation to maximise the strength of the prototype.

### 2.2.10 Summary of Foam cutting RP Machines

Nine different foam cutting RP machines were reviewed in order to provide a state-of-the-art overview of recent technological advances in foam cutting. The majority of modern foam cutting RP systems use layered manufacturing to progressively build models from layers cut with hot-wires. Other manufacturing methods include water jet cutting, hot-ribbon cutting and rapid heat ablation. A small number of systems have been commercialised including the VLM Rapid Shaper series by Menix Engineering Co. Ltd, and the Stratoconcept HW series by Croma.

The majority of the systems aim to produce large prototypes and concept models for signage, visual concept verification, architecture, aerospace (in the form of composite cores) and investment casting.

Figure 2.23 summarizes the difference in potential model size and model complexity between the nine reviewed systems. The Stratoconcept HWC system has the largest build volume with its largest machine capable of producing parts with a cross-section of up to 6 m<sup>2</sup> [49]. The VLM series machines are capable of producing the most complex and accurate parts with dimensional errors limited to 1.1% in the build direction [43].

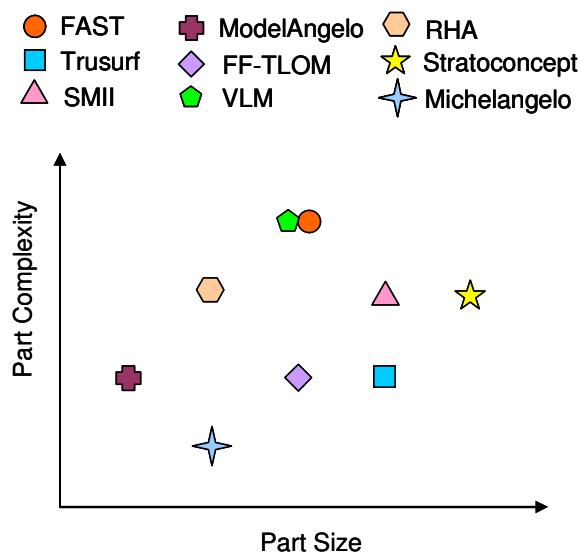


Figure 2.23. Qualitative comparison of complexity and size of parts made with nine foam cutting RP machines.

Table 2.2 summarizes the different build strategies, cutting tools and relative build times of the nine reviewed systems. It should be noted that the qualitative descriptions given are relative to the foam cutting RP machines reviewed and not to RP processes in general and only take into account the information presented in the referenced sources. Also the build speed does not include assembly time for layer based methods.

**Table 2.2. Comparison of foam cutting RP machines.**

System	Property		
	Cutting Tool	Build Strategy	Build Speed
FAST	Hot-ribbon	Direct sculpting	0
Trusurf	Water jet	Layer based	0
SM II	Hot-wire	Layer based	0
ModelAngelo	Hot-wire	Direct sculpting	- -
FF-TLOM	Hot-ribbon	Layer based	DATUM
VLM	Hot-wire	Layer based	+
RHA	Hot tool	Direct sculpting	-
Stratoconcept	Hot-wire	Layer based	0
Michelangelo	Hot-wire	Direct sculpting	++

<p>Key: 0 = Same as Datum          - = Less than Datum          + = Greater than Datum</p>
--

Several ideas were gathered from the review that could prove useful if applied to the FAST system. These include:

- The use of a two axis turntable to tilt and rotate the work piece to allow greater reachability of the robot. This would greatly increase the potential build volume of the system.
- The innovative swarf management technique developed by Hamade et al with ModelAngelo. This would prevent swarf from rejoining the work piece.
- Many of the systems exhibited a high level of automation. In particular the automatic generation of tool paths directly from CAD data was common among the systems. The automation of data creation (tool paths, control programs etc.) is very important if the fast, reliable production of sculpted objects is to be realised.

## 2.3 Empirical Studies of Factors in Foam Cutting

This section provides details of experimental research on foam cutting mechanics that has been carried out by researchers around the world and will focus specifically on the factors important to hot-wire, hot-ribbon and hot-tool foam cutting.

To-date experimental cutting trials have been the primary method of determining optimum cutting parameters for new cutting methods and for understanding foam cutting mechanisms. The factors important in PFC can be divided into three groups – energy parameters, material properties and tool geometry – as shown in figure 2.24.

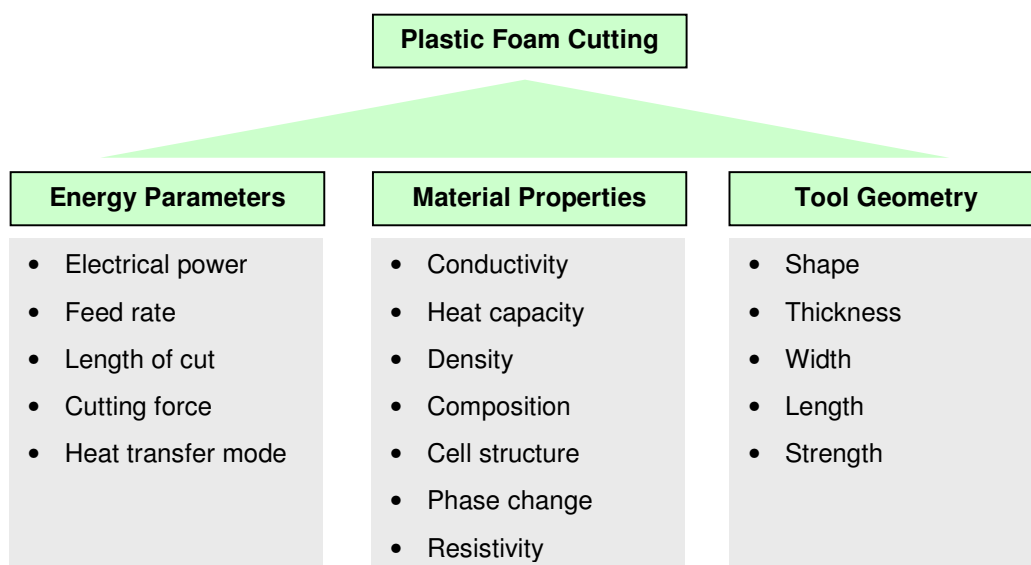


Figure 2.24. Factors important in PFC

### 2.3.1 Energy Parameters

PFC is associated with the transfer of heat, which is generated in the cutting tool, to the plastic foam material being cut. Heat transferred into the foam is restricted to the three modes of heat transfer; conduction, convection and radiation. In extreme cases the energy associated with cold mechanical cutting (shearing and tearing) may be of importance.

It has been shown that the primary factors involved in the heat transfer are the energy absorption properties of the foam material, electrical power and feed rate.

### 2.3.1.1 Electrical Power

Heat is created within the various reported cutting tools [14, 39, 42] by passing an electric current through a resistive metal. This is known as the *Joule heating effect* and is defined by the following equation:

$$Q = I^2 \cdot R \quad (\text{Eq. 2.1})$$

Where the units of Q, I and R are power (Watt), current (Ampere) and resistance (Ohm) respectively. In the case of a hot-wire the heat generated can be defined as a linear volumetric heat flux as shown in Eq. 2.2:

$$Q_L = \frac{Q}{L_e} \quad (\text{Eq. 2.2})$$

Where  $L_e$  represents the length of wire in the cut. In order to consider the influence of the heat input and the cutting speed together, the effective heat input is described as shown in Eq 2.3:

$$Q_{eff} = \frac{Q_L}{V_c} \quad (\text{Eq. 2.3})$$

Where  $V_c$  is the cutting velocity in m/s and  $Q_{eff}$  has the units  $W \cdot s/m^2$  or  $J/m^2$ . Ahn et al from the Korea Advanced Institute of Science and Technology (KAIST) have carried out a number of experiments investigating the relationship between the effective heat input, cutting speed and kerf width [42, 44, 45]. Experimental parameters were chosen such that the maximum cutting velocity coincided with the speed at which the cutting force was sufficient to start bending the wire. The authors concluded that within the experimental range, relationships between the kerf width ( $\eta$ ) and the effective heat input were linear and can be defined by the following equation:

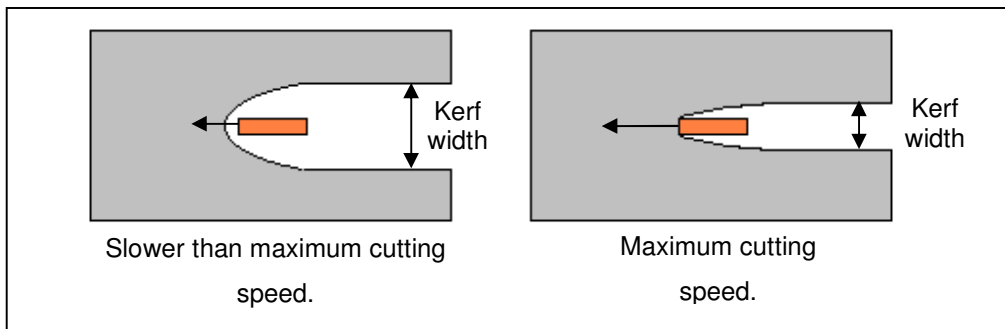
$$\eta = A_1 \cdot Q_{eff} + A_2 \quad (\text{Eq. 2.4})$$

Where  $A_1$  and  $A_2$  are experimentally determined constants.

Broek et al from the Delft University of Technology carried out similar experiments using a hot-ribbon or blade as the cutting tool [35, 39]. The high aspect ratio of the ribbon provides strength in the cutting direction which resists bending forces and allows the ribbon to take non-linear profiles. One disadvantage of using hot-ribbon cutting tools is the large surface area normal to the cutting direction from which heat is radiated. This surplus heat increases the kerf width of the cut and therefore decreases the accuracy of the manufactured surface. The authors describe a non-linear



relationship between heat input, cutting speed and kerf width in which increased heat input or decreased cutting speed increases the kerf width as shown in figure 2.25.



**Figure 2.25. Kerf width under different cutting speed conditions.**

Broek et al carried out 48 cuts each time varying one parameter to isolate its effect on the surface finish and accuracy. For each cut the energy per centimetre ( $Q_A$ ) of the blade was calculated in W/cm.

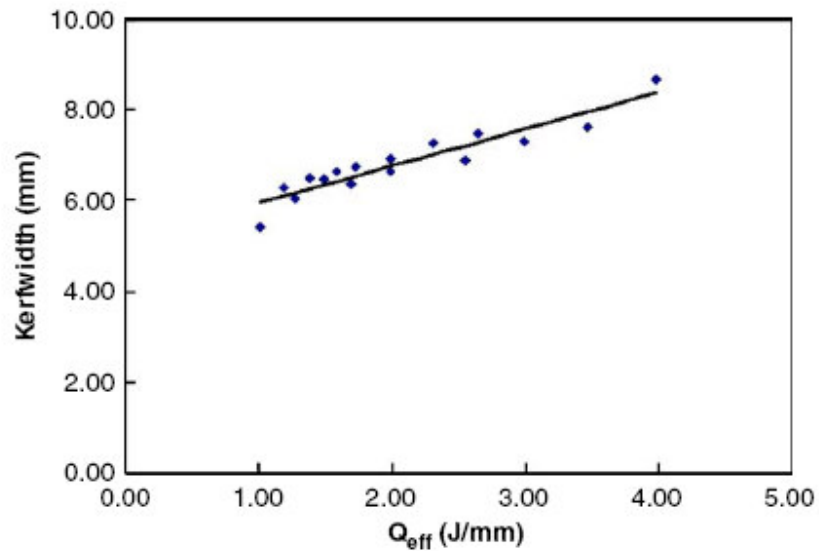
$$Q_A = \frac{Q}{A_c} \quad (\text{Eq. 2.5})$$

Dividing this value by the cutting velocity in cm/s ( $V_c$ ) gives a value for the effective heat input in W·s/cm<sup>2</sup> or J/cm<sup>2</sup>.

$$Q_{eff} = \frac{Q_A}{V_c} \quad (\text{Eq. 2.6})$$

This value represents the dissipated thermal energy per square centimetre of surface that was cut. In this particular experiment it was found that an effective heat input between 3 and 7 J/cm<sup>2</sup> produced the best surface finish.

Similar experiments were carried out by Kim et al [10] which found a linear relationship between kerf width and effective heat input for rapid heat ablation within a certain experimental range, as shown in figure 2.26. The  $Q_{eff}$  in this case has units (J/mm) because the tool cuts a line instead of an area. The authors then suggested the information could be used to describe the size of a virtual tool used to plan future cutting tool paths and minimise cutting inaccuracies.



**Figure 2.26. Relationship between kerf width and effective heat input for RHA [10].**

The concept of the effective heat input is developed significantly further in later chapters. For reasons that will become clear in chapter 3, the effective heat input as derived in equation 2.4 and 2.5 shall be called the *area specific effective heat input* to reflect the fact the units are  $J/m^2$ .

### 2.3.1.2 Cutting Force

As mentioned in previous sections it is the cutting force that directly affects the surface finish of the cut. High effective heat inputs result in zero force cuts, which lead to large kerf widths, while low effective heat inputs result in high force cuts which can break or bend the cutting tool. Optimum surface finishes (surfaces with low roughness) are achieved by using an effective heat input such that the cutting force is a low non-zero value. This is the condition when the cutting tool is just hot enough to melt the adjacent foam without increasing the kerf width.

Broek et al [39] defined a 'cutting speed window' for a given heat input, which limits the cutting speed within a range that simultaneously minimises the cutting force and the kerf width, as shown in figure 2.27. In this figure the maximum kerf width is arbitrarily placed however in practice it would be chosen to suit the tolerances of the application.

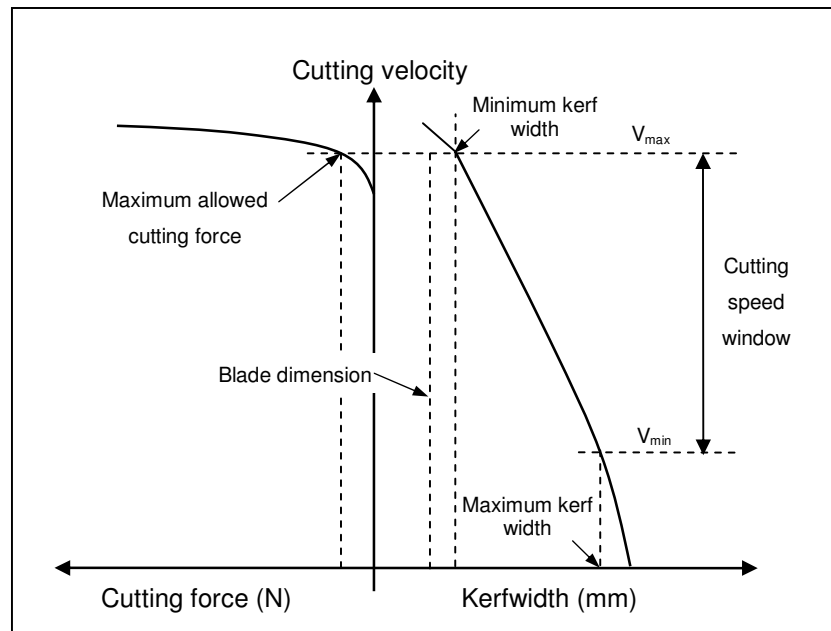


Figure 2.27. Definition of cutting speed window defined by Broek et al [39].

The mechanical power imparted on the work piece by PFC tools can be calculated by multiplying the cutting force by the cutting speed. This value is usually very small compared to the thermal energy (< 1%) due to the fact that low cutting forces are the norm.

## 2.3.2 Material Properties

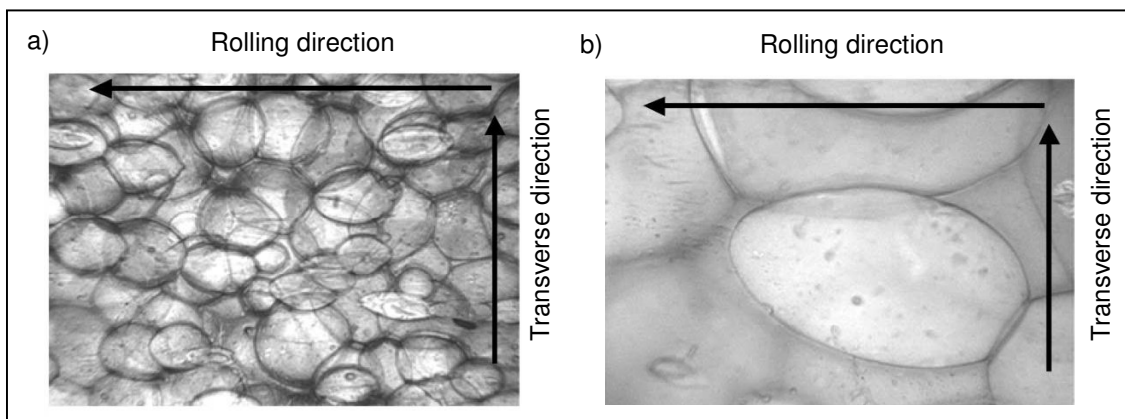
### 2.3.2.1 Plastic Foam

Plastic foams come in a plethora of different chemical compositions, cell structures and densities. The manufacturing methods often dictate the cell structure and ultimately how the PF will behave during cutting. Central to the study of plastic foam cutting mechanics is the way in which plastic foams degrade with increasing temperature. For any FEA to be accurate it is important to know how the thermal properties change with temperature and also what temperatures cause the various physical transitions present in plastic foam cutting.

Most of the groups researching plastic foam cutting adopt material property values from literature, often using inappropriate values and greatly over simplifying the material characteristics. For example Ahn et al [42, 44, 45] assume a melting temperature based on the melting point of solid crystalline PS instead of foamed amorphous PS. Also they extrapolate the temperature dependant properties, such as specific heat, to cover temperature ranges far beyond the referenced data. This is not ideal but understandable as the correct data is hard to find or is not published in readily accessible places. Some effort has been made by Ahn et al to experimentally

determine the anisotropic properties of rolled EPS and the decomposition temperature of molten PS foam.

The VLM process requires EPS sheets to be rolled in order to ensure accurate sheet thickness. In this process the foam becomes anisotropic as figure 2.28 shows. Cutting trials were carried out to determine the relationship between maximum cutting speed and heat input in the rolled and transverse directions in order to determine the effects of anisotropy of a rolled EPS sheet. The results of the experiment revealed the maximum cutting speed of the hot-wire in the transverse direction was only 64% that of the rolling direction. This is because the linear density in the transverse direction is higher than that of the rolled direction.



**Figure 2.28. Microstructure of expandable polystyrene foam sheet. (a) 100x enlarged. (b) 400x enlarged [45].**

This experiment highlights the need to understand the material properties of the foam in order to make relevant predictions based on experiments.

PFC involves the melting and subsequent decomposition of the melted foam, hence knowing the thermal decomposition characteristics of the plastic foam is important. Thermal Gravimetric Analysis (TGA) was carried out by Ahn et al [45] to determine the relationship between percentage weight loss and temperature. The samples were  $6.25 \text{ kg/m}^3$  EPS. The results of this experiment showed that the weight loss expressed as a percentage begins to rapidly increase at  $390^\circ\text{C}$  as shown in figure 2.29. These results offer an insight into the way EPS decomposes from its molten state and provides crucial data that can be used in a numerical model.

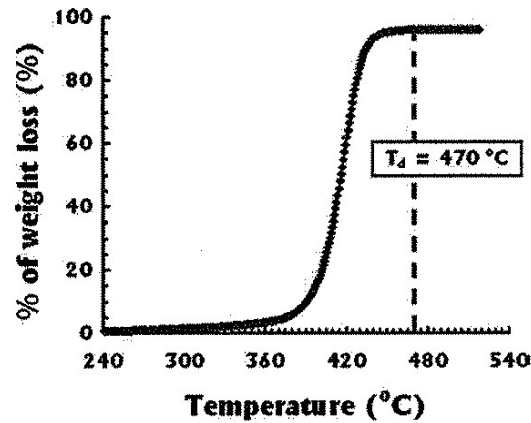


Figure 2.29. Relationship between weight loss and temperature [45].

### 2.3.2.2 Cutting Tools

The material of the cutting tool influences the cutting process in several ways. The material determines the electrical behaviour of the cutting tool, it influences the strength and the shape stability of the cutting tool and it directly influences the radiative heat transfer which relies on the emissivity of the surface. An ideal cutting tool material will have a high specific resistance, high temperature strength and good creep properties.

Ti alloys have high resistivity, which allows the material to quickly respond to changes in electrical power. They also have good strength at high temperature. Due to the high cost of titanium it is not widely used. The most common cutting tool materials are Nickel alloys due to the relative low cost, high specific resistance and high temperature strength. Alloy steels can also be used in low end applications where the wires may be shorter and the cutting temperatures not as high.

## 2.3.3 Tool Geometry

PFC machines that use hot-ribbons or other non-wire cutting tools need to consider the effect tool geometry will have on the cutting process. The tool geometry will influence the tool in a number of ways including, shape stability, size of the cut, shape of the cut, radiation pattern and tool paths.

### 2.3.3.1 Tool Cross-section

The cross sectional shape together with the tool material determines the stiffness and bending behaviour of the tool. This is important for resisting normal cutting forces but also buckling and torsion. It can be intuitively reasoned that different cross-sections will show different cutting behaviour and produce different surface qualities. The tool path and tool tip control may also be influenced by the tool cross-section, for example a circular cross section tool can cut in all

directions while a rectangular tool is best suited cutting along the longitudinal axis of the cross-section [39].

### 2.3.3.2 Radiation Pattern

The heat radiation pattern of the tool is determined by the shape of the cutting tool, the material it is made of and its colour. For high tool temperatures it can be expected that this pattern will impact on the cutting behaviour of the tool. It may be possible to design a tool such that the cutting edge dissipates the most energy thereby optimising the cutting behaviour [39].

Kim et al developed a ball-end type hot tool with tangential grooves to attempt to optimise the radiation pattern [46]. The tool is a cylinder with a semi spherical end and tangential grooves along the shaft, as shown in figure 2.30. The tangential grooves have been designed to minimise the heat affected zone of the work piece and hence improve the accuracy. The outer surfaces are cooler and melt the foam while the inner surfaces are hotter and decompose the melted foam. In this way the melted foam region is minimised while there is sufficient heat to decompose and remove the melted material.

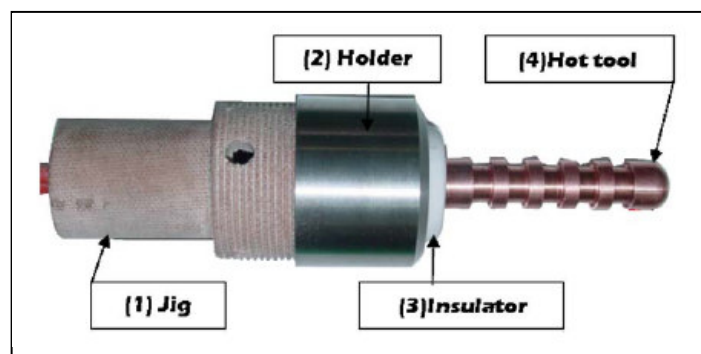


Figure 2.30. RHA hot-tool.

### 2.3.4 Summary of Empirical Studies

The majority of the empirical data published on plastic foam cutting (PFC) was carried out by two groups; Ahn et al from the Department of Mechanical engineering, KAIST, Korea and Broek et al from the Faculty of Design, Engineering and Production, Delft University of Technology, Netherlands. Ahn et al investigated hot-wire cutting of EPS in relation to their VLM process, while Broek et al investigated hot-ribbon cutting of XPS in relation to the FF-TLOM process. Their combined efforts covered many aspects of PFC and helped to bring the subject of hot-tool foam cutting under scientific scrutiny.

After examination of the aforementioned literature a number of areas have been identified where more research was required. These research areas formed the bases for the experiments described in chapter 3 and are listed below:

- Hot-tool cutting of different foam materials (namely 30 kg/m<sup>3</sup> XPS and 15, 26, 30 kg/m<sup>3</sup> EPS). This is to determine what effects different cellular structures and densities have on the PFC process.
- The effect of cutting tool geometry and size (namely hot-ribbon and hot-wires of different sizes). This is to determine if there are differences in the way different size and different shape tools interact with the foam and may also reveal clues to optimising tool shape design.
- Both Ahn et al and Broek et al failed to accurately measure the cutting force of their respective cutting tools. The cutting force is an important parameter as it limits the possible range of cutting parameters such as feed rate and power and directly influences the surface texture.
- A method of classifying surface textures based on cutting mechanisms is needed.
- Both Ahn et al and Broek et al failed to accurately measure the temperature of the hot-tools whilst cutting. This is a crucial parameter to quantify as the tool temperature is directly related to the kerf width. The longitudinal and transverse temperature profiles along the tool need to be studied in order to understand the effect temperature gradients within the tools have on the surface form.
- The transient nature of hot-tool cutting needs to be investigated. Ahn et al assumed that the wire is always in equilibrium (which is only possible with temperature control) and Broek et al state that equilibrium conditions were never obtained during their cutting trials (i.e. the temperature of the cutting tool was still changing at the end of the cuts). It is important that the cutting conditions that prevail whilst the cutting tools are in thermal equilibrium are identified.
- A method of mathematically relating all the cutting parameters should be formulated which, once the empirical data has been found, allow the cutting conditions for a wide variety of cutting parameters to be predicted.

## 2.4 Numerical Simulations

As mentioned earlier, the results from analytical models for PFC are rarely reliable due to the many assumptions necessary to simplify the model and because of the nonlinear material properties and heat transfer modes. Therefore, numerical simulations were found to be the most common method of investigating the influence of cutting parameters on temperature distribution around the cutting elements and to determine the optimal cutting conditions.

Numerical simulations of PFC were first carried out by Ahn et al for hot-wire cutting using the finite element method (FEM) [42, 44]. They first simulated the case where the wire was set perpendicular to a foam sheet to investigate the temperature distribution around the wire and later varied the cutting angle. Finite element analysis (FEA) software called SYSWELD+ was used to predict the temperature distribution in the EPS foam sheet. A number of assumptions were made in the formulation of the FE model: the hot-wire was modelled as a line heat source, the work piece was fixed and the hot-wire moved at constant speed, thermal conductivity and specific heat were assumed to be temperature dependant. The temperature of the wire was set constant at 973 K (700 °C) and the effects of radiation were ignored. Figure 2.31 shows the model geometry and boundary conditions.

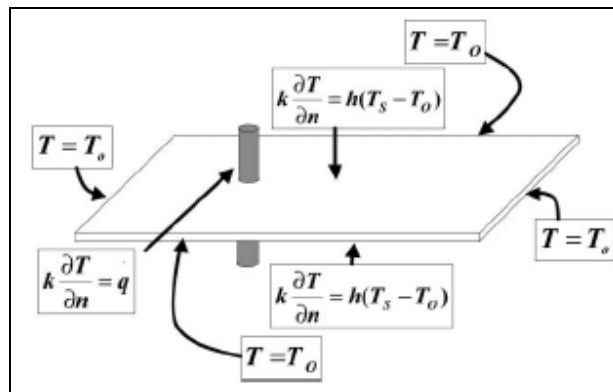


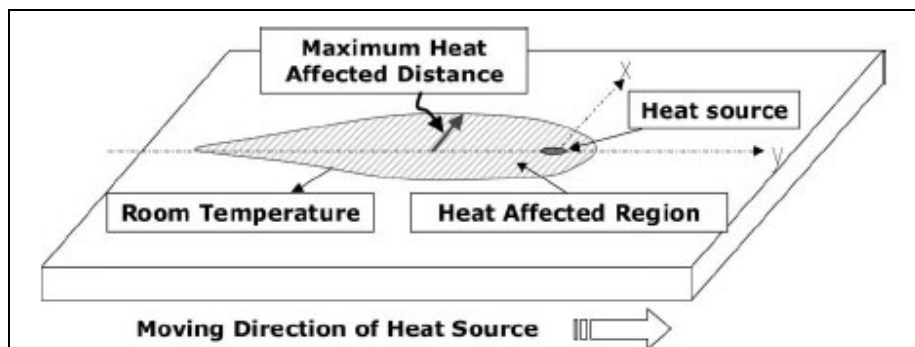
Figure 2.31. Boundary conditions of local analysis. Reproduced from [42].

The hotwire was simulated by a volumetric heat flux. In the case of a circular beam the radial heat flux  $q(r)$  of the work piece was expressed by the following equation:

$$q(r) = \frac{4Q_L}{\pi d^2} \quad (\text{Eq. 2.7})$$



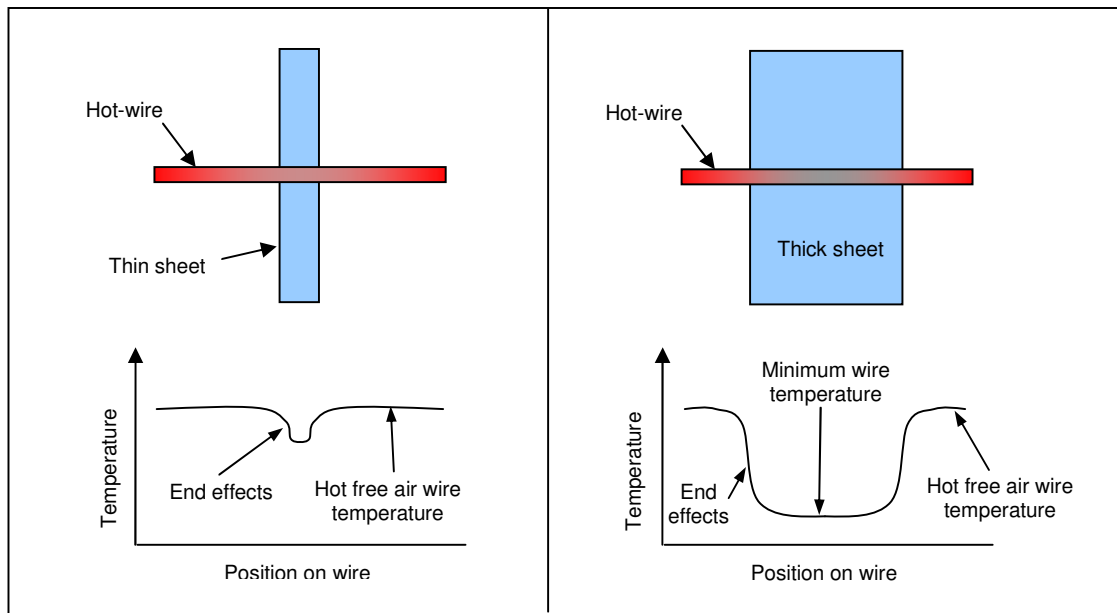
The heat input used for the analysis was  $5.71 \text{ W/mm}^3$ . The analysis was purely thermal and so isothermal contours around the wire were used to determine the maximum heat affected distance as shown in figure 2.32.



**Figure 2.32. Schematic of thermal field showing heat affected region and maximum heat affected distance. Reproduced from [42].**

The heat affected region shown in figure 2.32 is defined in this analysis as the area contained by an isothermal line at the melting temperature of the foam. The authors used a commonly quoted melting temperature of  $240^\circ\text{C}$  for crystalline solid PS. It should be noted however, that EPS is amorphous and therefore does not have a defined melting point: in fact the foam begins to soften at the glass transition temperature between  $80\text{-}120^\circ\text{C}$  and the cells collapse at approximately  $160^\circ\text{C}$  [50]. For these reasons the results gathered while using an isothermal line at  $240^\circ\text{C}$  could be seen as somewhat arbitrary and are more useful as showing trends than the actual melted widths.

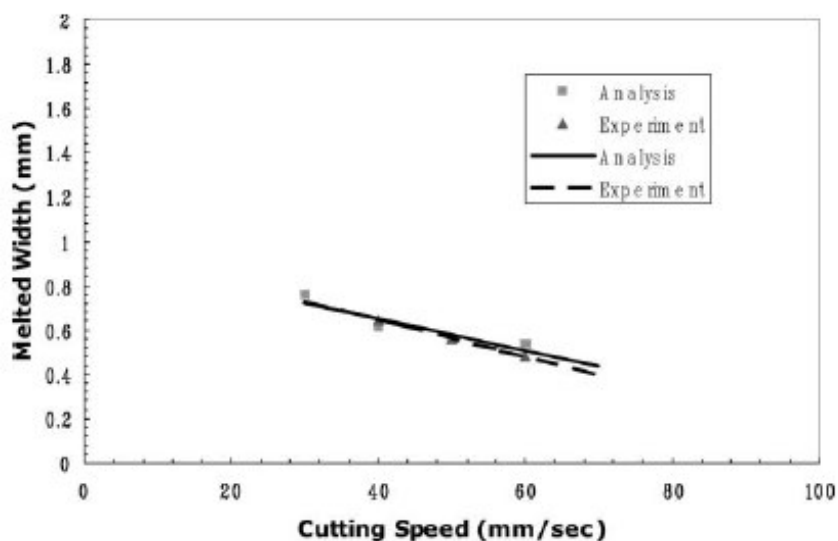
The authors also assume the free air wire temperature of  $700^\circ\text{C}$  stays constant throughout the cut. This assumption is somewhat valid for very thin foam sheets (where wire edge effects play an important role); however it will not hold for thicker sheets as the wire engaged in the cut drops to much lower temperatures. Figure 2.33 shows the temperature distribution across a hot-wire cutting a thin sheet and a thick sheet. The thin sheet causes a small decrease in temperature, however, the hot-wire on either side of the cut keeps the wire in the centre from reaching its minimum temperature. When a hot-wire cuts a sufficiently thick sheet of foam the wire in the centre of the cut is far from the hot wire on either side, therefore the minimum wire temperature can be reached.



**Figure 2.33. Wire temperature for thick and thin cuts.**

It should be noted that once a foam sheet is sufficiently thick so that the end effects can be ignored, further thickening of the sheet will not decrease the minimum wire temperature. The minimum wire temperature will inevitably be different for each feed rate and power combination (unless the area specific effective heat input is the same).

The model adopted by Ahn et al assumes that heat is transferred solely by conduction, as the hot-wire contacts the foam at all points around the circumference of the wire. In reality this is inaccurate because only the leading edge of the wire directly contacts the foam.



**Figure 2.34. Comparison of experimental and analytical results with respect to melted width.**

**Reproduced from [42].**

Despite these shortcomings the analytical and empirical results showed good agreement with respect to the melted width of the cut as figure 2.34 shows. One explanation for the concurring results is the conductivity of EPS is similar to the conductivity of air, approximately 0.027 W/mK and 0.0257 W/mK respectively. Therefore while the FE model assumes the hot-wire is touching the foam at all points on its circumference the inaccuracy is negligible.

Simulations where the cutting angle was varied showed that the effect this has on melted width is small compared to other factors such as power and feed rate [44].

Kim et al, also from KAIST numerically simulated the RHA process for a hot tool to determine the temperature distribution in EPS foam and the shape of the ablated surface. This was done by assuming radiation was the only heat transfer mode and by defining a view factor for simplified tool geometry. This view factor represents the amount of radiation that leaves the tool surface and is intercepted by the workpiece. Figure 2.35 shows the model geometry and boundary conditions.

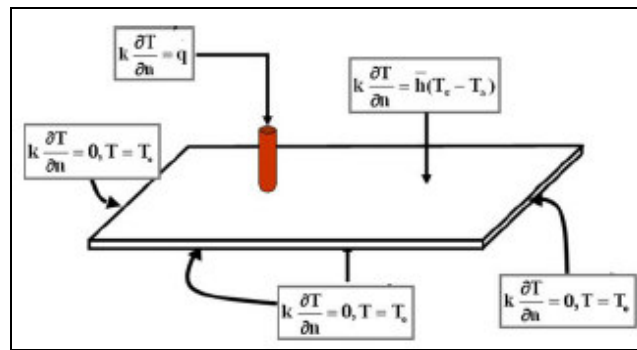
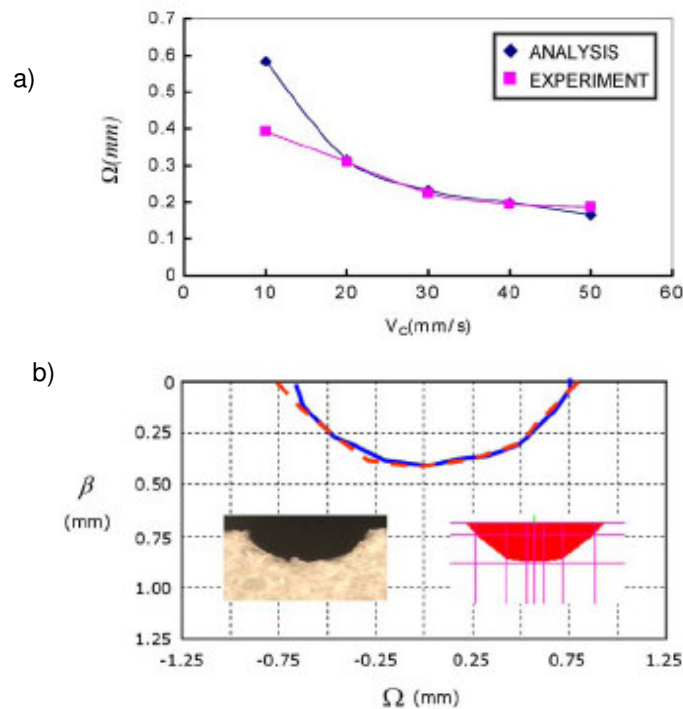


Figure 2.35. Geometry and boundary conditions of local analysis. Reproduced from [9].

Again the analysis was purely thermal and the melted area is defined as the area within the isothermal line at the melting point of the material,  $T_m$ , because material in this zone is assumed to melt or decompose. The results showed that the dominant parameters were power, feed rate and the distance between the tool and the work piece. The kerf width was also found to have a linear relationship with the effective heat input per unit gap. The analytical results agreed well with the experimental results and the numerical model is useful for predicting the shape of the groove cross-section as the temperature distribution can be successfully calculated. Figure 2.36a shows the relationship between kerf width and feed rate. As can be seen the simulated and experimental results are similar for feed rates 20 mm/s and higher. Figure 2.36b shows the shape of the groove, again the calculated results are in excellent agreement with the experimental data.



**Figure 2.36. Comparison between analysis and experiment. a) Kerfwidth vs. heat input b) Cross-sectional shape of ablated groove. Reproduced from [9].**

### 2.4.1 Summary of Numerical Simulations

To the author's knowledge Ahn and Kim et al were the first and only group to attempt the numerical simulation of hot-tool plastic foam cutting prior to the work contained in this thesis. They simulated three main scenarios, i.e. straight hot-wire cutting, hot-wire cutting with the wire angled in the cutting plane and rapid heat ablation (RHA). All simulations were two dimensional and purely thermal i.e. no modelling of mechanical forces.

After examination of the aforementioned literature a number of areas have been identified where more research is required. The research areas listed below form the bases for the finite element analysis described in chapters 4 and 5:

- The finite element (FE) model should allow a wide variety of hot-tools to be simulated including wires of different sizes and ribbons.
- The FE model should be accurate for both main types of polystyrene foam, i.e. EPS and XPS.
- The FE should use experimentally verified thermal material property data with minimal assumptions.

- The FE model should be able to simulate cuts of increased complexity, such as curved cuts.

## 2.5 Summary of Literature Review

This chapter has provided background information on plastic foam cutting and has given an overview of foam cutting RP machines. Some key points and concluding remarks can be made about foam cutting research to date:

- A number of foam cutting RP machines are currently being developed in institutions around the world of which two have been commercialised [24, 51]. The main aim of said machines is to construct large ( $>1 \text{ m}^3$ ) prototypes quickly and inexpensively. With most foam cutting RP machines the ability to produce intricate detail is sacrificed to produce large models. The prototypes are suitable for applications in a wide range of industries including aerospace, architecture, sport, health care, advertising and product development.
- The two main methods of fabrication are; layered manufacturing in which individual layers are cut and assembled, and direct sculpting which uses an entirely subtractive method of producing models. Generally, layered methods have the advantage of producing large parts with internal features while direct sculpting is potentially faster and can create parts with increased surface complexity.
- Two main cutting elements are used in the reviewed systems, these are hot-wires and hot-ribbons. Hot-wires are ideally suited for cutting 2D profiles or ruled surfaces while hot-ribbons can be used to cut double concave surfaces and difficult geometries such as pockets. Another cutting tool reviewed is the ball-end shaped hot tool for rapid heat ablation. This tool completely ablates the foam and can be used in much the same way as a ball-end milling tool; in fact tool paths generated for ball-end mills can be used directly for RHA.
- Effort has been made to experimentally determine the factors important to foam cutting. The main factors can be categorised into three groups: energy parameters, material properties and tool geometry. Empirical equations relating effective heat input and kerf width for hot-wires have been documented. Material properties have been shown to affect the cutting characteristics, also the relationship between cutting force and cutting speed was investigated for hot-ribbons.

- The parameters important in PFC are: electrical power, feed rate, cutting force, material composition, cell structure and tool cross-section. However, the experimental work is time consuming and the reported quantitative results cannot be generally applied.
- PFC is too complex to be fully understood through analytical modelling. A numerical approach has been employed in order to investigate the influence of the cutting parameters on the temperature distribution around the cutting elements and to determine the optimal cutting conditions [42]. Satisfactory results were achieved through computational simulations providing kerf widths based on isothermal temperature contours. However, the simulations used questionable material properties data and boundary conditions. Also no information on the numerical simulation for the generation of complex surfaces is available.

## **3 Empirical Studies of Factors in Foam Cutting**

---

### **3.1 Introduction**

This chapter presents experimental research undertaken by the author, that investigates the important factors in hot-wire and hot-ribbon plastic foam cutting. It explores the relationships between foam material, electrical power, feed rate, cutting force, wire temperature, kerf width and surface finish. Ideal cutting conditions are identified and a method of using force feed-back control to maintain constant wire temperature is presented. Important material properties are also determined experimentally for use in the finite element analysis of later chapters.

The following section describes the objectives of the foam cutting trials. A detailed description of the materials used in the trials is given, as well as the experimental apparatus and the experimental method. The experimental results are split into two sections containing information on the hot-wire and hot-ribbon cutting trials respectively.

### **3.2 Objectives**

Firstly, experimental research to-date on PFC has been sparse with experimental data often presented for a narrow range of parameters or in a qualitative fashion [35, 42]. Most of the



published results focus on the relationship between feed rate, cutting force and kerf width, while factors influencing wire temperature and surface finish have been largely overlooked [35, 39, 42, 52]. The cutting trials carried out for this thesis have provided a large pool of information from which important trends were observed and the underlying thermomechanical interactions have been identified.

Secondly, the wide range of cutting conditions used in the tests inevitably revealed the optimum cutting settings for the given experimental apparatus and materials. This has enabled the author to propose a general predictive cutting strategy for EPS and XPS foams.

Thirdly, the cutting trials provided a practical and methodical base for testing temperature control strategies. The findings of such tests were compared with cuts for which the temperature was not controlled to provide an unbiased assessment.

Lastly, the experimental data collected from the trials are used to test the accuracy of the finite element analysis of later chapters.

Quantitative measurements of the surface roughness and form, of cuts made with hot-tools, will not be addressed in this thesis. This body of work is currently under investigation by a colleague within the FAST group.

### **3.3 Materials**

This section describes the materials used in the cutting trials and the experiments used to determine material properties for the finite element computer simulations. It begins with a description of common polystyrene foams (EPS and XPS) as they were consistently used in the trials, followed by a description of the cutting element materials.

#### **3.3.1 Polystyrene Foams**

The main type of plastic foam used in the cutting trials is polystyrene (PS) foam. PS foams are currently the most common material used in the foam cutting industry. PS foams are inexpensive and are widely available, the low density and rigid cell structure of PS foams mean they are well-suited for a wide range of applications and the physical properties make it ideal for thermal plastic foam cutting.

Two different density EPS foam were used for the cutting trials: S-grade and VH-grade from Bondor. Table 3.1 gives the technical information for the foam.

Table 3.1. Technical Information of Expanded Polystyrene (Bondor: S-grade &amp; VH-grade)

Material	Bondor S-grade	Bondor VH-grade
Structure	Amorphous, closed-cell foam	
Density	15 kg/m <sup>3</sup>	30 kg/m <sup>3</sup>
Max. Temperature for use	50 to 70 °C, on a short-term basis 60 to 80 °C	
Melting point	200 - 250 °C	
Unstable against:	Esters, ketones, Ether, gasoline, aromatic hydrocarbons, chlorinated hydrocarbons	
Resistant against:	Acids and bases, methyl alcohol, ethanol, i-propanol, silicone oils	
Processing temperature:	110 to 120 °C	
Form of delivery:	Granular material, prefoamed granular material	
Uses:	Thermal insulation, step sound reduction, packaging, casting	
Compressive performance	25 kPa	50 kPa
Thermal conductivity (k-value) at reference temperature 15 °C	k=0.038 W/m.K.	k=0.034W/m.K.
Compression stress at 10 % deformation	85 kPa	165 kPa
Cross breaking strength	165 kPa	320 kPa
Glass transition temperature	83 – 120 °C	

### 3.3.1.1 Extruded Polystyrene (XPS)

The XPS used in the cutting trials is 30 kg/m<sup>3</sup> Styrofoam from Dow Chemical Company. Table 3.2 gives the technical information for the foam.

**Table 3.2. Technical Information of Extruded Polystyrene (Styrofoam, DOW).**

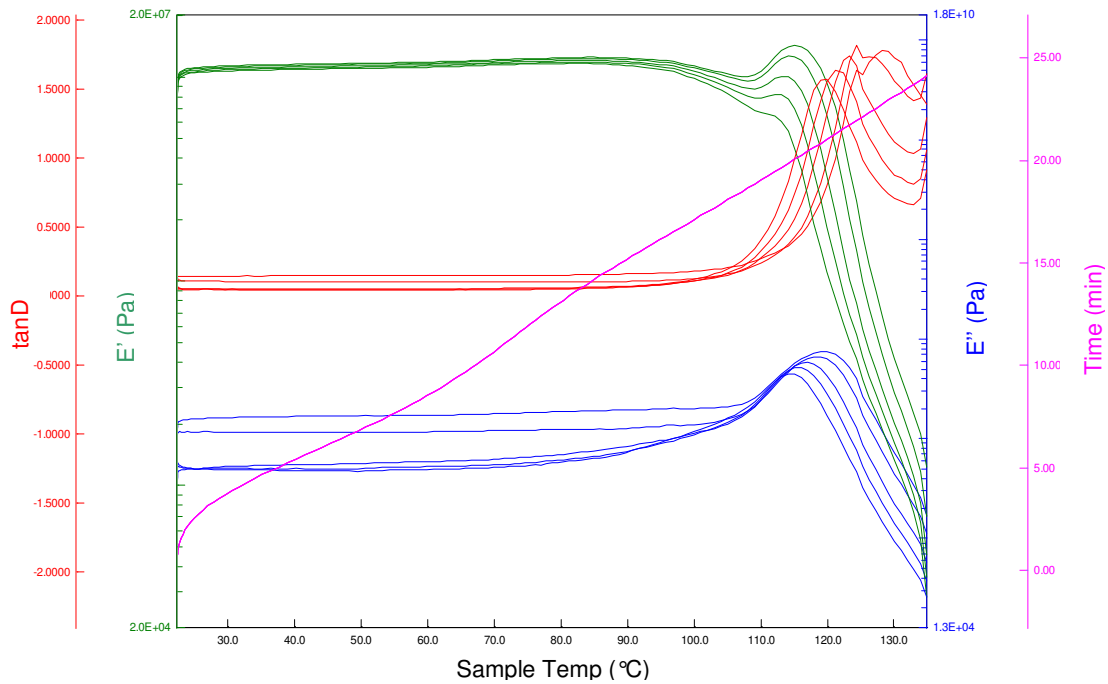
<b>Material</b>	<b>Styrofoam</b>
<b>Structure</b>	Closed cell
<b>Density</b>	30 kg/m <sup>3</sup>
<b>Tensile strength</b>	500 kN/m <sup>2</sup>
<b>Melting temperature</b>	200 – 250 °C
<b>Glass Transition Temp.</b>	80 - 120 °C
<b>Unstable against:</b>	Esters, ketones, Ether, gasoline, aromatic hydrocarbons, chlorinated hydrocarbons
<b>Resistant against:</b>	Acids and bases, methyl alcohol, ethanol, i-propanol, silicone oils
<b>Uses:</b>	Insulation, helmet, protection
<b>Compressive performance</b>	210 kN/m <sup>2</sup>
<b>Thermal conductivity</b>	0.027 W/mK
<b>Compression stress at 10 % deformation</b>	300 kN/m <sup>2</sup>

### 3.3.1.2 Thermal Material Properties of Polystyrene Foams

The great variety of PS foams available means there is also a wide variety of material properties. Some characteristics, such as the glass transition temperature and the thermal decomposition profile are related to the chemical composition, which is essentially the same for all PS foams. The multitude of different densities and cellular structures are what differentiates the thermal material properties of different PS foams at ambient temperatures. At high enough temperatures all PS foams ‘melt’ and return to their un-foamed high density state. At this point the thermal characteristics of all PS ‘foams’ are similar to that of molten PS plastic.

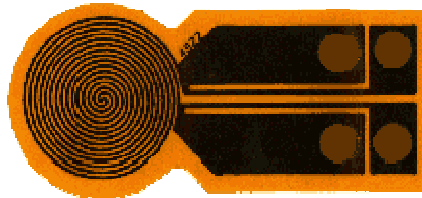
To determine the glass transition temperature, conductivity and specific heat of the foams used in the cutting trials, a set of experiments were carried out using Dynamic Mechanical Analysis (DMA) and Hot Disk Analysis. DMA is a technique that measures the modulus and energy dissipation of materials as they are periodically stressed. Various material properties can be measured by subjecting a sample to frequency and temperature effects over time [53]. DMA was carried out on both EPS and XPS foams to determine the glass transition temperature and activation energy. The samples were slowly heated from 20 to 140 °C at frequencies varying from 1 to 50 Hz at a rate of 5 °C/min. Using this method the glass transition temperature was found to

be between 103 and 118 °C for EPS and XPS. Figure 3.1 shows the results for an XPS sample. The blue lines show how the loss modulus ( $E''$ ) changes with temperature. The peak loss modulus is a function of frequency and temperature and occurs at the glass transition temperature. The glass transition temperature values were found to match common industry quoted values. The green lines shows the modulus ( $E'$ ) while the red lines show the ratio of  $E'/E''$ .



**Figure 3.1. DMA storage and loss modulus for XPS foam.**

Hot Disk Analysis is a technique for measuring the thermal properties of materials using a hot disk analyser (HDA). Measurements are made by placing a disk sensor (figure 3.2) between two pieces of the sample material. The disk is then heated by a constant electrical current for a short period of time. The heat generated in the disk then heats up the surrounding sample material and the disk itself. The average transient temperature increase is simultaneously recorded by monitoring the change in electrical resistance.



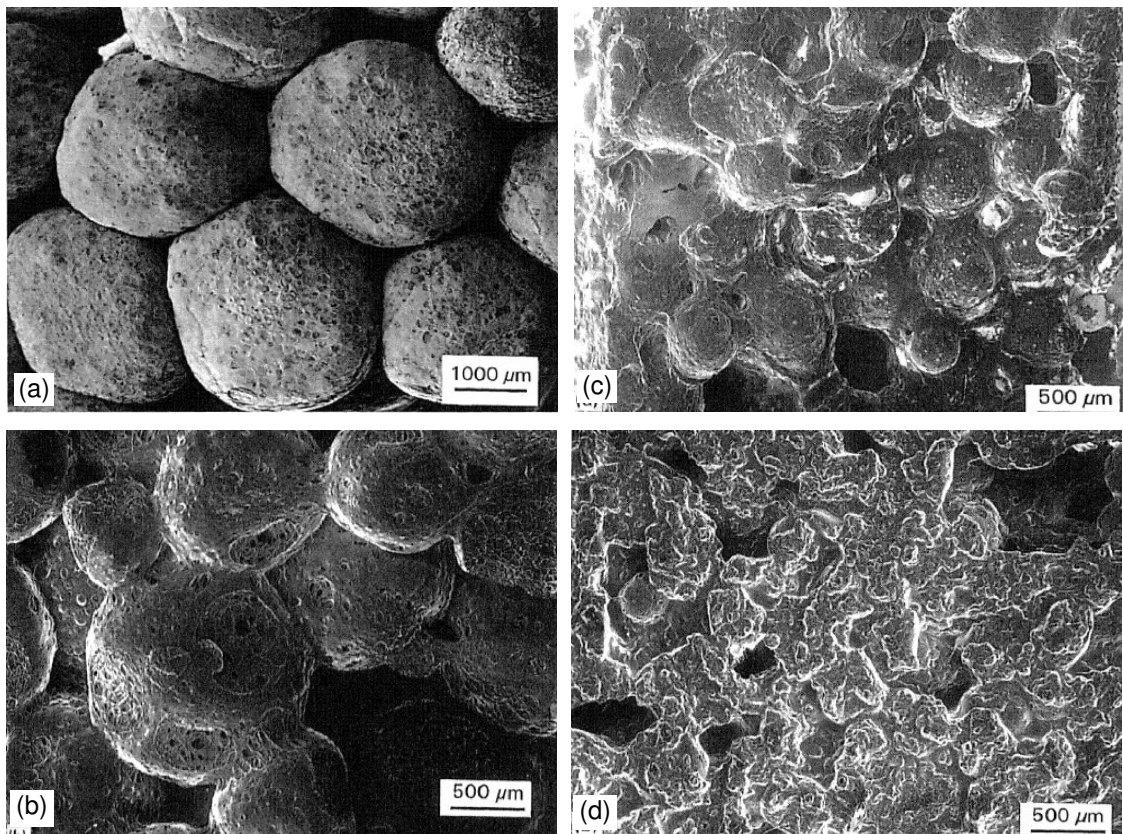
**Figure 3.2. Hot disk sensor.**

The associated software is then used to calculate the conductivity and specific heat of the samples. The average conductivities for EPS and XPS at 20°C were found to be 0.0327 W/mK and 0.0316 W/mK respectively. The average specific heats were found to be 1973 J/kgK for EPS and 2167 J/kgK for XPS. These values are close to those found in literature and will be used to develop the material models for the finite element analysis.

### **3.3.1.3 Thermal Degradation of Polystyrene Foams**

Central to the study of plastic foam cutting mechanics is the way in which plastic foams degrade with increasing temperature. For any FEA to be accurate it is important to know how the thermal properties change with temperature and also what temperatures cause the various physical transitions present in plastic foam cutting. For this reason it is important to know how the values presented in literature were found and how well they apply to the thermal cutting of polystyrene foams.

Mehta et al investigated the thermal degradation of foamed polystyrene patterns whilst studying the expendable pattern casting (EPC) process and found a number of interesting degradation characteristics applicable to the thermal cutting of EPS foam [50]. The experimental procedure involved submerging EPS samples in water or wax which had been heated to a specific temperature. Water was used for the temperature range between 50 and 100°C while wax was used for temperatures between 100 and 170°C. The samples were submerged for 30 seconds before being taken out and cooled to room temperature. Subsequently the samples were prepared for imaging with a scanning electron microscope (SEM). The resulting images (figure 3.3) show how the cellular structure of EPS changes with increasing temperature. Up to temperatures of 100°C the visual appearance of the cell structure does not change. As the temperature increases above 110°C the cells begin to collapse rapidly. This collapse temperature compares well with the commonly reported glass transition temperature range of 80 to 120°C; and is well below the commonly quoted melting temperature of crystalline PS of 240°C. At 160°C the cells have completely returned to their unexpanded state. The collapse temperatures were found to be the same regardless of EPS density and cell size.



**Figure 3.3. SEM photograph showing effect of temperature on EPS cell structure. (a) 20°C, (b) 110°C, (c) 120°C, (d) 160°C. Reproduced from [50].**

Mehta et al also carried out thermo-gravimetric analysis (TGA) and differential scanning calorimetry (DSC) on EPS of various densities. The TGA results show EPS volatilisation begins at about 275°C with maximum volatilisation rates occurring between 400 to 420°C as shown in figure 3.4. To ensure there was no difference in the degradation characteristics of the foam used in the above study and the foam used in the following cutting trials; an independent TGA experiment was carried out. This test revealed there is very little difference in the thermal degradation characteristics of XPS and EPS and that both foams have TGA profiles very close to the one reported by Mehta et al and Ahn et al [45, 50]. To see the independent TGA data see appendix A.

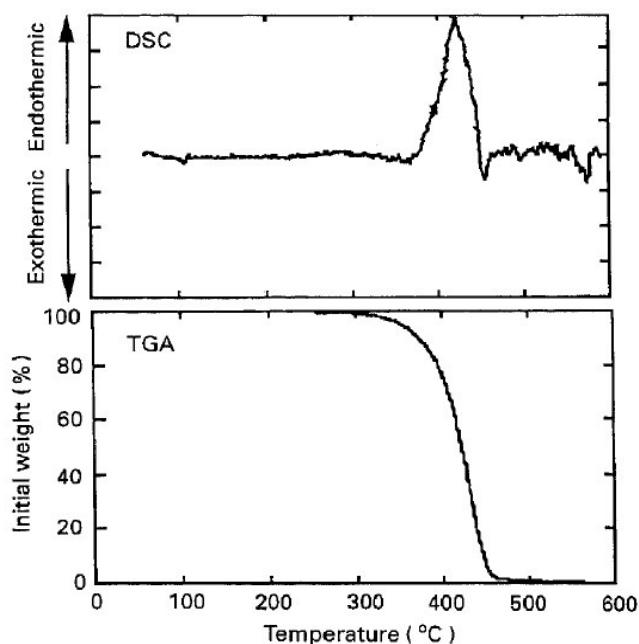


Figure 3.4. Typical TGA and DSC plots for EPS (0.024g/cm<sup>3</sup>). Reproduced from [50].

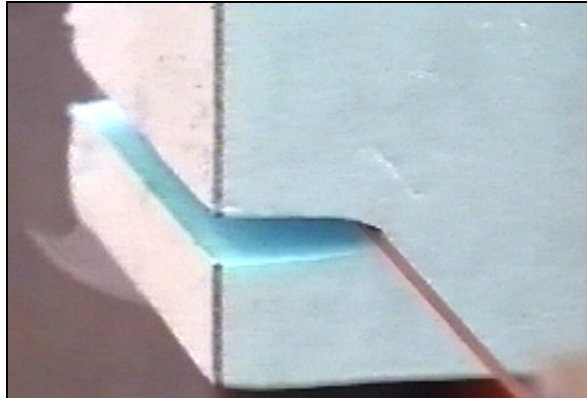
The thermal degradation of EPS is a highly endothermic process as shown by the peak in the DSC data. The heat of degradation can be calculated from the area under the endothermic peak. The average heat of degradation was found to be approximately 912 J/g for a range of densities. Importantly the degradation of EPS in plastic foam cutting will cause a chilling effect on the hot cutting tool. If some basic assumptions are made it is possible to calculate the decrease in temperature of a hot cutting tool such as a hot-wire based on the thermal degradation of a known amount of EPS. For example, if a taut  $\varnothing$  0.64 mm Nichrome wire is used to cut a 50 mm long EPS sample producing a 1.2 mm kerf; the wire will decrease in temperature by about 270°C over the length of the cut (see appendix B for the assumptions and working). Of course in practice not all the plastic in the cutting zone is fully degraded; nevertheless volatilisation can consume a significant portion of the energy available for cutting.

### 3.3.2 Cutting Tool Materials

The most common materials used for the thermal cutting of plastic foams are nickel-chromium (Nichrome) alloys, stainless steel alloys and titanium alloys. The suitability of a material for use as a foam cutting tool depends on the electrical, thermal and mechanical properties as well as the material cost.

Stainless steel wires are the most inexpensive and are suitable for many applications. Hobbyists and craftsmen often report of success when using stainless steel wires however these wires lack longevity at high temperatures. Computer controlled foam cutting machines are often large and

therefore require longer wires, which in turn require greater wire tension in order to prevent excessive wire deflection. For this reason stainless steel wires are rarely used with commercial foam cutting machines. Titanium alloy wires are the most expensive and have the most desirable material properties for large CNC foam cutting machines. Nichrome wires benefit from good corrosion resistance at high temperatures and have favourable resistive properties. The modest cost and appropriate material properties of Nichrome wires strike a good balance between cost and performance. For this reason Nichrome alloys were used for all cutting trials in this thesis.



**Figure 3.5 Nikrothal N80 Ø 0.64 mm wire cutting XPS foam.**

The wire used in this research project was Nikrothal N80 wire produced by Kanthal Corporation. The Nikrothal N80 wire (Figure 3.5) has a density of 8.53 g/cm<sup>3</sup> and a melting range between 1380 °C - 1400 °C. The basic chemical, mechanical and physical properties of this alloy are summarized in Table 3.3 below.

**Table 3.3. Chemical, mechanical and physical properties of Nikrothal N80 hotwire.**

<b>Chemical, thermal and mechanical properties of Nikrothal N80 wire.</b>						
Chemical Composition %	Ni	Cr	Fe	Si	Mn	C
	72.4	21.0	2.0	1.7	1.0	0.1
Tensile Strength at 20 °C	760 MPa					
Wire elongation at failure	30%					
Temperature coefficient of resistance, 20 – 500 °C	140 μΩ.m					
Melting point	1400 °C					
Maximum continuous operating temperature	1200 °C					
Density	8530 kg/m <sup>3</sup>					



### 3.4 Experimental Apparatus

The following sections introduce the main equipment used for the hot-wire and hot-ribbon cutting trials. The cutting apparatus comprised of an industrial robot (Kuka KR6), a hot-wire cutting head, a hot-ribbon cutting head, an electrical power supply, and a material sample holding device. Time, current, voltage, wire/ribbon temperature, air temperature and cutting force were recorded for every cut. The measurements were logged onto a computer where the data was calibrated and assessed. Figure 3.6 below shows how the different components are related within the foam cutting system.

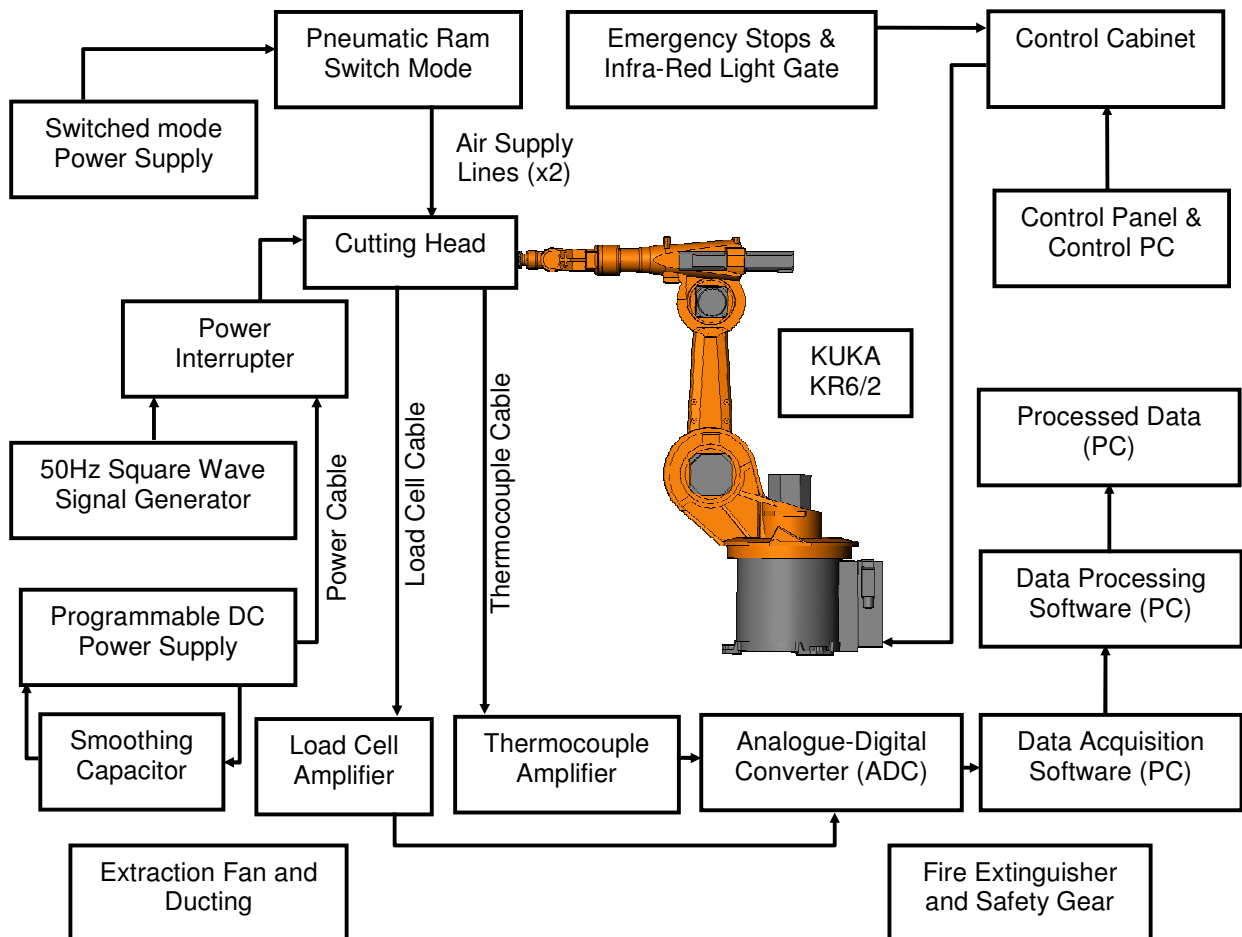


Figure 3.6. Schematic of plastic foam cutting system.

#### 3.4.1 Cutting Heads

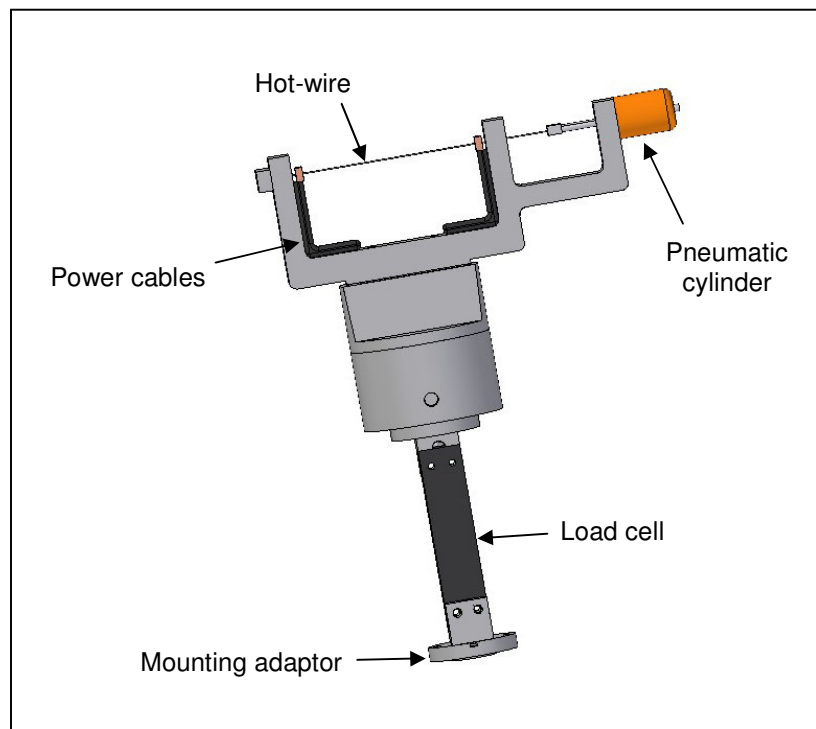
Two cutting heads were developed for the cutting trials. One employs the use of a hot-wire while the other uses a hot-ribbon. The hot-wire cutting head can be used to cut simple 2D profiles or

objects with convex surfaces. The simple geometry of the hot-wire also allows the relationships between various cutting parameters to be investigated without the added complication of multifaceted tool geometries.

The hot-ribbon cutting head was developed for use with the FAST system. The cross-section of the rectangular hot-ribbon cutting elements provides strength in the cutting direction and therefore allows almost any cutting tool geometry to be made. By forming the hot-ribbon cutting elements into appropriate shapes the hot-ribbon cutting head can be used to sculpt double concave features and pockets.

#### 3.4.1.1 Hot-wire Cutting Head

The cutting head shown in Figure 3.7 was used throughout the hot-wire cutting trials. It has been designed to mount directly onto the robot as well as a rigid steel frame. During the cutting trials the cutting tool was mounted on a floor mounted steel frame to prevent the load cell recording inertial forces created by the acceleration and deceleration of the robot. A foam sheet holding device was then attached to the robot to allow the foam to be moved through the stationary hot-wire.



**Figure 3.7. Hot-wire cutting head.**

Power is supplied directly to the wire via detachable cables. The hot-wire circuit is electrically isolated from the remainder of the metallic cutting head components using a combination of nylon

bushes and ceramic inserts. The robot has a maximum loading capacity of six kilograms on the tool mount so the cutting head was made entirely from aluminium in order to minimise weight.

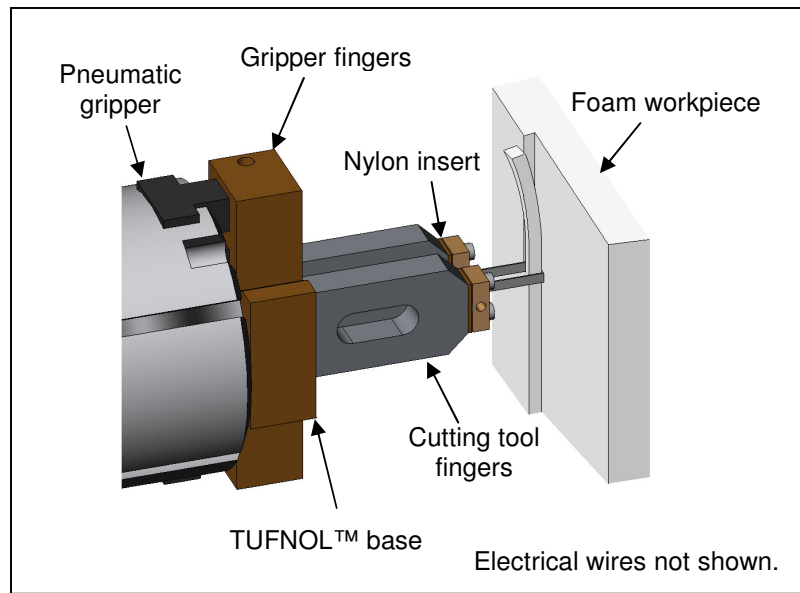
The hot-wire stretches between the major arms of the tool and is tensioned using a pneumatic ram that is mounted between the minor arms of the cutting tool. The ram used is a Norgren Martonair cylindrical ram with 2" stroke, rated to 8 bar. In contrast to other systems that have been used to provide wire tension such as springs, this technique does not require regular manual adjustment. The tension remains constant regardless of wire temperature and can be easily varied by adjusting the pressure. Maintaining a constant level of pre-tension in the wire has been found to be an important element in producing a good surface finish. When carrying out cuts over a wide range of wire temperatures it is important to adjust the wire tension to suit the modified yield strength of the wire and avoid breakages.

Drawings of the hot-wire cutting head can be found in appendix C.

#### **3.4.1.2 Hot-ribbon Cutting Head**

The hot-ribbon cutting head shown in figure 3.8 was used throughout the hot-ribbon cutting trials and for the proof of concept sculptures made by the FAST system. It has been designed to mount directly onto the robot or onto a steel frame. During the cutting trials the cutting head was fixed to the floor mounted rigid steel frame to prevent the load cell recording inertial forces created by the acceleration and deceleration of the robot. A foam sheet holding device was then attached to the robot to allow the foam to be moved through the stationary hot-ribbon.

The fingers of the hot-ribbon cutting head can be adjusted to hold different sized hot-ribbon tool profiles. The wider profiles are used for roughing cuts while the narrow profiles are used for finishing cuts. The cutting tools can be changed very efficiently using the pneumatic gripper and an automated robot sequence that releases the roughing tool and subsequently clamps the finishing tool.

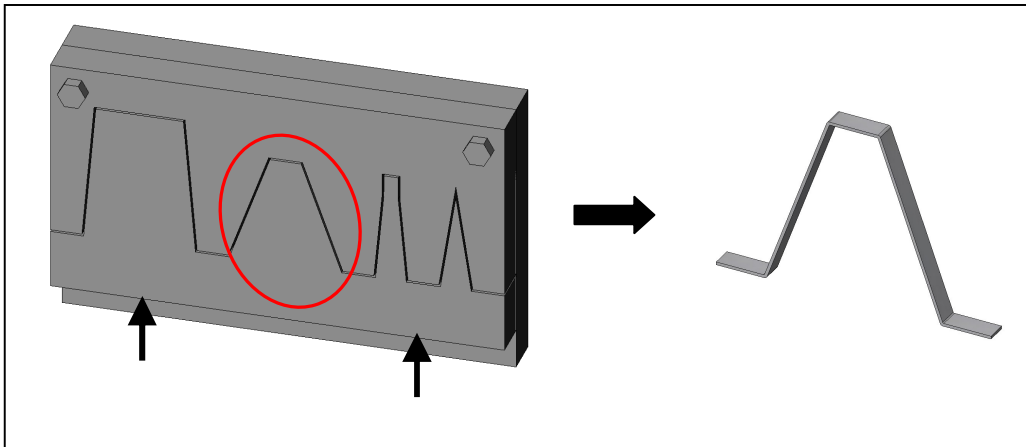


**Figure 3.8. Hot-ribbon cutting head.**

Power is supplied to the hot-ribbon via brass contacts on the gripper fingers. This allows the cutting tool to be replaced without the need to detach/reattach the power cables. The hot-ribbon circuit is electrically and thermally isolated from the remainder of the metallic cutting head using a combination of nylon inserts and TUFNOL™ parts.

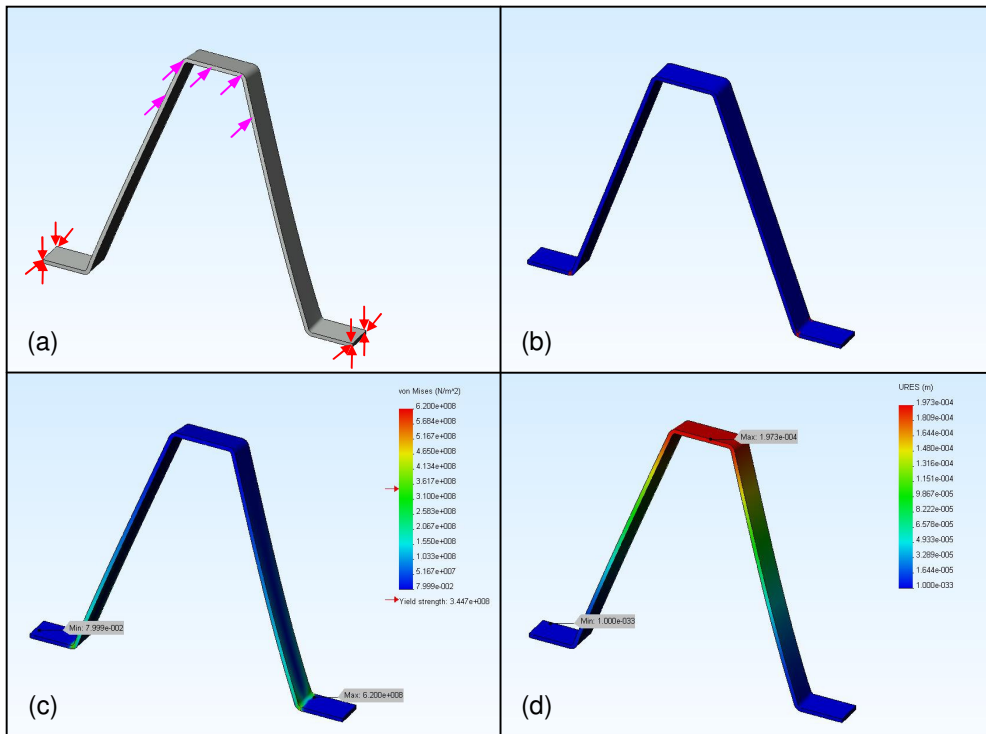
The hot-ribbon is held firmly in position by two brass contacts at the end of the cutting tool fingers. The hot-ribbon is orientated such that the tool cross-section perpendicular to the cutting direction is minimised therefore reducing potential cutting forces. The width of the ribbon is wide enough to provide sufficient strength to prevent bending in reasonable cutting conditions.

To achieve consistency when forming the hot-ribbons, a die was created. The die contains a number of profiles from which roughing and finishing cutting elements can be formed. Figure 3.9 shows the die with the different cutter profiles. The die produces cutting elements with consistent geometric shapes and dimensions and allows the cutting elements to be shaped efficiently. The highlighted profile was used for the majority of the hot-ribbon cutting trials. Drawings of the hot-ribbon cutting tool and ribbon forming die can be found in appendix C.



**Figure 3.9. Hot-ribbon forming jig showing the profile selected for the cutting trials.**

Finite element analysis was carried out in COMOSXpress on the hot-ribbon cutting element to ensure it is rigid enough to withstand the forces experienced during cutting. A cutting force of 12 N was used in the simulation as this was the highest force measured whilst producing reasonable surfaces with this ribbon profile. Figure 3.10 (a) shows how the loads and constraints were applied to the model; (b) shows that the factor of safety  $> 1$ ; (c) shows that the maximum stress is located at the bottom of the legs; (d) shows that the ribbon is displaced by less than 0.2 mm at the tip.



**Figure 3.10. FE analysis of hot-ribbon cutting element. (a) Boundary conditions and loading (b) FOS (blue>1) (c) Von Mises stress (d) Displacement.**

These results indicate that the ribbon is of an appropriate gauge to withstand relatively high cutting loads and will be rigid enough to prevent excessive deflection which would otherwise impact on the surface accuracy.

### 3.4.1.3 Power Source

The initial hot-wire cutting trials were conducted using an ITECH IT6831 programmable power supply. The power supply has a voltage range of 0 to 19 Volts, a current capacity of 0 to 10 Ampere and can be used in constant current or constant voltage mode. Constant current mode was used for all the cutting trials conducted in this thesis.

The hot-ribbon cutting elements required substantially more power to heat than the hot-wires. For this reason the ITECH IT6831 power supply was replaced with a POWERTECH MP3090 DC regulated power supply. The POWERTECH MP3090 has a current capacity of 40 Ampere. An external circuit which modifies the electrical output was created to allow the power supply to be controlled via PC software. The software allows the duty cycle to be modified and the power to be switched between alternate levels based on inputs from a load cell and predetermined cutting force limits.

### 3.4.2 Industrial Robot

The KUKA KR6 robot is a six axis industrial robot capable of point to point and continuous controlled path tasks. The rated payload is 6 kg on the end effector which can be moved at maximum speed, even with the arm fully extended. The robot is equipped with a controller (CR2), whose control and power electronics are integrated in a common cabinet. Figure 3.11 shows the robot in its experimental configuration.

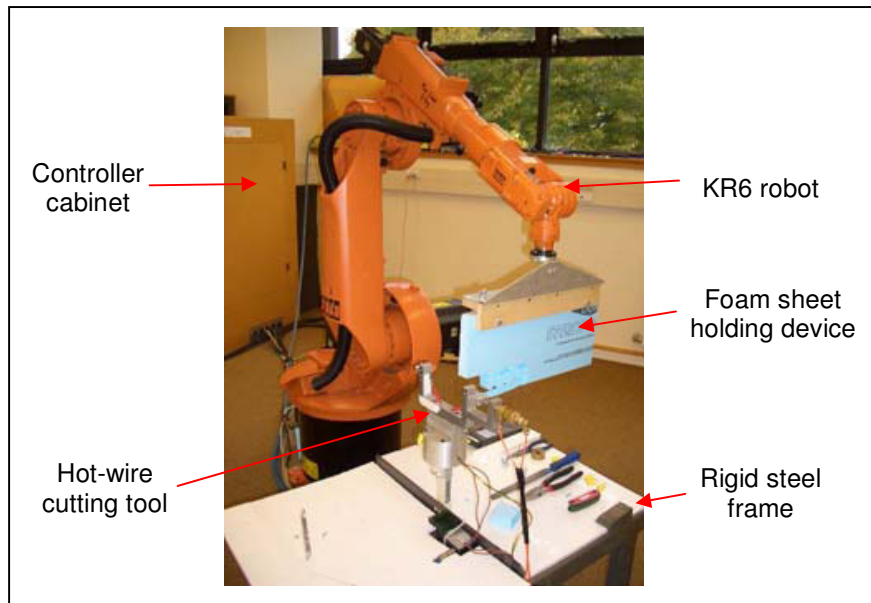


Figure 3.11. Hot-wire cutting trial experimental setup.

### 3.4.3 Measurement Devices

This section describes the various devices used to measure important parameters in the plastic foam cutting process and the systems used to log the data.

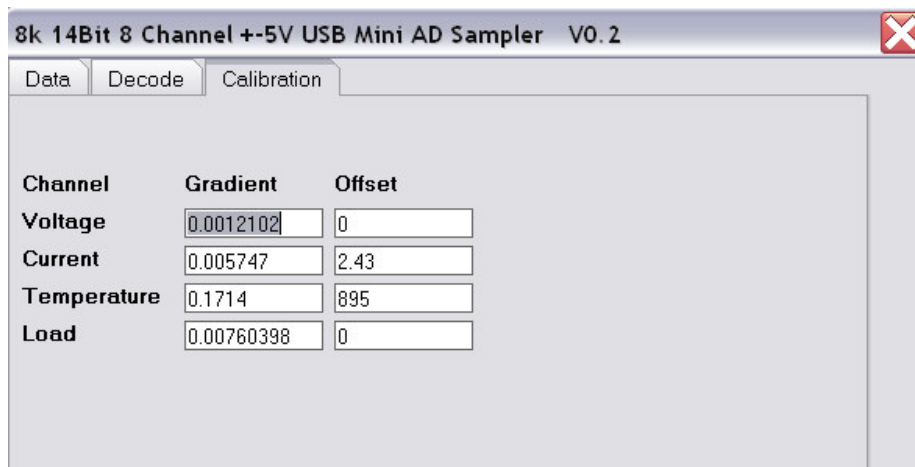
#### 3.4.3.1 Cutting Force Measurement System

The cutting force is an important factor influencing both surface finish and life time of the cutting tool. The cutting force measurement system installed in the facility consists of a proprietary load cell and analogue signal amplifier. The load cell is mounted between the cutting tool and the floor mounted table as shown in Figure 3.11 and 3.12.



**Figure 3.12 Load cell used in the cutting trials.**

The output of the signal amplifier is fed into an analogue to digital converter, which in turn is connected to a data logging PC. The data is converted to a force measurement in real time by a data acquisition (DAQ) system that contains the necessary calibration data for the load cell. The calibration of the load cell is a simple exercise involving the use of weights and a frictionless pulley. The calibration is carried out in the cutting position and the load is applied at the centre of the wire/ribbon that is in the cutting head. Data is gathered using several different weights and then plotted to give a calibration curve. Due to the proprietary nature of the load cell, the data obtained is highly linear, with a high level of repeatability. The gradient and axis intercept of the calibration curve are entered into the appropriate boxes on the calibration page and, from these, the software gives direct force readings (Figure 3.13).



**Figure 3.13. Calibration page.**

### 3.4.3.2 Temperature Measurement System

The most technically challenging problem encountered during the cutting trials was the issue of temperature measurement. Understanding how the temperature of the wire changes over time and along the length of the hot-tool provides insights into how the cutting strategy can be improved and how the end effects impact the surface form. Measuring the hot-tool temperature is difficult for a number of reasons: the first is location, the hot-tool is surrounded by foam and only



visible through a narrow gap; also the hot-tool has low thermal inertia, therefore physically contacting the wire with a measuring instrument inevitably changes the local temperature of the tool. Measuring the hot-tool temperature by monitoring the change in resistivity proved ineffective because the resistivity of Nichrome changes minimally with temperature. Also only a small portion of the wire is engaged in the cut so the effect is averaged across the wire.

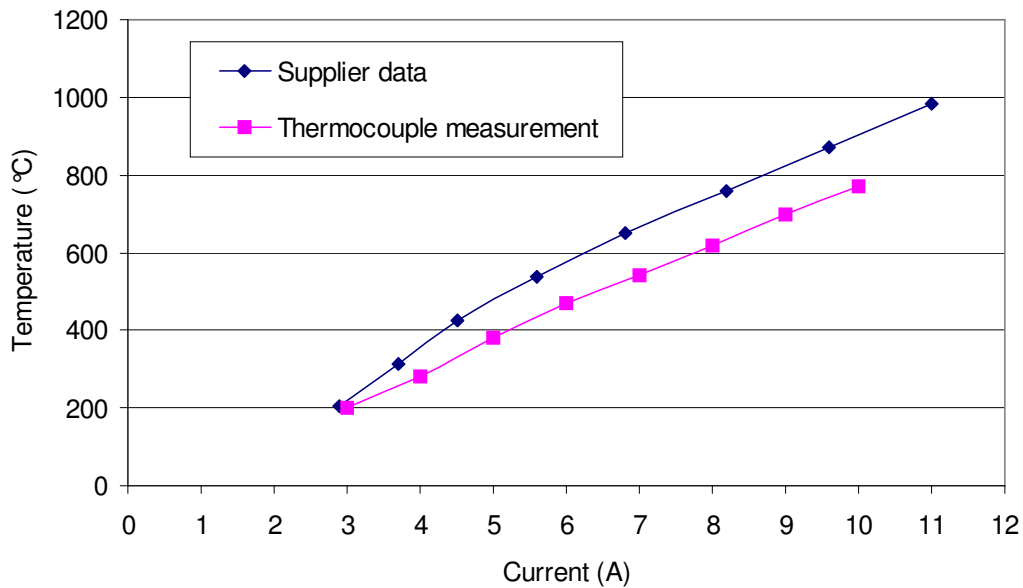
Nevertheless there were two main options available for measuring the wire temperature during cutting; these are thermocouples and thermal imaging cameras. Both temperature measurement technologies have shortcomings when applied to foam cutting, however these were overcome with the right experimental method, and it was therefore possible to obtain high quality temperature data.

Thermocouples were chosen for all the temperature measurements in the initial stages of the cutting trials because their low cost and general availability. After the initial cutting trials a thermal imaging camera with appropriate specifications was acquired to validate the thermocouple data and to observe transverse temperature effects not able to be measured with thermocouples.

### **Thermocouples**

Thermocouples have two main shortfalls; the first arises because of the low thermal inertia of the hot-tool. Inevitably the thermocouple acts as a heat sink for the wire and therefore cools the local temperature of the wire thus giving a false reading. The second problem is the electromotive force (EMF), produced by the current running through the hot-tool, which interferes with the minute voltage difference thermocouples create to measure the temperature. To overcome these problems it was necessary to somehow compensate for the heat sink effect and to simultaneously control the current in the wire so that it can be briefly turned off each time a temperature measurement is made without affecting the tool temperature.

By comparing the thermocouple measurements with supplier data it was possible to apply a temperature dependant offset to correct the measured thermocouple data. Figure 3.14 below shows the temperature/current relationship for Nichrome (Nikrothal N80, Ø0.64 mm) wire. The two curves provide a direct comparison between suppliers' data and that measured with the thermocouple, as used in the documented experiments.



**Figure 3.14. Comparing suppliers wire temperature data with experimental.**

To allow the thermocouple to measure the hot-wire temperature without EMF interference the hot-wire current had to be momentarily stopped. In this way reliable temperature data was collected while the wire was electrically inactive. In practice the thermocouple continuously recorded both the good and bad data and the erroneous data was subsequently removed with a filter program run in MATLAB<sup>®</sup>. The data was collected at a much higher rate than was actually needed (1000 measurements per second) so it was possible to remove well over 50% of the data without negatively effecting the usefulness of the information. For all of the cutting trials a 50% duty cycle was adopted. The electrical currents quoted throughout the thesis are the average currents. The electrical power used in the calculations of the effective heat inputs were based on the actual power cycle, not the average current. The period of the duty cycle was small (0.01 seconds) so that any heating and cooling that occurred over the power cycle could be assumed negligible (i.e. the wire temperature is a function of the average power, not the instantaneous power). For more information on why a duty cycle of 50% was chosen and how the temperature data was filtered please see appendix D.

### **Thermal Imaging Camera**

The main problems with using thermal imaging cameras to obtain the hot-tool temperatures are; line of sight, camera resolution and determination of the emissivity. The camera must also meet the specifications for the cutting trials which include; a wide temperature range (100 to 1000°C), high thermal sensitivity (to determine the temperature difference between the front and back of the cutting tool), and high resolution so that at least three pixels cover the hot-tool being observed. As the wire is only 0.64 mm in diameter the resolution must be at least 0.2 mm/pixel.

A FLIR S65 camera with a 200  $\mu\text{m}$  (64 mm x 48 mm/150 mm) close-up lens was chosen which met all the above specifications (figure 3.15). The camera was able to store images at a rate of 25 Hz and could therefore capture in great detail the transient temperature profiles of the cutting tool being measured. The technical specification of the camera is given in appendix E.



**Figure 3.15. FLIR S65 thermal Imaging Camera.**

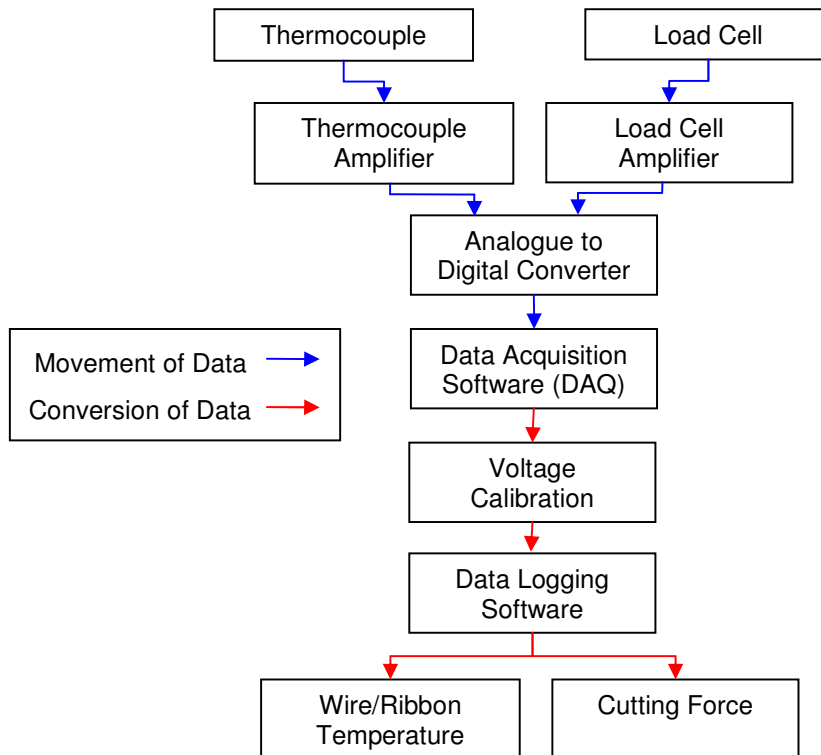
The camera was positioned behind the stationary cutting tool and just to the side of the advancing foam sample so that a direct view of the tool during cutting was possible. A small weight was attached to the bottom of the foam block so that each time a sliver of material was parted from the main block it curved under gravity and created an opening through which the cutting tool (hot-wire/ribbon) could be seen. Without the addition of such a weight it would have been very difficult to see the entire width of the cutting tool within the cut.

The emissivity value of the wire/ribbon was calculated by painting a small portion of the wire/ribbon with a high temperature black paint of known emissivity. Then the emissivity value within the camera was changed so that the temperature of the un-painted portion of cutting tool matched the previous temperature of the painted portion. The emissivity of the hot tools were found to vary over a wide range of values however eventually a value between 0.29 and 0.37 was found that was repeatable dependant on which tool was used. One reason for the difficulty in determining the emissivity with a high level of precision is because the surface of the cutting tools changed over time. Unused Nichrome tools are clean, polished and silver coloured while after cutting at high temperatures the surface oxidises and becomes slightly green and dull (due to the formation of chromium oxide). This oxidation of the surface along with possible contamination with pyrolysed polystyrene varies the radiative properties of the surface.

The thermal imaging camera was operated independently of the data acquisition system which is described in the next section.

### 3.4.3.3 Data Acquisition and Processing System

A software data acquisition system (DAQ) was installed to collect and store the numerical data generated by the force and temperature measurement systems. The raw measurements from the instruments were converted into digital format using an analogue to digital converter (ADC) and the data was retrieved from the ADC by the DAQ through a USB interfacing system. The flow of information through the system is depicted in the flowchart below.



**Figure 3.16. Movement of data through various components of the data acquisition system.**

The data generated during the data collection process was stored as a \*.bin file. The data in the \*.bin file was then decoded into a more useful \*.txt format. At this stage it was also possible to choose whether the raw or calibrated data was decoded. Data in this format can be readily imported into most commercial spreadsheet applications.

Importantly the data received by the DAQ could be viewed in real time via the DAQ user interface. The data page displayed whether the data was currently being recorded and displayed both the raw voltage and calibrated values for cutting tool temperature, cutting force, current (DC equivalent), voltage (DC equivalent) and percentage duty cycle. The data page also provided two alternative methods of controlling the power. These are shown in figure 3.17 as Control Method 4 and 5. Control method 4 works by adjusting the 100% current on the power supply to an

appropriate level then selecting the percentage duty cycle desired. Control Method 5 allowed the power to be modulated in real time based on predetermined cutting force limits. Control method 5 is explained in greater detail in section 3.6.7.

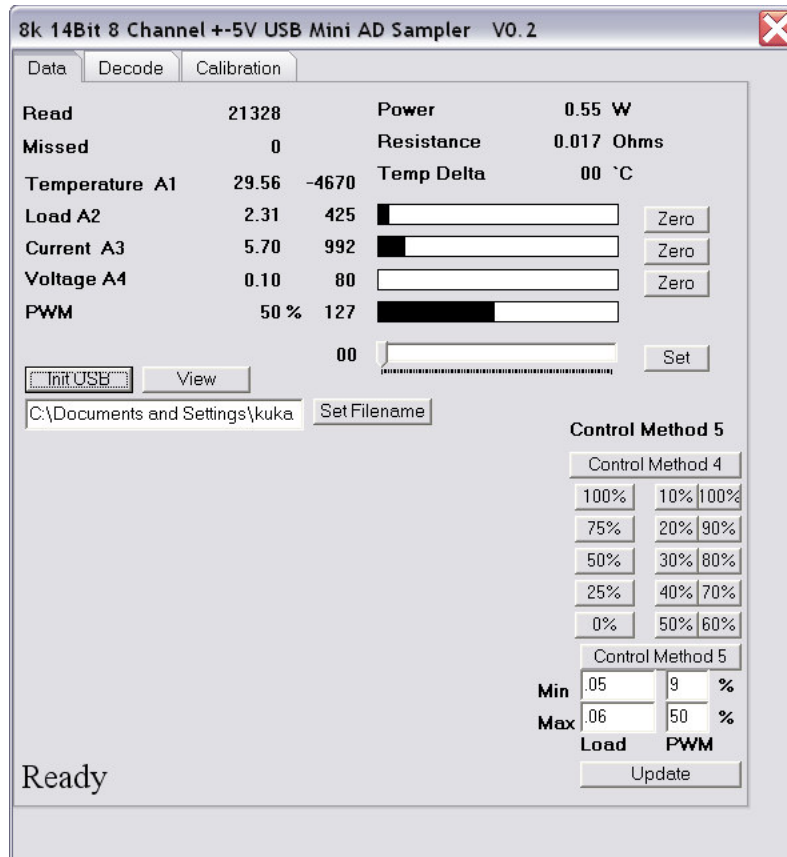


Figure 3.17. Data page of DAQ user interface.

### 3.4.4 Safety

The KUKA KR6/2 industrial robot is capable of moving at speeds of up to  $3 \text{ ms}^{-1}$  and can accelerate extremely quickly which presented a serious safety issue considering the small size of the robot's working envelope. The cutting of polystyrene by means of vaporisation and melting posed another health and safety issue. The safety measures put in place to ensure no personal injury or damage to equipment by the robot or cutting of polystyrene included:

- The robot's working envelope was clearly marked with 'danger' tape on the floor. In addition several photoelectric sensors wired to the emergency stop circuit of the robot's control PC were used as 'light barriers'. The robot was shutdown immediately when someone crossed the light barrier. The barriers needed to be reset to resume operation once they had been triggered.

- All new control programs created were run at a reduced velocity and were run in the 'Test 2' control state. The 'Test 2' control state requires the user to engage a paddle like switch with their fingers while they hold their thumb on a button to execute the program. The robot stops instantly if the paddle like switch is released or the pressure on the execution button is relieved. In addition, the robot is also stopped if the paddle like switch is depressed with excessive force (this is designed to accommodate panic responses by the user).
- Three emergency stop buttons within easy reach around the room were wired to the emergency stop circuit of the robot's control PC. If the buttons were pressed, the system would need to be rebooted in order to reset them.
- A large extractor fan with adequate ducting to the outside was used to remove fumes and smoke during cutting.
- A fire extinguisher was on hand to extinguish any possible fire caused by the cutting of the polystyrene.

### **3.5 General Experimental Method**

The cutting trials consisted of over 800 individual cuts from which a vast number of measurements were made. The general cutting procedure for all the cutting tests was as follows:

- a) A sheet of material was held vertically in the clamping device which was manipulated by the robot.
- b) Power was supplied to the hot-wire or hot-ribbon by fixing the current and allowing the voltage to float. The temperature of the wire was then allowed to stabilise.
- c) A robot programme was run to initiate the linear cutting of the foam sample at a predetermined feed-rate.
- d) As a result of step c above, a 10 mm sliver of material was pared from the parent sheet by the hot-wire or hot-ribbon. The cutting force was monitored throughout and logged to a computer, and the surface finish was subsequently examined.
- e) The robot programme was then necessarily modified to advance the cutter path by 10 mm. Steps b-d were then repeated measuring the temperature in the centre of the sample throughout the cut. This was done independently of the force measurement to ensure the thermocouple did not introduce errors into the force measurement.

- f) Steps b to e were then repeated changing the test conditions (current, feed rate, material and cutting tool) as necessary.

The following table summarises the range of variables used in the cutting trials.

**Table 3.4. Experimental range of parameters.**

Cutting Tool	PS Foam	Feed-rate (m/s)	Current range (A)
Ø 0.64 mm Nichrome wire	S-grade EPS (15 kg/m <sup>3</sup> )	0.003 to 0.050	3.0 to 8.0
	H-grade EPS (26 kg/m <sup>3</sup> )	0.003 to 0.050	3.0 to 8.0
	VH-grade EPS (30 kg/m <sup>3</sup> )	0.003 to 0.050	3.0 to 8.0
	XPS (30 kg/m <sup>3</sup> )	0.003 to 0.038	3.0 to 8.0
Ø 0.32 mm Nichrome wire	XPS (30 kg/m <sup>3</sup> )	0.013 to 0.020	1.8 to 2.6
Ø 0.91 mm Nichrome wire	XPS (30 kg/m <sup>3</sup> )	0.013 to 0.020	6.0 to 9.0
3.175 x 0.457 mm Nichrome ribbon	H-grade EPS (26 kg/m <sup>3</sup> )	0.050 to 0.098	12 to 22
	XPS (30 kg/m <sup>3</sup> )	0.040 to 0.076	16 to 22

The above procedure was used to produce the bulk of the data in this thesis including the cutting force, electrical current, feed rate and surface texture relationships, however additional tests were carried out to obtain other measurements of interest. These tests included:

- Measuring the hot-wire/ribbon temperature inside a cut.
- Measuring the kerf width of cut samples.
- Trialling a temperature control strategy for the hot-wire.
- Observing the effect of cutting orientation.

A description of the testing procedure for each of the above additional experiments will be included in the relevant sections.

### 3.6 Hot-wire Cutting Trials



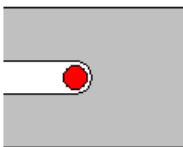
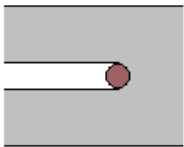
This section contains noteworthy results gathered during the hot-wire cutting trials and discusses how the information can be used to improve on current cutting strategies. Also included with the relevant data is an explanation of how the data was collected and the experimental procedures. The particular results shown were chosen because they demonstrate clearly the trend in discussion. In some cases the same cutting conditions are used consistently so as to create a link between various tests and results.

#### 3.6.1 Cutting Stages

Preliminary cutting trials revealed the transient nature of hot-wire cutting with constant current cutting conditions. In these tests the wire was heated in free air to a stable temperature before the cutting sequence was started. Once the wire entered the foam it was visually apparent that the wire cooled. In some cases the wire changed colour from red to black or the cutting force on the wire increased. Further cutting tests revealed this to be a transient phenomenon whereby the cutting mechanism changes from thermal cutting to thermomechanical or mechanical cutting.

Three main cutting stages were identified to help classify the different phases of cutting. Stage I and stage II are unstable phases where the hot-wire is in an “overheated” state in the cutting environment. Stage II is the transitional phase where the cutting mechanisms of stage I transition to the cutting mechanisms of stage III. Stage III is an equilibrium stage in which the thermal energy generated in the wire is balanced by the heat transferred from the wire into the surroundings. Determining the influential cutting parameters in stage III is of high importance as these conditions prevail for the majority of the cut and are the easiest to control.

**Table 3.5. Diagrammatic representation of the three cutting stages with a hot-wire.**

Wire in “free air”	Stage I	Stage II	Stage III
			
Stable high temperature wire	Unstable high temperature wire	Wire cooling	Wire stable at lower temperature

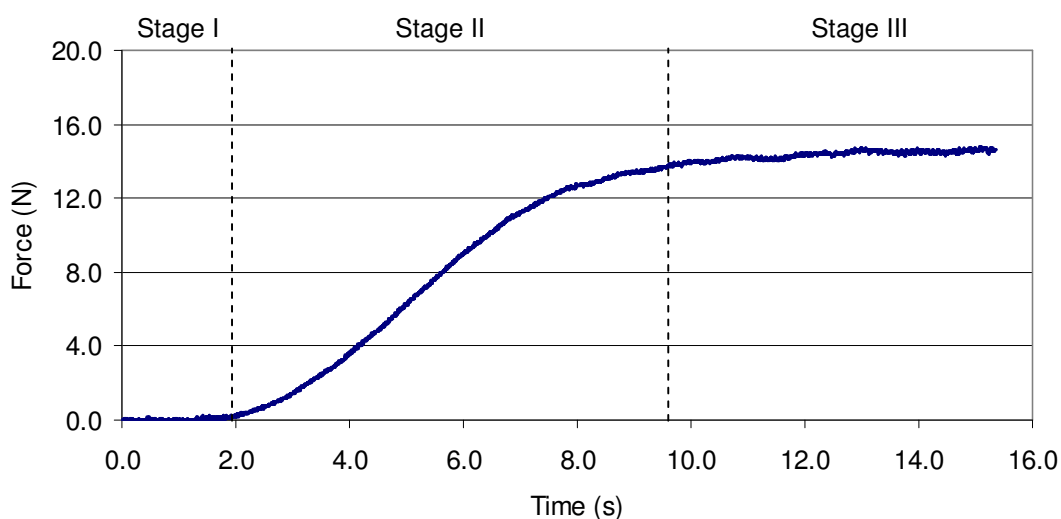
#### 3.6.2 Characteristic Cutting Force

The first area of interest to be investigated was the cutting force experienced by the wire. This is because the cutting force provides direct limits for the range of potential successful cutting



parameters. If the cutting forces are excessively high for a particular current/feed rate combination then the wire will break. Therefore, finding the upper limit for appropriate cutting force values was a logical place to start.

The general experimental method described in section 3.5 was used to measure the cutting force of cuts with a wide range of parameters. Each individual combination of electrical power and cutting velocity was found to produce a characteristic cutting force profile. High electrical currents and low cutting velocities produced very low cutting forces while low electrical currents and high cutting velocities produced high cutting forces. However, all cutting force profiles which do not use temperature control exhibit an 'S' shape curve with low cutting forces at the beginning followed by a transition period, followed by a steady state force. The three stages of table 3.5 are related to the characteristic 'S' curve as shown in figure 3.18.

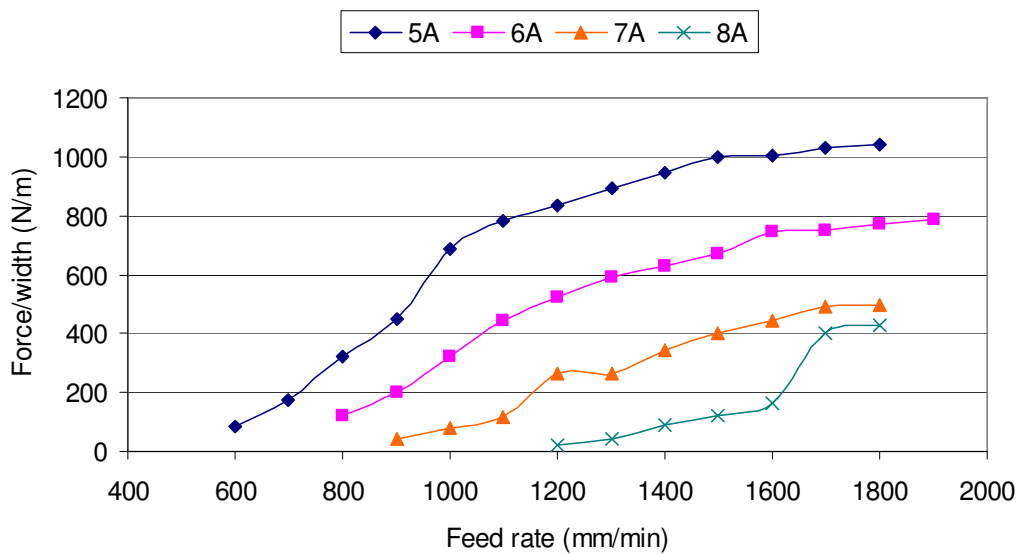


**Figure 3.18 Characteristic cutting force profile of a XPS sample (5A - 0.02 m/s)**

The cutting force is directly related to the degree of physical contact between the wire and the foam and also the viscosity of the plastic it is contacting. For a more in depth analysis of the characteristic force profile of cuts made with different cutting parameters see the attached prior published work (appendix J).

The equilibrium cutting force present in stage III was calculated for a wide range of feed rates and currents by averaging the force in the stable region and plotting all the average stage III cutting forces on one graph. Figure 3.19 shows the relationship between equilibrium cutting force, feed rate and electrical current for XPS samples cut with a  $\varnothing$  0.64 mm wire.

The trend lines show that the equilibrium cutting force does not increase linearly with the feed rate but tends to follow an 'S' shape curve. The wire temperature or power input has an obvious effect on the cutting force, that is, higher power inputs lower the cutting force. It is important to note that the 'S' shaped curves of figure 3.19 represent the equilibrium cutting force of many cuts not the transient cutting force of one cut, like in figure 3.18. The low equilibrium cutting forces associated with low feed rates are due to the fact the wire has sufficient energy to melt any adjacent foam before it contacts the wire. Therefore, for any wire over the 'melting' temperature of the foam there exists a feed rate below which zero force cutting conditions will prevail.



**Figure 3.19. Stage III cutting force vs. feed rate for various free air wire temperatures in XPS.**

The equilibrium force curves of figure 3.19 all seem to approach an upper limit of cutting force, however the limit is different for each data series. This upper limit is most evident in the 5,6 and 7A data series which are constant at approximately 1040, 800 and 500 N/m respectively. As long as the wire is sufficiently strong the maximum achievable cutting force depends on the force required to tear (or shear) the foam. This suggests the limiting cutting force values seen in the above graph are determined by the temperature dependant shear strength of the foam material. The last two data points in the 8A series are notably higher than what would be expected from the trends of the other series. This could be because of a change of wire (due to creep at high temperatures the wire did not last long when using 8A), a new foam sample, large differences in the ambient temperature or a combination of any/all of these things. While anomalies such as this have been noticed in other graphs, there is no single apparent connection and they are often not repeatable. A similar 'bump' in the data can be seen for the VH-grade data series in figure 3.20.

Figure 3.20 shows the equilibrium cutting force versus feed rate trends for a variety of PS foams. As can be seen all three PS foam types exhibit the same general 'S' shape profile. The difference in cutting force arises from the different cellular structures, densities and molecular weights of the foams. The difference between the 30 kg/m<sup>3</sup> VH grade EPS and the 15 kg/m<sup>3</sup> S grade EPS show that reducing the density of the foam reduces the cutting force. This is because the less dense material is 'melted' with less energy per unit volume and therefore the gap surrounding the wire is larger, resulting in less mechanical interaction between the wire and the foam. The difference between the 30 kg/m<sup>3</sup> XPS and the 30 kg/m<sup>3</sup> VH grade EPS is thought to be due to the different cell structures and molecular masses of the foams. The finer cellular structure of XPS may result in higher mechanical shear strength. Also experimental data gained in these cutting trials suggest that the XPS foam had a higher molecular mass than the EPS, resulting in higher glass transition activation energies and higher cutting forces for the same amount of electrical energy. This is explained further in later sections.

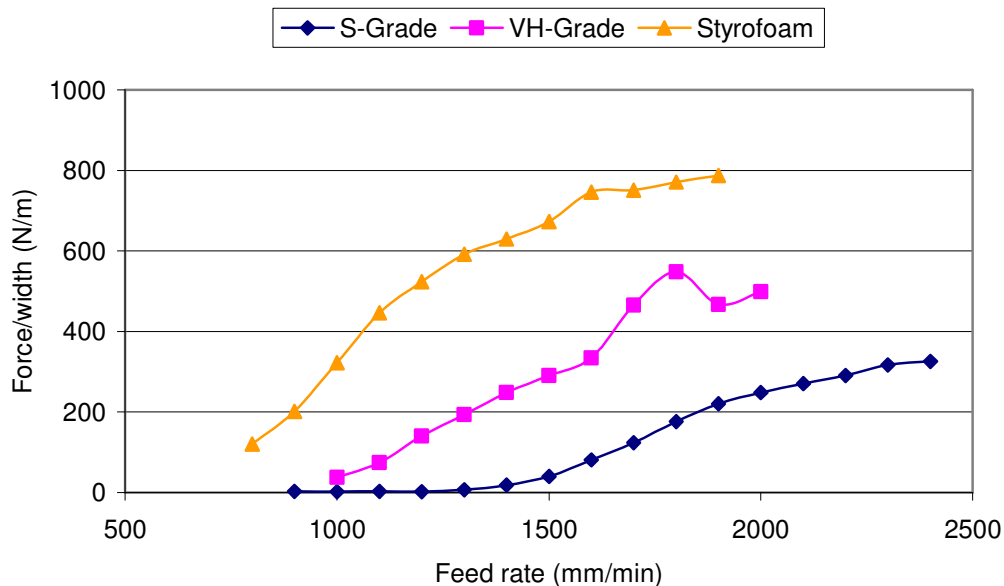


Figure 3.20. Cutting force vs. feed rate for different PS foams cut with 6A.

The following section investigates the connection between cutting force and cutting orientation.

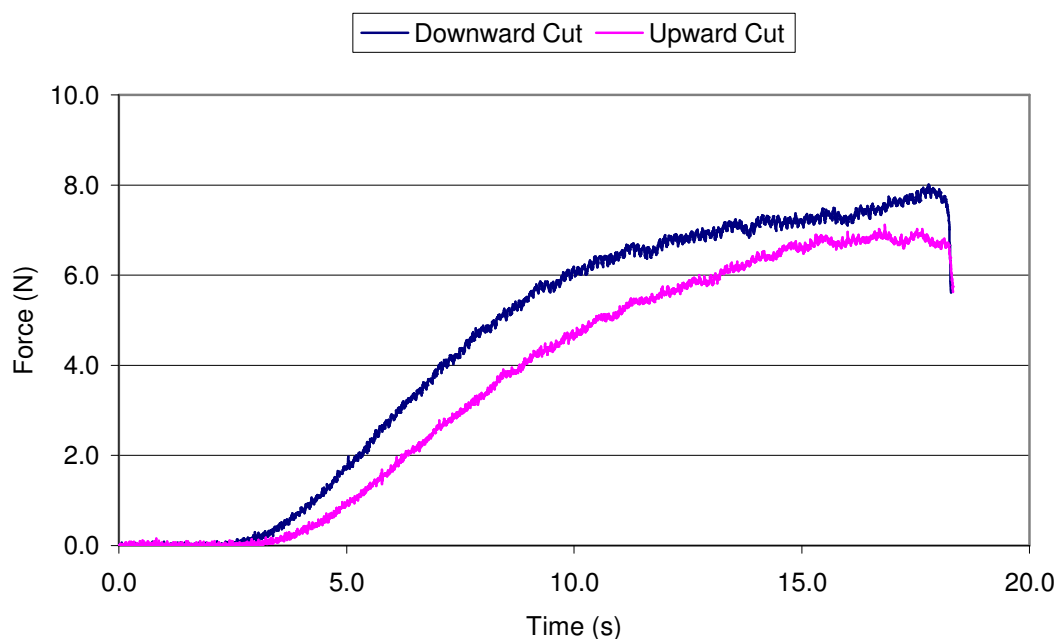
### 3.6.3 Cutting Orientation

All of the cutting tests that have been discussed thus far were performed in the horizontal plane, meaning the hot-wire was held horizontally and the foam was moved perpendicular to the wire axis and parallel to the floor. The choice for this experimental configuration was based largely on the most appropriate orientation for the load cell, as it was preferable to have the load cell straight up and down to remove the effects of gravity. Choosing the horizontal cutting plane also meant

the cutting conditions will not be affected by cutting direction. It is well known that heat rises and because hot-wire cutting depends on how the heat is transferred to the surrounding foam it is important to know whether cutting orientation has an effect on PFC and how large that effect is.

To measure the effect of cutting orientation the robot code was changed to cut vertically, up and down. The rigid steel frame, which had the cutting head mounted on, was turned on its side so that the load cell and cutting tool were cantilevered horizontally from the steel frame. The load cell was then zeroed to remove the force associated with self weight of the cutting head and load cell assembly. Eight cuts were then made; four in EPS and XPS respectively. Each material was cut with high and low currents (7A and 5A) in both directions (up and down) with a feed rate of 0.0167 m/s.

Figure 3.21 shows the results of vertical cuts in XPS using a 0.64 mm Nichrome wire with 5A. The cutting force when the wire was moving up relative to the foam (upward) was found to be slightly less than the cutting force in the opposite (downward) direction. Also the hot-wire took slightly longer to reach stable cutting conditions when cutting upwards. This verifies the theory that some of the heat generated in the cutting tool rises due to natural convection. When the rising heat is in the same direction as the cut the convective heat aids the cutting process. When cutting downwards some of the convective heat is free to move upwards reducing the heat available for cutting, resulting in higher cutting forces. It is expected that the cutting force for a horizontal cut made with the same cutting conditions will lie in-between the two force profiles in figure 3.21.



**Figure 3.21. Effect of cutting orientation on the cutting force (5A, 0.0167 m/s, XPS).**

While the effect of orientation on the cutting force was detectable the resulting surface textures were very similar. It should be noted that the difference in cutting force detected in the cutting tests represents the worst case scenario. In practice the cutting strategy can be chosen so that the majority of cuts lie in the horizontal plane.

In summary, the effect of cutting orientation on the cutting surface is measurable and should be considered in situations when the cutting tool is cutting in the vertical plane and high accuracy is required. For most situations the effect of cutting orientation will be negligible and can be ignored. The effect is small compared to changing the electrical current or the feed rate.

The rest of the results discussed in this chapter relate to horizontal cutting. The following section links the cutting force with the surface texture.

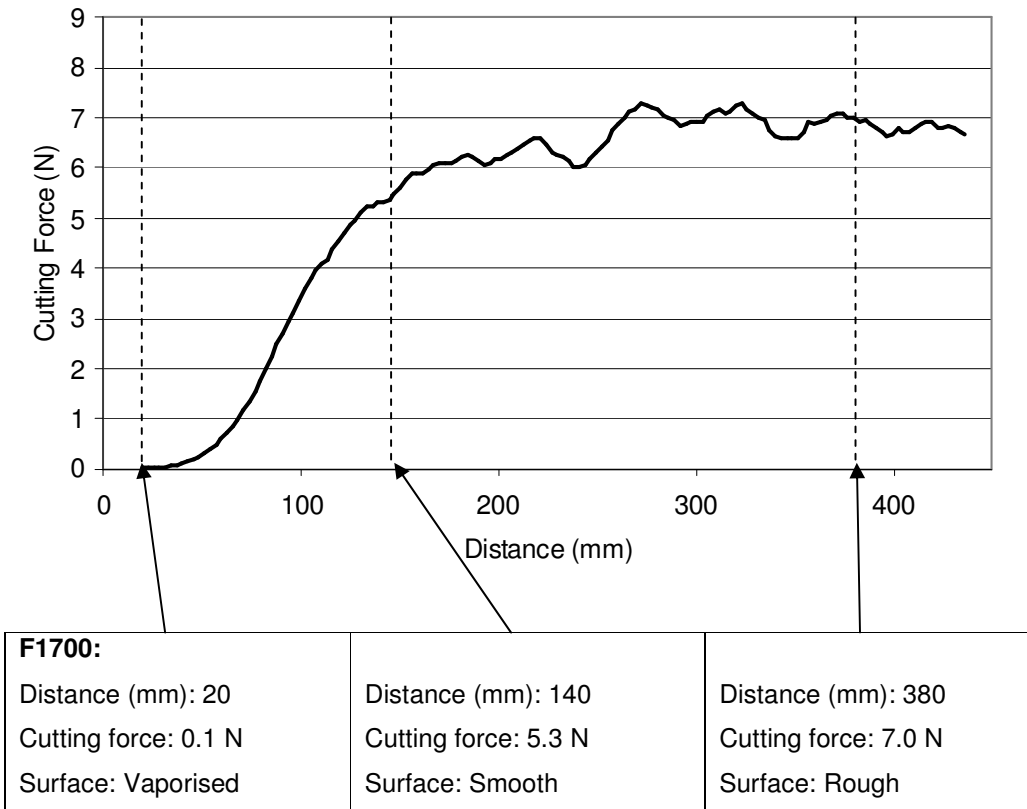
### 3.6.4 Surface Texture

This section describes the relationship between cutting force and surface texture and proposes mechanisms that might explain how the different wire/foam interactions impact on the surface quality.

Most polystyrene foam material removal processes, such as sawing or milling, leave a rough or furry texture on polystyrene as they pull out entire cells or tear them apart. This is acceptable for some conventional plastic foam prototyping or manufacturing processes as they often require

post-processing to finish the product (e.g. sanding or coating with strengthening mesh and stuccoes). However, to be suitable for a wider range of RP&M applications including product design and lost foam casting, hot-wires provide a much smoother surface texture. Under correct cutting conditions hot-wires can obtain very smooth surfaces (Ra values of approximately 25 μm for XPS) which require no further post-processing for most applications. There is very little information on how to quantitatively measure the surface texture and surface form of plastic foams. The main problems are due to the cellular structures, the wide range of roughness values and the softness of the materials. For this reason the descriptions of surface texture in this work are qualitative not quantitative. Ongoing research within the manufacturing group in the University of Canterbury is aimed at addressing this issue.

Figure 3.22 below shows a cutting force profile of a 20 mm wide EPS sample cut with a feed rate of 0.0283 m/s and 5A electrical current. Beneath the graph are stereo-photographs of various sections of the sample surface. As can be seen the surface texture of the sample changes dramatically along the length of the cut.





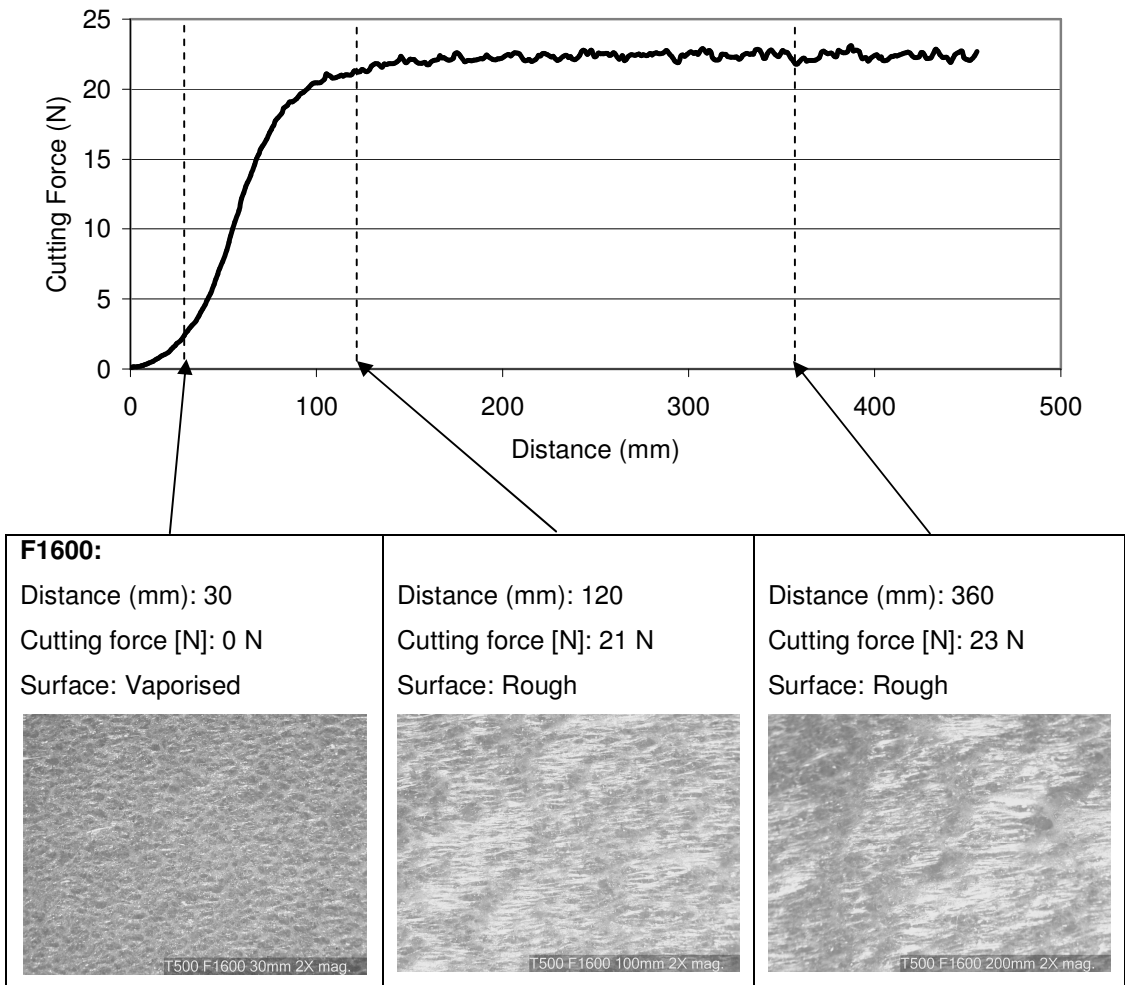
**Figure 3.22. Cutting force/surface finish relationship for S-grade EPS (5A – 0.0283m/s).**

In the leftmost image the cell structure is easily visible due to preferential melting of the cell boundaries. This vaporised surface is caused by pure thermal cutting where the heat from the wire is sufficient to ‘melt’ the plastic without contacting it. The middle image shows a much smoother surface. Upon closer inspection it is possible to see plastic filaments smeared across the surface. These filaments fill in any cracks in the cell boundaries and provide the smoothest possible surface. The rightmost image is visually very bumpy due the high cutting forces causing the wire to oscillate in a path of least resistance through the foam.

Excessively high cutting forces result in rough surfaces. Obviously it is desirable to avoid the rough surface at all times; not only because of the high Ra value and poor geometric form, but also because the hot-wire has a high chance of failure. The vaporised surface is most suited to roughing cuts or when a smooth surface texture is not critical because it is relatively easy to produce and keeps the cutting forces low. The smooth surface is most desirable for applications where low surface roughness is important, such as lost foam casting patterns. To achieve the smooth surface a low non-zero cutting force must be maintained; this requires a delicate combination of heating and shearing of the plastic.

Similar effects are seen with XPS but on a much smaller scale. Because XPS is not made with pre-expanded beads it is much more homogeneous and the cells are much smaller. Figure 3.23 below shows a force profile of a 30 mm XPS sample cut with a feed rate of 0.0267 m/s and an electrical current of 7A. As can be seen the high equilibrium cutting force in this cut resulted in a rough surface for the majority of the cut.

The vaporised (leftmost) surface has an average roughness on the order of the cell size which is notably smoother than the equivalent surface in EPS. It is also possible to produce a smooth surface finish in XPS similar to the smooth surface described for EPS; however this is harder to achieve than pure thermal cutting (due to the narrow range of parameters for which smooth cutting exists).



**Figure 3.23. Cutting force/surface finish relationship for XPS (7A - 0.0267m/s).**

Table 3.6 summarises the stage III surface textures observed for a wide range of XPS samples. The surface finish of each sample was examined and assigned a label (vaporised, smooth or irregular). Vaporised surfaces are characterised by a textured surface and occur when the wire is very hot. Smooth surfaces are created by thermo-mechanical cutting in which the cutting forces



are low. The irregular surface category encompasses both wavy surfaces and ripped surfaces, caused by wire oscillations and cutting forces over the shear strength of the foam respectively.

High electrical currents and low feed rates result in vaporised surfaces while low currents and high feed rates result in irregular surfaces. Most importantly, it can be seen that the smooth surface exists in a relatively small band that runs diagonally across the range of parameters. Interestingly the ratio of current to feed rate remains relatively constant over the smooth (green) band. The reason for this will become clear in section 3.6.7.

**Table 3.6. Qualitative summary of XPS surface textures for a range of feed rates and currents cut with a 0.64 mm diameter Nichrome wire.**

Styrofoam, 30kg/m <sup>3</sup> (XPS)					
Feed rate (mm/min)	Amps (A)				
	4	5	6	7	8
300	Smooth	Vaporised	Vaporised	Vaporised	Vaporised
400	Smooth	Vaporised	Vaporised	Vaporised	Vaporised
500	Smooth	Smooth	Vaporised	Vaporised	Vaporised
600	Irregular	Smooth	Vaporised	Vaporised	Vaporised
700	Irregular	Smooth	Vaporised	Vaporised	Vaporised
800	Irregular	Smooth	Smooth	Vaporised	Vaporised
900	Irregular	Irregular	Smooth	Smooth	Vaporised
1000	Irregular	Irregular	Smooth	Smooth	Vaporised
1100	Irregular	Irregular	Irregular	Smooth	Vaporised
1200	Irregular	Irregular	Irregular	Smooth	Smooth
1300	Irregular	Irregular	Irregular	Smooth	Smooth
1400	Irregular	Irregular	Irregular	Irregular	Smooth
1500	Irregular	Irregular	Irregular	Irregular	Smooth
1600	Irregular	Irregular	Irregular	Irregular	Smooth
1700	Irregular	Irregular	Irregular	Irregular	Irregular
1800	Irregular	Irregular	Irregular	Irregular	Irregular

For more hot-wire cutting tables showing the relationship between surface texture, current and feed rate for S and VH grade EPS see appendix F.

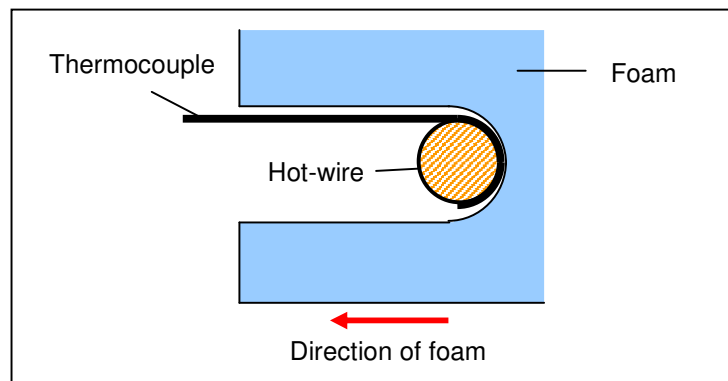
### 3.6.5 Wire Temperature

The characteristic cutting force profiles of previous sections showed that the cutting forces changed over time until equilibrium was reached even though the electrical power stayed constant. This fact suggests that the cutting force is more directly related to the wire temperature and not necessary the electrical power. Measuring the temperature of a hot cutting tool

throughout a cut proved critical to verifying the underlying cutting mechanisms and also to help devise an effective temperature control strategy.

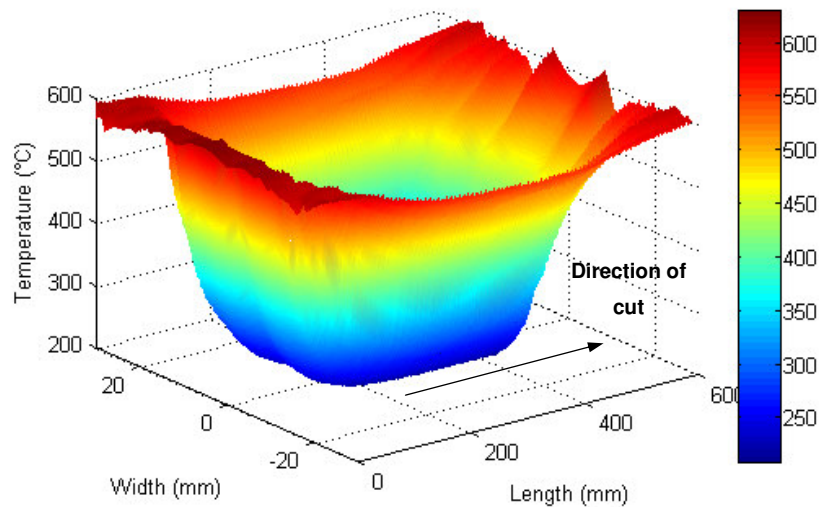
### Thermocouple Measurement

As mentioned in section 3.4.3.2 finding an accurate method of measuring the temperature of the hot-wire proved difficult. In the early stages of research the general experimental procedure outlined in section 3.5 was used. A small thermocouple was used to hook onto the wire and directly measure the temperature in the cutting zone (figure 3.24). Obviously this method of measurement has many disadvantages (such as the thermocouple acting as a heat sink and impacting the local surface) however due to the low cost, simple operational use and real time results able to be obtained, it was still a valuable tool.



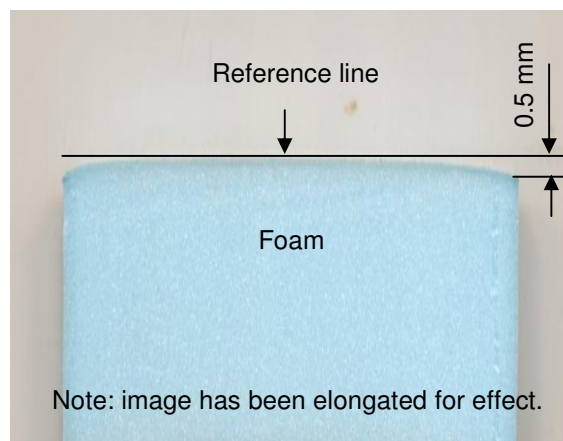
**Figure 3.24. Position of the thermocouple on the hot-wire during cutting.**

Using the thermocouple configuration shown above, an experiment was planned that provided a map of the temperature distribution along the length of the wire over time. The thermocouple was attached to the stationary wire and the foam sample was traversed across the wire with constant velocity. After each run the foam was returned to the start position and incrementally moved along the wire 1 mm, before starting the next cut. The temperature versus distance data for all the runs were compiled to create a single 3D graph (figure 3.25). The figure not only represents the dynamic temperature gradients along the wire, but also reveals the thermal history of the wire as a complete cut is made, from workpiece penetration to exiting. Surprisingly, for the applied conditions, the wire temperature decreased from the nominal 'free air' temperature of 600 °C to a stable 'in cut' temperature of around 250 °C before exiting the foam. It is this stable, minimum temperature that is critical to the cut surface texture and accuracy in stage III cutting.



**Figure 3.25. 3D image of wire temperature during the cutting process (XPS, 1100mm/min, 7A).**

The transverse temperature profile revealed the degree to which foam on the edge of the sample experienced higher temperatures. For the case shown, the very edge of the foam experienced wire temperatures 60°C hotter than in the middle of the cut. This gradient can have an undesirable effect on the surface form of the cut sample. Figure 3.26 shows the cross sectional form of a sample cut with the same cutting parameters as detailed above. The sample was carefully cut with a knife to create a thin cross section which was scanned on a flat bed scanner.



**Figure 3.26. Thin slice of foam sample showing the cross-sectional surface form (XPS, 7A, 1100mm/min).**

The thermal gradient in the wire at the edge of the sample clearly has a barrelling effect on the foam surface with the centre of the sample raised almost half a millimetre from the edge. This barrelling effect is amplified with higher power inputs and higher feed rates due to the greater temperature difference between the wire in free air and the wire in the cut.

### Thermal Imaging Camera

A thermal imaging camera was used to verify the thermocouple temperature measurements and to determine the transient temperature profile of the hot-wire over the length of a cut. Figure 3.27 below shows a typical image of the hot-wire during a cut. The temperature range is between 300 and 890 °C. The figure shows the stationary wire with the foam moving from left to right and out of the page. The temperature profile along the centre of the wire is determined by drawing a straight line over the wire in the temperature analysis software Quickreport and exporting this information to Excel. An average of six images were taken at different positions along each 300 mm long cut.

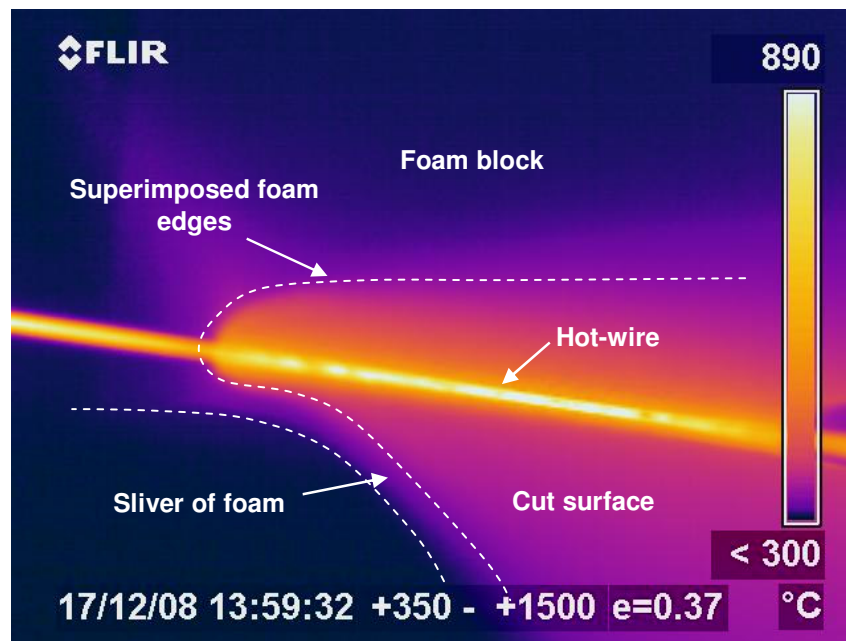
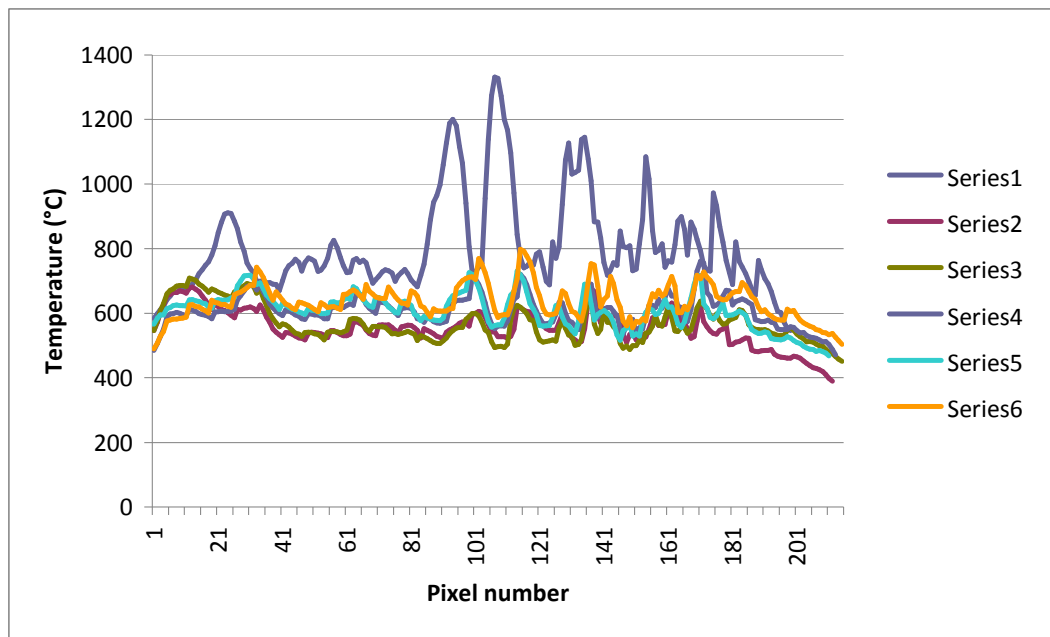


Figure 3.27. S65 thermal camera image of hot-wire cutting (XPS, 8A, F0.0150).

Figure 3.28 shows the temperature profiles generated from the group of images from which the above image was taken. The different series represent successive images in time. As is expected series 1 is warmer as the wire has not yet had time to cool down. Series 2 to 4 show that the wire has cooled to a stable temperature. In series 5 and 6 the wire is exiting the foam and starting to warm up again. The average temperature of the wire during stable stage III cutting is 530 °C. The variation in temperature along the wire length is due to differences in emissivity. Small amounts of pyrolysed PS in the form of a fine ash powder, is sometimes left on the wire after a cut has been made. That is why the various peaks and troughs in the different temperature profiles are in phase. The nominal wire temperature was defined as the average temperature over the length of the wire engaged in the cut.



**Figure 3.28. Wire temperature profiles recorded with the thermal imaging camera (XPS, 8A, F0.0150).**

To verify the thermocouple readings an individual experiment was carried out which directly compared the thermocouple readings with the measurements from the thermal imaging camera. The experiment compared free air wire temperatures between 100°C and 900°C in 100°C intervals. The thermocouple could only measure the local wire temperature while the camera simultaneously measured the temperature of the wire away from the thermocouple and the thermocouple itself. Figure 3.29 shows the thermal image of the wire and the thermocouple with the temperature readings. As can be seen the thermocouple is cooler than the rest of the wire.

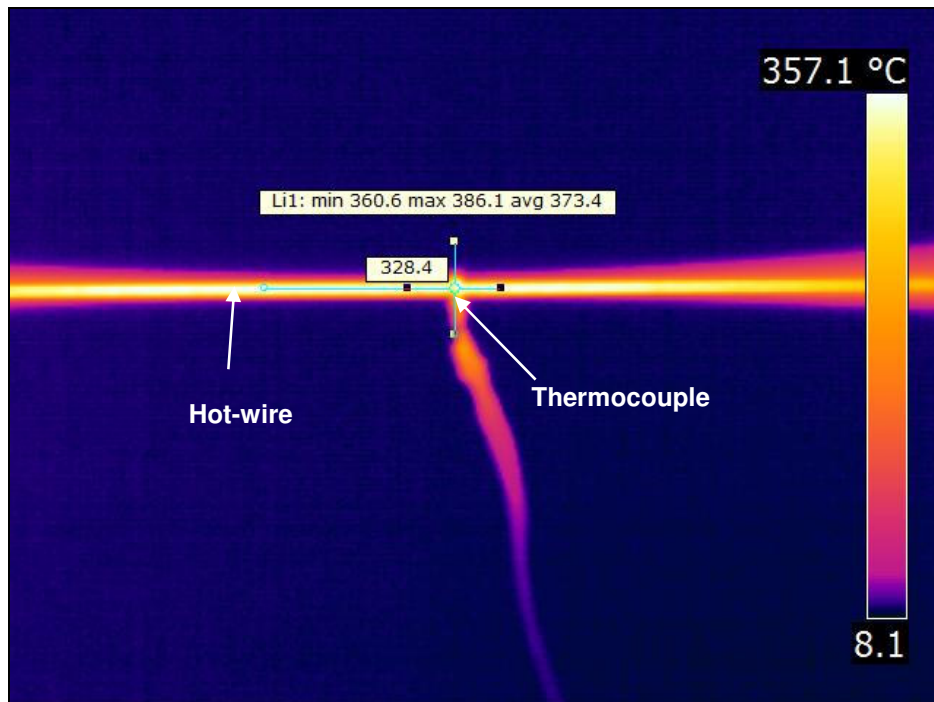


Figure 3.29. Thermal image of the hot-wire and thermocouple in free air.

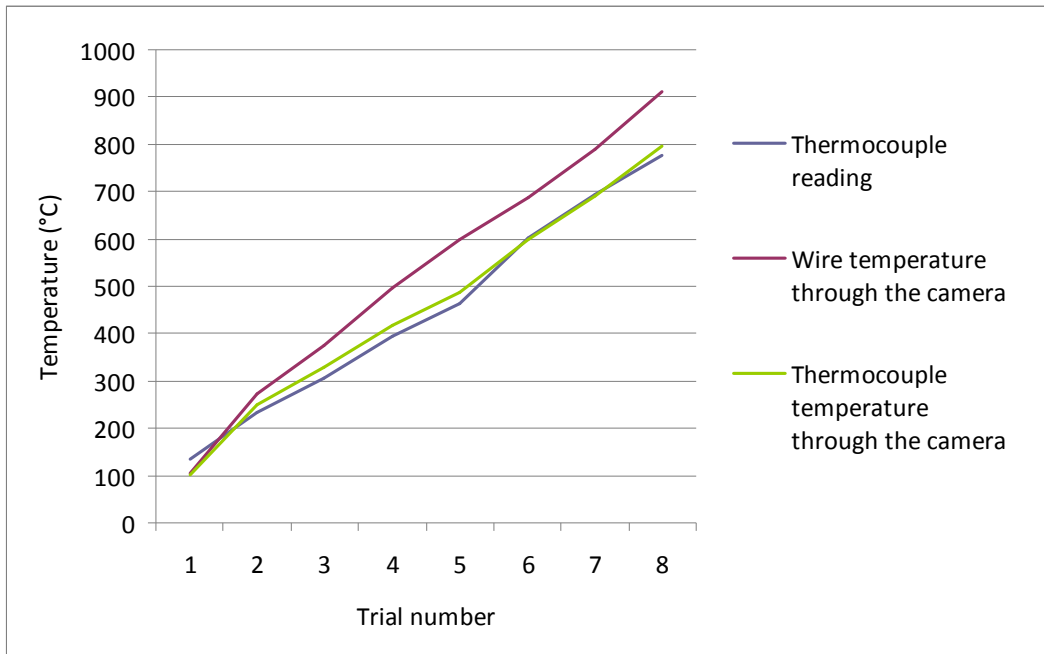
The results of this experiment are shown in figure 3.30. The thermal imaging camera records a higher wire temperature than the thermocouple. This proves the initial assumption that the thermocouple acts as a heat sink and therefore records lower than expected wire temperatures. The thermocouple reading and the temperature of the thermocouple as seen by the camera were essentially identical; proving the camera and the thermocouple were well calibrated. The difference in wire temperature between points on the wire away from the thermocouple and in contact with the thermocouple varies almost linearly with temperature; therefore, applying a temperature dependant offset to thermocouple measurements is a valid temperature correction strategy. The correction formula is as follows:

$$T_{wire} = 1.16 \times T_{Thermocouple} - 3.75 \quad \text{Eq. (3.1)}$$

Where:

$T_{wire}$  = the correct wire temperature

$T_{Thermocouple}$  = the temperature measured by the thermocouple

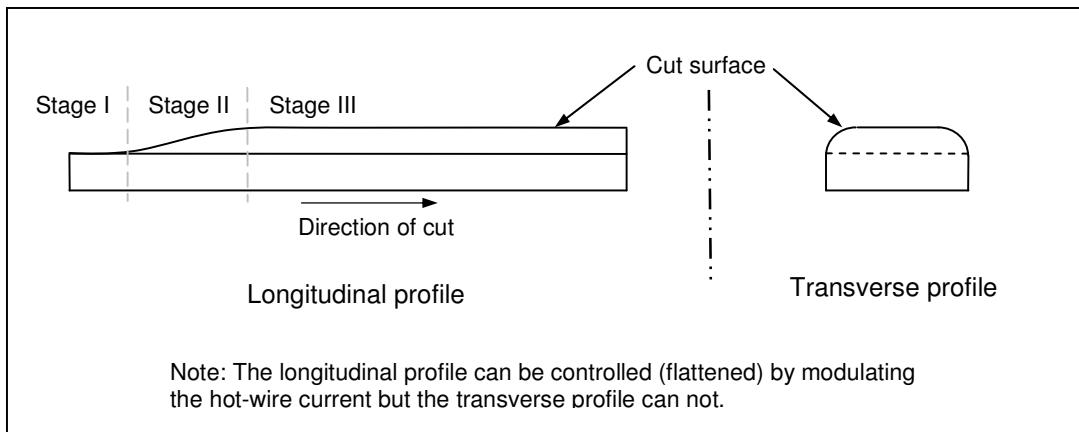


**Figure 3.30. Comparison of the different temperature readings from the thermal imaging camera and the thermocouple.**

The next section describes how the kerf was measured and relates the wire temperature with the kerf width.

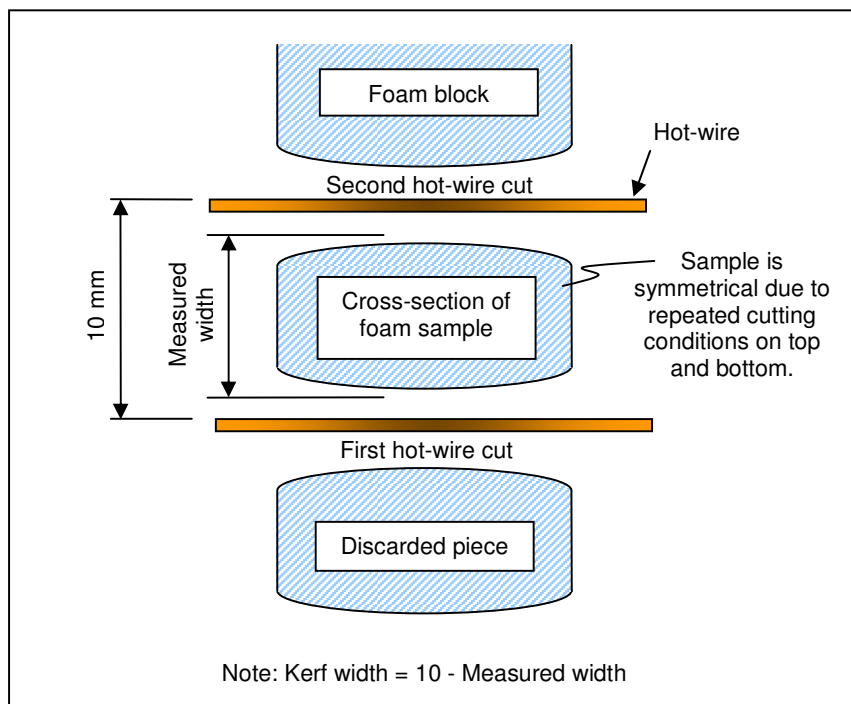
### 3.6.6 Kerf width

Kerf is a common manufacturing term describing the gap created behind a cutting tool. In plastic foam cutting (PFC) the kerf width varies depending on the material being cut, the temperature of the wire, the speed of the cut and the shape of the cutting tool. Because of the wide range of cutting mechanisms present in hot-wire PFC, from vaporisation to ripping, the kerf width was found to vary between approximately 1.4 and 6 times the diameter of the 0.64 mm wire. To ensure the location of the cut surface is accurate the kerf width must be known in advance and compensated for. The kerf width is directly related to the wire temperature, therefore if the wire temperature changes over the length of the cut and along the wire, the kerf will also vary longitudinally and transversely. Figure 3.31 shows the longitudinal and transverse kerf variations found with constant current cutting.



**Figure 3.31. Longitudinal and transverse kerf variations.**

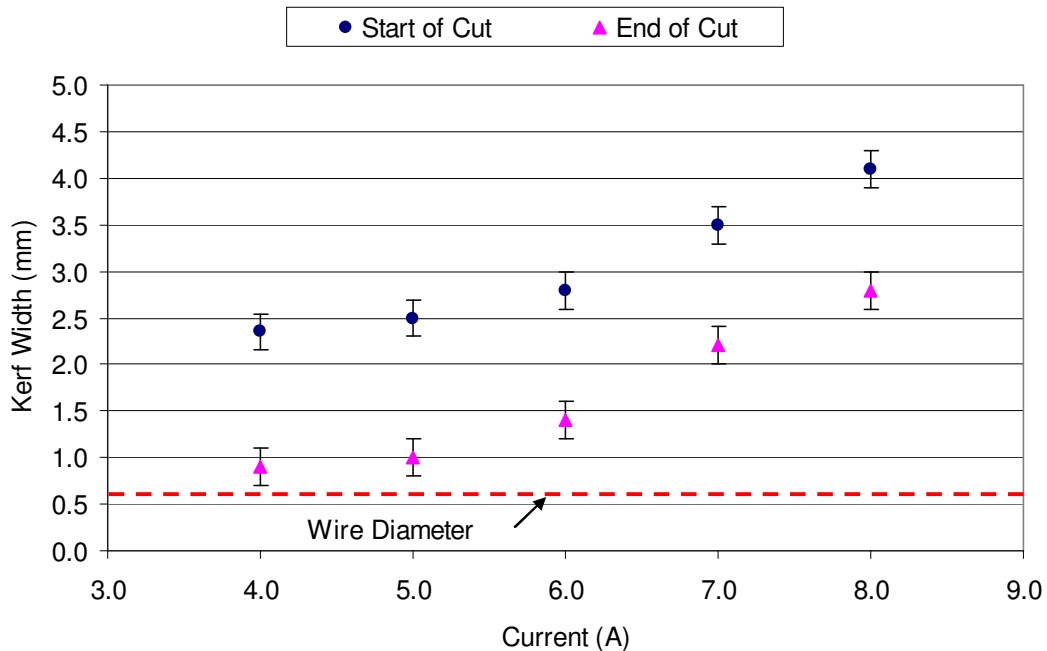
To measure how the longitudinal kerf width profile changes with different power inputs, a range of 30 mm wide EPS and XPS samples were cut changing the current and feed rate each time. Each sample was created by making two successive cuts separated by 10 mm using the same cutting conditions each time. In this way the kerf width could be measured by subtracting the measured sample thickness from the known wire offset of 10 mm. This experiment was carried out for wire diameters of 0.36, 0.64 and 0.91 mm. The samples were measured across the centres of the foam samples to negate any edge effects of the hot-wire, as shown in figure 3.32.



**Figure 3.32. Measurement strategy for determining kerfwidth of hotwire cutting.**

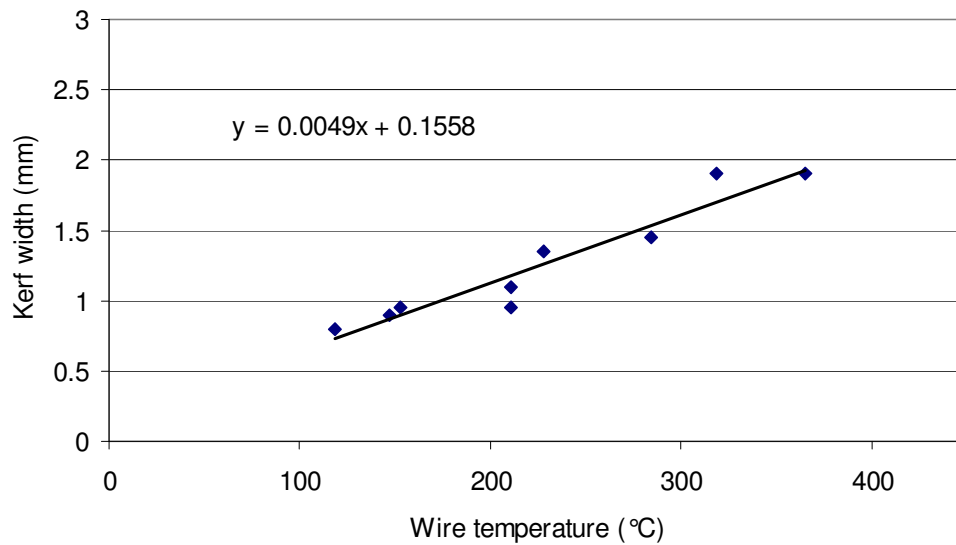


The results are plotted in figure 3.33 for XPS samples cut with a feed rate of 0.0150 m/s and varying constant currents. The kerf width was found to change as the cut progressed. The two different data points for each current represent the kerf at the start of the cut and at the end of the cut, 0 mm and 300 mm respectively. The kerf width is constant after approximately 100 mm and therefore the kerf width at the end of the cut may be considered the steady-state value. The kerf is always much larger at the start of the cut due to the initial high wire temperatures. For low power inputs the kerf width approaches the diameter of the hot-wire; however this usually results in high cutting forces and poor surface textures. Another reason (separate from surface texture) why temperature control is needed is because it is much easier to apply an offline constant tool offset to cancel out the effect of kerf, than to apply an online temperature dependant offset.



**Figure 3.33. Kerfwidth vs. current for XPS cut at 0.0150m/s at two different positions along the sample length.**

Plotting the steady state or stage III kerf width against the corresponding wire temperatures reveals a linear relationship as shown in figure 3.34. The wire temperature is a function of electrical power input, feed rate and material properties and is therefore difficult to calculate from first principles. The linear kerf width versus wire temperature relationships were used to provide temperature inputs to the finite element models developed in later chapters, which would be difficult to determine any other way.



**Figure 3.34. Kerfwidth vs. wire temperature for EPS foam cut with a 0.64 mm diameter Nichrome wire.**

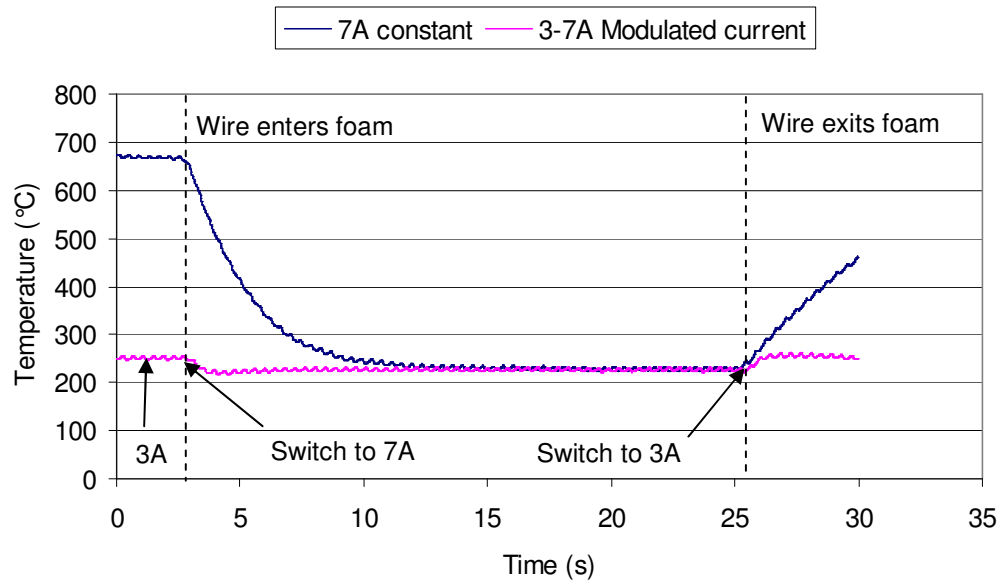
The following section describes a preliminary attempt at controlling the wire temperature to achieve constant cutting conditions.

### 3.6.7 Temperature Control

While the temperature gradients along a straight wire are largely unavoidable, the electrical power input can be controlled to produce a consistent wire temperature profile over time. Maintaining a constant temperature profile throughout a cut means the wire will be in thermal equilibrium and thus a desirable surface may be produced for the entire length of the cut.

When using a constant current it was apparent that the wire temperature was always hotter in free air than in a cut. It is then logical to assume that to obtain a constant wire temperature the current in free air and in the cut would have to be different. A search through the hot-wire temperature data revealed a number of in cut and free air currents that resulted in identical wire temperatures. For example, the equilibrium wire temperature inside a cut (XPS, 0.0183m/s), using 7A, was approximately the same as the wire temperature in free air using 3A. This relative equivalence led to a cutting test in which the current was switched between 3A in free air and 7A in the cut to maintain a constant wire temperature. The results shown in figure 3.35 reveal the difference in wire temperature using thermocouple temperature measurement with constant and adaptive current. The temperature of the constant current cut started at 680°C and fell to 250°C over 10 seconds. If the hot-wire had a larger diameter the time to reach thermal equilibrium for the constant current cut would be even longer; this is certainly the case for hot-ribbons. The

temperature of the modulated current cut stayed approximately constant at 250°C in both free air and whilst cutting.



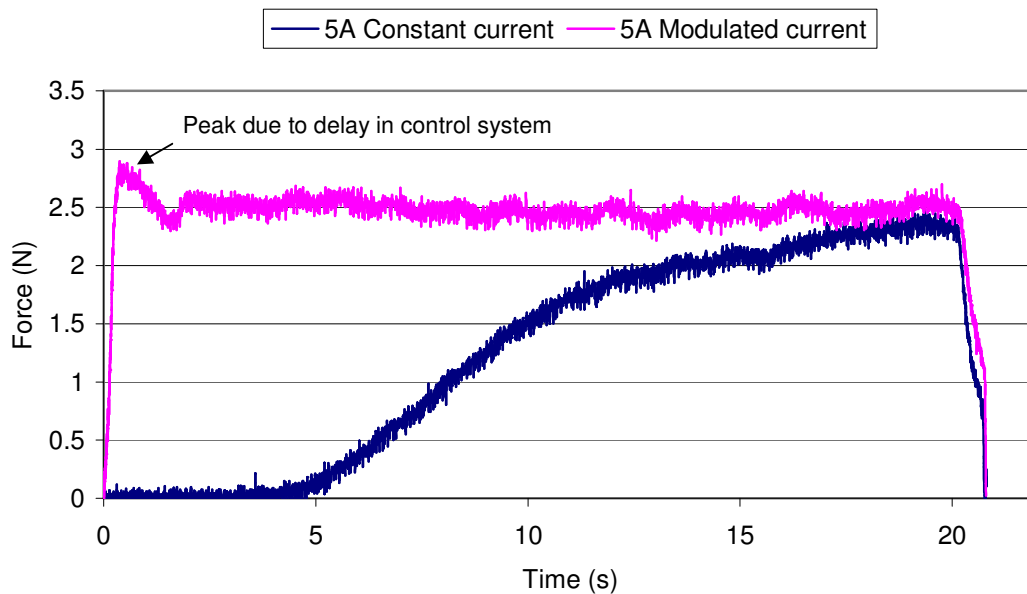
**Figure 3.35.** Shows the wire temperature in the cut with and without temperature control (XPS, 0.0183m/s).

The success of the simple test carried out above led to the development of a simple control system which automatically changes the electrical power based on the real time cutting force. The DAQ software was altered to allow the current duty cycle to change depending on preset cutting force values. The load cell measures both the magnitude and direction of any applied loads and the software uses the calibrated absolute force readings to allow bidirectional controlled cutting. Figure 3.36 shows the user form used to enter the parameters which control the cutting. Minimum and maximum cutting force thresholds go in the left-hand side while the different duty cycles go in the right-hand side. At this stage prior experimental experience was required to choose the 'free air' and 'in cut' duty cycles that keep the wire temperature constant. In the future FEA simulations could provide a means to predict the required values without the need for extensive cutting trials.

Control Method 5		
Min	.05	9 %
Max	.06	50 %
	Load	PWM
Update		

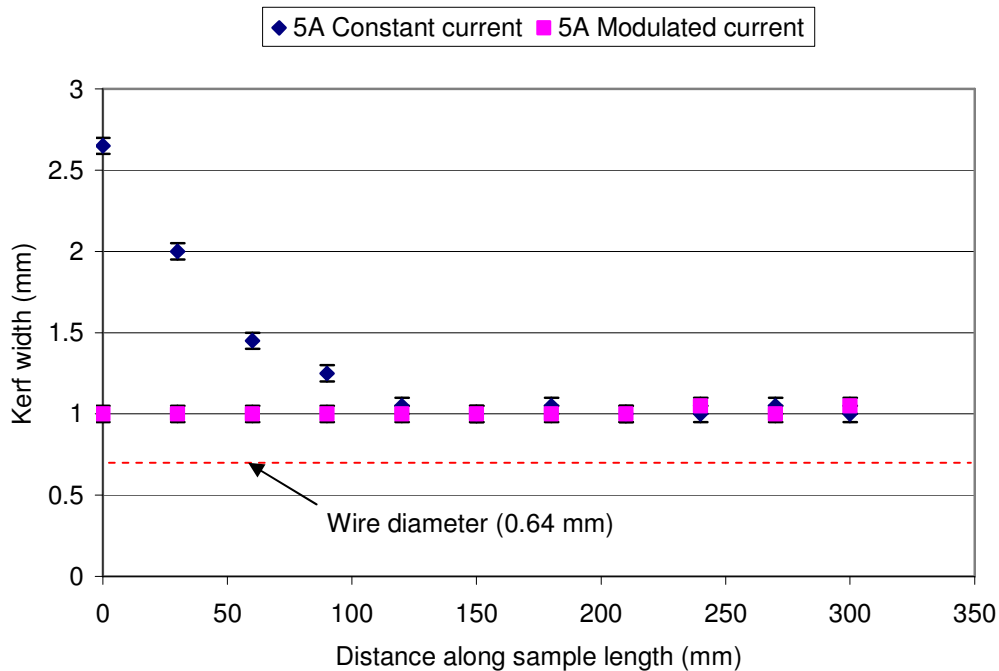
**Figure 3.36.** Part of the DAQ user form used to adjust the force feed-back wire temperature control.

To evaluate the success of the force feed-back control system the cutting force was measured for a range of cuts for which the wire temperature was controlled and these were compared against identical cuts in which the input power remained constant. Figure 3.37 below shows the cutting force profiles of two XPS samples with a feed rate of 0.0150m/s and a nominal current of 5A. The temperature control strategy was very effective in providing a constant cutting force over the length of the cut compared with the constant current sample. The small peak in cutting force at the start of the cut of the controlled sample is due to a slight delay in the response of the control system.



**Figure 3.37. Force profiles of constant and modulated current cuts (XPS, 0.0150m/s).**

The aim of the temperature control system was to produce constant cutting conditions from the time the wire first entered the foam until it exited, to ensure consistent surface textures and kerf widths. Figure 3.38 shows the kerf width of the same two samples used for figure 3.37 as measured at 30 mm intervals along the samples lengths. The kerf width measurement strategy is explained in the previous section. As can be seen the kerf width of the cut made with constant current varies by over 1.5 mm compared with the controlled cut which varies by only 0.1 mm. Achieving a high level of dimensional and geometrical accuracy of a cut surface is highly desirable and is much easier to obtain with constant kerf widths.



**Figure 3.38. Kerf width of hot-wire with and without force feedback temperature control (XPS, 0.0150m/s).**

These results confirm that force feedback temperature control of hot-wire cutting can be used successfully to provide surfaces with constant surface texture and kerf width. In practice there are a number of barriers to be overcome in order to implement this temperature control strategy in realistic 3D sculpting operations:

1. The effective length of the cutting tool interacting with the foam will vary depending on its location on the tool path. This means that the cutting force will constantly change even if the cutting conditions do not. This could make it hard to choose appropriate 'trigger' loads.
2. If the cutting tool is mounted on the robot (which is the most practical place as it maximises the sculpting area) the load cell will pick up inertial forces which will impair the cutting force readings.
3. A variety of different cutting tools may be used in the transition from roughing to finishing and for specialist surface textures. Each cutting tool will have a different electrical resistance and the cutting forces can be expected to change significantly. This means different power settings will be required for each cutting tool configuration.

Further cutting tool development is required to overcome these shortfalls. One possible alternative solution is to predetermine the modulated power input so that the high and low power

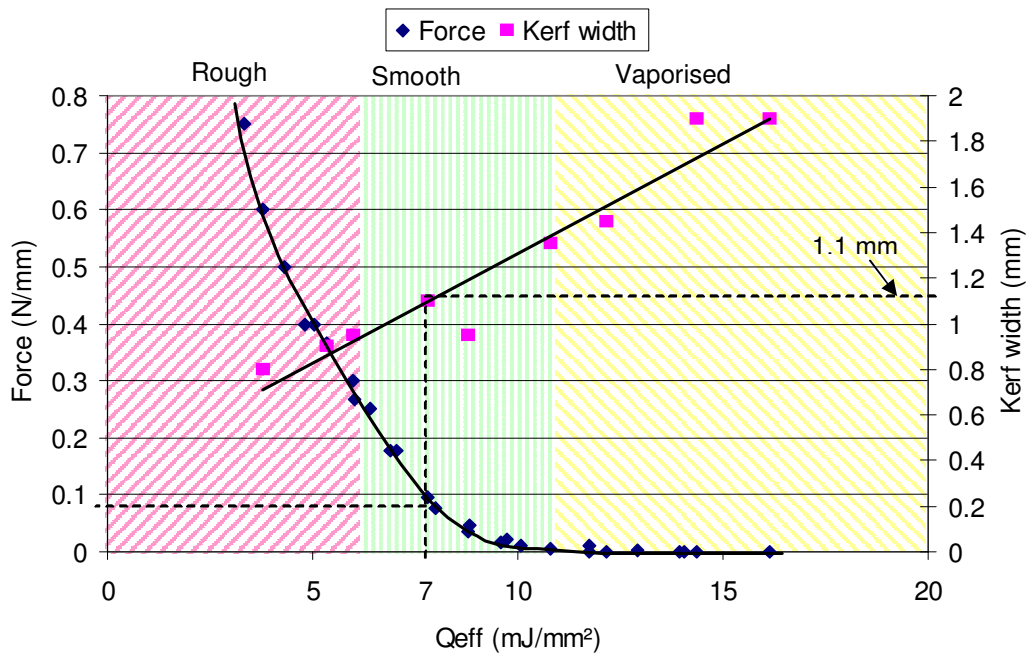
settings coincide with the tool path simulation. In this way the power settings for 'free air' and 'in cut' modes can be predetermined in an offline simulation. The challenge with this control strategy is to accurately predict the wire temperatures and match the timing of the cutting tool power supply with that of the robot movements and the foam blank geometry; however this could be done by integrating the wire temperature control model with the tool path generation software. This type of control strategy is analogous to CNC milling where the spindle speed, cutting depth or feed rate are predicted (based on cutting tool and material definitions) in place of the wire temperature.

Mastercam is a popular machining package that allows intelligent feed rate optimisation to increase machining efficiency [22]. Mastercam allows the user to define the machine characteristics as well as tool and material libraries so that the software can automatically calculate tool specific feed rates and spindle speeds (see appendix F). In much the same way models relating the kerf width, wire temperature and cutting force could be combined with tool and material libraries to automatically calculate hot-tool feed rates, surface offsets and power inputs to maximise cutting speed or minimise power use.

The following section describes the relationship between the area specific effective heat input (as described by Ahn et al), kerf width and cutting force, and explains how the effective heat input theory can be extended much further to provide a powerful mathematical model.

### 3.6.8 Effective Heat Input

The area specific effective heat input,  $Q_{eff}$ , is calculated by dividing the electrical power input by the feed rate and has units  $J/m^2$  (section 2.3.1.1). Physically this value represents the amount of electrical/thermal energy used to create a unit area of cut surface. It is a very useful parameter as it allows a wide range of cutting data to be presented on a single graph. Ahn et al used  $Q_{eff}$  to observe how the kerf width changes with energy input, however much more information can be gained if the cutting force is also plotted on a secondary axis. Figure 3.39 shows the relationship between cutting force per unit length of wire and kerf width against the effective heat input for VH grade EPS.



**Figure 3.39. Force and kerfwidth vs. effective heat input for VH Grade EPS.**

The force data follows an exponential decay or ‘elbow’ pattern across the range of  $Q_{eff}$ . This ‘elbow’ represents a change from one dominant cutting mode to another; the high forces on the left (red region) represent thermomechanical cutting while the almost nonexistent forces on the right (yellow region) represent pure thermal cutting. The kink in the elbow as represented by the green region represents smooth cutting conditions as described in section 3.6.3. The kerf width varies linearly over the experimental range of parameters despite the fact the range of cutting conditions included both high force, low power thermomechanical cutting, as well as low force, high power pure thermal cutting.

It is not hard to see how the cutting data displayed in the above graph can be used to predict the surface texture and kerfwidth of future cuts (assuming the same material and wire diameter are used). For example, to obtain a smooth surface in VH-grade EPS a small non-zero cutting force is required, this relates to an effective heat input of approximately 7 mJ/mm<sup>2</sup> (as shown by the dotted line). This also correlates to a kerfwidth of 1.1 mm, which can then be used to determine the wire offset needed to negate the effects of kerf on the dimensional accuracy of the surface. In this case the wire offset would be 0.55 mm (half of 1.1 mm).

### The Volume Specific Effective Heat Input

The concept of unifying the power and the feed rate to represent the amount of energy used to create a cut surface can be taken one step further. Dividing the area specific effective heat input,  $Q_{eff}$ , by the corresponding kerf width produces the volume specific effective heat input (Eq. 3.2).

$${}^{Vol}Q_{eff} = \frac{Q_{eff}}{\lambda} \quad (\text{Eq. 3.2})$$

Where:

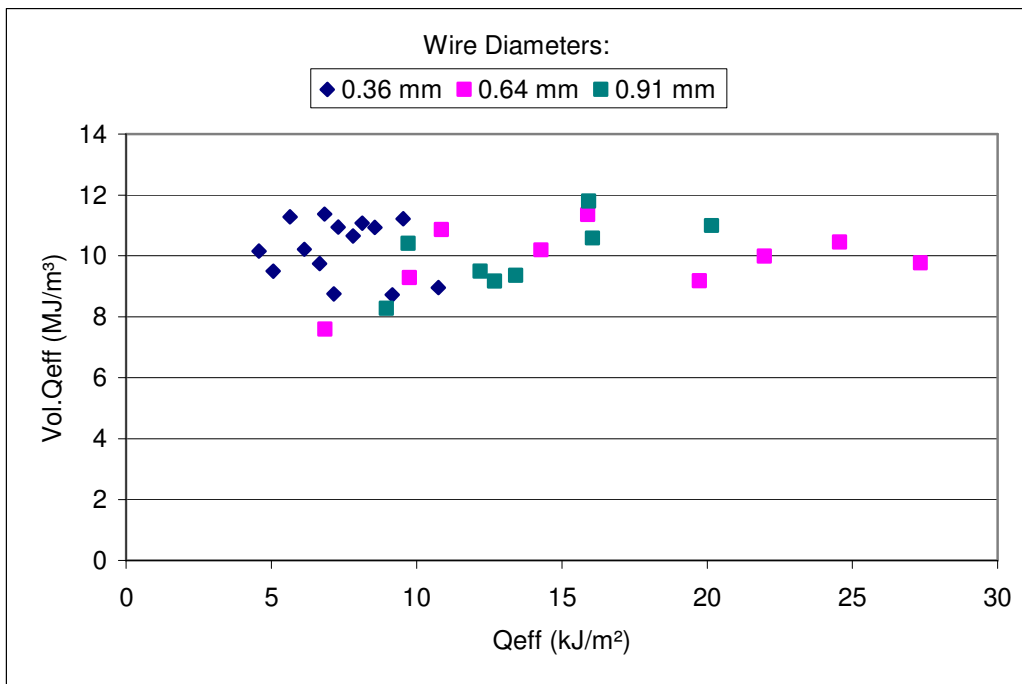
$Q_{eff}$  = the area specific effective heat input in J/m<sup>2</sup>

$\lambda$  = kerf width in m

The volume specific effective heat input,  ${}^{Vol}Q_{eff}$ , physically represents the amount of electrical/heat energy needed to 'melt' a unit volume of foam and has the dimensions J/m<sup>3</sup>. In this situation the term 'melt' is used to express the process by which the foam near the wire reduces in volume (not necessarily actual melting). This value will not be found in previous literature; it is a function of the temperature dependant foam material properties, the cutting tool geometry, heat transfer characteristics and is almost impossible to determine from first principles.

Figure 3.40 below shows the volume specific effective heat input for XPS with different wire diameters plotted against the area specific effective heat input. It is clearly evident that all of the cuts have the same  ${}^{Vol}Q_{eff}$  value (within the experimental errors) independent of the  $Q_{eff}$  and the diameter of the wire. The average  ${}^{Vol}Q_{eff}$  value over the entire XPS hot-wire cutting trials was found to be 10.1 MJ/m<sup>3</sup> with a standard deviation of 10%. The corresponding value for EPS is 7.71 MJ/m<sup>3</sup> with a standard deviation of 10%.





**Figure 3.40. Volumetric effective heat input for XPS cuts with different wire diameters.**

The first point to note is that the energy required to create a unit volume of kerf in XPS or EPS with a hot-wire is constant (within the experimental range of parameters). The second point to note is that this is true regardless of what wire is used (i.e. it is independent of wire size and material). The third point is once the  $^{Vol} Q_{eff}$  value is known for a given plastic foam material, it is possible to calculate the kerf width for any wire, feed rate and power input combination within a practical range of parameters. To demonstrate the usefulness of this fact, consider the following scenario:

*A CNC foam cutting operator is required to cut a block of XPS foam with high dimensional accuracy. Before the cut is made the operator must decide what electric current and feed rate to use and what the resulting kerf width will be. The operator can then set a wire offset to counter the effect of the kerf and achieve the desired block dimensions without trial and error. If, for example the foam cutting machine was fitted with a 0.36 mm diameter Nichrome wire (with a resistance of 10.58  $\Omega/m$ ), and the operator chose a current of 3A and a feed rate of 0.0150 m/s, the kerf width can be calculated from a rearranged version of Eq. 3.2.*

The method for doing this is as follows:

$$^{Vol} Q_{eff} = \frac{Q_{eff}}{\lambda} \quad (\text{Eq. 3.2})$$

$${}^{Vol}Q_{eff} = \frac{Q_l}{v_c} \cdot \frac{1}{\lambda}$$

$${}^{Vol}Q_{eff} = \frac{I^2 \cdot R}{v_c} \cdot \frac{1}{\lambda}$$

Rearranging for  $\lambda$  gives

$$\lambda = \frac{I^2 \cdot R}{v_c} \cdot \frac{1}{{}^{Vol}Q_{eff}} \quad (\text{Eq. 3.3})$$

Substituting the known values provides the solution

$$\underline{\lambda = 0.63mm}$$

In the above example there were three unknowns, the current, the feed rate and the kerf width. The operator chose to fix the current and feed rate and change the wire offset, however the operator could have just as easily fixed the kerf width and calculated the required current or feed rate. If more than one parameter is able to be varied at the operators' discretion, then he/she can simply choose values for all the unknowns except for the one that is most easily controlled.

### The Mass Specific Effective Heat Input

For plastic foams which have identical molecular structures and differ only by density, such as S, H and VH grade EPS, the volume specific effective heat input can be converted into an even more powerful tool by dividing  ${}^{Vol}Q_{eff}$  by the density of the material (Eq. 3.4).

$${}^{Mass}Q_{eff} = \frac{{}^{Vol}Q_{eff}}{\rho_f} \quad (\text{Eq. 3.4})$$

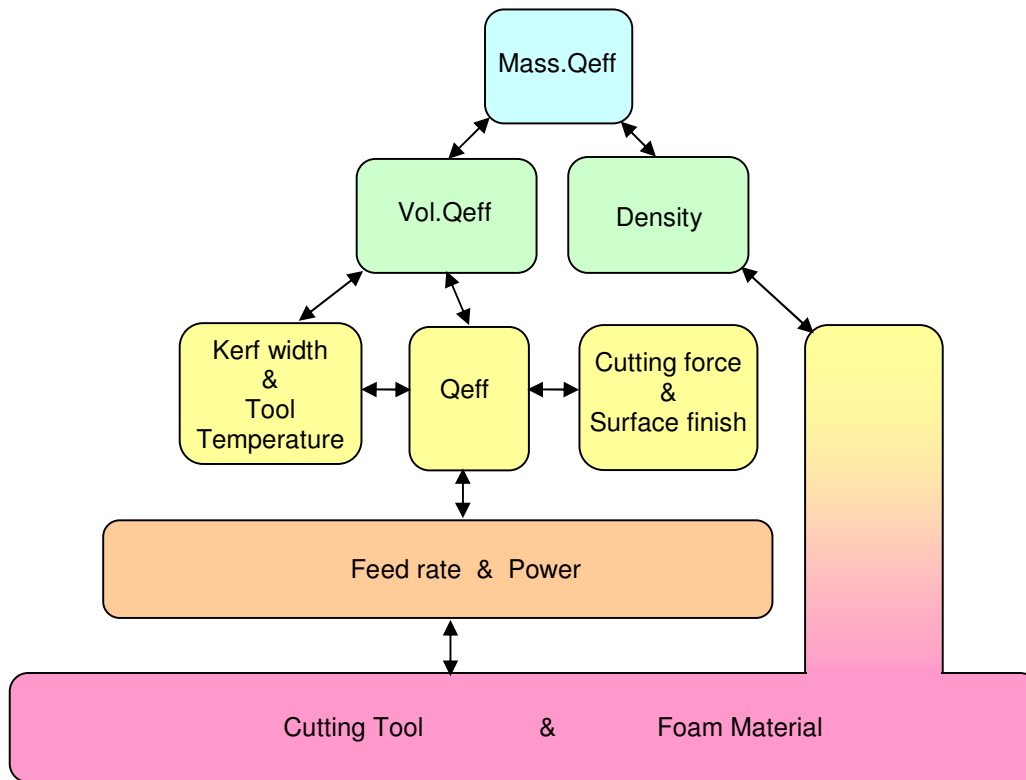
Where:

${}^{Mass}Q_{eff}$  = the mass specific effective heat input

$\rho_f$  = density of the foam.

The mass specific effective heat input is the same for all EPS foams of different densities that have the same molecular structure. It is now possible to carry out the same exercise for EPS as was previously done with XPS, however this time the density of the material can also be a variable. The mass specific heat input now provides the basis for a powerful predictive mathematical model relating all the important parameters in foam cutting i.e. the kerf width, power, feed rate, material and cutting tool.

The  $^{Mass}Q_{eff}$  represents the summation of all the information gained in the cutting trials so far. Figure 3.41 shows the various hot-tool foam cutting parameters studied in the cutting trials and how they relate to each other.



**Figure 3.41. Summary of relationships between foam cutting parameters.**

The primary parameters are the cutting tool and the foam material as they are constants for each cutting trial set. The feed rate and power input are secondary parameters as they can be varied within a permissible range, as limited by the primary parameters. The feed rate and power input determine the area specific effective heat input,  $Q_{eff}$ , which is directly related to the kerf width, and surface finish, which are related to the tool temperature and cutting force respectively. Combining  $Q_{eff}$  and kerf width data produces the volume specific effective heat input,  $^{Vol}Q_{eff}$ . Combining the  $^{Vol}Q_{eff}$  data and material density data leads to the mass specific heat input,  $^{Mass}Q_{eff}$ , which sits at the apex of figure 3.41 and unifies all the parameters into one mathematical model. The reason the density is shown separate from the primary material parameter is because foams of the same molecular structure can have widely varying densities, thus it is useful to keep density as an independent variable.

A hot-tool cutting calculator (HCC) was developed in Excel that allows any of the variables in Eq. 3.3 and 3.4 to be calculated from the other five variables. Technically the HCC can be used for

any plastic foam and hot-wire combination, however finding the right range of parameters, such as wire resistance, an appropriate current range and feed rate does require some expert knowledge. Figure 3.42 shows a screen shot of the HCC with necessary data.

Hot-tool cutting calculator		
Inputs		
<b>Enter 0 for the one unknown</b>		
Mass.Qeff	297000	J/kg
Foam density	15	kg/m <sup>3</sup>
Wire resistance	3.6	ohm/m
Feed rate	0.02133	m/s
Current	6	A
Kerfwidth	0	mm
Outputs		
<b>Answer for the one unknown</b>		
Mass.Qeff	0	J/kg
Foam density	0	kg/m <sup>3</sup>
Wire resistance	0	ohm/m
Feed rate	0	m/s
Current	0	A
Kerfwidth	1.3638497	mm

EPS, XPS and Nichrome data:

Mass.Qeff:  
336000 J/kg for XPS  
297000 J/kg for EPS

Common foam densities:  
15, 26 and 30 kg/m<sup>3</sup> for EPS  
30 kg/m<sup>3</sup> for XPS

Nichrome wire resistances:  
10.5 ohm/m for 0.36 mm diameter  
3.6 ohm/m for 0.64 mm diameter  
1.65 ohm/m for 0.91 mm diameter

Nichrome wire current ranges:  
2.5 - 4.2 A for 0.36 mm  
5.6 - 11.0 A for 0.64 mm  
8.5 - 12.7 A for 0.91 mm

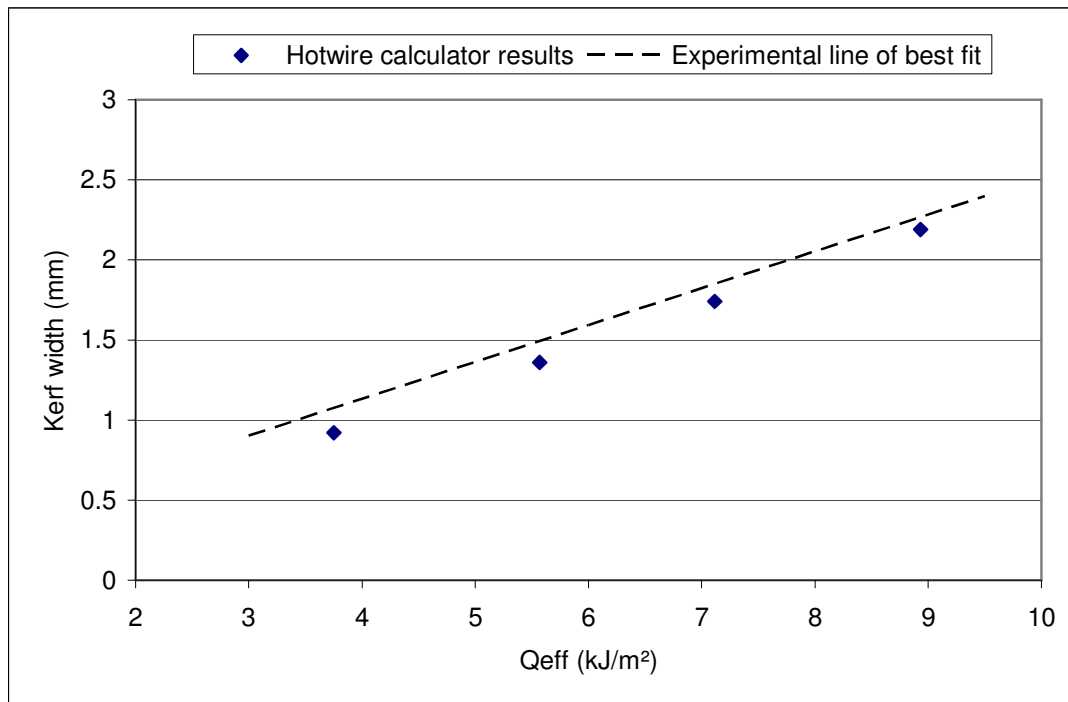
Kerf width ranges:  
0.45 - 1.20 mm for XPS and 0.36 mm wire  
0.90 - 2.35 mm for XPS and 0.64 mm wire  
0.80 - 1.90 mm for EPS and 0.64 mm wire  
0.93 - 1.83 mm for XPS and 0.91 mm wire

**Figure 3.42. Hot-wire cutting calculator and necessary data.**

It is possible to successfully use the HCC without prior knowledge of an appropriate range of feed rates. This can be done by estimating an initial value for the feed rate and iterating until the calculated kerf width is large enough to provide a low non-zero cutting force. Experimental data carried out in the cutting trials showed this occurs when the kerf width is approximately 1.5 times the diameter of the hot-wire or 2.7 times the height of the hot-ribbon.

The  $^{Mass}Q_{eff}$  value of 297 kJ/kg for EPS was calculated using experimental data collected using 26 kg/m<sup>3</sup> EPS. To validate the ability of the HCC to predict the kerf widths of foams with different densities, four calculations were made to predict the kerf width of cuts made with 15 kg/m<sup>3</sup> EPS. This is important because the 15 kg/m<sup>3</sup> kerf width measurements were not used to calculate the  $^{Mass}Q_{eff}$  and therefore provide an independent verification. The calculated kerf widths were then compared with the experimentally found line of best fit. Figure 3.43 below shows that the calculated kerf widths match well with the experimentally determined line of best fit, however there is a constant small negative offset of approximately 0.15 mm. One possible reason for the

slight negative offset is the fact the 15 kg/m<sup>3</sup> EPS was obtained from a different supplier than the 26 kg/m<sup>3</sup> EPS and may have a slightly different composition. Due to the fact there is a 10% standard deviation in the  $^{Mass}Q_{eff}$  values the experimental data is within the error range of the HCC predictions.



**Figure 3.43. Hot-wire calculator results vs. the experimental line of best fit.**

Because the kerf width and wire temperature are linearly related, it is also possible to predict the wire temperature using the HCC and a simple equation relating the kerf width to the wire temperature (figure 3.34). Different foam materials will inevitably yield different kerf width versus hot-wire temperature relationships; however, a database of these relationships could be built into automated tool path generation software similar to Mastercam (appendix G). Figure 3.44 shows how offline automated tool path generation software would work within the FAST system.

Maintaining constant cutting speeds is inefficient because the robot does not have the same maximum speed everywhere in the working volume. This is because each of the robot's six axes have rotational velocity and acceleration limits, which may prevent the tool from reaching its ideal speed. Using the equations embedded in the HCC with the proposed user defined tool and material libraries, automated tool path generation software could reduce cutting time by simultaneously varying the feed rate and power to maintain constant kerf widths and surface texture. This would enable parts to be sculpted faster and more accurately. To the authors' knowledge the mass specific heat input and the mathematical model behind the HCC is a new

development in the understanding of foam cutting mechanics and provides a significant step toward the aim of automated and intelligent sculpting technology.

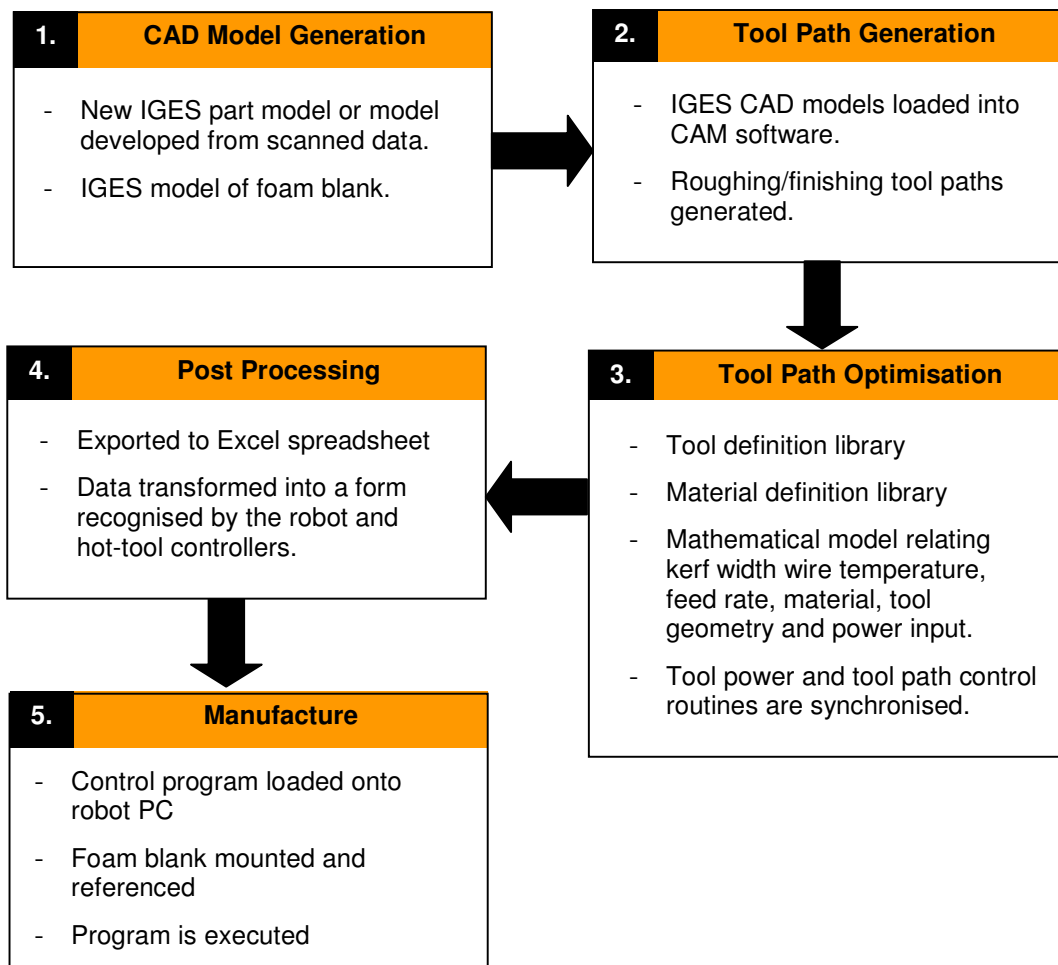


Figure 3.44. Tool path generation and optimisation within the FAST system.

### 3.6.9 Summary

The hot-wire cutting trials carried out in this thesis were extensive. Over 400 individual cuts were made, not including the repeatability, thermal imaging camera and force feed back temperature control tests which were just as numerous. A complete compilation of the cutting data with associated graphs is available in a DVD accompanying this thesis. The cutting trials included two main material sets, EPS and XPS, three different wire diameters and a wide range of feed rates and power inputs. For each cut the cutting force, wire temperature and kerf width were measured as well as observations of the surface texture. The main outcomes of these trials are as follows:

- When using constant current cutting the cutting mechanisms change over the length of the cut. These changes can be described in three unique stages. Stage I is characterised

by low cutting forces. Stage II represents the transition from stage I to stage III. Stage III is characterised by stable relatively high cutting forces.

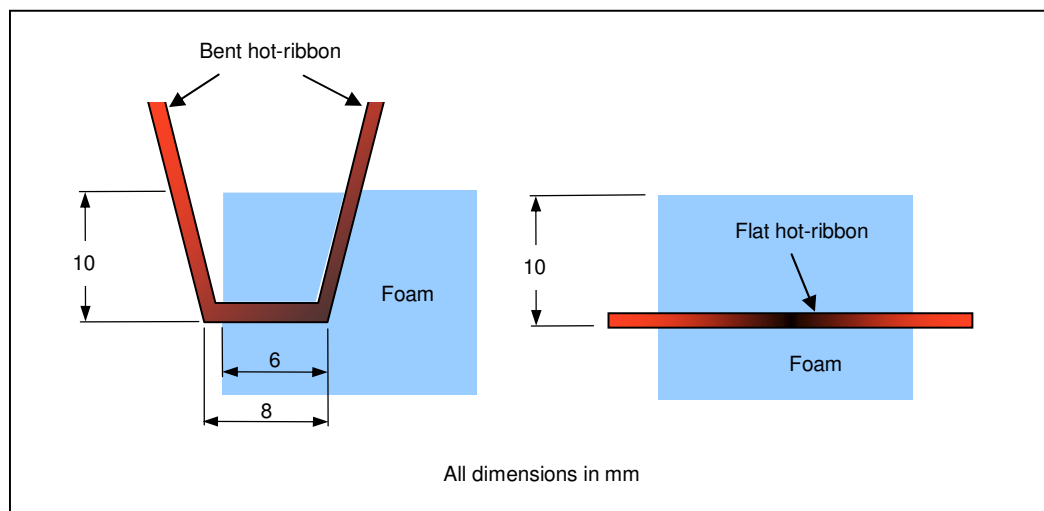
- The surface texture along a sample cut with constant current changes depending on the cutting force present at that position. High cutting forces result in a mechanically ripped or wavy surface. Low non-zero cutting forces provide the smoothest surface as the wire shears the adjacent molten plastic filling in the cell boundaries. When cutting forces are zero the wire is sufficiently hot to melt the foam ahead of the wire resulting in a granular surface texture due to preferential melting at the cell boundaries.
- The wire temperature was measured with thermocouples and a thermal imaging camera and a 3D temperature map of the wire throughout a cut was created. The wire was found to cool as much as 250°C along the length of a cut. Higher wire temperatures at the edges of the cut were found to result in a barrelling effect on the surface of the foam.
- For constant power cutting the kerf width was found to vary between 1.4 to 6 times the diameter of the wire. Not knowing the kerf width could be a serious source of error when sculpting 3D objects.
- A method of controlling the wire temperature throughout a cut was developed which used force feedback to modulate the electrical power. It was successful in creating constant cutting conditions and therefore enabled cuts to be made with constant kerf widths and surface textures along the cut.
- New parameters were developed called the volume specific effective heat input and the mass specific effective heat input, which, once obtained, can be used to predict the kerf width that will result from using any foam/wire combination.
- A hot-tool cutting calculator (HCC) was developed utilising the mass effective heat input to provide an effortless way to predict the cutting conditions for a previously untested range of cutting conditions. The HCC can also be used to calculate the mass effective heat input from experimental data.
- A method of incorporating the equations embedded in the HCC into CAM software was suggested which could greatly increase the speed, accuracy and utility of automated sculpting technology.

### 3.7 Hot-ribbon Cutting Trials

This section contains results gathered during the hot-ribbon cutting trials. The general experimental method (section 3.5) was used for all of the hot-ribbon cutting trials with slight modifications for temperature measurement (as will be discussed in the following sections). Many similarities were found between the hot-ribbon and hot-wire cutting trials. For this reason, more focus is placed on the differences between hot-wire and hot-ribbon cutting than on repeating the explanations of section 3.6.

The main benefit of hot-ribbons over hot-wires is their ability to resist perpendicular cutting forces (as discussed in section 3.4.1.2). This means that the ribbon can be formed into a variety of shapes allowing the sculpting of double concave surfaces and features which are not possible with a straight hot-wire. To use hot-ribbons effectively multiple pass cutting strategies are required. The effect that multiple passes have on the surface was studied. For this reason both shaped and flat hot-ribbon profiles were used in the trials. Figure 3.45 shows the configuration of each hot-ribbon.

The shaped hot-ribbon tests were used to gain knowledge about the practical application of the tool. The shaped hot-ribbon interacts with the foam asymmetrically. One of the legs is always in free air while the other is cutting the foam. This creates a temperature gradient along the tip of the tool which needed to be investigated.



**Figure 3.45. Shaped and flat hot-ribbon configurations.**


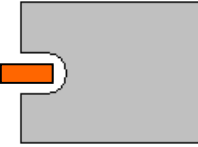
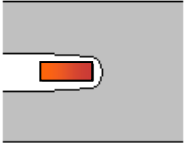
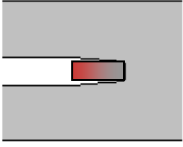
The flat ribbon was used to simplify the measurement of the ribbon temperature and kerf width. With the flat ribbon the kerf was calculated with the same technique as used for the hot-wire cutting trials (section 3.6.5).



One disadvantage of hot-ribbons is that they create large kerf widths and have higher thermal inertia than hot-wires, which means it is more difficult to find stable cutting conditions compared to hot-wires. The width of the ribbon adds an extra complication as a temperature gradient is established between the leading and trailing edges of the ribbon. This temperature gradient is different for every feed rate and power combination.

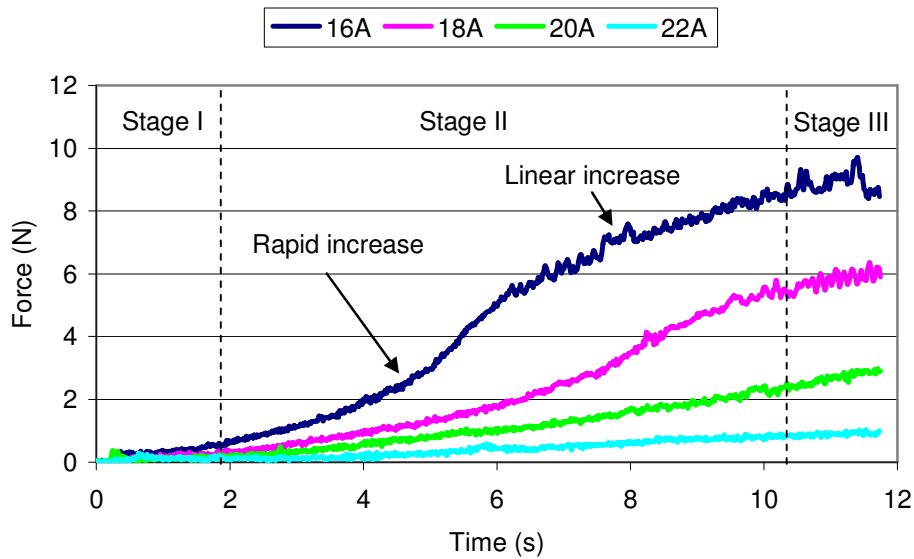
The transient cutting characteristics of constant cutting with a hot-ribbon can be described with three stages. Table 3.7 shows the three cutting stages for a hot-ribbon.

**Table 3.7. Diagrammatic representation of the three cutting stages with a hot-ribbon.**

Ribbon in "free air"	Stage I	Stage II	Stage III
			
Stable high temperature ribbon	Unstable high temperature ribbon	Ribbon cooling	Ribbon stable at lower temperature

### 3.7.1 Characteristic Cutting Force

The characteristic cutting force profile for a hot-ribbon follows a similar 'S' shape curve as the characteristic hot-wire force profile. Figure 3.46 shows the effect of the current on the cutting force profile for a feed rate of 0.052 m/s in XPS. The cutting force takes much longer to stabilise with the hot-ribbon than it does with the hot-wire (the samples needed to be 600+ mm long compared to 300 mm long for hot-wire cutting). This is thought to be because of the extra thermal inertia and the geometry of the ribbons. After the initial rapid increase in cutting force the force increases at a slower almost linear rate. This is thought to be because the leading edge first cools to a stable temperature, then the rest of the blade slowly cools until a steady state temperature gradient is formed across the width of the ribbon.



**Figure 3.46. Characteristic force profiles for hot-ribbon cutting of XPS at 0.052m/s using various currents.**

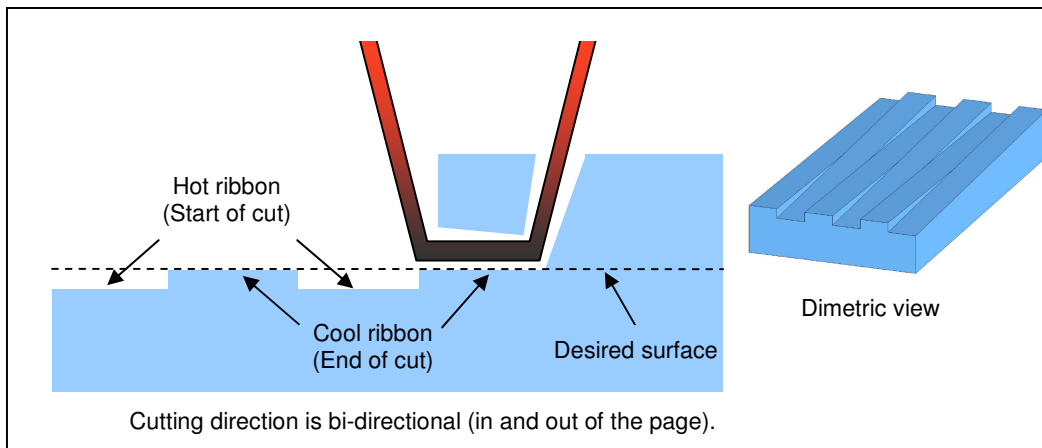
The cutting force directly influences the surface finish of the cut. High cutting forces cause ripped or wavy surfaces while low cutting forces result in vaporised surfaces. Smooth surfaces are also possible with low non-zero cutting forces.

Force feedback temperature control was successfully used to create stable stage III cutting conditions, which enabled cuts to be made with constant cutting force. This was a particularly important accomplishment for bi-directional cutting where the thermal effects of adjacent passes are exaggerated (figure 3.47).

The following section describes the effect of the asymmetric cutting conditions on the cut surface.

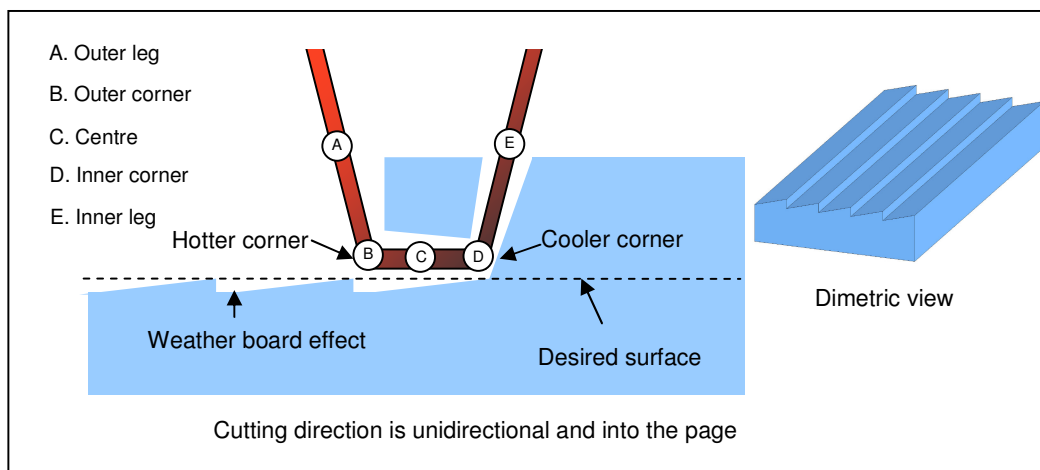
### 3.7.2 Asymmetric Surface Effects

There are two main asymmetries present when using a shaped hot-ribbon and constant currents. The first, most apparent asymmetry is due to the change in temperature over the length of the cut. This is due to the ribbon heating up in the free air at either end of the cut and can be largely eliminated using force feedback temperature control (figure 3.47).



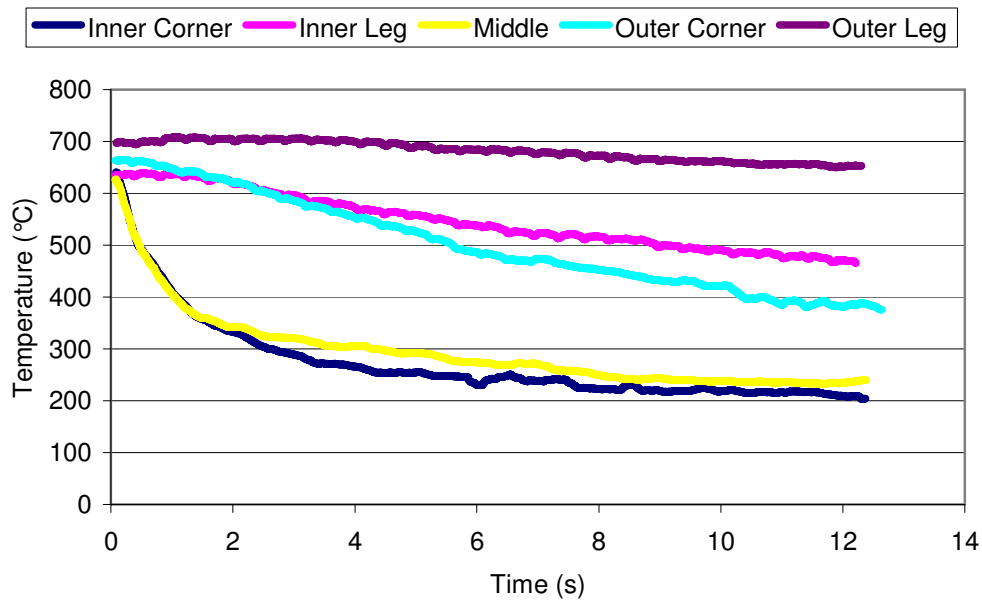
**Figure 3.47. Longitudinal hot-ribbon surface effects.**

The second asymmetry comes from the necessary cutting strategy in which multiple passes are required to create an arbitrary freeform surface. In the example below the cutting direction is unidirectional i.e. always into the page. Figure 3.48 demonstrates this asymmetry.



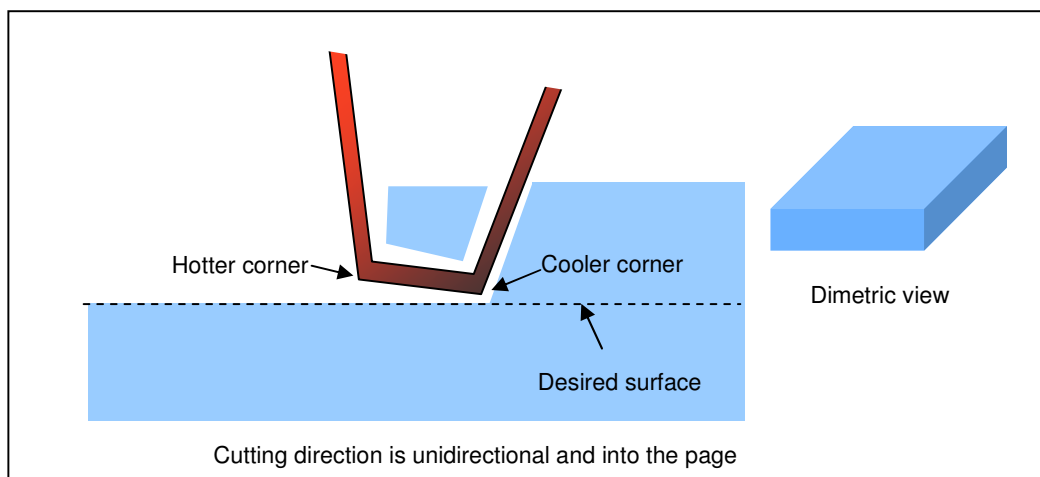
**Figure 3.48. The weather board effect created by asymmetric cutting conditions.**

The temperatures at points A, B, C, D and E were recorded for a range of cutting parameters. Figure 3.49 shows the temperatures of the different positions for a cut made in EPS with 16A and a feed rate of 0.050 m/s. The important temperatures to note are those at points B and D, the inner and outer corners respectively. After four seconds the temperature difference is approximately 300 °C, by the end of the cut the temperature difference appears to have stabilised at approximately 200 °C. This indicates that the weather board effect decreases over the length of the cut; however even with steady-state cutting conditions the weather boarding is still clearly observable.



**Figure 3.49. Temperature at different parts of the shaped hot-ribbon cutting tool (EPS, 16A, F0.050).**

One possible solution to this problem is to form the ribbon so that the flat tip is angled up from the cool corner to the hot corner resulting in a flat surface (figure 3.50).



**Figure 3.50. Geometric temperature compensation for asymmetrical cutting with a hot-ribbon.**

More research is needed in this area. Finite element analysis could be used to optimise the ribbon shape for varying feed rate and power combinations (unfortunately there was not time to pursue this line of inquiry in this thesis).

### 3.7.3 Transverse temperature profile

Initial cutting trials revealed that the cutting force continued to increase for a long time after the apparent ribbon temperature had stabilised. One possible explanation was that the thermocouple used to measure the ribbon temperature was (due to contact issues) only measuring the leading edge of the ribbon. This would mean that the rest of the ribbon may still be cooling, leading to increasing cutting forces.

To test this idea a thermal imaging camera was used to observe a transverse section of a ribbon whilst cutting. This was done by cutting a narrow slot (<1 mm wide) down the centre of a foam sample. The slot was small so that any local change in temperature was negligible. The camera was then positioned directly underneath the ribbon so that a small transverse section of the ribbon could be seen through the slot. Figure 3.51 shows a thermal image of the ribbon in the slot (EPS, 18A, F0.062).

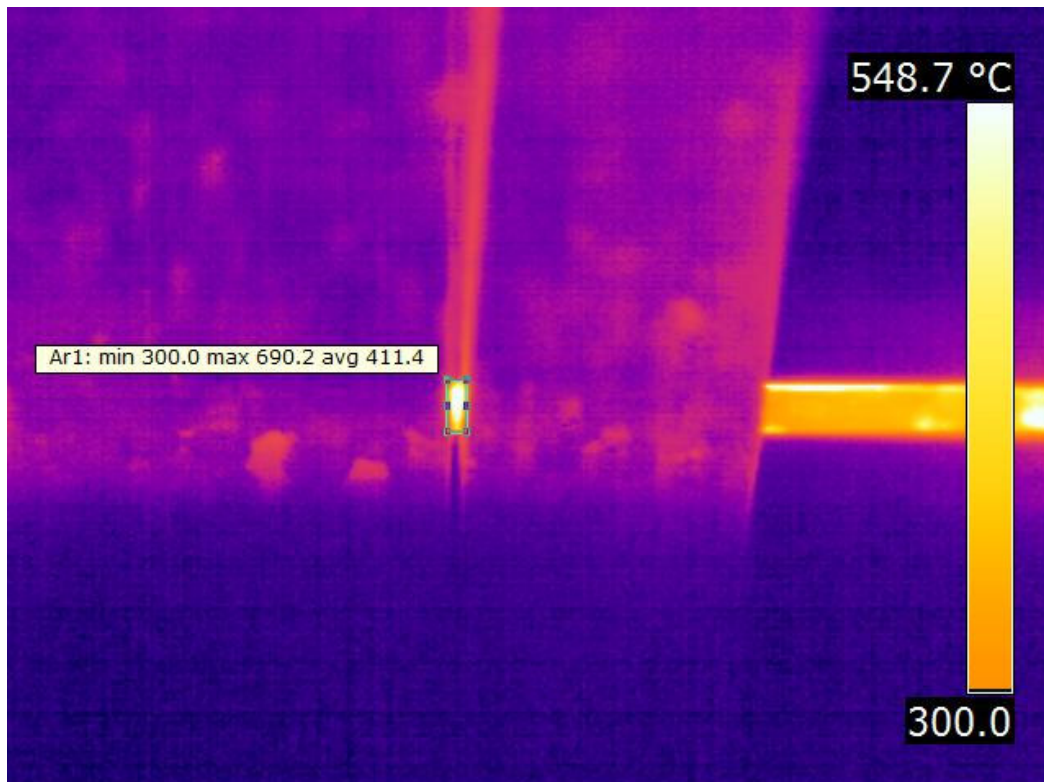
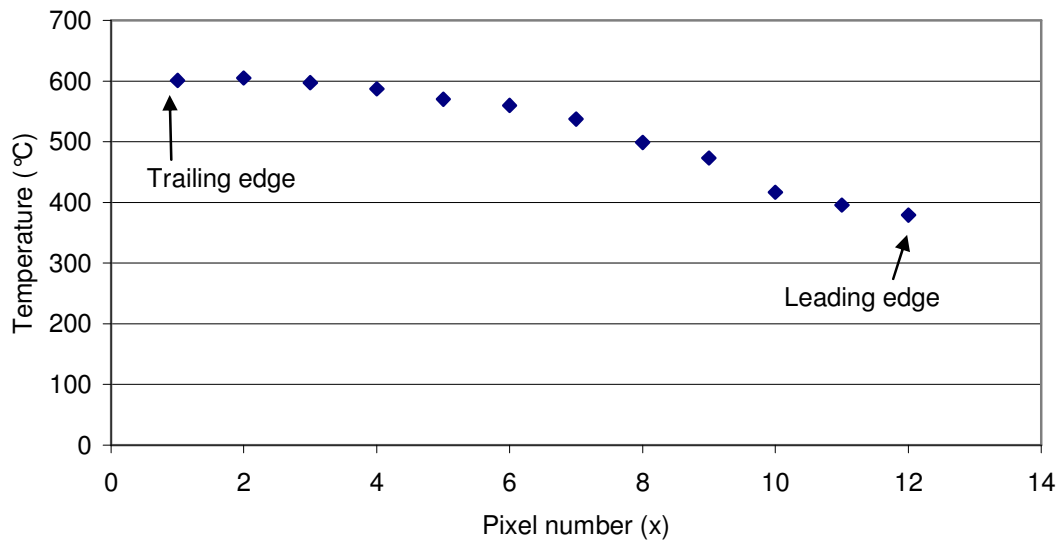


Figure 3.51. Picture of the ribbon while cutting from underneath through a small slot (EPS, 18A, 0.062 m/s).

Each pixel in the thermal image corresponds to a temperature value. A software package called Quickreport was then used to export the temperature values for each pixel into Excel. Figure 3.52 shows the temperature values in the centre of the selected area. The left and right sides of the graph represent the temperature of the trailing and leading edges respectively.



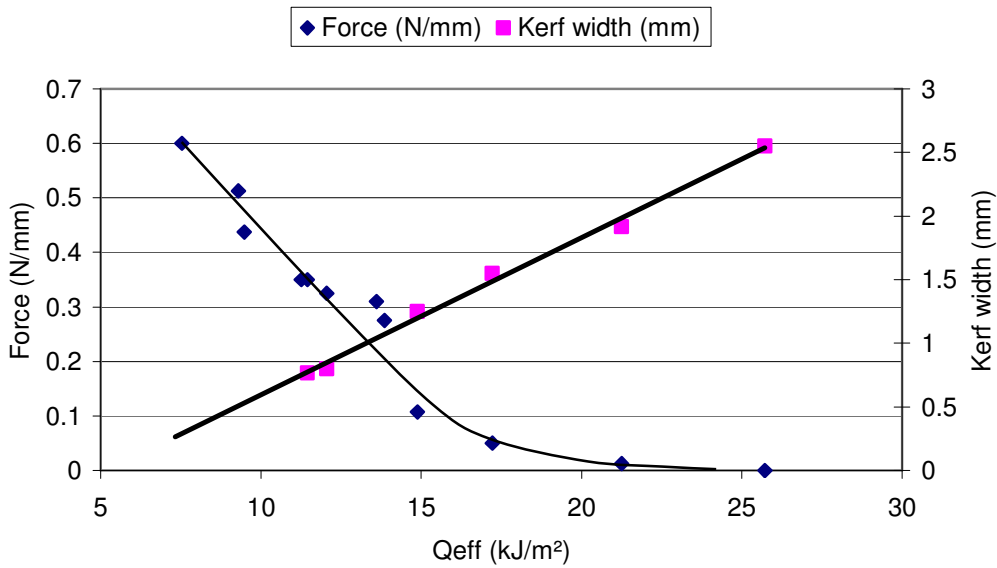
**Figure 3.52. Centreline temperature plot of the small area shown in the preceding thermal image.**

The above graph shows there is a definite trend in the temperature along the X axis (ribbon width) and confirms the assumption that the temperature of the ribbon is cooler at the leading edge and hotter at the trailing edge. The temperature difference in this case was approximately 200°C. This temperature difference is considerable and should be taken into account when developing future thermomechanical finite element models.

Close examination of similar graphs, which were constructed at different times along a cut, show the temperature gradient does in fact change over time. It is thought that the slowly changing transverse temperature gradient changes the amount of frictional shear stress present across the width of the ribbon until equilibrium conditions are met. This would explain the linearly increasing cutting force seen in figure 3.46.

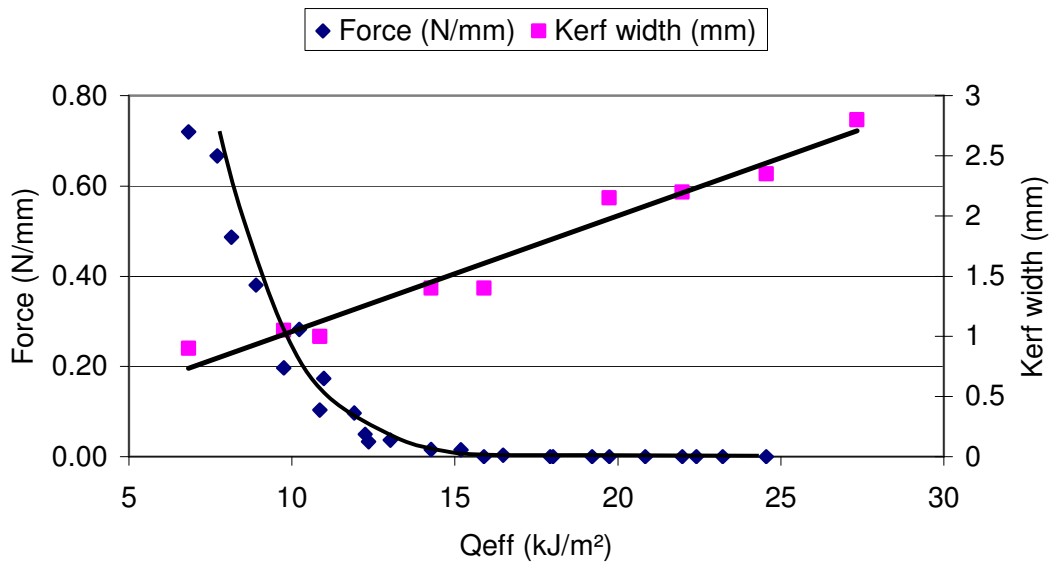
### 3.7.4 Kerf width

Flat hot-ribbon cutting trials were carried out to determine the relationship between the area specific effective heat input,  $Q_{eff}$ , and the kerf width (see section 3.6.5 for the experimental method). The kerf width was found to vary linearly over the experimental range of parameters (figure 3.53). The cutting force in XPS greatly increases for any  $Q_{eff}$  values less than 15 kJ/m<sup>2</sup>.



**Figure 3.53. Cutting force and kerfwidth against area specific effective heat input for XPS for hot-ribbon cutting.**

Comparing this graph with the equivalent graph for hot-wire cutting, figure 3.54, shows a remarkable similarity. The hot-wire uses much less energy to achieve zero force cuts than the ribbon (16 kJ/m<sup>2</sup> compared to 25 kJ/m<sup>2</sup>).



**Figure 3.54. Cutting force and kerfwidth against area specific effective heat input for XPS for hot-wire cutting.**

Therefore the  $Q_{eff}$  can be used as an indication of the relative efficiency of the cutting tools. The hot-ribbon is thought to be less thermally efficient due to the small portion of its perimeter

engaging with the foam. In contrast almost half of the perimeter of the hot-wire is actively involved in cutting.

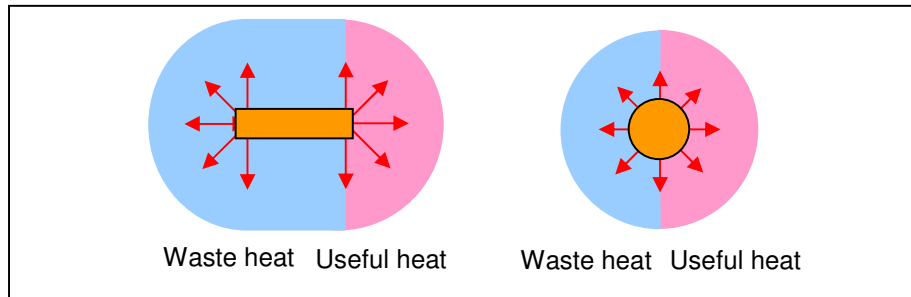


Figure 3.55. Simplified representation of heat flows for hot-tools with different efficiency.

### 3.7.5 The Mass Specific Effective Heat Input

The volume specific effective heat input,  $^{Vol}Q_{eff}$ , for EPS and XPS was found to be 8.4 MJ/m<sup>3</sup> and 11 MJ/m<sup>3</sup> with standard deviations of 4% and 7% respectively. Figure 3.56 shows the spread of  $^{Vol}Q_{eff}$  values found for EPS.

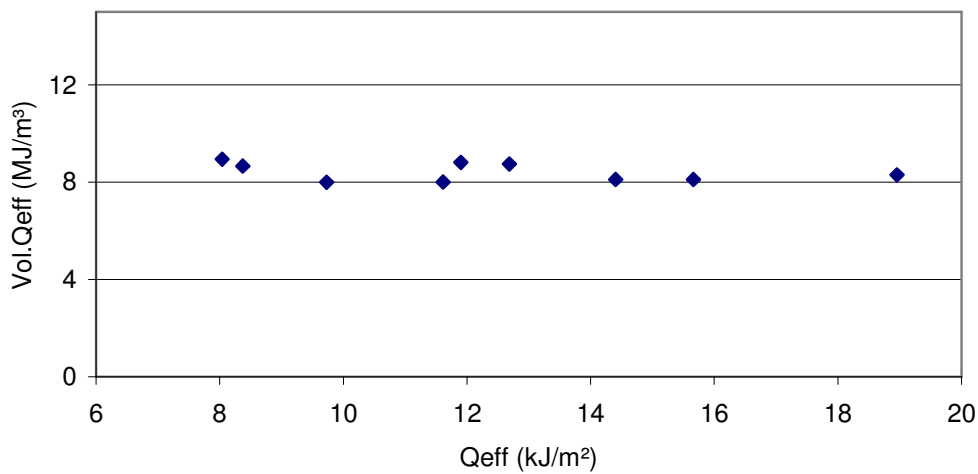


Figure 3.56. Volume specific effective heat input for EPS cuts made with a hot-ribbon.

The mass specific effective heat input,  $^{Mass}Q_{eff}$ , for EPS and XPS was found to be 0.32 MJ/kg and 0.37 MJ/kg respectively. These values are remarkably close to those found for hot-wire cutting (0.31 MJ/kg for EPS and 0.34 MJ/kg for XPS) differing by 3% for EPS and 9% for XPS. This suggests that the  $^{Mass}Q_{eff}$  is only slightly dependant on tool geometry and the effects of tool size are small (as shown by the different hot-wire diameters).



The  $^{Mass}Q_{eff}$  values found in the hot-ribbon cutting trials may also be used in the hot-tool cutting calculator (HCC) described in section 3.6.8. Using the mathematical model embedded in the HCC, offline tool path generation and optimisation is a real possibility for hot-ribbon cutting in the near future.

### 3.7.6 Summary

The hot-ribbon cutting trials consisted of over 300 cuts. The cutting trials included two main material sets, EPS and XPS, two different ribbon configurations and a wide range of feed rates and power inputs. For each cut the cutting force, wire temperature and kerf width was measured as well as observations of the surface texture and surface form. A complete compilation of the cutting data with associated graphs is available in a DVD accompanying this thesis. The main outcomes of these trials are as follows:

- When using constant current cutting the cutting mechanisms change over the length of the cut. These changes can be described in three unique stages. Stage I is characterised by low cutting forces. Stage II represents the transition from stage I to stage III. Stage III is characterised by stable relatively high cutting forces. Force feedback temperature control was successfully used to eliminate this problem.
- Cutting with a shaped or bent hot-ribbon introduces thermal asymmetries which impacts the cut surface form. Altering the shape of the tool is one possible solution to this problem.
- A transverse temperature gradient was successfully measured using a thermal imaging camera. The leading edge of the ribbon was found to be as much as 200°C cooler than the trailing edge. This temperature profile should be included in any future FE models developed.
- The  $Q_{eff}$  can be used as a relative measure of cutting tool efficiency. The hot-ribbon was found to be less efficient than the hot-wire.
- $^{Mass}Q_{eff}$  values of 0.32 and 0.37 MJ/kg were calculated for EPS and XPS respectively. This also allows the hot-tool cutting calculator to be used for calculating variables in hot-ribbon cutting.
- The mathematical equations behind the HCC could be integrated into CAM software to greatly increase the speed, accuracy and utility of automated foam sculpting technology.

## 4 Finite Element Method ---

### 4.1 Introduction

The previous chapter presented experimental cutting trials and derivations of empirical formula. The following two chapters are focussed on advancing the numerical study of foam cutting processes. This chapter begins with a brief review of the theoretical background of the finite element method (FEM) employed in the analysis of plastic foam cutting. The two dimensional partial nonlinear differential equations representing the thermal fields are developed into finite element equations through the finite element discretization process. The finite element method is then used in chapter five to perform computer simulations of hot-tool cutting.

FEM is a computer-based numerical method developed to solve engineering problems involving solid mechanics, fluid flow and heat transfer among others. Due to its versatility, the method can be used to solve coupled problems and problems with complex geometries where solutions are highly non-linear [54]. The essence of the finite element method is to take a complex problem whose solution may be difficult or impossible to calculate analytically, and decompose it into geometrically simpler pieces for which a local approximation of the solution may be constructed. Then the local approximate solutions are combined to obtain a global approximate solution.

In practice the geometry to be modelled is discretized into elements. Each element has nodes that are used to represent the value of the field variables (for example, temperature, stress, displacement) over the element by an interpolation function. Individual matrix equations are generated for each element and assembled together to find the overall system equations. Known nodal field values (known as boundary conditions) are imposed on the system equations and the unknown nodal values of the problem are obtained by solving the system equations.

## 4.2 Heat Diffusion Equation [55]

Consider a homogeneous two-dimensional medium and a temperature distribution  $T(x, y)$  which is expressed in Cartesian coordinates. Using the law of conservation of thermal energy the temperature distribution in an infinitesimally small control area defined in the medium is governed by the following general differential equation:

$$\rho c_p \frac{\partial T}{\partial t} = \frac{\partial}{\partial x} \left( k \frac{\partial T}{\partial x} \right) + \frac{\partial}{\partial y} \left( k \frac{\partial T}{\partial y} \right) + \dot{q} \quad \text{Eq. (4.1)}$$

where:

$\rho$  = the density of the medium

$c_p$  = the specific heat of the medium

$k$  = the thermal conductivity of the medium

$\dot{q}$  = the rate at which heat is generated per unit volume of the medium

$\rho c_p \frac{\partial T}{\partial t}$  = the time rate of change of the thermal energy of the medium per unit volume

$k \frac{\partial T}{\partial x}$  and  $k \frac{\partial T}{\partial y}$  = the rate of heat transfer per unit area (heat flux) at the x, and y coordinates respectively.

Eq. (4.1) is the two-dimensional form of the *heat diffusion equation*. This equation provides the basic tool for heat conduction analysis. From its solution, the temperature distribution  $T(x, y)$  is obtained as a function of time.

To solve the above differential equation, Eq. (4.1) it is necessary to define the boundary conditions on selected surfaces and nodes.

For a specified nodal temperature,  $T_n$ ,

$$T_{(x,y,t)} = T_n \quad \text{for } t > 0 \quad \text{Eq. (4.2a)}$$

For initial nodal temperatures,  $T_i$ ,

$$T_{(x0,y0)} = T_i \quad \text{for } t = 0 \quad \text{Eq. (4.2b)}$$

For specified surface heat flux,  $q''$ ,

$$-k\nabla T = q'' \quad \text{for a finite heat flux} \quad \text{Eq. (4.2c)}$$

$$\nabla T = 0 \quad \text{on adiabatic heat flux} \quad \text{Eq. (4.2d)}$$

For surface convection,

$$-k\nabla T = h[T_\infty - T_{(x,y,t)}] \quad \text{Eq. (4.2e)}$$

Where  $h$  = the convective heat transfer coefficient.

For surface radiation,

$$-k\nabla T = \alpha q_r'' - \sigma \varepsilon T_{(x,y,t)}^4 \quad \text{Eq. (4.2f)}$$

where  $\nabla T = \left( \frac{\partial T}{\partial x} + \frac{\partial T}{\partial y} \right)$ ,  $\alpha$  = the surface absorptivity,  $\sigma$  = the Stefan-Boltzmann constant and  $\varepsilon$  = the surface emissivity.

The problem is nonlinear due to temperature-dependant material properties. The following section shows the derivation of the finite element equations, based on Huebner [56].

### 4.3 Finite Element Equation Formulation

A general formulation of element equations for transient heat transfer in a medium can be derived for a two-dimensional solid,  $\Omega$ , bounded by a surface,  $\Gamma$ , as shown in figure 4.1.

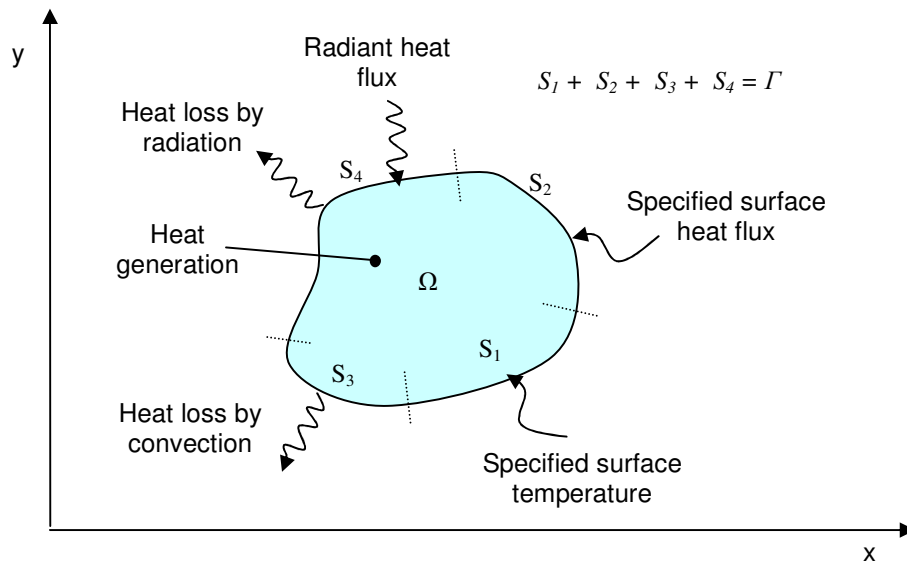


Figure 4.1. Various modes of heat transfer in a two-dimensional solid.

The solution domain  $\Omega$  is divided into  $M$  elements, and each element has  $r$  nodes. The usual procedure is used to express the temperature and temperature gradients within each element ( $e$ ) as:

$$T^{(e)}(x, y, t) = \sum_{i=1}^r N_i(x, y) T_i(t) \quad \text{Eq. (4.3a)}$$

$$\frac{\partial T^{(e)}}{\partial x}(x, y, t) = \sum_{i=1}^r \frac{\partial N_i}{\partial x}(x, y) T_i(t) \quad \text{Eq. (4.3b)}$$

$$\frac{\partial T^{(e)}}{\partial y}(x, y, t) = \sum_{i=1}^r \frac{\partial N_i}{\partial y}(x, y) T_i(t) \quad \text{Eq. (4.3c)}$$

or in matrix notation:

$$T^{(e)}(x, y, t) = [N(x, y)]\{T(t)\} \quad \text{Eq. (4.4a)}$$

$$\left\{ \begin{array}{l} \frac{\partial T}{\partial x}(x, y, t) \\ \frac{\partial T}{\partial y}(x, y, t) \end{array} \right\} = [B(x, y)]\{T(t)\} \quad \text{Eq. (4.4b)}$$

where  $[N]$  is the temperature interpolation matrix and  $[B]$  is the temperature-gradient interpolation matrix.

$$[N(x, y)] = [N_1 \ N_2 \ \dots \ N_r] \quad \text{Eq. (4.6a)}$$

$$[B(x, y)] = \begin{bmatrix} \frac{\partial N_1}{\partial x} & \frac{\partial N_2}{\partial x} & \dots & \frac{\partial N_r}{\partial x} \\ \frac{\partial N_1}{\partial y} & \frac{\partial N_2}{\partial y} & \dots & \frac{\partial N_r}{\partial y} \end{bmatrix} \quad \text{Eq. (4.6b)}$$

For a single element, the method of weighted residuals is used to derive the element equations starting with the energy equation, Eq. (4.1):

$$\int_{\Omega^{(e)}} \left( \frac{\partial q_x}{\partial x} + \frac{\partial q_y}{\partial y} - \dot{q} + \rho c_p \frac{\partial T}{\partial t} \right) N_i d\Omega = 0 \quad \text{Eq. (4.7)}$$

where  $\Omega^{(e)}$  = the domain for the element (e).

By *Gauss's theorem*, which introduces surface integrals of the heat flow across the element boundary  $\Gamma^{(e)}$ . The term  $\int_{\Omega^{(e)}} \left( \frac{\partial q_x}{\partial x} + \frac{\partial q_y}{\partial y} \right) N_i d\Omega$  is integrated and the following re-arranged form of Eq. (4.7) is presented below:

$$\int_{\Omega^{(e)}} \rho c \frac{\partial T}{\partial t} N_i d\Omega - \int_{\Omega^{(e)}} \left[ \frac{\partial N_i}{\partial x} \frac{\partial N_i}{\partial y} \right] \begin{Bmatrix} q_x \\ q_y \end{Bmatrix} d\Omega = \int_{\Omega^{(e)}} Q N_i d\Omega - \int_{\Gamma^{(e)}} (q \cdot \hat{n}) N_i d\Gamma, \quad i = 1, 2, \dots, r \quad \text{Eq. (4.8)}$$

Next we express the surface integral as the sum of integrals over  $S_1$ ,  $S_2$ ,  $S_3$  and  $S_4$  and introduce the boundary conditions, Eq. (4.3):

$$\int_{\Omega^{(e)}} \rho c \frac{\partial T}{\partial t} N_i d\Omega - \int_{\Omega^{(e)}} \left[ \frac{\partial N_i}{\partial x} \frac{\partial N_i}{\partial y} \right] \begin{Bmatrix} q_x \\ q_y \end{Bmatrix} d\Omega = \int_{\Omega^{(e)}} Q N_i d\Omega - \int_{S_1} (q \cdot \hat{n}) N_i d\Gamma + \int_{S_2} q_s N_i d\Gamma - \int_{S_3} h(T - T_{(e)}) N_i d\Gamma - \int_{S_4} (\sigma \varepsilon T^4 - \alpha q_r) N_i d\Gamma, \quad i = 1, 2, \dots, r \quad \text{Eq. (4.9)}$$

As the last step we introduce the element temperatures from Eq. (4.5a) and heat flow components from Fourier's law. Fourier's law is expressed with Eq. (4.5b) as follows:

$$\{q''\} = -[k][B]\{T\} \quad \text{Eq. (4.10)}$$

Finally, after some manipulation the resulting element equations become

$$[C_p] \left\{ \frac{dT}{dt} \right\} + [[K_c] + [K_h] + [K_r]] \{T\} = \{R_T\} + \{R_Q\} + \{R_q\} + \{R_h\} + \{R_r\} \quad \text{Eq. (4.11)}$$

For a simplified two-dimensional FEA of hot-tool foam cutting where the dominant mode of heat transfer is conduction, the heat flows due to convection and radiation can be assumed negligible (this is explained further in chapter 5). As plastic foams are excellent thermal insulators the outside edges of the foam are assumed to be adiabatic (i.e. perfectly insulated). When these factors are taken into account Eq. (4.11) reduces to:

$$[C_p] \left\{ \frac{dT}{dt} \right\} + [K_c] \{T\} = \{R_{T_s}\} + \{R_Q\} \quad \text{Eq. (4.12)}$$

where:

$$[C] = \text{element capacitance matrix} = \int_{\Omega^{(e)}} \rho c \{N\} [N] d\Omega \quad \text{Eq. (4.13a)}$$

$$[K_c] = \text{element conductance matrix} = \int_{\Omega^{(e)}} [B]^T [k] [B] d\Omega \quad \text{Eq. (4.13b)}$$

$$\{R_T\} = \text{heat load vector arising from specified temperatures} = - \int_{S_1} (q'' \cdot \hat{n}) \{N\} d\Gamma \quad \text{Eq. (4.13c)}$$

$$\{R_Q\} = \text{heat load vector arising from internal heat generation} = - \int_{\Omega} Q \{N\} d\Omega \quad \text{Eq. (4.13d)}$$

Eq. (4.11) represents the general nonlinear formulation of element equations for transient heat conduction in a medium. In order to obtain the system equations, the element equations are assembled by the standard procedure.

For the general nonlinear transient case (for example, the hot-wire foam cutting case), the formulations are written as follows:

$$[C_p(T)] \{\dot{T}\} + [K_c(T)] \{T\} = \{R_{T_s}(T, t)\} + \{R_Q(T, t)\} \quad \text{Eq. (4.14)}$$

Eq. (4.14) shows that the element matrices and the heat load vectors are both temperature and time dependant, and a solution by an iterative, time marching scheme is required. In the following section a commonly used method of solving nonlinear equations, such as the one presented above, is described.

## 4.4 Solving Nonlinear Transient Equations

Nonlinear transient equations are common in heat transfer analysis. Material properties are often temperature-dependant; phase changes absorb or liberate heat and change material properties; surface heat fluxes due to convection and radiation are also highly nonlinear. Eq. (4.14) describes a nonlinear transient heat transfer problem.

Eq. (4.14) can be presented in general matrix form as:

$$[K]\{u\} = \{F^a\} \quad \text{Eq. (4.15)}$$

where for thermal equations:

$[K]$  = the conductivity coefficient matrix

$\{u\}$  = the unknown temperature DOF vector

$\{F^a\}$  = the vector of applied loads

If the coefficient matrix  $[K]$  is itself a function of the unknown DOF values (or their derivatives) then Eq. (4.15) is nonlinear. The most popular method for solving nonlinear equations is the Newton-Raphson iteration method, which is presented below [56-58].

$$[K_i]\{\Delta u_i\} = \{F^a\} - \{F_i^{nr}\} \quad \text{Eq. (4.16)}$$

$$\{u_{i+1}\} = \{u_i\} + \{\Delta u_i\} \quad \text{Eq. (4.17)}$$

where:

$[K_i]$  = the updated conductivity coefficient matrix,  $i$  = subscript representing current iteration

$\{F_i^{nr}\}$  = the resisting load vector calculated from the element heat flows

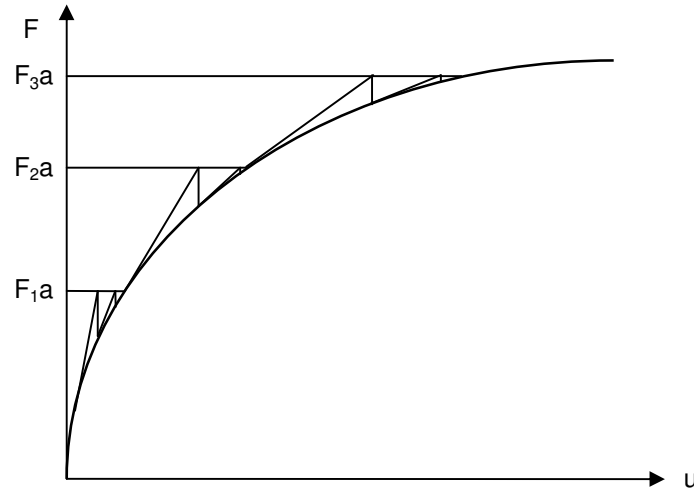
$\{\Delta u_i\}$  = temperature increment vector

Both  $[K_i]$  and  $\{F_i^{nr}\}$  are evaluated based on values given by  $\{u_i\}$ .  $\{\Delta u_i\}$  is computed from Eq. (4.16). The next approximation  $\{u_{i+1}\}$  is obtained from Eq. (4.17). This process is then repeated until the convergence criteria have been met.

If the analysis includes path-dependant nonlinearities, then the solution process requires that some intermediate steps be in equilibrium in order to correctly follow the load path. This is



accomplished by using the incremental Newton-Raphson procedure as shown in figure 4.2. Where  $\{F_n^a\}$  = the total applied load vector at time step n.



**Figure 4.2. Incremental Newton-Raphson Procedure.**

The Newton-Raphson method only guarantees convergence if the solution at any iteration is near the exact solution. Therefore the incremental approach is sometimes required even if path-dependant nonlinearities are not present. When the coefficient matrix is updated at every iteration the process is called the full Newton-Raphson method.

#### 4.4.1 Convergence

The iteration procedure described above continues until convergence is achieved. Convergence is assumed when:

$$\|\{R\}\| < \epsilon_R R_{ref} \quad (\text{out of balance convergence}) \quad \text{Eq. (4.18)}$$

$$\|\{\Delta u_i\}\| < \epsilon_U u_{ref} \quad (\text{DOF increment convergence}) \quad \text{Eq. (4.19)}$$

where:

$$\{R\} = \text{the residual vector} = \{F^a\} - \{F^{nr}\}$$

$$\{\Delta u\} = \text{the DOF increment vector of load step } n$$

$\epsilon_R$  and  $\epsilon_U$  = tolerances.

Popular FEA software, ANSYS (used to simulate the hot cutting process in the next chapter), uses a default tolerance of 0.001 for both  $\epsilon_R$  and  $\epsilon_U$ , however these values can also be customised to suit the type of problem or the accuracy required.

## 4.5 Summary

This chapter provided a brief description of the concept of the FEM and the derivation of the finite element equations from the partial nonlinear differential equations of the heat transfer problem. It also presented a nonlinear solution algorithm for the solution of the matrix equations. The key points of the chapter are summarised below:

- FEM is a computer-based numerical method used to solve continuum problems. The problem domain is discretized into elements with nodes which are used to represent the variation of the field variables over the element via interpolation functions. In this case the FEM is used to simulate plastic foam cutting by calculating the thermal fields surrounding a heat source in a medium.
- The finite element equations were formulated assuming conduction was the only mode of heat transfer. The contribution from radiation is negligible and the model geometry omits the air gap required for convection.
- The finite element equation for conductive heat transfer was derived from the law of conservation of energy using the weighted residuals approach.
- The full Newton-Raphson iteration procedure was presented as a means of solving nonlinear equations.
- The convergence criteria required for the Newton-Raphson method was also described.

## **5 Finite Element Analysis of Hot-tool Plastic Foam Cutting** \_\_\_\_\_

### **5.1 Introduction**

This chapter investigates the thermal responses of the plastic foam materials during hot-tool cutting via finite element simulations. It develops a nonlinear, transient, two-dimensional thermal model for hot-tool plastic foam cutting. The finite element models are built using a scripting language, APDL (ANSYS Parametric Design Language) provided by the commercial code ANSYS [57]. A number of different simulations were carried out to validate the finite element model for different size cutting tools, different shape cutting tools, different types of PS foam and different tool paths. A detailed analysis of the simulation results is presented. The simulations are also validated by comparing the results with experimental data.

This chapter begins with a brief description of the hot-tool cutting process. Then the heat transfer model is described followed by an explanation of the results and a comparison with experimental data.

## 5.2 Process Description

The configuration of the hot-tool plastic foam cutting process used in the cutting trials is shown in figure 5.1. In practice the foam was held in a holding device and moved with constant velocity relative to the wire, however for the simulations the hot-tool was moved from an initial position near the left side of the block to the right while the foam block was held stationary. The hot-tool was given constant temperature boundary conditions to represent the steady-state wire temperatures found in experiments. Other parameters used in the simulations come directly from parameters used in the cutting trials, so a direct comparison can be made between the FEA results and the experimental data. A table of parameters and their values used for the simulations are listed in table 5.1.

**Table 5.1. Parameters and values used for simulations.**

Cutting Tool	Material	Feed-rate range (m/s)	Temperature range (°C)
Ribbon	EPS	0.0380 to 0.0740	200 to 400
Ribbon	XPS	0.0280 to 0.0640	162 to 247
Wire (0.64 mm)	EPS	0.0267 to 0.0300	131 to 427
Wire (0.64 mm)	XPS	0.0150 to 0.0167	176 to 505
Wire (0.36 mm)	XPS	0.0133 to 0.0200	188 to 260
Wire (0.91 mm)	XPS	0.0133 to 0.0200	213 to 319

A second set of simulations that modelled curved cuts with different radii was carried out for a hot-ribbon with a temperature of 315°C cutting EPS with a feed rate of 0.050 m/s. The radii were varied from 0 mm to 15 mm to determine what effect the finite width of the ribbon has on the kerf width for curved cuts with varying radii. This test provided information on the minimum radius possible to cut with the chosen hot-ribbon.

The plastic foam materials used in the cutting trials are described in section 3.3. The thermal material property models used in the simulation are described in section 5.3.3.

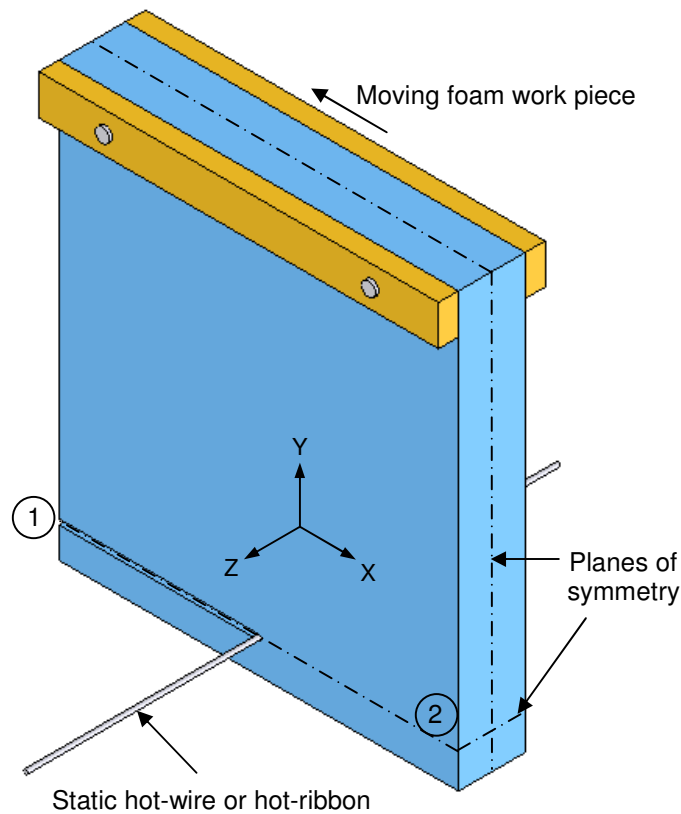


Figure 5.1. Graphical representation of the hot-tool cutting process.

## 5.3 Heat Transfer Model

Temperatures transferred to the plastic foam by conduction from the hot-tool can be calculated via the nonlinear transient thermal finite element equation (see Eq. 4.14). The following sections describe the temperature-dependant material properties of the foam and the time dependant heat loads embedded in equation 4.14. Also described in this section are the assumptions, elements and mesh management used in the simulations.

### 5.3.1 Assumptions

A number of assumptions have been made in developing the finite element model, including:

- The temperature distribution across the centreline is assumed symmetrical.
- The foam material is isotropic and homogeneous.
- Thermal expansion is negligible; therefore the model geometry is constant.

- The conductivity of the foam is low and therefore heat transfer on the surfaces far away from the wire is negligible. The surfaces can be treated as adiabatic.
- The hot-tool is perfectly surrounded by foam at all times; therefore conduction is the only mode of heat transfer.
- Thermal degradation of the PS plastic at temperatures over 400°C is assumed negligible.
- The kerf width is represented by the maximum width of the isotherm at the temperature at which the cells collapse. A value of 160°C was adopted from literature [50].

These assumptions allow the model to be made half the size, using symmetry to reduce the number of elements required. The main assumption in the model is that the hot-tool is always surrounded by foam. This inevitably leads to more heat being conducted into the foam than if an air gap were surrounding a portion of the cutting element. This effect is somewhat balanced by the fact that the conductivity of air is relatively close to that of EPS and XPS (e.g. conductivity of air at 100°C = 0.031 W/mK and the conductivity of XPS at 100°C = 0.032 W/mK). Also the radiated energy from the hot-tools is approximately 1% and can be assumed negligible. It is expected that the FEA results will depart from experimental data for high energy cuts as the air gap surrounding the wire increases. Thermal degradation of the PS has also been ignored for two main reasons; firstly the cutting tool temperature is rarely over 400°C and therefore has no effect on the majority of cases, and secondly it greatly simplifies the model and reduces computing time. Because thermal degradation of PS is an endothermic reaction, ignoring it will result in higher temperatures in the foam and larger recorded kerf widths when compared to experimental data.

### 5.3.2 Elements Used

The element chosen for this FEA is a two dimensional quadrilateral element with four nodes (called PLANE55). This element is suited for 2D, steady-state or transient thermal analysis. Figure 5.2 shows the geometry, node locations and coordinate system for PLANE55 elements. Heat fluxes and convections can be applied as surface loads on the element faces and temperature constraints can be applied directly to the nodes.

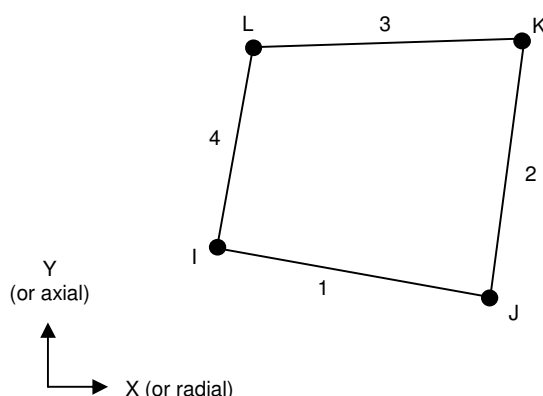
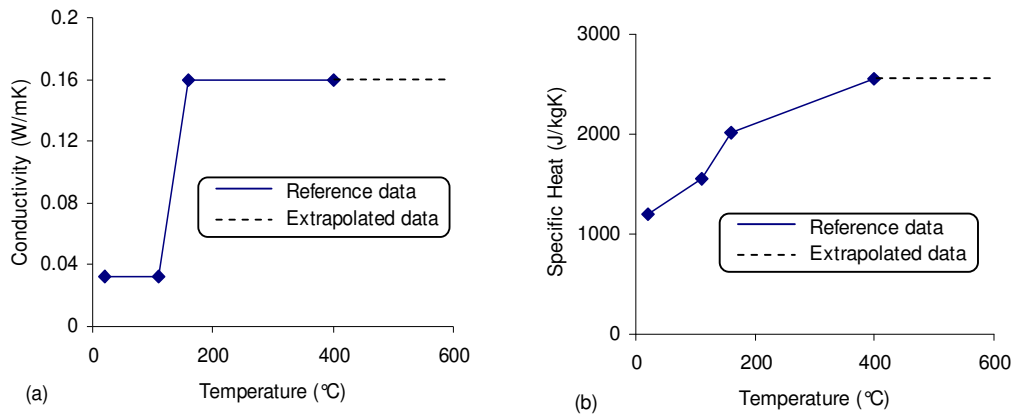


Figure 5.2. Element PLANE55 geometry.

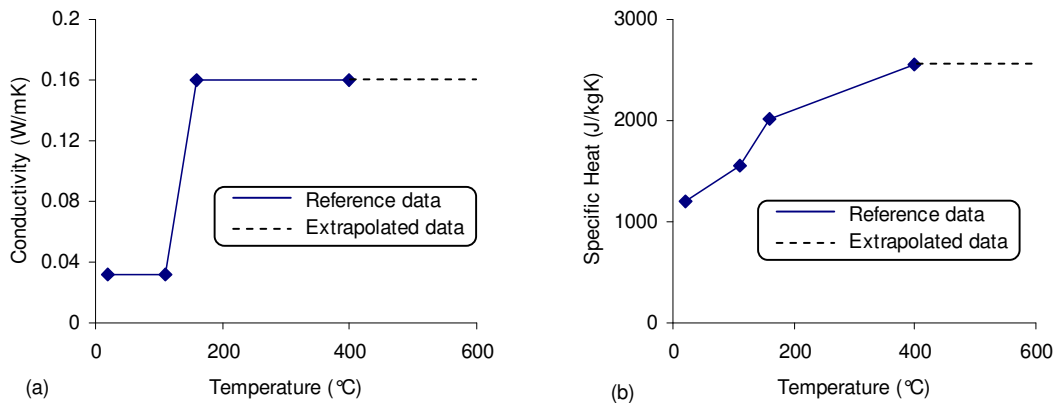
### 5.3.3 Material Properties

Temperature responses in a material with high heat fluxes are determined by the thermal material properties such as thermal conductivity, specific heat and density, which are themselves dependant on temperature. The thermal material properties need to be known accurately for the subsequent finite element analysis to be reliable. It was very difficult to find thermal material property data over the required temperature range in the literature. Often when data for various properties such as conductivity and specific heat were found they were from disparate sources. For this reason considerable effort was spent measuring the material properties of the specific PS foams used in the cutting trials and validating data found in literature (see section 3.3).

The thermal material properties for EPS and XPS used in the simulation are shown in figure 5.3 and 5.4 respectively. The conductivity of the foams was measured experimentally with a Hot Disk Analyser (HDA) giving values of; 0.033 W/mK for EPS and 0.032 W/mK for XPS at 20°C. These values were verified against commonly quoted industry values. At temperatures over 160°C foam cells collapse returning the foam to a high density (non-foamed) state [50]. At this stage there is a large change in the conductivity of the foam due to the removal of air gaps within the foam. A conductivity of 0.16 W/mK was used for all temperatures over 160°C [59]. This value was assumed to be valid for both plastic types as they are chemically, thermally and mechanically very similar at this stage. The specific heat data for temperatures up to 400°C was taken from literature [60] and is assumed to be the similar for all PS plastics. The specific heat increases linearly from room temperature to the glass transition temperature of 110°C. The glass transition activation energy or 'latent heat' is responsible for the jump in specific heat between 110 and 160°C, after which the trend continues linearly up to 400°C. In all cases after 400°C the thermal material properties are considered to have constant values. In reality PS starts to thermally degrade at temperatures above 400°C, however for the wire temperatures used in the simulations the effect is assumed negligible.



**Figure 5.3. Thermal material properties of EPS. a) Conductivity b) Specific Heat.**



**Figure 5.4. Thermal material properties of XPS. a) Conductivity b) Specific Heat.**

Density values for EPS and XPS were determined experimentally to be  $26 \text{ kg/m}^3$  and  $30 \text{ kg/m}^3$  respectively. These values were kept independent of temperature to ensure that the overall mass of the foam block was conserved throughout the analysis. As there is no thermal expansion mass must be conserved for the conservation of energy.

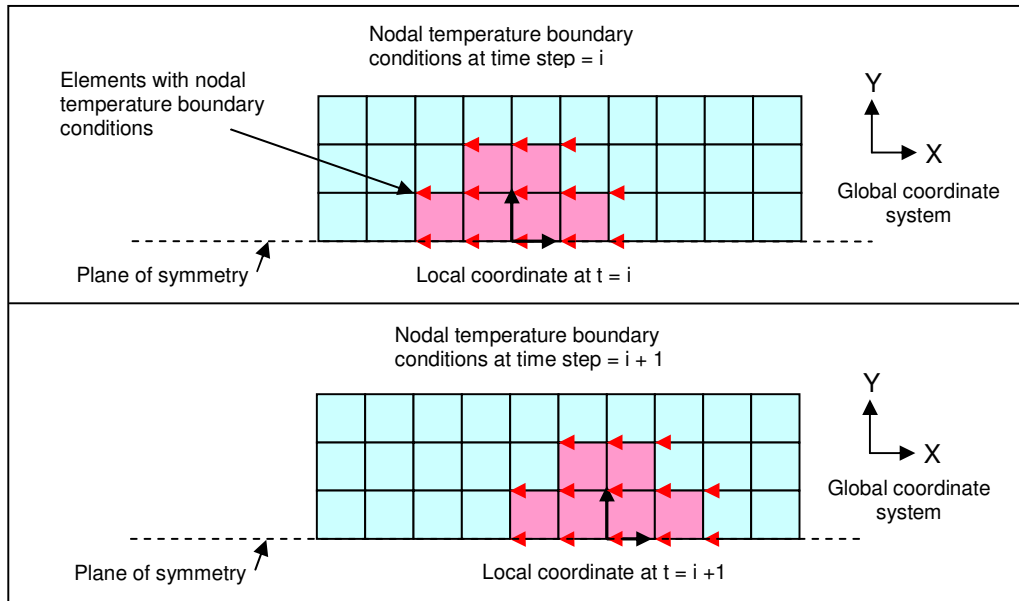
In order to define the temperature dependant material property data in ANSYS, temperatures are defined in tables using the MPTEMP command first, followed by the data associated with the material property using the MPDATA command.

### 5.3.4 Mesh Management and Nodal Boundary Conditions

Due to symmetry in the cutting plane of straight cuts only half of the foam block (i.e. approximately  $5 \text{ mm} \times 40 \text{ mm}$ ) is used for generating the mesh (figure 5.5). The mesh pattern is made of uniform rectangles as this simplifies the application of the boundary conditions and



analysis of the results. The element size is directly related to the size of the cutting tool (e.g. six elements are used to simulate the top half of each hot-wire and one row of 14 elements simulate the top half of the hot-ribbon). The width and height of the foam block is chosen to be exact multiples of the element size to ensure that the elements are not automatically resized by the software; this is important as the kerf width is determined by counting the number of elements inside the 160 °C isotherm.



**Figure 5.5. Nodal boundary conditions applied at nodes relative to the local coordinates for two successive time steps.**

The hot-wire is simulated by imposing constant temperature boundary conditions on a select group of nodes for a predefined amount of time. After each successive time step the old temperature boundary conditions are deleted and a new set are imposed in a new location. The locations of the temperature boundary conditions are determined by moving a set of local coordinates along the foam block a distance of two elements each time step. The group of nodes are selected in such a way as to approximate the shape of the hot-tool being simulated. For example, to simulate a hot-wire with a diameter of 0.64 mm a cylindrical local coordinate system is used to select all the nodes within a 360° arc about the origin and within the radius of the wire. The local coordinates are moved a distance of two elements each time step to allow sufficient approximation of the actual continuous process. The time step ( $TS$ ) is calculated by the following equation:

$$TS = \frac{(2 \times \text{elements size})}{\text{feedrate}} \quad \text{Eq. 5.1}$$

To simulate the hot-ribbon making a curved cut the local coordinate system was simply moved along a path tangent to the chosen radius of the curve.

For more detailed information on the formation of the models for hot-ribbons and hot-wires see the APDL input codes in the appendix H.

## 5.4 Simulation Results

This section reports the results of over 50 hot-tool plastic foam cutting simulations using the finite element models developed. The feed rates and temperatures used for the simulations were adopted from prior experimental work to create a link between the various tests and results. The temperature field of selected samples are shown as well as an explanation of how the kerf width was measured. The final results of the FEA are evaluated against experimental data and displayed graphically.

### 5.4.1 Hot-wire Simulations

Each hot-wire simulation has four main input parameters; wire diameter, material, wire temperature and feed rate. Figure 5.6 shows the temperature distribution in EPS foam for a 0.64 mm diameter hot-wire with a feed rate of 0.030 m/s and a wire temperature of 252°C. The bottom portion of the image shows the whole model with temperature contours that span the entire temperature range. The hot-wire is represented by the red circle on the right hand side and the tail to the left shows how the heat dissipates after the wire has passed through the foam. The top image is identical to the bottom except for the fact it is zoomed in on the hot-wire and the temperature scale only goes up to 160°C (the temperature at which the foam cells collapse). The kerfwidth is calculated by counting the number of vertical elements in the grey (>160°C) area and multiplying them by the height of the elements (e.g. for the figure shown; kerf width = 7.6 x 0.16 mm = 1.2 mm).

The results from each simulation were then plotted against the effective heat input and compared against the experimentally determined kerf widths. For screenshots of simulations with other cutting parameters please see appendix I.

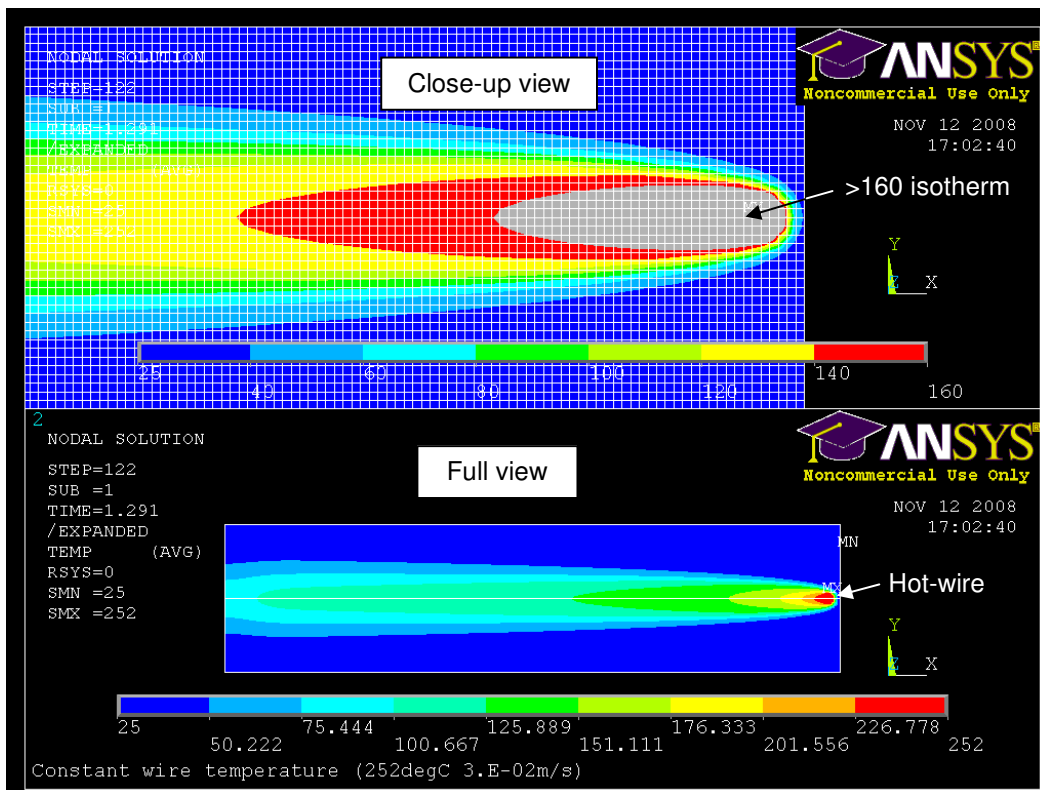


Figure 5.6. FEA temperature distribution for a hot-wire cut (EPS, 0.64 mm wire, F0.030).

Figure 5.7 and 5.8 show the results for XPS and EPS with a 0.64 mm hot-wire. The FEA kerf widths do not form a perfectly straight line because the temperature inputs came directly from experimentally determined wire temperatures and not from an equation defining a line of best fit. The FEA results match well with the experimental data for both XPS and EPS suggesting the assumptions made in previous sections are valid. For low values of  $Q_{eff}$  the FEA kerf widths are lower than the experimental trend line. This is because as the kerf width approaches the diameter of the wire there is more mechanical interaction between the wire and the foam which creates larger than calculated kerfs. For high  $Q_{eff}$  values the FEA kerf widths are greater than the experimental trend line. This is because the FE model does not take into account the effect of the insulating air gap which grows in size around the wire as the effective heat input increases.

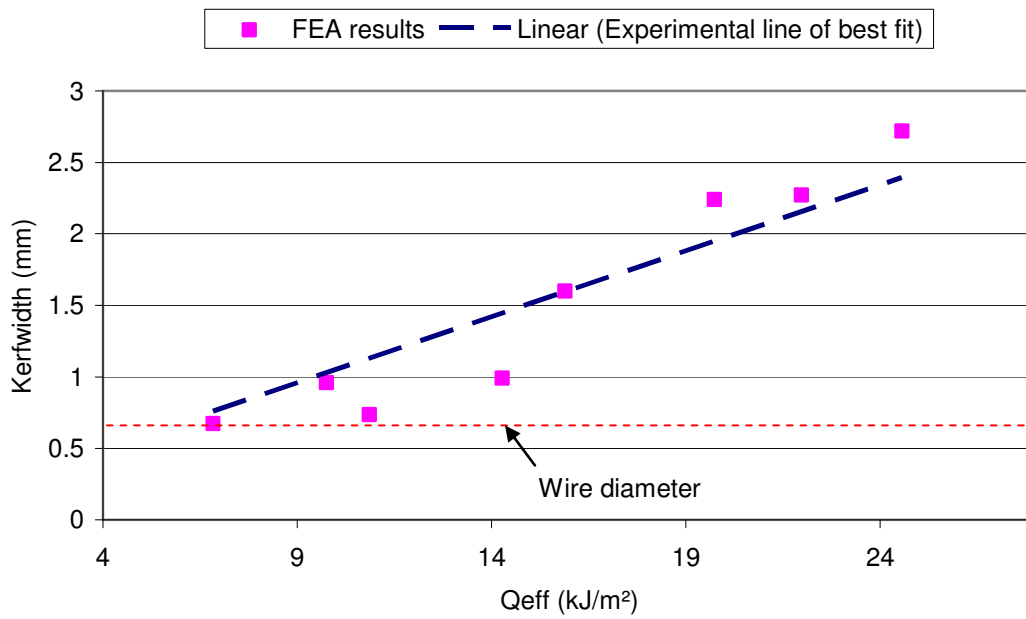


Figure 5.7. Comparison between FEA and experimental kerfwidhts (XPS, 0.64 mm wire).

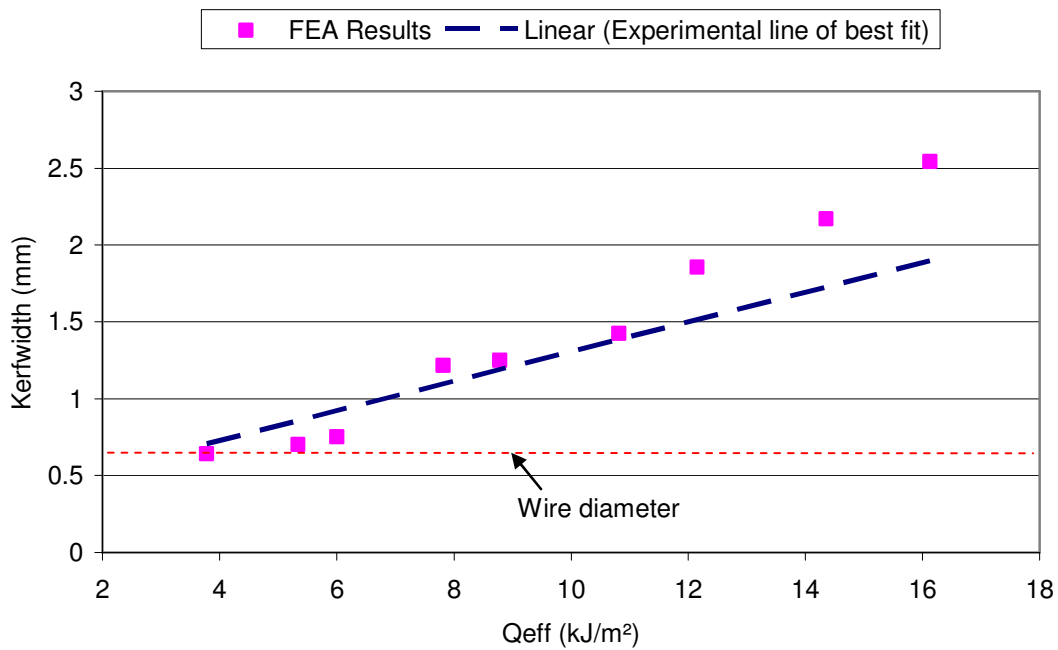


Figure 5.8. Comparison between FEA and experimental kerfwidhts (EPS, 0.64 mm wire).

The results for the 0.36 mm and 0.91 mm wires in XPS are shown below, figures 5.9 and 5.10 respectively. The results for the 0.36 mm wire are very close to the experimental data. For low Q<sub>eff</sub> values the FEA results are above the experimental line of best fit however the actual experimental results are horizontal below 5.5 kJ/m<sup>2</sup>. The range of Q<sub>eff</sub> values for both the 0.36

and 0.91 mm wires do not go as high as for the 0.64 mm wire graph, therefore the deviation in results at higher kerf widths is not seen.

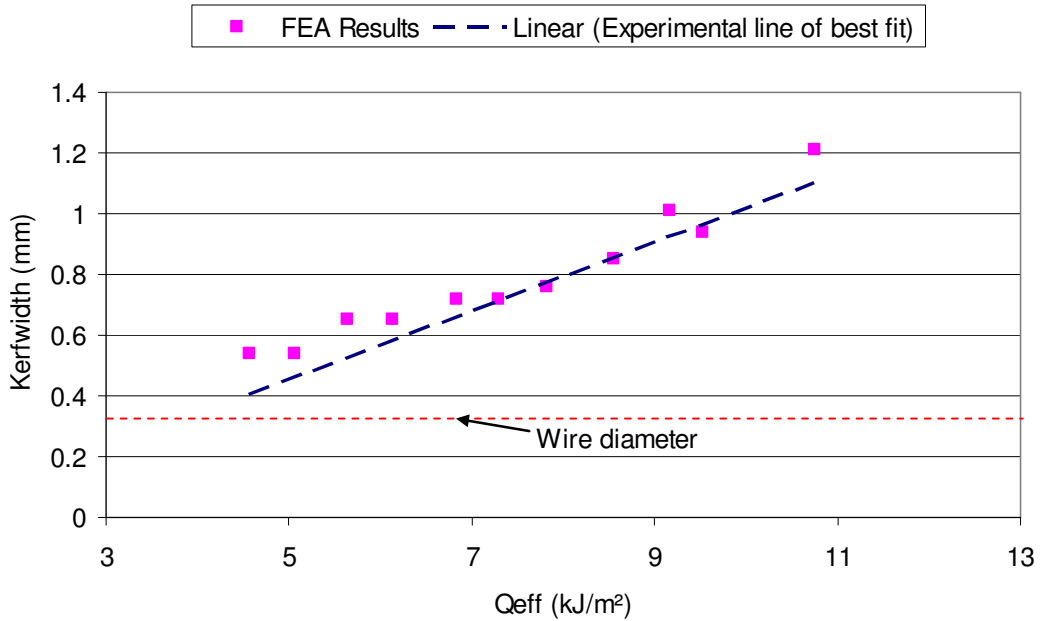


Figure 5.9. Comparison between FEA and experimental kerf widths (XPS, 0.036 mm wire).

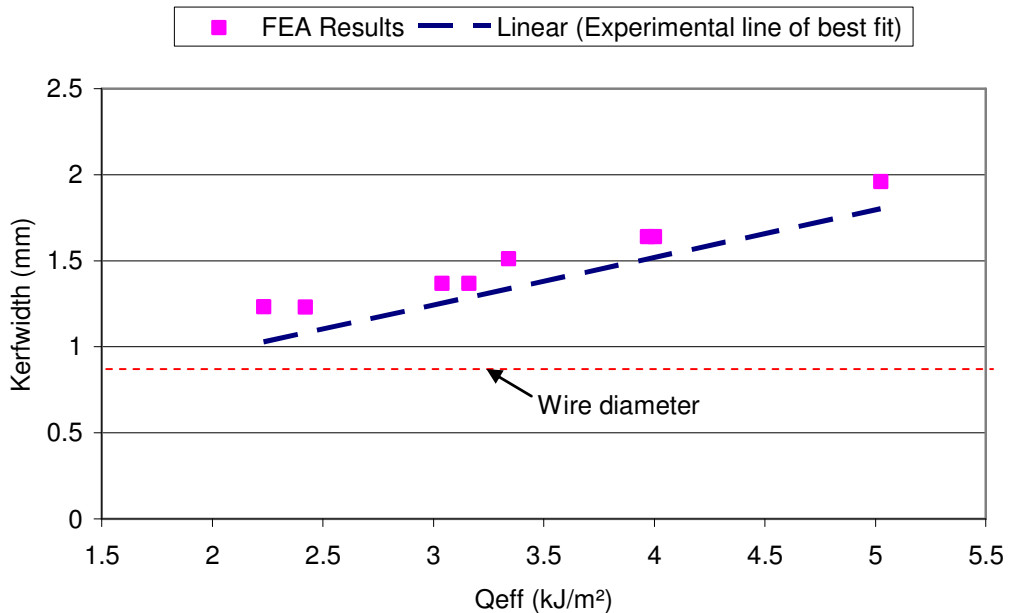


Figure 5.10. Comparison between FEA and experimental Kerfwidths (XPS, 0.91 mm wire).

The FEA results for the 0.91 mm wire in XPS are all parallel with the experimental line of best fit with a small positive offset. This could be because the range of effective heat inputs is quite low

and/or because some of the assumptions inherent in the model are not valid for large wire diameters.

In summary, the FE model was successful in predicting the kerf width for a wide variety of wire diameters and two different plastic foam types. The largest errors occurred at the maximum and minimum effective heat input values due to assumptions that became less valid with those conditions. It is believed that the accuracy of the model could be improved with more accurate material property data and temperature inputs.

## 5.4.2 Hot-ribbon Simulations

### 5.4.2.1 Hot-ribbon Straight Cuts

FEA was carried out using the same thermal model as in the previous section while changing the tool geometry to represent a ribbon. Figure 5.11 below shows the results for EPS with a ribbon temperature of 281 °C and a feed rate of 0.038 m/s. The kerf width is calculated by counting the maximum vertical number of elements within the 160 °C isotherm.

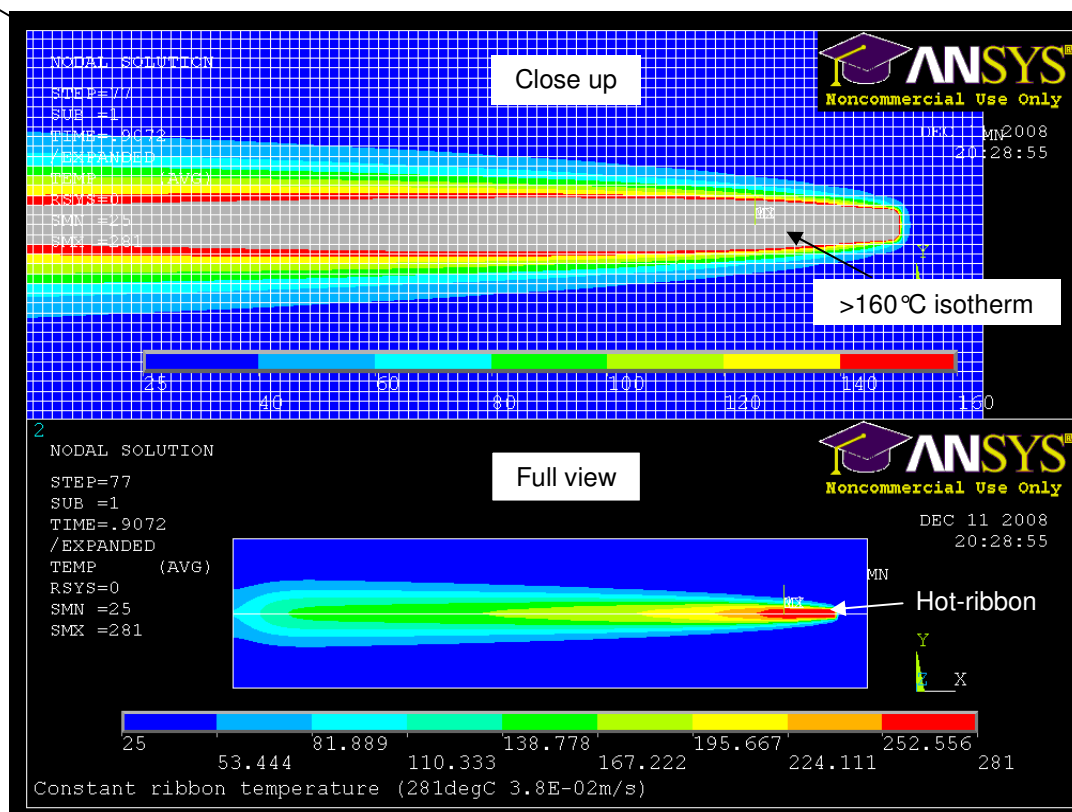


Figure 5.11. FEA temperature distribution for a hot-wire cut (EPS, ribbon, 281 °C, F0.038).

The results of all the simulations for the hot-ribbon are shown in figures 5.12 and 5.13 below. Overall the hot-ribbon simulations gave mixed results, the EPS FEA compared well with the experimental data while the XPS simulations were very poor.

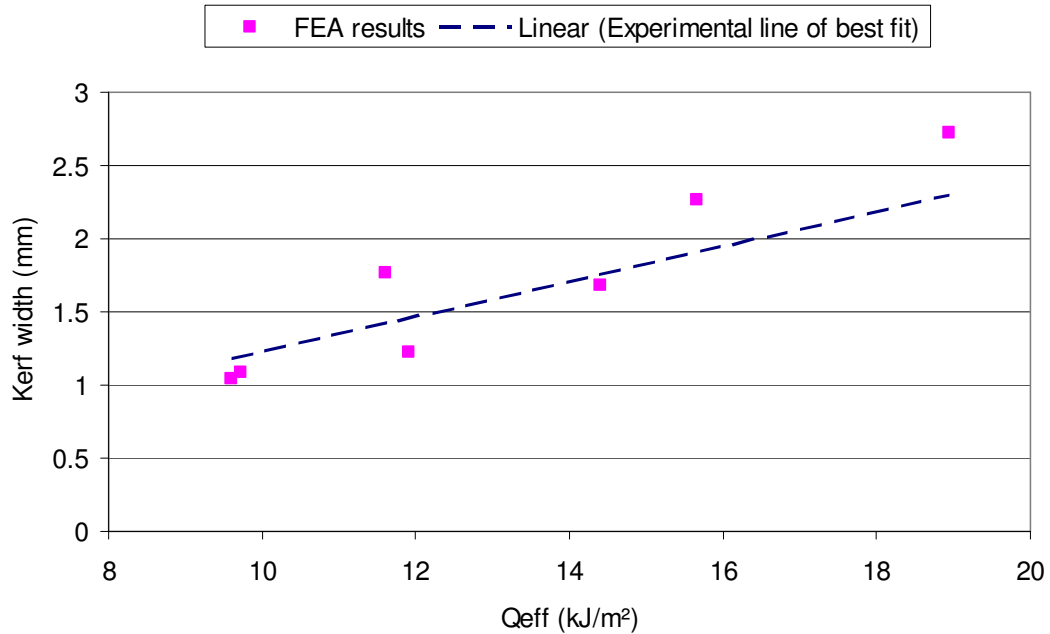


Figure 5.12. Comparison between FEA and experimental kerf widths (EPS, ribbon).

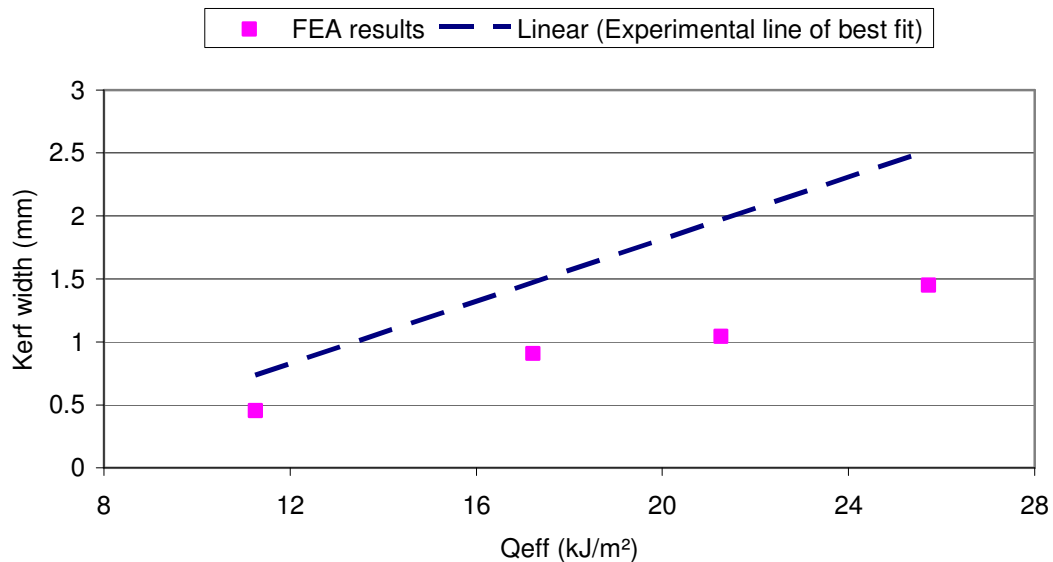


Figure 5.13. Comparison between FEA and experimental kerf widths (XPS, ribbon).

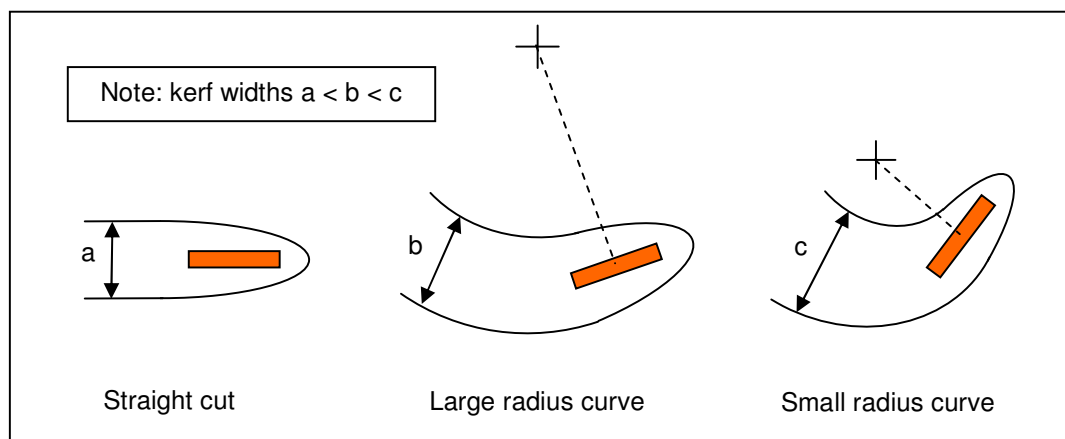
One possible reason for the poor correlation in results for XPS could be experimental error. All of the measured wire temperatures that were used in the simulations were much lower than would

normally be expected for the effective heat inputs. While the reason for this discrepancy is not known, it could have been caused by a faulty thermocouple which was not replaced until after the XPS hot-ribbon trial set or perhaps the wrong calibration numbers were used. Another possible reason is that the thermocouple selectively recorded the leading edge temperature by failing to contact the trailing edge which is much hotter. Further research is required to ensure that the poor predictions were due to faulty input data and not the thermal FE model.

In summary, the hot-ribbon FE model showed good potential in predicting the kerf widths of hot-ribbon cuts made in EPS and XPS. It is believed that much tighter correlations between the FE results and experimental results may be achieved by re-evaluating the accuracy of the hot-ribbon temperature measurements.

#### 5.4.2.2 Hot-ribbon Curved Cuts

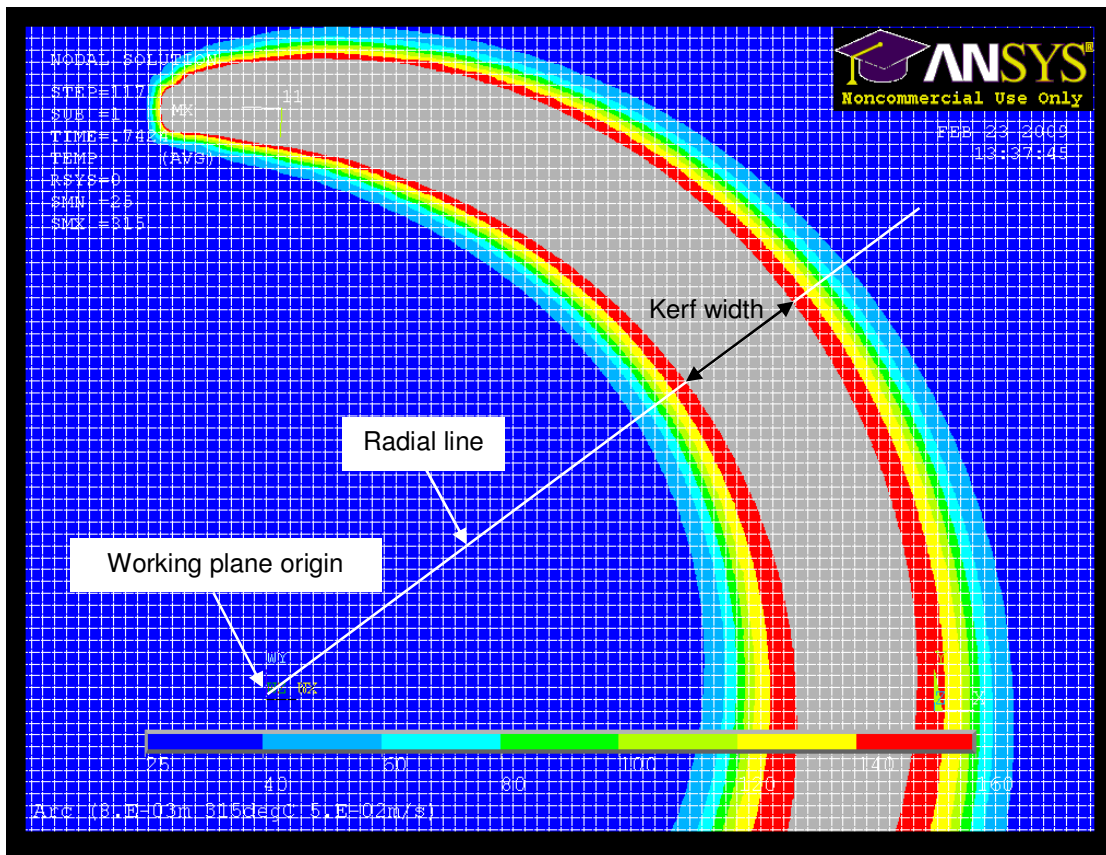
Once the FEA model was shown to provide reliable predictions of the kerf width in straight EPS cuts a second set of simulations was run in order to investigate curved cutting. Due to the fact the hot-ribbon is not symmetrical in all directions, moving the tool through an arced curve will produce different results than moving the tool in its optimum orientation in a straight line (figure 5.14).



**Figure 5.14. The effect of curve radius on kerf widths cut with a hot-ribbon.**

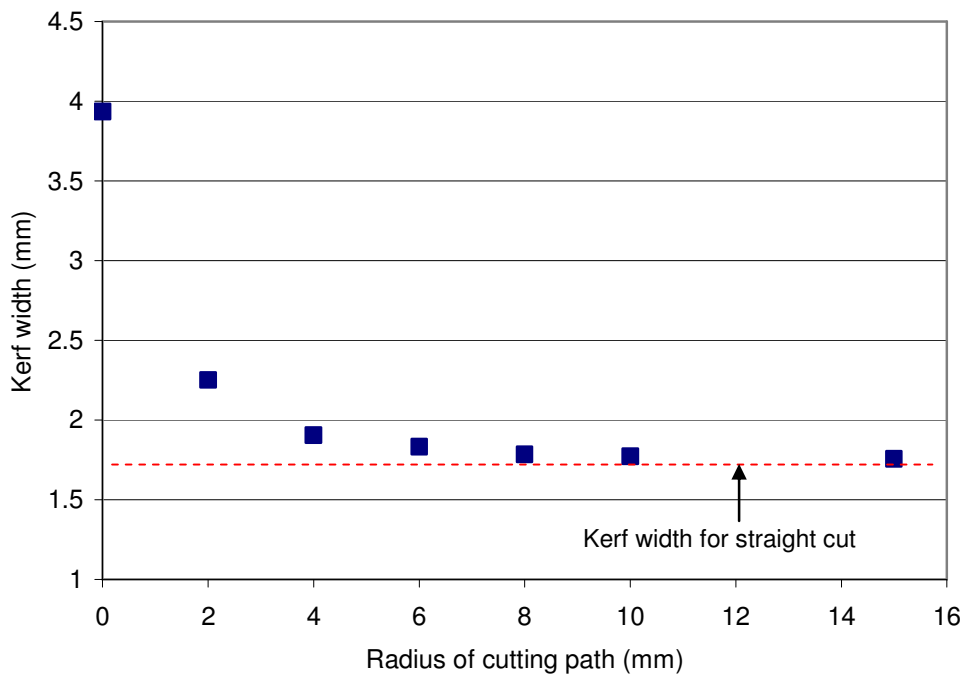
It is logical to assume that as the radius of the curve decreases the resulting kerf width will increase. Knowing how the kerf width increases relative to the cutting radius will provide limits to the minimum allowable radii for certain accuracy specifications. The simulations will also provide insights into how the cutting tool can be improved for curved cuts. Figure 5.15 shows the temperature distribution for a curved cut in EPS. The kerf width is determined by finding the largest distance within the 160°C isothermal line (grey area) that lies on a radial line from the working plane origin.





**Figure 5.15. Curved cut with a hot-ribbon in EPS (315°C, 0.050)**

The simulations were carried out for curve radii of 0, 2, 4, 6, 10 and 15 mm. They were also compared with a straight cut (representing a curve with an infinite radius). The results are summarised in figure 5.16.



**Figure 5.16. Kerf width versus radius of curve for hot-ribbon cuts (EPS, 315°C, 0.050m/s).**

The kerf width was found to increase with decreasing radii. For a cutting radius of 6 mm the kerf width was found to be 0.11 mm larger than the equivalent kerf width for a straight cut. For cutting radii less than 6 mm the kerf increases substantially. For the hot-ribbon used in this analysis it is suggested that sculpted features are limited to minimum radii over 6 mm. This is to ensure that the cutting tool can produce all detail to a sufficient level. The simulated hot-ribbon was 3.175 mm wide, which suggests a rule of thumb for calculating the minimum cutting radius is approximately twice the width of the tool (if the tool is wider than it is high, which is the case for all hot-ribbons).

Reducing the width of the ribbon will reduce the effect curved cuts have on the kerf width. Because hot-wires are symmetric in all directions the kerf width will not change for hot-wire curved cuts of different radii. To add intricate detail to sculpted parts secondary tools may be required for which the accuracy does not change when sculpting complex paths. One possible example of this kind of tool is the hot-tool developed by Ahn et al for the rapid heat ablation (RHA) process (see section 2.2.7).

## 5.5 Model limitations and Possible Improvements

The two dimensional thermal FE model developed in this chapter was considered a success, it consistently provided reasonably accurate predictions of kerf width based on wire temperatures. However, for this model to be a truly powerful predictive tool some improvements are required.

The first major limitation with the model in its current form is that the wire temperatures for each feed rate, power input and material combination need to be known in advance; which means you need to have already carried out the experiments you want to predict. Overcoming this limitation should be the first step when developing future foam cutting simulations.

The second major limitation with the model is how its predictions diverge from the experimental values at high and low values of the effective heat input. One possible method of minimising this problem is to incorporate the air gap that surrounds the tool into the model. This could be done by changing the material properties of all elements which are found to exceed the temperature at which the cells collapse (160°C for PS foams) from foam to air. The major difficulty with this solution would be accurately modelling the high density plastic layer formed by the collapsed foam. This is necessary to maintain conservation of mass and also conservation of energy.

The third limitation of the model is its inability to give any information regarding the cutting forces. While this would provide great insights into how to optimise the performance of cutting tools it would require a totally new and far more complex approach. The finite element model would need to do all of the things described above as well as model mechanical interactions involving plastic deformation, friction and adaptive meshing.

Unfortunately, due to time constraints the above improvements could not be implemented before the completion of this thesis.

## 5.6 Summary

In this chapter a finite element model was developed based on the 2D nonlinear transient thermal finite element equation derived in chapter four (Eq. 4.14). Important outcomes are as follows:

- A nonlinear transient thermal finite element model was developed with the purpose of predicting the kerf width from a wide range of feed rate and power combinations for XPS and EPS materials and tools of different sizes and geometries.

- The main assumptions in the FE model were; conduction is the only mode of heat transfer, there is no air gap surrounding the cutting tool and the kerf width is represented by the maximum height of the area enclosed by the 160 °C isotherm.
- A 2D quadrilateral element with four nodes called PLANE55 was chosen as it suited transient thermal analysis.
- The material property models were based on a mixture of experimental data and commonly accepted values found in literature.
- It is believed that the hot-tool temperature inputs, which were determined experimentally, provide the largest source of error in the final results.
- The hot-wire simulations all showed good agreement with the experimental data. The largest errors were often associated with the maximum and minimum effective heat input values for which the assumptions were less accurate.
- The hot-ribbon simulations matched the experimental data well for EPS, but poorly for XPS. This is thought to be the result of experimental error providing temperature inputs that were too low.
- FEA was used to simulate curved cuts with a hot-ribbon. For the hot-ribbon used in the simulation the kerf width was found to increase substantially when the cutting radius was below 6 mm.
- The limitations of the FE model in its current form were discussed as well as possible improvements.

## 6 Conclusions

---

This thesis has investigated hot-tool plastic foam cutting mechanics as applied to rapid prototyping and manufacturing foam cutting machines. The findings are applicable to most plastic foam cutting machines, but are particularly relevant to the FAST concept being developed at the University of Canterbury. The investigation involved the following topics:

- Assessment of current rapid prototyping and manufacturing foam cutting machines and the associated cutting mechanics found in literature.
- Empirical studies of factors that influence hot-wire and hot-ribbon cutting.
- Establishment of material properties data relevant to plastic foam cutting.
- Development of a force feedback temperature control system.
- Development of a *'Hot-tool cutting Calculator'* (HCC) based on empirical data which has the ability to predict the outcome, given a set of cutting parameters, or conversely can predict the ideal cutting parameters for a given outcome.
- Development of two-dimensional thermal finite element models of the hot-wire and hot-ribbon cutting processes.

## 6.1 Conclusions

The main achievements of the work described in this thesis are summarised in sub-sections, as follows:

### 6.1.1 Literature Review

A literature review on plastic foam cutting mechanics and foam cutting RP machines was carried out to determine what plastic foam cutting tools are being used and what previous research on plastic foam cutting mechanics had been published.

A number of large sized foam cutting RP machines were found, two of which were developed commercially [3, 6-8, 10, 11, 15, 32, 43, 49, 51]. The applications of foam prototypes can be used in a wide range of industries including: aerospace, architecture, sport, health care, advertising and product development. The two main methods of fabrication were layered manufacturing, where layers of cut foam were stacked on top of each other, and direct sculpting which uses an entirely subtractive method. The reviewed machines commonly used one of two cutting tools; either hot-wires or hot-ribbons. Hot-wires are better suited to two-dimensional profiles and ruled surfaces while hot-ribbons can be used for complex surfaces and features.

A large majority of the empirical data published on plastic foam cutting (PFC) prior to this thesis, was carried out by two groups; Ahn et al from the Department of Mechanical engineering, KAIST, Korea and Broek et al from the Faculty of Design, Engineering and Production, Delft University of Technology, Netherlands [6, 35, 42, 44, 45]. The main factors influencing plastic foam cutting can be categorised into three groups: energy parameters, material properties and tool geometry. Empirical equations relating the area specific effective heat input and kerf width have been documented. Isotropic material properties were shown to affect the cutting characteristics.

Examination of the literature revealed much experimental work was still required to elevate the understanding of foam cutting from a black art to a scientifically critiqued manufacturing process. This experimental work formed the basis for chapter 3.

PFC is difficult to model analytically from first principles because of the inherent non-linear relationships; therefore numerical methods are more commonly used. Finite element analysis was employed by Ahn et al [42] in order to investigate the influence of the cutting parameters on the temperature distribution around cutting elements and to determine the optimal cutting conditions. Satisfactory results were achieved through computational simulations providing kerf widths based on isothermal temperature contours. These simulations were highly simplified versions of the real processes and contained questionable inputs, such as boundary conditions and material properties. Also no information on the numerical simulation for the generation of

complex surfaces was available. Advancing the numerical simulation of plastic foam cutting was the motivation for chapters 4 and 5.

### **6.1.2 Empirical Studies of Plastic Foam Cutting**

The hot-wire and hot-ribbon cutting trials carried out in this thesis were extensive. Collectively over 800 individual cutting tests were made. The cutting trials included two main material sets, EPS and XPS, three different wire diameters, two hot-ribbon configurations and a wide range of feed rates and power inputs. For each cut the cutting force, wire temperature and kerf width was measured as well as observations of the surface texture.

When using constant current conditions the cutting mechanisms change over the length of the cut. These changes can be described in three unique stages. Stage I is characterised by low cutting forces. Stage II represents the transition from stage I to stage III. Stage III is characterised by stable relatively high cutting forces.

The surface texture along a sample, cut with constant current, changes depending on the cutting force present at that position. High cutting forces result in mechanically ripped or wavy surfaces. Low non-zero cutting forces provide the smoothest surfaces as the wire shears the adjacent molten plastic filling in the cell boundaries. When cutting forces are zero the wire is sufficiently hot to melt the foam ahead of the wire resulting in a granular surface texture due to preferential melting at the cell boundaries.

Thermocouples and a thermal imaging camera were used to observe the temperature profiles of hot-tools during cutting. 0.64 mm diameter Nichrome wires were found to cool as much as 250 °C along the length of a cut. Higher wire temperatures at the edges of the cut were found to result in a barrelling effect on the surface of the foam. A transverse temperature gradient was successfully measured during hot-ribbon cutting using a thermal imaging camera. The leading edge of the ribbon was found to be as much as 200 °C cooler than the trailing edge. This temperature profile helps to explain some of the transient temperature effects associated with hot-ribbon cutting and should be included in any future FE models developed. Asymmetrical temperature profiles were found to exist along the profile of shaped hot-ribbon tools. This asymmetry was caused by the necessary machining strategy used to cut complex surfaces whereby the cutting tool path is incrementally stepped with a small overlap. The result is one side of the tool is hotter than the other side, causing a 'weatherboarding' effect on the surface. A method of optimising the tool shape to compensate for this effect was proposed.

Kerf widths generated by hot-wires were found to vary between 1.4 to 6 times the diameter of the wire over the experimental range of parameters. Similar multipliers are seen with hot-ribbons.

This means that not knowing the kerf width could be a serious source of error when sculpting three dimensional objects.

A new parameter was formulated called the mass specific effective heat input,  $^{Mass}Q_{eff}$ , which, once obtained, can be used to predict the kerf width that will result from using a foam/tool combination. The  $^{Mass}Q_{eff}$  combines all the previously disparate parameters into a single entity representing the culmination of knowledge in the experimental portion of this thesis.

### 6.1.3 Material Property Tests

A range of material property tests were carried out to determine values that could not be found in the literature or to verify values obtained from disparate sources. Experiments were also carried out to verify common industry values against values obtained for the specific materials used in the cutting trials (as the material properties could have been highly batch dependant). The range of experiments conducted include; thermal gravimetric analysis (TGA), dynamic mechanical analysis (DMA), differential scanning calorimetry (DSC) and hot disk analysis (HDA).

The data from these experiments helped in two main ways: The data confirmed many of the values found in literature and provided reassurance that materials of the same grade differ only slightly between different manufacturers.

### 6.1.4 Force Feedback Control System

A method of controlling the temperature of hot-tools throughout a cut was conceived, designed and developed which used force feedback to modulate the electrical power. It was successful in creating constant cutting conditions and therefore enabled cuts to be made with constant kerf widths and surface textures. Maintaining constant cutting conditions during a rather dynamic cutting process is considered of the utmost importance for increasing the quality of PFC. While it is considered possible that off-line temperature control may be possible in the near future, force feedback temperature control provides another option that has proved effective. Limitations and improvements to the force feedback control system have also been suggested.

### 6.1.5 Hot-tool Cutting Calculator

A hot-tool cutting calculator (HCC) was developed utilising the  $^{Mass}Q_{eff}$  to provide an effortless way to predict the cutting conditions for previously untested cutting conditions. The HCC can also be used to calculate the  $^{Mass}Q_{eff}$  from experimental data.

A method of incorporating the equations embedded in the HCC into CAM software was suggested which could greatly increase the speed, accuracy and utility of automated sculpting



technology. The HCC is a step toward the future goal of adding artificial intelligence to the CAM process which will further increase the automation potential of the FAST system.

### **6.1.6 Numerical Model and Simulation**

A nonlinear transient thermal finite element model was developed with the purpose of predicting the kerf width of a wide range of feed rate and power combinations for XPS and EPS materials and tools of different sizes and geometries.

The main assumptions in the FE model were: conduction was the only mode of heat transfer; there was no air gap surrounding the cutting tool; and the kerf width was represented by the maximum height of the area enclosed by the 160°C isotherm (160°C being the temperature at which the cellular structure of foam collapses). A FEA software package called ANSYS was used to simulate the plastic foam cutting. A 2D quadrilateral element with four nodes called PLANE55 was chosen as it was well suited to transient thermal analysis. The material property models were based on a mixture of experimental data and commonly accepted values found in literature.

With the exception of the XPS hot-ribbon cuts the simulations showed good agreement with the experimental data. The reason for the poor agreement between the FEA and the experimental kerf width for the XPS hot-ribbon cuts is thought to be poor ribbon temperature inputs. The measured temperature inputs were lower than expected and thus resulted in smaller calculated kerf widths. All of the other simulations showed good agreement and thus the model is thought to be reliable. The largest errors were often associated with the maximum and minimum effective heat input values for which the assumptions were less accurate.

### **6.1.7 Summary**

This study has added considerably to the pool of knowledge for foam cutting with a hot-tool. In general, much of the work reported herein has not been previously published. This work provides the most advanced study of foam sculpting work available to date.

Other works carried out by the author that have been accepted for publication or are currently being reviewed are in appendix J. Further work is currently being drafted.

## 7 Recommendations ---

Important recommendations for future research in improving plastic foam cutting techniques arise from discussions in the main text and from the conclusions. The following sections summarise these potential research works.

### 7.1.1 FAST Machine Technology

The size of objects able to be sculpted with FAST (without an indexing table) is restricted by the reachability of the robot. Currently this is a severe limitation of the system as the robot needs to be able to reach both sides of the foam blank. Improving the build size of the robot system should be a high priority objective of further research. One possible solution to this problem is to add a foam holding device with two rotational degrees of freedom, similar to that used by Zhu et al [11]. Ideally the foam holding device will resemble a turntable that can turn the foam blank so the robot can easily sculpt both sides of the object. The turntable should also be capable of tilting the foam towards and away from the robot to allow the top and bottom of the foam to be cut. A way of attaching the foam to the turntable will need to be designed so the foam can be efficiently attached and removed without damaging the foam. The two extra axes should move synchronously with the robot to allow maximum feed rates to be achieved.

### 7.1.2 Further Experimental Studies

One aspect of PFC not covered in this thesis is the quantitative assessment of surface texture and surface form. It has been found that depending on the cutting mechanisms present a wide

range of surface textures are possible. This is further complicated by the fact that different foams, such as EPS and XPS, have very different cellular structures. Accurately knowing the surface roughness of sculpted parts and how to improve the surface for different applications is crucial for the development of high accuracy sculpting. Coordinate measuring machines (CMMs) with stylus type probes are not ideal for measuring foam surface form because foam surfaces are relatively soft and the stylus can damage the surface. In light of this problem it is suggested that non-contact measurement methods are developed, such as optical scanners. It may turn out that there is no one measuring method that will obtain highly accurate measurements for both surface texture and surface form for both EPS and XPS and multiple measurement methods will need to be developed. This is a topic currently being studied by a colleague at the University of Canterbury.

While the cutting trials in this thesis were extensive only a small fraction of hot-tool/foam material combinations were studied in detail. There is still no source available whereby an operator of a foam cutting machine can find information on how a wide range of foams should be cut for best results. A database is needed whereby the mass specific effective heat input,  $^{Mass} Q_{eff}$ , for many material/tool combinations are recorded, as well as equations relating the tool temperature to the kerf width. Not only would this database be useful for all foam cutting applications it could form the basis for expert knowledge relationships within a CAM system.

### 7.1.3 Tool path Generation and Optimisation

The main motivation for research into plastic foam cutting mechanics was to understand the cutting mechanisms so that the quality of foam cut objects may be improved. Work carried out in this thesis led to the development of the Hot-tool Cutting Calculator (HCC) which calculates the steady state kerf width as a function of the  $^{Mass} Q_{eff}$ , electrical power, feed rate and the material density. The current FAST system uses semi-automated tool path generation with constant velocity cuts. To increase the sculpting speed of FAST tool path generation software is required that allows the cutting tool to accelerate and decelerate whilst cutting. This way the cutting tool can be moved at maximum speed at all locations within the robots working volume. The HCC with the aid of a database could be used to adjust the electrical power to the cutting tool to maintain constant tool temperature during intermittent cutting and when the tool is changing speed within the foam.

### 7.1.4 Numerical Simulations

This thesis has presented simulations of hot-wire and hot-ribbon cutting by modelling the heat transferred from the cutting tool to the surrounding foam material via conduction. While this

model was found to be useful for the prediction of the kerf width, there are four main issues that need to be addressed to make the model more useful for generalised hot-tool foam cutting.

Firstly, the simulations should not require any prior information that requires experimental testing. This means that the only inputs should be known material properties, cutting tool and foam geometries, power inputs, cutting paths and cutting velocity, all of which are known beforehand. It is not currently known how this may be done in practice, however if it is possible then the simulations could be used to calculate the  $^{Mass}Q_{eff}$  without need for time consuming and expensive experiments.

Secondly, the simulations should model the air gap necessary for actual foam cutting. This is a prerequisite to modelling the mechanical tool/foam interactions. The air gap in front of the wire will depend on the wire temperature and may be zero (i.e. perfect contact).

Thirdly, the model should allow the simulation of complex cuts in addition to linear cuts. This is crucial for determining the effects of tool geometry and tool paths and will allow the analysis of special cutting conditions (e.g. when a hot-ribbon is used to cut a highly curved surface or to create a pocket by plunging into foam end on).

Lastly, modelling the mechanical interaction between the cutting tool and the wire will provide additional information on tool life and surface texture, which could be used to predict the range of allowable cutting conditions.

Implementing any or all of these suggested improvements to the numerical simulations would greatly increase the usefulness of the simulations by reducing the information needed as inputs and improving cutting tool design.

### **7.1.5 Numerical Optimisation of Cutting Tool Design**

The above computational simulations of plastic foam cutting remain limited to predicting the result of inputted cutting parameters. Design optimisation could be used to design cutting tools uniquely suited to the cutting strategies of different foam cutting machines. For example, the shape of hot-ribbons may be optimised for strength in the cutting direction or to minimise the effect of asymmetrical heating.

### **7.1.6 Design for Manufacturability (DFM) Rules**

Design for Manufacturability (DFM) is the process of designing a product in such a way that reduces the cost and improves manufacturability. It is much less expensive to intercept manufacturing problems at the design phase than it is in the manufacturing phase.

A set of DFM rules should be formulated to aid the manufacture of plastic foam objects cut with hot-tools. One such rule may be to eliminate the need for sharp (> 6 mm) radii features or holes in objects that will be sculpted with a hot- ribbon.

## 8 References

---

- [1] D. Klemptner and K. C. Frisch, *Handbook of polymeric foams and foam technology*. Munich ; New York: Hanser ; Distributed in U.S.A. and Canada by Oxford University Press, 1991.
- [2] A. Novac, Kaza, S., Wang, Z., Thomas, C., "Techniques for Improved Speed and Accuracy in Layered Manufacturing," in *Proceedings of Solid Free-form Symposium*, Austin, Texas, 1996, pp. 609-617.
- [3] R. L. Hope, Roth, R.N., Rieck, A.T., "Layer building with sloping edges for rapid prototyping of large objects," in *5th European Conference on Rapid Prototyping and Manufacturing.*, Helsinki, Finland., 1996.
- [4] M. Jouaneh, A. Hammad, and P. Datseris, "A flexible automated foam cutting system," *International Journal of Machine Tools and Manufacture*, vol. 37, pp. 437-449, 1997.
- [5] D. G. Ahn, S. H. Lee, and D. Y. Yang, "Investigation into development of progressive-type variable lamination manufacturing using expandable polystyrene foam and its apparatus," *Proceedings of the I MECH E Part B Journal of Engineering Manufacture*, vol. Volume 216, pp. pp. 1239-1252, 1 September 2002 2002.
- [6] J. J. Broek, I. Horvath, B. de Smit, A. F. Lennings, Z. Rusak, and J. S. M. Vergeest, "Free-form thick layer object manufacturing technology for large-sized physical models," *Automation in Construction*, vol. 11, pp. 335-347, 2002.

- [7] D. R. Aitchison and R. Sulaiman, "A new adaptable rapid prototyping & manufacturing approach for producing a variety of foam-based product solutions," in *NordDesign 2004 – Product Design in Changing Environment* Tampere, Finland, 2004.
- [8] R. F. Hamade, F. Zeineddine, B. Akle, and A. Smaili, "Modelangelo: a subtractive 5-axis robotic arm for rapid prototyping," *Robotics and Computer-Integrated Manufacturing*, vol. 21, pp. 133-144, 2005.
- [9] H. C. Kim, D. G. Ahn, S. H. Lee, and D. Y. Yang, "A study on thermal characteristics of non-contact hot-tool for rapid feature detailing (RFD) process," *International Journal of Machine Tools and Manufacture*, vol. 45, pp. 345-353, 2005.
- [10] H. C. Kim, S. H. Lee, and D. Y. Yang, "Development of a rapid heat ablation (RHA) process using a hot tool," *International Journal of Machine Tools and Manufacture*, vol. In Press, Corrected Proof, 2006.
- [11] J. Zhu, R. Tanaka, T. Tanaka, and Y. Saito, "An 8-axis robot based rough cutting system for surface sculpturing," in *11th International Conference on Precision Engineering (11th ICPE)*, Tokyo, Japan, 2006, pp. p139-144
- [12] D. Aitchison, H. Brooks, R. Kandula, B. Kraus, and M. Taylor, "Feed-rate, Temperature and Feed-force Relationships for Foam Plastics Cut by a Taut Hot-wire," in *International Conference on Manufacturing Science and Technology* Melaka, Malaysia: Proceedings of ICOMAST2006, 2006.
- [13] D. Aitchison and R. Sulaiman, "Determining the surface form of polystyrene through the coordinate measurement machine," *Proceedings of the Institution of Mechanical Engineers, Part C: Journal of Mechanical Engineering Science*, vol. V217, pp. 839-844, 2003.
- [14] H. Brooks and D. Aitchison, "Thermal Plastic Foam Cutting Mechanics for Rapid Prototyping and Manufacturing Purposes," in *9th National Conference on Rapid Design, Prototyping and Manufacturing.*, Lancaster University, 2008, pp. 33-40.
- [15] M. G. Taylor, "Semi-automated Robotic Sculpting of Freeform Surfaces for Direct Digital Manufacture," in *International Conference on Mechanical & Manufacturing Engineering (ICME2008)*, Johor Bahru, Malaysia, 2008.
- [16] MegaPlot, "Photo Gallery," <http://www.foamcutter.pl/index.php?id=286>, 2007.
- [17] Joseph J. Beaman, Joel W. Barlow, David L. Bourell, and Richard Crawford, *Solid Freeform Fabrication : A New Direction in Manufacturing: With Research and Applications in Thermal Laser Processing*: Kluwer Academic Publishing, 1997.
- [18] Digital Division, "Glossary," [www.digital-division.com/1\\_3d\\_digitalisieren\\_folder\\_e/glossary.html](http://www.digital-division.com/1_3d_digitalisieren_folder_e/glossary.html), 2007.
- [19] Prototype Magazine, "Roland MDX 540," in *Prototype Magazine*, 2007.
- [20] T. Grim, *User's Guide to Rapid Prototyping*. Dearborn, Michigan: Society of Manufacturing Engineers, Rapid Prototyping Association of SME, 2004.
- [21] T. Wohlers, "Wohlers Report 2006," Fort Collins, Colorado, USA, Executive Summary 2006.
- [22] Mastercam, <http://www.mastercam.com/Default.aspx>, 2009.

- [23] C. K. Chua, S. M. Chou, and T. S. Wong, "A study of the state-of-the-art rapid prototyping technologies," *The International Journal of Advanced Manufacturing Technology*, vol. V14, pp. 146-152, 1998.
- [24] K. G. Cooper, *Rapid Prototyping Technology: Selection and Application*. New York, Basel: Marcel Dekker, Inc., 2001.
- [25] P. Gallina, "Delayed reference control for hotwire cutting of expandable polystyrene foam," *Journal of Manufacturing Science and Engineering, Transactions of the ASME*, vol. 128, pp. 360-365, 2006.
- [26] MegaPlot, "Available Models," <http://www.foamcutter.pl/index.php?id=242>, 2007.
- [27] Demand Products Inc, "Foam Cutting," <http://www.demandproducts.com/foamcut.html>, 2007.
- [28] 3D Custom Foam Inc, <http://www.3dcustomfoam.com/s/Home.asp>, 2007.
- [29] D. Aitchison, J. Bain, H. Brooks, A. Posthuma, and M. Taylor, "Transient Temperature Effects in Hot-wire Plastic Foam Cutting," in *4th International Conference and Exhibition on Design and Production of MACHINES and DIES/MOLDS*, Cesme, Turkey, 2007, pp. 219-224.
- [30] Johan Tangelder, "Automated fabrication of shape models of free-form objects with a sculpturing robot," in *Department of Computer Science Utrecht: Utrecht University*, 1998.
- [31] J. Broek, I. Horvath, B. de Smit, A. Lennings, and J. Vergeest, "A Survey of the State of Art in Thick Layered Manufacturing of Large Objects and the Presentation of a Newly Developed System," in *First International Seminar and Workshop on Engineering Design in Integrated Product Development - EDIPROD'98*, Zielona Gora, Poland, 1998, pp. IV-1..IV-12.
- [32] A. Posthuma, "Development of a novel robotically effected plastic foam sculpting system for rapid prototyping and manufacturing," in *Department of Mechanical Engineering*. vol. M.E. Christchurch: University of Canterbury, 2007, p. 144.
- [33] R. L. Hope, Jacobs, P.A., Roth, R.N., "Rapid prototyping with sloping surfaces," *Rapid prototyping journal*, vol. vol 3, pp. pp 12-19, 1997 1997.
- [34] C. L. Thomas, T. M. Gaffney, S. Kaza, and C. H. Lee, "Rapid prototyping of large scale aerospace structures," in *Aerospace Applications Conference, 1996. Proceedings., 1996 IEEE*, 1996, pp. 219-230 vol.4.
- [35] B. De Smit, J. Broek, and I. Horvath, "Experimental Investigation Of Factors Influential For The Flexible Blade Based Prototyping Process," in *The 1999 ASME Design Engineering Technical Conference*, Las Vegas, Nevada, USA, 1999.
- [36] I. Horvath, J. S. M. Vergeest, J. J. Broek, Z. Rusak, and B. de Smit, "Tool profile and tool path calculation for free-form thick-layered fabrication," *Computer-Aided Design*, vol. 30, pp. 1097-1110, 1999.
- [37] B. De Smit, J. Broek, I. Horvath, and L. Lennings, "Implementation of the Freeform Thick Layered Object Manufacturing Technology (FF-TLOM), a status review," in *The 9th European Conference on Rapid Prototyping and Manufacturing*, 2000, pp. 311 - 321.
- [38] B. De Smit, J. Broek, I. Horvath, A. Medland, and A. F. Lennings, "Comparative Analysis and Experimental Verification of the Computed Shape of a Flexible Blade Tool for FF-

- TLOM," in *5th ASME Design for Manufacturing Conference*, Baltimore, Maryland, USA, 2000.
- [39] J. Broek, I. Horvath, and B. de Smit, "Exploration of Influential Parameters for Speed Control of the Flexible Blade Cutting Process," in *TMCE*, Wuhan, China, 2002.
- [40] B. De Smit, A. Kooijman, J. Broek, and I. Horvath, "Developing a Tool for the Direct Cutting of Freeform Surfaces out of Extruded Polystyrene Foam," in *Euro-u Rapid 2002 Conference*, 2002.
- [41] B. De Smit, P. De Jager, A. Kooijman, and H. Broek, "Experimental Results on the Application of FF-TLOM Technology for the Creation of a Large Freeform Shape," Faculty of Design Engineering and Production, Delft University of Technology, 2001.
- [42] D. G. Ahn, S. H. Lee, and D. Y. Yang, "Investigation into thermal characteristics of linear hotwire cutting system for variable lamination manufacturing (VLM) process by using expandable polystyrene foam," *International Journal of Machine Tools and Manufacture*, vol. 42, pp. 427-439, 2002.
- [43] D. G. Ahn, S. H. Lee, and D. Y. Yang, "Development of transfer type variable lamination manufacturing (VLM-) process," *International Journal of Machine Tools and Manufacture*, vol. 42, pp. 1577-1587, 2002.
- [44] D. G. Ahn, S. H. Lee, and D. Y. Yang, "A study on the influence of the sloped cutting angle on kerfwidth and part quality in the hotwire cutting of EPS foam for the VLM- rapid prototyping process," *International Journal of Machine Tools and Manufacture*, vol. 43, pp. 1447-1464, 2003.
- [45] D.-G. Ahn, S.-H. Lee, and D.-Y. Yang, "Influence of process parameters on the surface roughness in hotwire cutting of EPS foam sheet for VLM-S rapid prototyping process," *Journal of Materials Science*, vol. 40, pp. 5699-5702, 2005.
- [46] H. C. Kim, S. H. Lee, and D. Y. Yang, "A study of tool design for minimization of heat-affected zone in rapid heat ablation process," *Journal of Materials Processing Technology*, vol. 187-188, pp. 51-55, 2007.
- [47] J. Zhu, T. Tanaka, and Y. Saito, "3D mesh simplification for freeform surfacing," in *Tehran International Congress on Manufacturing Engineering (TICME2005)*, Tehran, Iran, 2005, pp. (CD-ROM Proceeding).
- [48] Cirtes, "Computer-Assisted Foam-Cutting Systems for Rapid Prototyping Enhanced by Stratoconception Technology," in *European Tool and Mould Making*, 2007, p. 22.
- [49] Croma, "Foam Processing Technologies," <http://www.croma-foamcutter.com/>, 13/03/2008.
- [50] S. Mehta, S. Biederman, and S. Shivkumar, "Thermal degradation of foamed polystyrene," *Journal of Materials Science*, pp. 2944-2949, 1995.
- [51] L. Menix Engineering Co., "Rapid Shaper." vol. <http://www.rapidshaper.com> Korea, 2008.
- [52] R. Svecko, A. Chowdhury, M. Bolcina, and R. Tusck, "Computer Controlled Machine for Cutting Expanded Polystyrene," *Electrotechnical Review, Ljubljana, Slovenija*, vol. Elektrotehnisiki vestnik 67(2), pp. 145-151, 19-01-2000 2000.



- [53] B. Wunderlich, A. Boller, I. Okazaki, and S. Kreitmeier, "Modulated differential scanning calorimetry in the glass transition region," *Journal of Thermal Analysis and Calorimetry*, vol. 47, pp. 1013-1026, 1996.
- [54] T. Osswald and J. P. Hernandez-Ortiz, *Polymer Processing: modelling and simulation*. Munich: Carl Hanser, 2006.
- [55] F. P. Incropera, *Fundamentals of Heat and Mass Transfer*, 6th ed. New York: John Wiley & Sons, Inc, 2007.
- [56] K. H. Huebner and E. A. Thornton, *Finite Element Method for Engineers*, Second Edition ed. New York: Wiley - Interscience, 1942.
- [57] "ANSYS software," Version 11.0 ed, USA: ANSYS Inc, 2007.
- [58] R. D. Cook, D. S. Malkus, M. E. Plesha, and R. J. Witt, *Concepts and Applications of Finite Element Analysis*, Fourth Edition ed. University of Wisconsin - Madison: John Wiley & Sons, Inc., 2002.
- [59] Y. S. Touloukian, *Thermophysical properties of matter: [the TPRC data series: a comprehensive compilation of data]*, 1999 ed. vol. v2,10. New York: IFI/Plenum, 1970-79.
- [60] Y. S. Touloukian and C. Y. Ho, *Thermal Conductivity of Nonmetallic Solids*. New York: Plenum Press, 1972.

## **Appendices** \_\_\_\_\_

# Appendix A

## Materials Testing Data

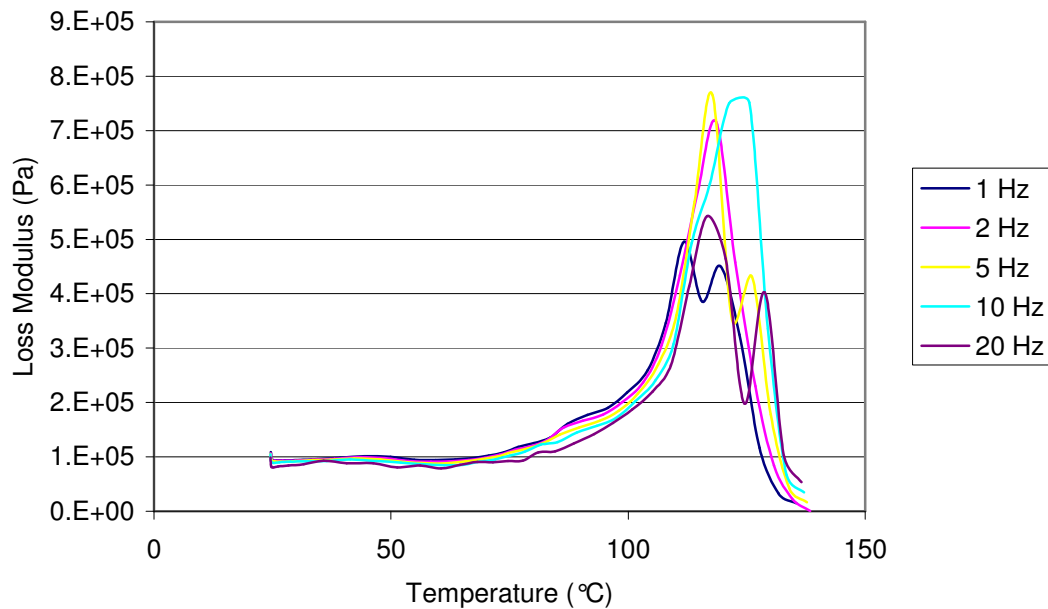


Figure A1. XPS loss modulus, normal direction.

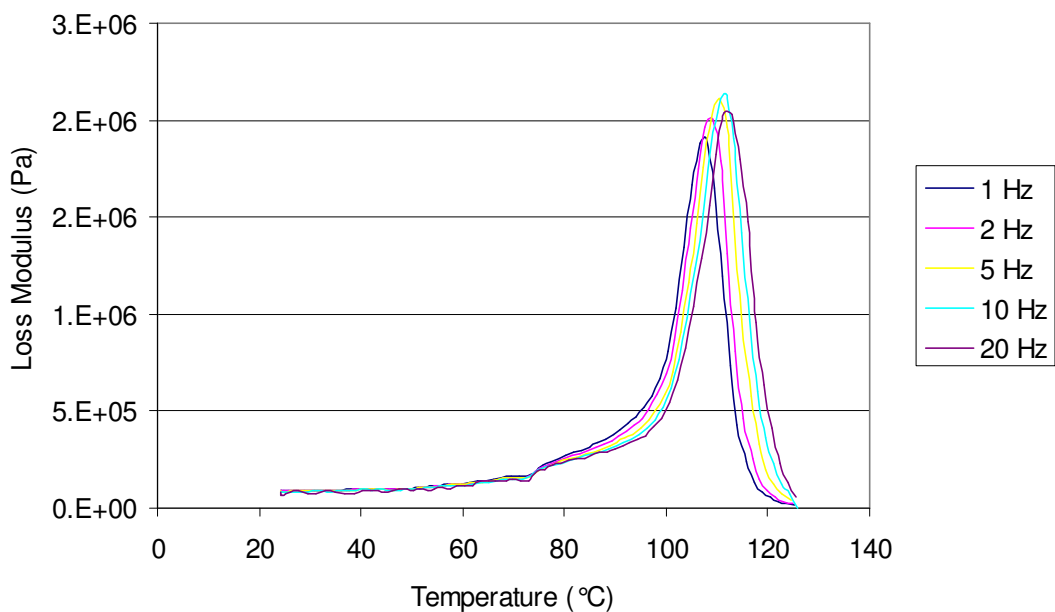


Figure A2. XPS loss modulus, parallel direction.

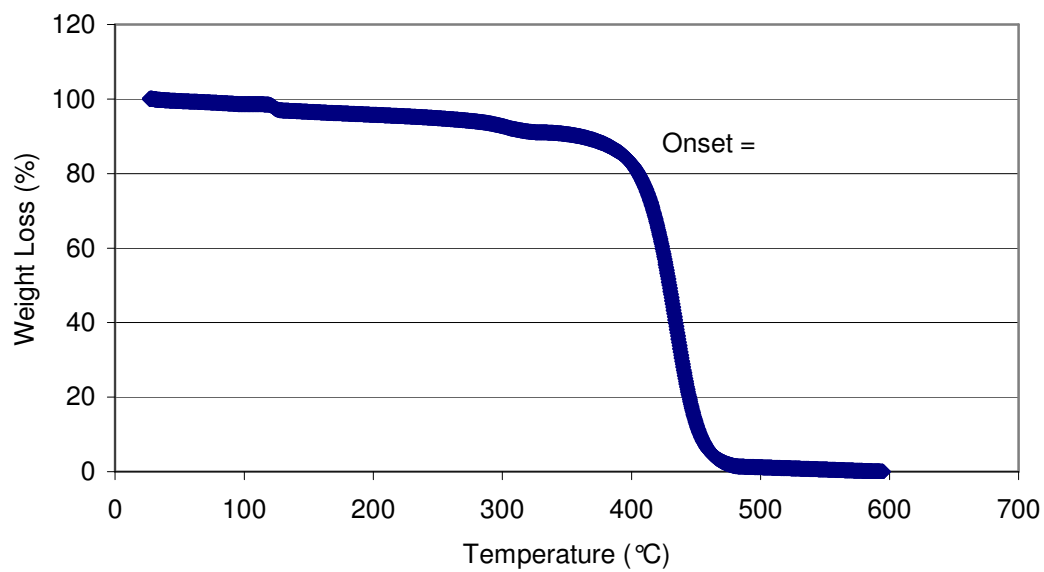


Figure A3. XPS TGA, 25 °C/min.

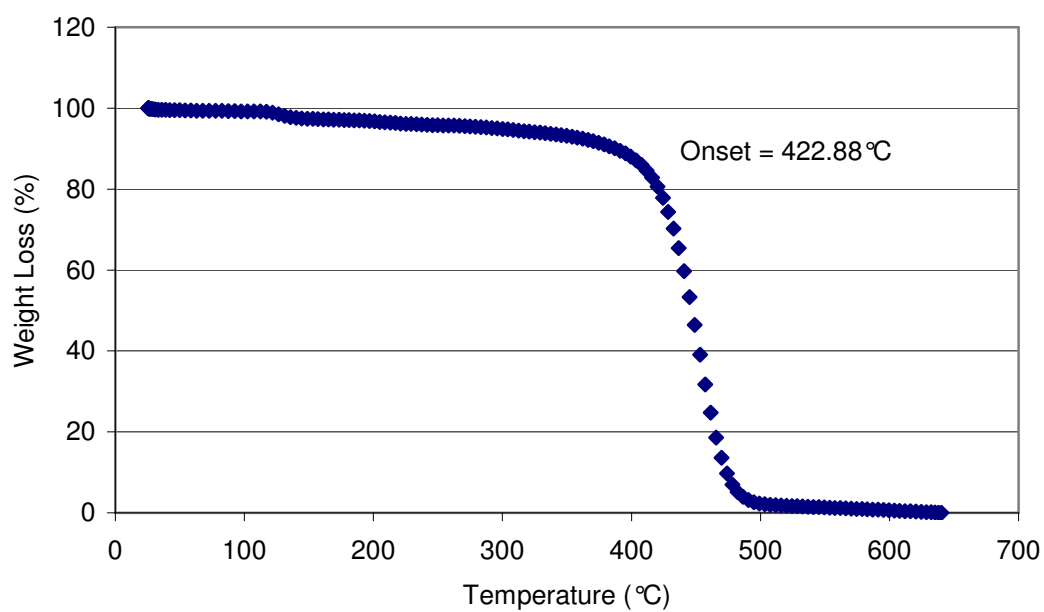


Figure A4. EPS TGA, 50 °C/min.

**Table A1. Nichrome wire properties.**

		Degrees F	400	600	800	100	1200	1400	1600	1800	2000
		Degrees C	205	315	427	538	649	760	871	982	1093
AWG Size	□ (Inches)	□ (mm)	Current (Amperes)								
8	0.128	3.2512	22.4	32	41	52	65	79	95	111	128
9	0.114	2.8956	18.8	26.8	34.5	44	55	67	80	94	108
10	0.102	2.5908	16.2	23.3	29.7	37.5	46	56	68	80	92
11	0.091	2.3114	13.8	19.2	24.8	31.5	39	48	57	67	78
12	0.081	2.0574	11.6	16.1	20.8	26.5	33.5	40.8	48	56	65
13	0.072	1.8288	9.8	13.6	17.6	22.5	28.2	34.2	41	48	55
14	0.064	1.6256	8.4	11.6	15	18.8	23.5	29	34.6	40.5	46
15	0.057	1.4478	7.2	10	12.8	16.1	20	24.5	29.4	34.3	39.2
16	0.051	1.2954	6.4	8.7	10.9	13.7	17	20.9	25.1	29.4	33.6
17	0.045	1.143	5.5	7.5	9.5	11.7	14.5	17.6	21.1	24.6	28.1
18	0.04	1.016	4.78	6.5	8.2	10.1	12.2	14.8	17.7	20.7	23.7
19	0.036	0.9144	4.3	5.8	7.2	8.7	10.6	12.7	15.2	17.8	20.5
20	0.032	0.8128	3.8	5.1	6.3	7.6	9.1	11	13	15.2	17.5
21	0.0285	0.7239	3.36	4.3	5.3	6.5	7.8	9.4	11	12.9	14.8
22	0.025	0.635	2.9	3.7	4.5	5.6	6.8	8.2	9.6	11	12.5
23	0.0226	0.57404	2.58	3.3	4	4.9	5.9	7	8.3	9.6	11
24	0.02	0.508	2.21	2.9	3.4	4.2	5.1	6	7.1	8.2	9.4
25	0.0179	0.45466	1.92	2.52	3	3.6	4.3	5.2	6.1	7.1	8
26	0.0159	0.40386	1.67	2.14	2.6	3.2	3.8	4.5	5.3	6.1	6.9
27	0.0142	0.36068	1.44	1.84	2.25	2.73	3.3	3.9	4.6	5.3	6
28	0.0126	0.32004	1.24	1.61	1.95	2.38	2.85	3.4	3.9	4.5	5.1
29	0.0113	0.28702	1.08	1.41	1.73	2.1	2.51	2.95	3.4	3.9	4.4
30	0.01	0.254	0.92	1.19	1.47	1.78	2.14	2.52	2.9	3.3	3.7
31	0.0089	0.22606	0.77	1.03	1.28	1.54	1.84	2.17	2.52	2.85	3.2
32	0.008	0.2032	0.68	0.9	1.13	1.36	1.62	1.89	2.18	2.46	2.76
33	0.0071	0.18034	0.59	0.79	0.97	1.17	1.4	1.62	1.86	2.12	2.35
34	0.0063	0.16002	0.5	0.68	0.83	1	1.2	1.41	1.6	1.8	1.99
35	0.0056	0.14224	0.43	0.57	0.72	0.87	1.03	1.21	1.38	1.54	1.71
36	0.005	0.127	0.38	0.52	0.63	0.77	0.89	1.04	1.19	1.33	1.48
37	0.0045	0.1143	0.35	0.46	0.57	0.68	0.78	0.9	1.03	1.16	1.29
38	0.004	0.1016	0.3	0.41	0.5	0.59	0.68	0.78	0.88	0.98	1.09
39	0.0035	0.0889	0.27	0.36	0.42	0.49	0.58	0.66	0.75	0.84	0.92
40	0.0031	0.07874	0.24	0.31	0.36	0.43	0.5	0.57	0.64	0.72	0.79
Source: <a href="http://www.wiretron.com/nicrdat.html">www.wiretron.com/nicrdat.html</a>											

## Appendix B

### Endothermic Cooling Effect Calculations

The thermal degradation of EPS is a highly endothermic process as shown by the peak in the DSC data. The heat of degradation can be calculated from the area under the endothermic peak. The average heat of degradation was found to be approximately 912 J/g for a range of densities. Importantly the degradation of EPS in plastic foam cutting will cause a chilling effect on the hot cutting tool.

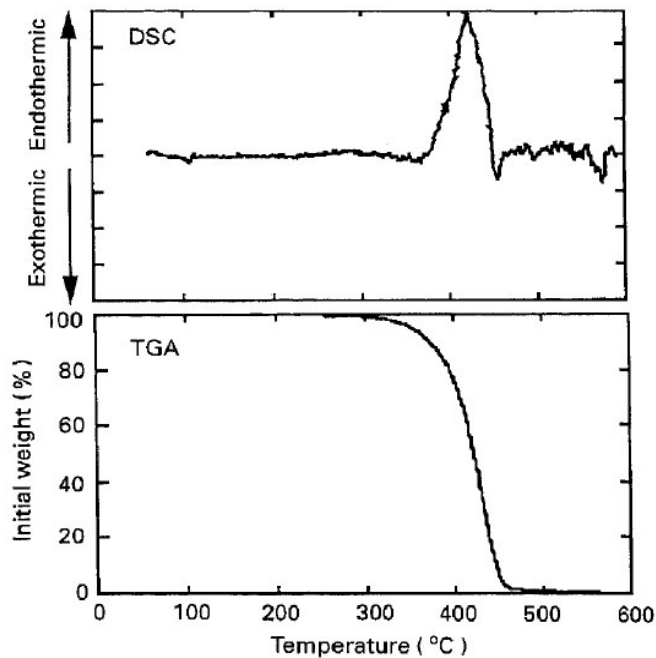


Figure B1. Typical TGA and DSC plots for EPS (0.024 g/cm<sup>3</sup>). Reproduced from [50].

If some basic assumptions are made it is possible to calculate the decrease in temperature of a hot cutting tool such as a hot-wire based on the thermal degradation of a known amount of EPS. For example, if a taut  $\varnothing$  0.64 mm Nichrome wire is used to cut a 50 mm long EPS sample producing a 1.2 mm kerf; the wire will decrease in temperature by about 270°C over the length of the cut.

Working:

$$\text{Unit volume of cut} = 1.2 \text{ mm} \times 1 \text{ mm} \times 50 \text{ mm} = 60 \text{ mm}^3$$

$$\text{Density of EPS} = 2.4 \times 10^{-5} \text{ g/mm}^3$$

$$\text{Unit volume of wire} = \frac{\pi D^2}{4} \times 1 \text{ mm} = 1.29 \text{ mm}^3$$

$$\text{Density of wire} = 8.4 \times 10^{-3} \text{ g/mm}^3$$

$$\begin{aligned}
 \text{Energy required to degrade EPS} &= \text{heat of degradation} \times \text{density of EPS} \times \text{volume of cut} \\
 &= 912 \text{ J/g} \times 2.4 \times 10^{-5} \text{ g/mm}^3 \times 60 \text{ mm}^3 \\
 &= \underline{1.313 \text{ J}}
 \end{aligned}$$

$$\text{Specific heat of wire} = 450 \text{ J/kg}^\circ\text{C} = 0.45 \text{ J/g}^\circ\text{C}$$

Amount of energy required to cool the wire by 1 °C is:

$$\begin{aligned}
 &= 0.45 \text{ J/g}^\circ\text{C} \times 8.4 \times 10^{-3} \text{ g/mm}^3 \times 1.29 \text{ mm}^3 \\
 &= \underline{4.88 \times 10^{-3} \text{ J/}^\circ\text{C}}
 \end{aligned}$$

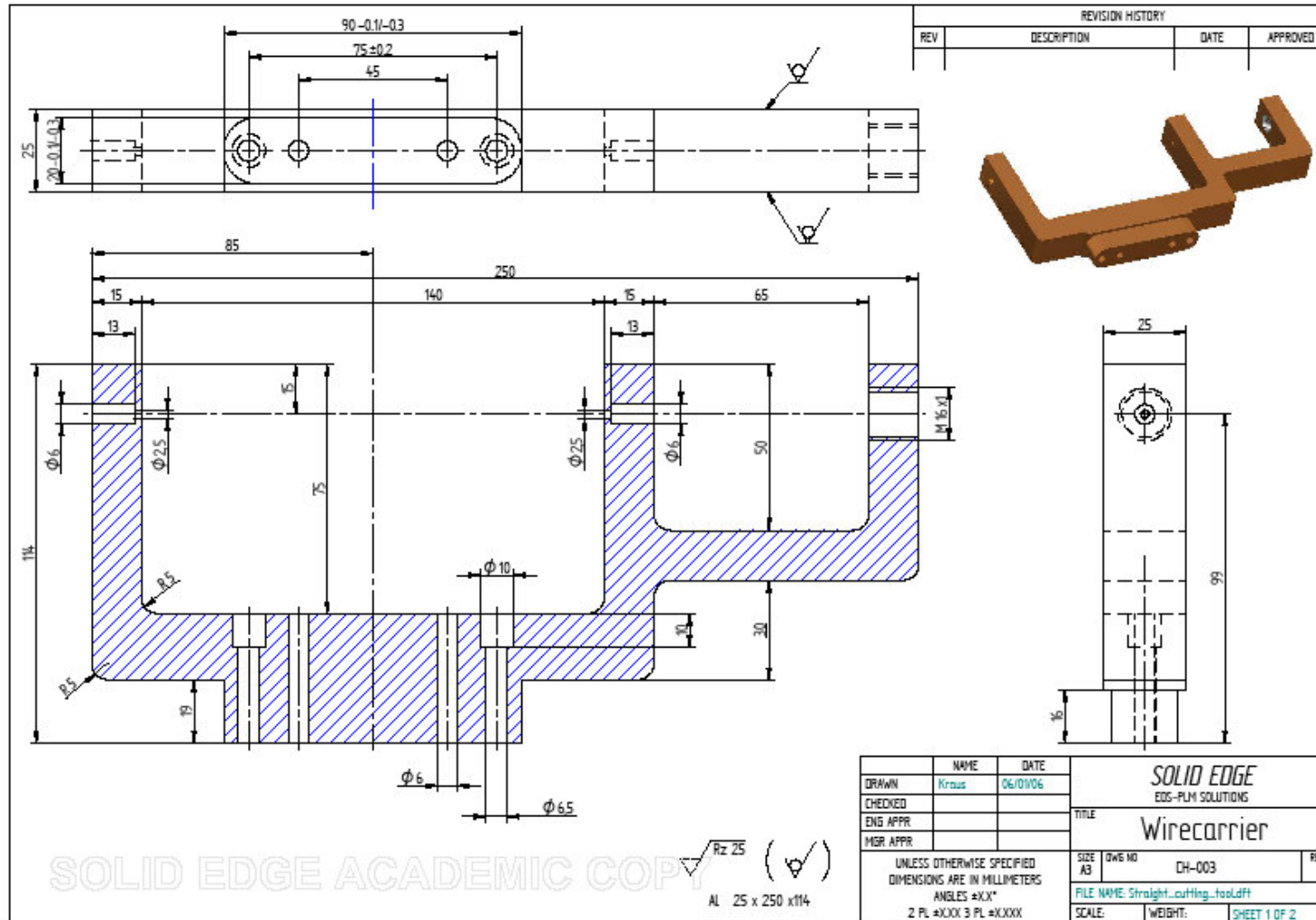
Therefore:

$$\text{Change in wire temperature} = (1.313 \text{ J}) / (4.88 \times 10^{-3} \text{ J/}^\circ\text{C}) = \underline{270 \text{ }^\circ\text{C}}$$

Of course in practice not all the plastic in the cutting zone is fully degraded and the wire will be continuously heated; nevertheless volatilisation can consume a significant portion of the energy available for cutting.

# Appendix C

## Cutting Head Drawings





The diagram shows an exploded view of a cutting head assembly. The main assembly is shown at the top left, with a grey frame, a teal cover, a tan housing, a purple load cell, and a red carrier. A pneumatic cylinder and hotwire are attached to the frame. The exploded view below shows the individual components: 1. Cover (teal), 2. Housing (tan), 3. Wirecarrier (grey), 4. Fitting (green), 5. Fitting (red), 6. Carrier (red). A purple load cell is also shown. A KUKA end effector is shown at the top right.

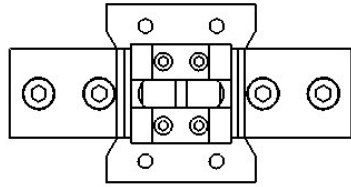
REVISION HISTORY			
REV	DESCRIPTION	DATE	APPROVED

Item Number	Document Number	Title	Material	Quantity
1	CH-001	Cover	Al 4 100/60	1
2	CH-002	Housing	Al 4 100/60	1
3	CH-003	Wirecarrier	Al 20/220/14	1
4	CH-004	Fitting	Al 4 60/2	1
5	CH-005	Fitting	Al 4 60/2	1
6	CH-006	Carrier	Al 20/40/30	2

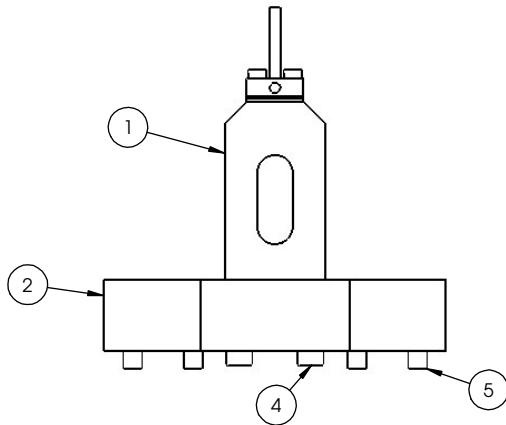
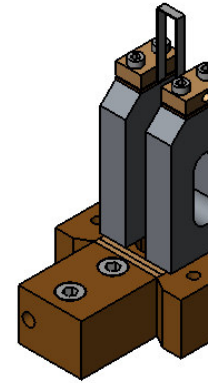
Screws and spring pins according to requirements

NAME	DATE	SOLID EDGE	
DESIGN	06/2016	UGS - The PLM Company	
CHECKED		Cutting Head Assembly	
ENG APPR		NO. 0010	CH-007
FOR APPR		FILE NAME	20160607_01
UNLESS OTHERWISE SPECIFIED DIMENSIONS ARE IN MILLIMETERS HOLE SIZE		SCALE	1:1
2 PL 40X3 3 PL 40X03		WEIGHT	SHEET 1 OF 1

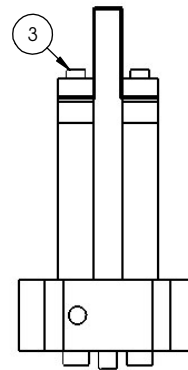
SOLID EDGE ACADEMIC COPY



PLAN



FRONT



SIDE

ITEM NO.	PART NUMBER	DESCRIPTION	QTY.
1	Tool Assembly	Dwg. 8	1
2	Finger Assembly	Dwg. 1 & 2	2
3	M3 10mm	Not to be made	4
4	M4 25mm	Not to be made	4
5	M5 20mm	Not to be made	4

TOTAL ASSEMBLY



SCALE : N/A

ALL DIMENSIONS IN mm

**UNIVERSITY OF CANTERBURY**  
**MECHANICAL ENGINEERING DEPT.**  
CH, CH, N, Z

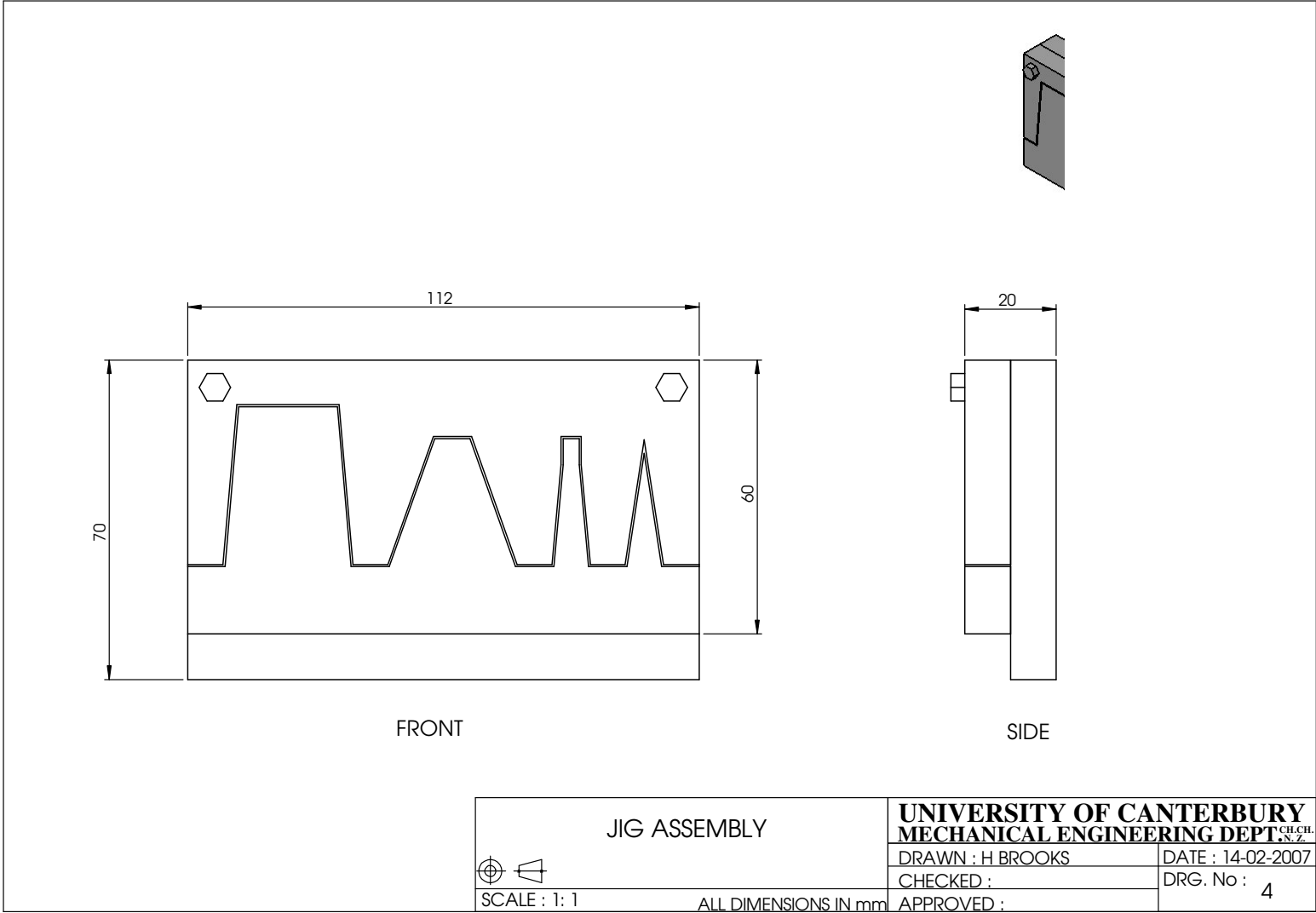
DRAWN : H BROOKS

DATE : 16-11-2006

CHECKED :

DRG. No : 9

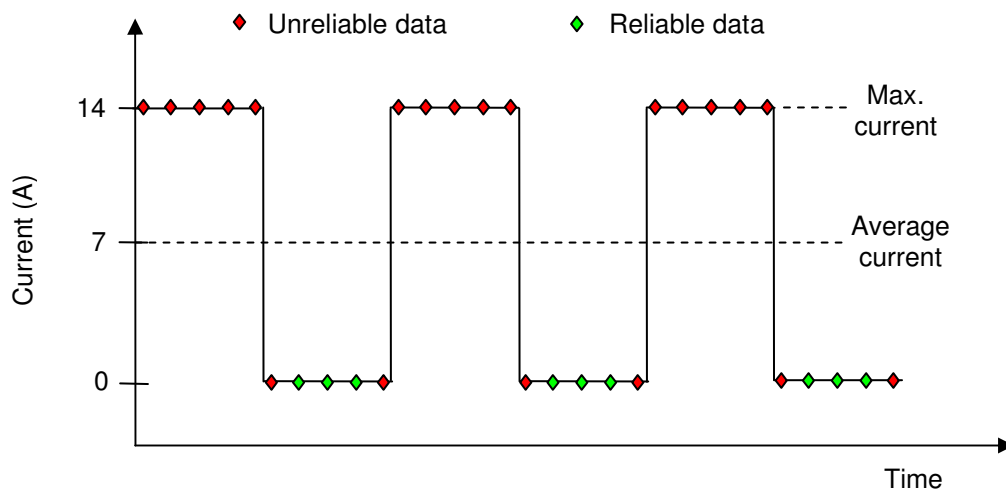
APPROVED :



## Appendix D

### Thermocouple Temperature Measurement

To allow the thermocouple to measure the hot-tool temperature without EMF interference the hot-wire current had to be momentarily stopped. In this way reliable temperature data was collected while the wire was electrically inactive. In practice the thermocouple continuously recorded both the good and bad data and the unreliable data was subsequently removed with the filter program run in MATLAB<sup>®</sup> shown below. The data was collected at a much higher rate than was actually needed (1000 measurements per second) so it was possible to remove well over 50% of the data without negatively affecting the usefulness of the information. For all of the cutting trials a 50% duty cycle was adopted (see figure below).



**Figure D1. Graph of current vs. time for a 50% duty cycle with superimposed thermocouple data points.**

The electrical currents quoted throughout the thesis are the average currents. The electrical power used in the calculations of the effective heat inputs were based on the actual power cycle, not the average current. The period of the duty cycle was small (0.01 seconds) so that any heating and cooling that occurred over the power cycle could be assumed negligible (i.e. the wire temperature is a function of the average power, not the instantaneous power).

#### MATLAB data filtering code

```
clear all, clc

beer = load('Data.txt');
m = length(beer);
ale = beer(1:1:m,:);
bigpizza = zeros(1,9);
```

```
n = length(ale);
for i=1:n;
    if ale(i,9) > 1;
        ale(i,9) = 3;
    else ale(i,9) = 0;
    end
end

for ii=1:n-2;
    if ale(ii+1,9) == 3;
        ale(ii,9) = 2;
        ale(ii+1,9) = 2;
    if ale(ii+2,9) == 0;
        ale(ii+2,9) = 2;
    end
    end
end

for iii=1:n-1;
    if ale(iii,9) == 0;
        pizza = ale(iii,:);
        bigpizza = [bigpizza;pizza];
    end
end

end
bigpizza(1,:) = [];
plot(bigpizza(:,1), bigpizza(:,3));
save 7A_0.0233_unfiltered.txt beer -ASCII
save 7A_0.0233_filtered.txt bigpizza -ASCII
```

# Appendix E

## Thermal Imaging Camera Specifications

### ThermaCAM™ S65 Infrared Camera

ThermaCAM™ S65



- IMAGING PERFORMANCE
- IMAGE PRESENTATION
- MEASUREMENT
- IMAGE STORAGE
- LENSES (OPTIONAL)
- SYSTEM STATUS INDICATOR
- LASER LOCATIR™
- BATTERY SYSTEM
- ENVIRONMENTAL SPECIFICATION
- PHYSICAL CHARACTERISTICS
- INTERFACES

<b>IMAGING PERFORMANCE</b>	
Thermal:	
Field of view/min focus distance	24°x18°/0.3 m (with 35 mm lens)
Spatial resolution (IFOV)	1.3 mrad
Thermal sensitivity	0.08 °C at 30 °C
Image frequency	50/60 Hz non-interlaced
Focus	Automatic or manual
Electronic zoom function	2,4,8 interpolating
Detector type	Focal Plane Array (FPA), uncooled microbolometer 320 x 240 pixels
Spectral range	7.5 to 13µm
Digital image enhancement	Normal and enhanced
Visual:	
Built-in digital video	640 x 480 pixels, full color
<b>IMAGE PRESENTATION</b>	
Video output	RS170 EIA/NTSC or CCIR/PAL composite video and IEEE-1394 FireWire output (full radiometric data)
Viewfinder	Built-in, high-resolution color LCD (TFT)
External display	4" LCD with integrated remote control
<b>MEASUREMENT</b>	
Temperature range	-40 °C to +1,500 °C (-40 °F to +2,732 °F)
	Up to +2,000 °C (3632 °F), optional
Accuracy	±2 °C, ±2% of reading
Measurement mode	Spot/manual (up to 10 movable), automatic placement and reading of max. and min. temperature within area.

	Area (circle or box, up to 10 movable), isotherm (2), line profile, Delta T
Atmospheric transmission correction	Automatic, based on inputs for distance, atmospheric temperature and relative humidity
Optics transmission correction	Automatic, based on signals from internal sensors
Emissivity correction	Variable from 0.1 to 1.0 or select from listings in pre-defined materials list
Reflected ambient temperature correction	Automatic, based on input of reflected temperature
External optics/window correction	Automatic, based on input of optics/window transmission and temperature
<b>IMAGE STORAGE</b>	
Type	Removable Flash-card (256 MB) - Built-in Flash memory (50 images)
	Built-in RAM memory for AVI and burst recording
File formats - Thermal	Standard JPEG, 14 bit measurement data included
File formats - Visual	Standard JPEG (including movable marker) linked with corresponding thermal image
Voice annotation of images	30 sec. of digital voice "clip" stored together with the image
	Bluetooth wireless headset
Text annotation of images	Predefined text selected and stored together with the image
<b>LENSES (OPTIONAL)</b>	
Field of view/min focus distance	7°x5.3°/4 m (with 122 mm lens)
	12°x 9°/1.2 m (with 71 mm lens)
	45°x 34°/0.1 m (with 18 mm lens)
	80°x 60°/0.1 m (with 9 mm lens)
	200µm close-up (64 mm x 48 mm/150 mm)
	100µm close-up (34 mm x 25 mm/80 mm)
	50µm close-up (15 mm x 11 mm/19mm)
	18µm close-up (6 mm x 4 mm/7mm)
Lens identification	Automatic
<b>SYSTEM STATUS INDICATOR</b>	
LCD Display	Shows status of battery and storage media. Indication of power, communication and storage modes
<b>LASER LOCATIR™</b>	
Classification	Class 2
Type	Semiconductor AlGaInP Diode Laser: 1mW/635 nm red
<b>BATTERY SYSTEM</b>	
Type	Li-Ion, rechargeable, field replaceable

Operating time	2 hours continuous operation
Charging system	in camera (AC adapter or 12 V from car) or 2 bay intelligent charger
External power operation	AC adapter 110/220 V AC, 50/60 Hz or 12 V from car (cable with Std plug: optional)
Power saving	Automatic shutdown and sleep mode (user selectable)
<b>ENVIRONMENTAL SPECIFICATION</b>	
Operating temperature range	-15 °C to +50 °C (5 °F to 122 °F)
Storage temperature range	-40 °C to +70 °C (-40 °F to 158 °F)
Humidity	Operating and storage 10% to 95%, non-condensing
Encapsulation	IP 54 IEC 529
Shock	Operational: 25G, IEC 68-2-29
Vibration	Operational: 2G, IEC 68-2-6
<b>PHYSICAL CHARACTERISTICS</b>	
Weight	2.0 kg incl. battery and top handle (includes remote control, LCD, video camera and laser) - 1,4 kg excluding battery and remote control with LCD
Size	100mm x 120mm x 220 mm (3.9"x4.7"x8.7") camera body
Tripod mounting	1/4" - 20
<b>INTERFACES</b>	
FireWire	IEEE-1394 FireWire output (standard, full radiometric data)
USB / RS-232	Image (thermal and visual), measurement, voice and text transfer to PC
IrDA	Wireless communication
Remote control	Top carrying handle with video camera, Laser LocatIR and LCD





VH-grade, 30 kg/m <sup>3</sup> (EPS)					
Feedrate (mm/min)	Amps (A)				
	4	5	6	7	8
300	Smooth	Vaporised	Vaporised	Vaporised	Vaporised
400	Smooth	Vaporised	Vaporised	Vaporised	Vaporised
500	Irregular	Vaporised	Vaporised	Vaporised	Vaporised
600	Irregular	Smooth	Vaporised	Vaporised	Vaporised
700	Irregular	Smooth	Vaporised	Vaporised	Vaporised
800	Irregular	Smooth	Smooth	Vaporised	Vaporised
900	Irregular	Smooth	Smooth	Vaporised	Vaporised
1000	Irregular	Smooth	Smooth	Vaporised	Vaporised
1100	Irregular	Irregular	Smooth	Vaporised	Vaporised
1200	Irregular	Irregular	Smooth	Smooth	Vaporised
1300	Irregular	Irregular	Smooth	Smooth	Vaporised
1400	Irregular	Irregular	Smooth	Smooth	Vaporised
1500	Irregular	Irregular	Irregular	Smooth	Vaporised
1600	Irregular	Irregular	Irregular	Smooth	Vaporised
1700	Irregular	Irregular	Irregular	Smooth	Smooth
1800	Irregular	Irregular	Irregular	Smooth	Smooth
1900	Irregular	Irregular	Irregular	Irregular	Smooth
2000	Irregular	Irregular	Irregular	Irregular	Smooth
2100	Irregular	Irregular	Irregular	Irregular	Smooth
2200	Irregular	Irregular	Irregular	Irregular	Smooth
2300	Irregular	Irregular	Irregular	Irregular	Smooth
2400	Irregular	Irregular	Irregular	Irregular	Smooth
2500	Irregular	Irregular	Irregular	Irregular	Irregular
2600	Irregular	Irregular	Irregular	Irregular	Irregular
2700	Irregular	Irregular	Irregular	Irregular	Irregular
2800	Irregular	Irregular	Irregular	Irregular	Irregular
2900	Irregular	Irregular	Irregular	Irregular	Irregular
3000	Irregular	Irregular	Irregular	Irregular	Irregular

<b>Styrofoam, 30kg/m<sup>3</sup> (XPS)</b>					
Feedrate (mm/min)	Amps (A)				
	4	5	6	7	8
300	Smooth	Vaporised	Vaporised	Vaporised	Vaporised
400	Smooth	Vaporised	Vaporised	Vaporised	Vaporised
500	Smooth	Smooth	Vaporised	Vaporised	Vaporised
600	Irregular	Smooth	Vaporised	Vaporised	Vaporised
700	Irregular	Smooth	Vaporised	Vaporised	Vaporised
800	Irregular	Smooth	Smooth	Vaporised	Vaporised
900	Irregular	Irregular	Smooth	Smooth	Vaporised
1000	Irregular	Irregular	Smooth	Smooth	Vaporised
1100	Irregular	Irregular	Irregular	Smooth	Vaporised
1200	Irregular	Irregular	Irregular	Smooth	Smooth
1300	Irregular	Irregular	Irregular	Smooth	Smooth
1400	Irregular	Irregular	Irregular	Irregular	Smooth
1500	Irregular	Irregular	Irregular	Irregular	Smooth
1600	Irregular	Irregular	Irregular	Irregular	Smooth
1700	Irregular	Irregular	Irregular	Irregular	Irregular
1800	Irregular	Irregular	Irregular	Irregular	Irregular

# Appendix G

## MasterCAM Brochure



Mastercam X2 Mill – Fast. Flexible. Reliable.



### A friendly familiarity

As you open Mastercam, there's an immediate comfort level with the look of the interface. Plus, we provide a set of training tools to help you get down to business creating toolpaths and cutting parts as quickly as possible. For instance, you can engage a learning mode designed for new users. And beyond the ease and comfort of the Mastercam interface is almost unlimited flexibility. You can customize its appearance and functionality. Even your keyboard and mouse shortcuts can be tailored to your preferences.

### Do more with less clicks

We understand that saving programming time can get you cutting chips faster, boosting productivity and your company's bottom line. There are numerous programming efficiencies designed into Mastercam. Several functions are consolidated within a single option, streamlining the number of programmer interactions. Mastercam's smart Ribbon Bar appears only when needed, putting crucial tools at your fingertips at just the right moment.

Also with Mastercam, newly created geometry is "live". Simply adjust the attributes to the existing geometry and move on to the next task.

### Toolpaths you can count on

At CNC Software, we have built our reputation for more than 20 years on creating the highest quality, most robust toolpath generation system in the world. The primary benefit that users continually cite about Mastercam is that they have complete command over all aspects of tool motion. Delivering comprehensive, clear tool control is crucial to programmers and one of many facets that sets us apart from the competition. With Mastercam X2, we have evolved our dominant toolpath system even further. It offers powerful toolpaths including new high speed cutting for any shop, advanced multi-axis features, and much more. It can also cut any type of CAD file, including mixed models comprised of any combination of wireframe, surface, or solid data.

### Plays well with others

Mastercam can use virtually any CAD source file in the world including SolidWorks®, Solid Edge®, AutoCAD®, CATIA, Pro/E®, and many more. And even better, it tracks new versions of these files, recognizes changes and helps you update the toolpaths. In addition, Mastercam is designed with an open architecture, allowing specialists around the world to create unique add-ins tailored for specific needs.

### Local experts, local support

Our company has the longest tenured Reseller channel in the business, which is a tremendous advantage for our customers. You have an exclusive Mastercam partner who is highly trained and experienced, ready to pass on his or her knowledge and to support you in every way possible. No other CAM software company has garnered such loyalty and strength. Our customers often remark about the significant role their Reseller has played in helping them achieve success and profitability with Mastercam.

### The power of X!

The Mastercam X family of CAD/CAM takes another leap forward with Mastercam X2, bringing powerful new techniques and faster programming to your shop.

### Mastercam X2.

CAD/CAM for the most important job – yours.

We established CNC Software, Inc. in 1983 to give shops a smarter, easier, offline method to program CNC machines. Today, Mastercam is the most commonly used CAM software worldwide\* and remains the program of choice among CNC programmers. When you invest in Mastercam, you get the best in CNC programming backed by the support and service of today's leading developer and our worldwide certified Resellers. Mastercam X2 represents the next generation of our popular Mastercam X CAD/CAM software, delivering the most comprehensive milling package with powerful new toolpaths and techniques.

\* Source: CIMdata, Inc.

**Quick access to basic functions** gets you familiar with the toolbar icons quickly – and lets you choose from a familiar text menu.

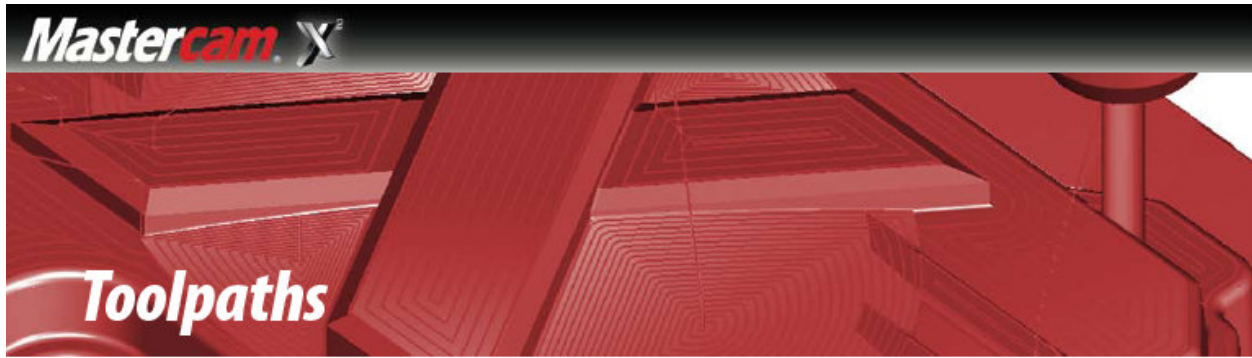
**Fully customizable interface** gives you instant access to the tools you need most.

**Smart Ribbon Bar** automatically changes based on what you are doing.

**Quick access history** keeps your most recently used functions at your fingertips.

**Active Operations Manager** gives dynamic access to all toolpath and solid model histories.

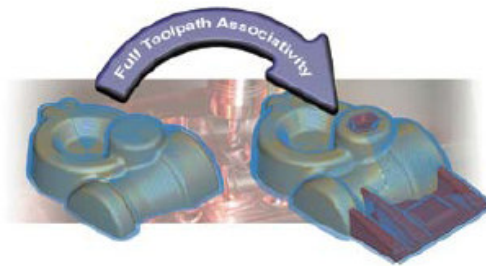




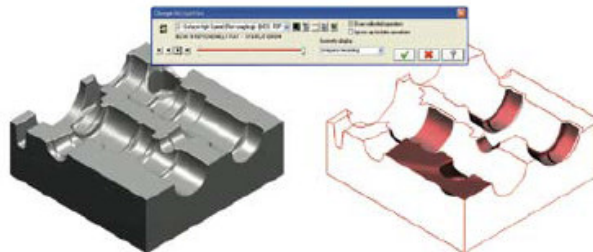
## Capture Your Machining Knowledge



Mastercam's full associativity gives you the power to capture your work and build on your experience. Once you program a part – any part – you can modify any element of the job and immediately get updated toolpaths without starting over. Mastercam's intelligent NC programming lets you build a library of machining strategies done the way you want them. Just choose the saved operations, apply them to a part, and Mastercam adapts them to the new model. Fast, easy, and productive. The way programming should be.



## CAD File Change Recognition & Toolpath Updating

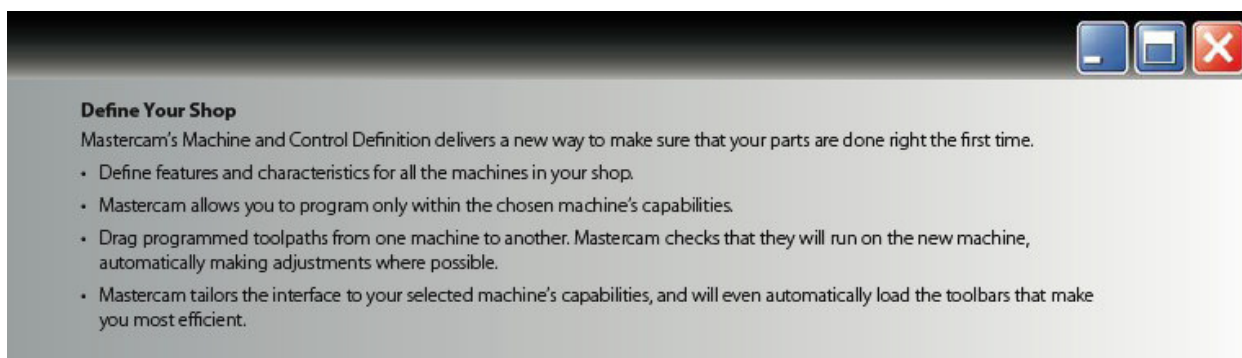


Every shop faces engineering changes. Often, it can be difficult to track which file is the latest, what modifications have been made, and what programming changes are needed.

Mastercam X2 includes two powerful new tools – File Tracking and Change Recognition – that give you an easy way to identify these issues and streamline programming an updated file.

- Create a checklist of files to watch including Mastercam, SolidWorks, Autocad, or other CAD files. Mastercam alerts you when a newer version of any file on the list is available.
- Mastercam's Change Recognition identifies modifications to any type of CAD geometry with no file type limitations – any combination of wireframe, solids, or surfaces.
- Mastercam marks any toolpaths affected by the updated CAD file. You can quickly select the new geometry and update the toolpaths.
- Once you update an affected toolpath, automatically update any additional toolpaths that use that geometry.

The real power of these tools becomes clear when receiving engineering changes to a large file with multiple operations. Something as simple as a few additional drill holes could be frustrating to identify. Now, with a few mouse clicks, you can immediately locate and program these changes, saving valuable time.



### Define Your Shop

Mastercam's Machine and Control Definition delivers a new way to make sure that your parts are done right the first time.

- Define features and characteristics for all the machines in your shop.
- Mastercam allows you to program only within the chosen machine's capabilities.
- Drag programmed toolpaths from one machine to another. Mastercam checks that they will run on the new machine, automatically making adjustments where possible.
- Mastercam tailors the interface to your selected machine's capabilities, and will even automatically load the toolbars that make you most efficient.



### Efficient NC Tools and Toolpath Management

- Full control over tool approach and retract.
- Wrap a toolpath around a diameter with rotary axis substitution.
- "Safe zones" help ensure safe tool retract in all toolpath types.
- Significantly reduce the size of a program with toolpath filtering.
- Use all your tooling including lollipop, slot, dovetail, tapered, and much more.
- Automatically generate customizable setup sheets.
- Subroutine support.
- User-customizable tool and material libraries automatically calculate feeds and speeds.
- Mastercam's Toolpath Manager stores all your job's operations in one place. Quickly create, edit, and verify your toolpaths, or copy and paste parameters from one operation to another. Use machine groups to organize your operations, and easily copy and paste toolpaths and tool definitions from one machine group to another.

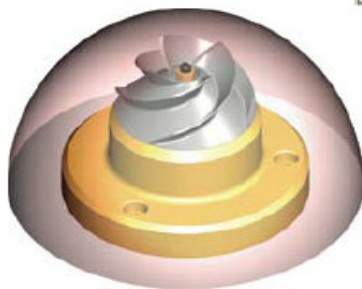


*"The 3D surfacing toolpath capability in Mastercam is wonderful. I use it to get the fine detail I need and the part comes out pretty near polished. Our chromer loves it."*

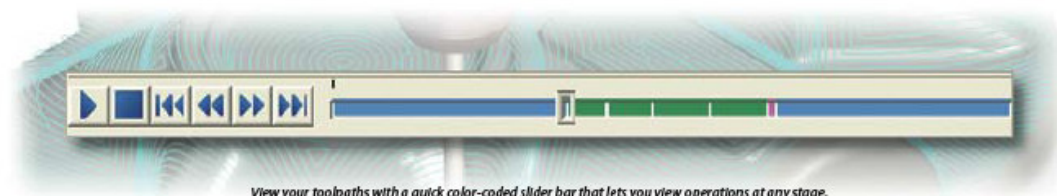
*Jim Quinn, Programmer  
Orange County Choppers  
Montgomery, NY*



### Dependable Toolpath Verification



- Watch and measure your part as it is cut from a solid block of material with Mastercam's solid model toolpath verification. The tool and holder are checked and displayed during simulation.
- "Play" the program with toolpath backplotting and get an estimate of machining time. Dynamically view all the vital information about tools and operations at any point, and even isolate specific areas to watch more closely.
- Quickly verify 2D toolpaths with a pixel paint of the full tool diameter to check the finish.



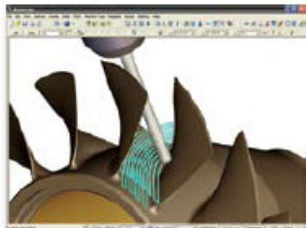
*View your toolpaths with a quick color-coded slider bar that lets you view operations at any stage.*



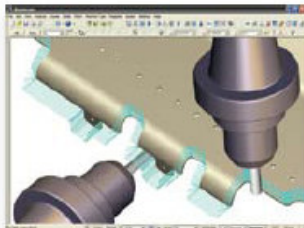
**A Wide Range of Strategies**

Multiaxis machining can dramatically increase a shop's competitiveness, and Mastercam offers a wide range of multiaxis machining strategies – both basic and advanced. With Mastercam, you have complete control over the three crucial elements of multiaxis machining: toolpath types, tool motion, and tool axis.

**Toolpath Types**



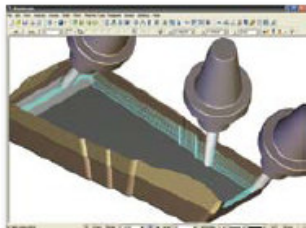
*Efficient multiaxis roughing techniques help ensure accurate cuts and short turnaround times.*



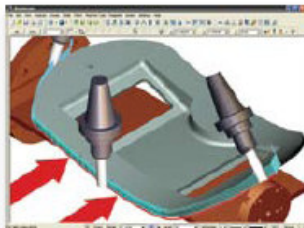
*5-axis contour cutting for easy part trimming.*



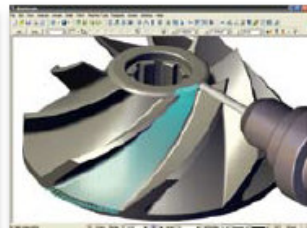
*Fast, efficient 5-axis drilling.*



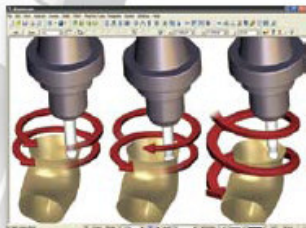
*Multisurface swarf cutting keeps the tool edge against drive surfaces for a smooth finish.*



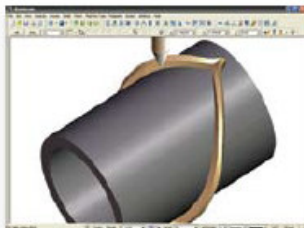
*'Rail' swarf cutting lets you control the cut using a lower rail.*



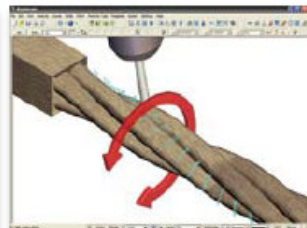
*5-axis flowline can machine a pattern that follows the natural shape of the part.*



*Mastercam gives you a variety of tool motion choices: one way cutting, zigzag cutting, and smooth spiral cutting.*



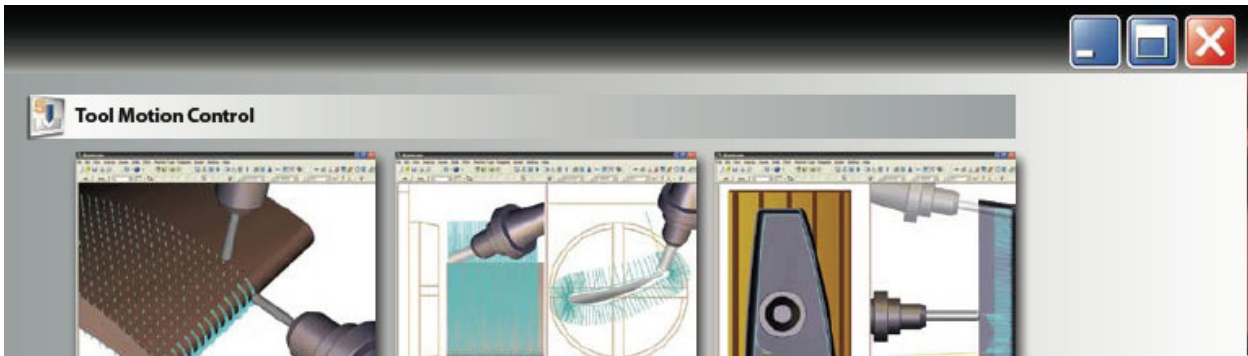
*4-axis roll die programming delivers easy programming specialized for roll dies and vertical walls on cylindrical parts.*



*Streamlined rotary 4-axis cutting.*

www.mastercam.com | 860.875.5006



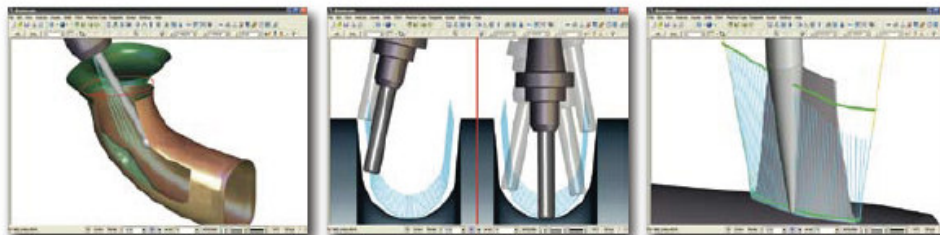


*Mastercam can add toolpath points to tightly curved areas for a smoother, more consistent finish.*

*Mastercam gives you complete control over your lead / lag and side tilt.*

*Full entry and exit control lets you determine exactly where and how the cutter enters and leaves your part.*

**Tool Axis Control**

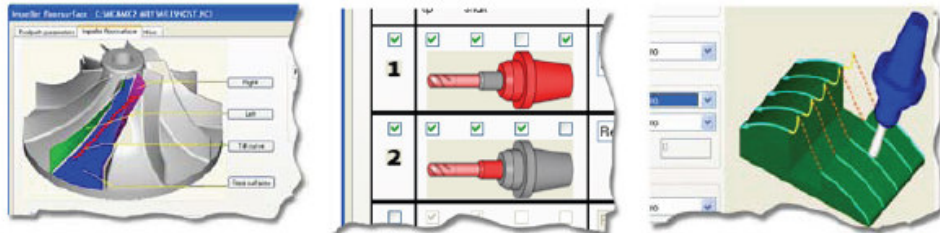


*Shank containment simplifies working in confined spaces.*

*Mastercam's axis limits controls tool motion between defined angles, ensuring the tool tilt will not violate part or machine tool limits.*

*Quickly control your tool axis with a simple set of geometry chains.*

**Clearly Illustrated Options**

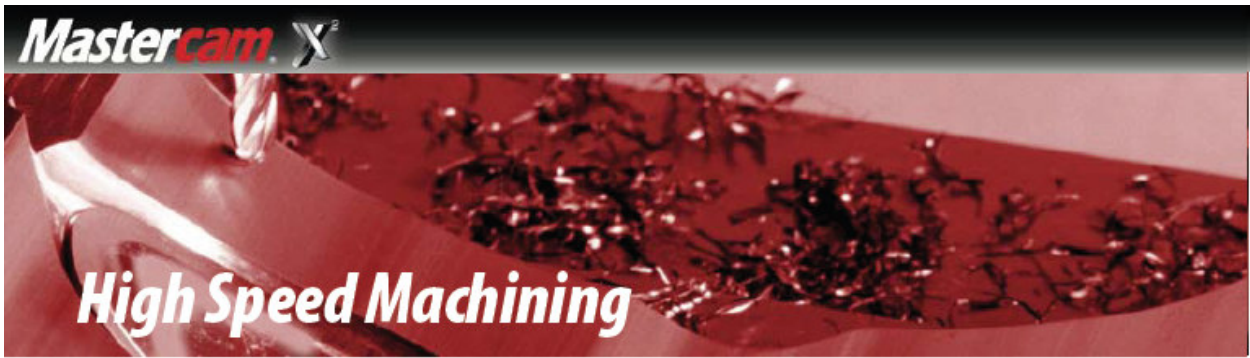


*Mastercam's advanced multiaxis machining lets you choose what type of project you are doing and adjusts the interface to show exactly what you need.*

*Advanced gouge checking helps ensure safe cuts in even the most complex operations.*

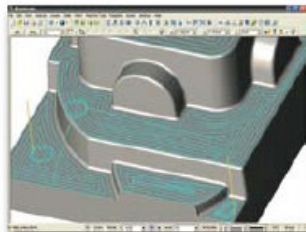
*Mastercam's link options offer complete control over entry / exit, cut-to-cut, and between cut moves.*

- Multisurface 5-axis roughing and finishing, including depth cuts, plunge roughing, and flowline machining.
- Machine 5-axis parts using spiral, zig zag, or one way tool motion.
- Swarf fanning and swarf machining over multisurface floors, plus "rail" swarf cutting for added control.
- Machine 5-axis curves with independent definitions of tool side angle and lead / lag angle.
- Create 5-axis contour toolpaths around surface edges for applications such as trimming vacuum-formed parts.
- Machine toward a single point for smooth tip cutting around an entire part.
- Easy 4-axis rotary axis and roldie programming, and 5-axis drilling.
- Automatic point generator adds greater precision in difficult areas.
- Create full 5-axis motion from a 3-axis projected toolpath.
- Special options for machining cylinder heads and converting probe data to machinable geometry.
- Advanced gouge checking and a 5-axis "safe zone" around the part.
- Complete control over the tool axis, lead / lag, entry / exit, and tilt simplifies even the most difficult multiaxis jobs.
- 3D tool compensation in machine controls and full tapered tool support.

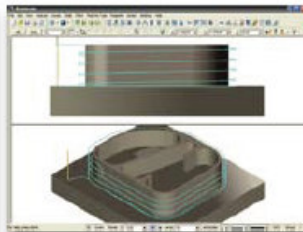


**Faster Turnaround and Superior Finish**

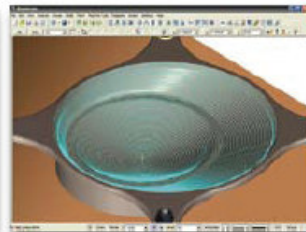
High Speed Machining is a powerful cutting method that combines high feed rates with high spindle speeds, specific tools, and specific tool motion. High Speed Machining can deliver faster turnaround and a superior finish. Mastercam includes a suite of High Speed Machining functions designed to help you make the most of this powerful technique, even if you don't have a high speed machine.



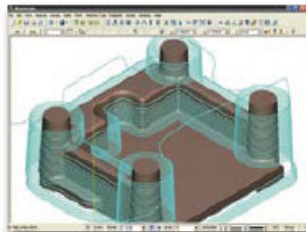
*Automatically machine flat areas using new time-saving minimum retracts and smooth entry, exit and cut motion.*



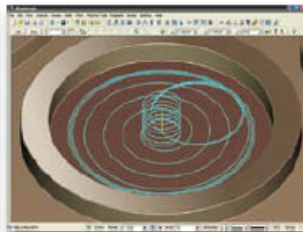
*Contour parts with smooth, consistent ramping motion.*



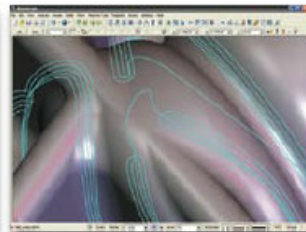
*Projected spiral finishing delivers a smooth cut with consistent material contact.*



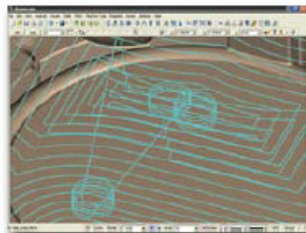
*High speed waterline cutting delivers constant Z moves with smooth entries and exits.*



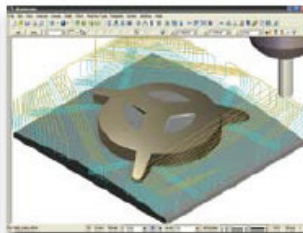
*Smooth, automated circle milling.*



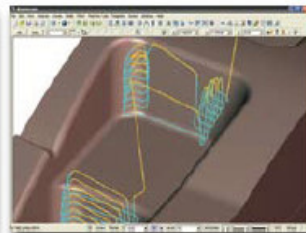
*Specialized high speed pencil tracing removes material from a previous finish pass.*



*High speed area clearance removes bulk material from the inside out with smooth motion.*



*Smart core roughing cuts from the outside in. If it encounters a pocket, it automatically switches to inside out.*



*High speed rest roughing smoothly removes material left from a previous rough pass.*

# Intelligent Feed Rate Optimization

## Save Time, Wear, and Money

Running an entire job at a single feed rate reduces efficiency. Running the same job at varying feed rates can save time, tool wear, and money. Our High Feed Machining function can optimize any 2-axis or 3-axis toolpath based on volume of material being removed and machine tool limitations to give you efficient, varied feed rates tailored to each job.

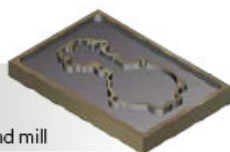
- Automatically vary feed rates based on volume. More material and the cutter moves slower; less material and the cutter moves faster.
- Automatically ease the tool into and out of corners.
- Create libraries of optimization settings for different jobs.

### Pocket

Material: aluminum

Tools used: 1/2" flat end mill and 3/15" flat end mill

	No Optimization	With Optimization	% Saved
Time	2:11	1:48	18.1%



### Constant Volume Removal

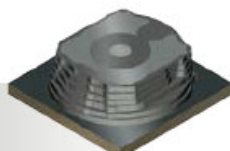
Mastercam slows the feed rate through deep material and speeds it up through more shallow stock.

### Multisurface Rough

Material: aluminum

Tool used: 1 1/4" flat end mill

	No Optimization	With Optimization	% Saved
Time	17:18	11:16	34.9%



### Smart Cornering

Based on the part and machine tool characteristics, Mastercam adjusts the feed rate around corners and small radii for smooth transition in tight areas.

### Multisurface Finish

Material: aluminum

Tool used: .375 ball end mill

	No Optimization	With Optimization	% Saved
Time	2:36:44	1:53:51	27.8%



# Appendix H

## ANSYS APDL Code

### 0.36 mm hot-wire code for a straight cut

! This log file is modified by Hadley Brooks in 2008.

! Test in ANSYS 11.0 = ok

! units: SI, mm - degree C - W - kg -sec - J

! In this analysis a temperature of temp (degC) is assumed with a feedrate of feed (m/s).

! The wire is approximated by moving a temperature BC each time step.

! The time step is such that the 'wire' moves at the correct speed.

finish

/clear

/title,AWG 27 wire (%temperature%degC %feed%m/s)

/filnam,smallwire\_xps\_294degC\_0.0133ms

/TRIAD,RBOT

/PREP7

!\*\*\*\*\* Cutting Parameters \*\*\*\*\*

! Choose foam material (XPS = 1, EPS = 2)

material = 1

! Choose wire temperature (deg C)

temperature = 294

! Choose feedrate (m/s)

feed = 0.0133

! choose element size (m)

elsize = 0.09020e-3

! Choose wire radius (m)

wirerad = 0.4034e-3/2

BLC4,0,3.608E-3,29.9464E-3,-3.608E-3

!half of 9.6\*30mm (because of symmetry)

aplot

ET,1,PLANE55

KEYOPT,1,1,0

KEYOPT,1,3,0 !2D plane problem

KEYOPT,1,4,0

KEYOPT,1,8,0

KEYOPT,1,9,0

\*if,material,eq,1, then

!\*\*\*\*\* XPS foam \*\*\*\*\*

MP,DENS,1,30, , ,

!kg/m3

MPTEMP,1,20,110,160,400

MPDATA,KXX,1,1,0.0316,0.0316,0.16,0.16,

!W/m-C\

MPTEMP,1,20,110,160,400

MPDATA,C,1,1,1200,1550,2020,2560

!W-s / kg-C

```

*endif

*if,material,eq,2, then
|***** EPS foam *****

MP,DENS,1,26,, , , !kg/m3
MPTEMP,1,20,110,160,400
MPDATA,KXX,1,1,0.0327,0.0327,0.16,0.16, !W/m-C\
MPTEMP,1,20,110,160,400
MPDATA,C,1,1,1200,1550,2020,2560 !W-s / kg-C

*endif

type,1
mat,1
ESIZE,elsize, !element size
MSHKEY,1
amesh,1 !Create area mesh

FINISH

/CONFIG,NRES,2000

/SOLU
ANTYPE,trans
TRNOPT,FULL
NROPT,FULL, ,
EQSLV,
SOLCONTROL,ON
AUTOTS,off
KBC,0 !step
OUTRES,ALL,LAST,
DSYM,SYMM,Y,0 !Set symmetry plane
!load step 1, initial conditions 25 C
TIME,0.001
DELTIM,0.001,,
TUNIF,25, !boundary conditions
solve
!load step 2..... , apply moving temp

timestep = (2*elsize)/feed

j=timestep

*DO,i,3,26.158e-3/elsize,2

TIME,j
DELTIM,0.01,,,

x0 = elsize*(i-2)
y0 = 0
local,11,1,x0,y0 !Set old local coords
nselect,s,loc,x,0,wirerad !select old wire position
DDELETE,all,temp !Delete old temp bc
allsel

x1 = elsize*i
y1 = 0
local,11,1,x1,y1 !Set new local coords

```



```

nselect,s,loc,x,0,wirerad          !Select new wire nodes
D,all,temp,temperature            !set temp bc
allselect
solve
j=j+timestep                        !time needed for a cutting speed of feed m/s => t=d/v =>
(2*elsize)/feed = timestep

*ENDDO
save

finish

/POST1
/EFACET,4
set,last
/WINDOW,1,top,
/WINDOW,2,bot,
/EXPAND,2,RECT,HALF,0,1E-12,0,
/CVAL,1,40,60,80,100,120,140,160,
/CVAL,2,
/FOCUS,1,0.025,0,0,0
/DIST,1,0.0020,0
/EDGE,1,1,
PLNSOL,TEMP, ,0,

```

#### 0.64 mm hot-wire code for a straight cut

```

! This log file is modified by Hadley Brooks in 2008.
! Test in ANSYS 11.0 = ok
! units: SI, mm - degree C - W - kg -sec - J

```

```

! In this analysis a temperature of temp (degC) is assumed with a feedrate of feed (m/s).
! The wire is approximated by moving a temperature BC each time step.
! The time step is such that the 'wire' moves at the correct speed.

```

```

finish
/clear

```

```

/title,AWG 22 wire (%temperature%degC %feed%m/s)
/filnam,medwire_xps_170degC_0.0150ms

```

```

/TRIAD,RBOT

```

```

/PREP7

```

```

!***** Cutting Parameters *****

```

```

! Choose foam material (XPS = 1, EPS = 1)
material = 1

```

```

! Choose wire temperature (deg C)
temperature = 170

```

```

! Choose feedrate (m/s)
feed = 0.0150

```

```

! choose element size (m)
elsize = 0.16e-3

```

```

! Choose wire radius (m)

```

wirerad = 0.74e-3/2

BLC4,0,4E-3,29.92E-3,-4E-3 !half of 9.6\*30mm (because of symmetry)  
aplot

ET,1,PLANE55  
KEYOPT,1,1,0  
KEYOPT,1,3,0 !2D plane problem  
KEYOPT,1,4,0  
KEYOPT,1,8,0  
KEYOPT,1,9,0

\*if,material,eq,1, then  
|\*\*\*\*\* XPS foam \*\*\*\*\*

MP,DENS,1,30, , , !kg/m3  
MPTEMP,1,20,110,160,400  
MPDATA,KXX,1,1,0.0316,0.0316,0.16,0.16, !W/m-C\  
MPTEMP,1,20,110,160,400  
MPDATA,C,1,1,1200,1550,2020,2560 !W-s / kg-C

\*endif

\*if,material,eq,2, then  
|\*\*\*\*\* EPS foam \*\*\*\*\*

MP,DENS,1,26, , , !kg/m3  
MPTEMP,1,20,110,160,400  
MPDATA,KXX,1,1,0.0327,0.0327,0.16,0.16, !W/m-C\  
MPTEMP,1,20,110,160,400  
MPDATA,C,1,1,1200,1550,2020,2560 !W-s / kg-C

\*endif

type,1  
mat,1  
ESIZE,elsize, !element size  
MSHKEY,1  
amesh,1 !Create area mesh

FINISH

/CONFIG,NRES,2000

/SOLU  
ANTYPE,trans  
TRNOPT,FULL  
NROPT,FULL, ,  
EQSLV,  
SOLCONTROL,ON  
AUTOTS,off  
KBC,0 !step  
OUTRES,ALL,LAST,  
DSYM,SYMM,Y,0 !Set symmetry plane  
!load step 1, initial conditions 25 C  
TIME,0.001  
DELTIM,0.001,,  
TUNIF,25, !boundary conditions  
solve

!load step 2..... , apply moving temp

timestep = (2\*elsize)/feed

j=timestep

\*DO,i,3,25.92e-3/elsize,2

TIME,j  
DELTIM,0.01,,,

x0 = elsize\*(i-2)  
y0 = 0

local,11,1,x0,y0  
nselect,s,loc,x,0,wirerad  
DDELETE,all,temp  
allselect

!Set old local coords  
!select old wire position  
!Delete old temp bc

x1 = elsize\*i  
y1 = 0

local,11,1,x1,y1  
nselect,s,loc,x,0,wirerad  
D,all,temp,temperature  
allselect

!Set new local coords  
!Select new wire nodes  
!set temp bc

solve  
j=j+timestep

!time needed for a cutting speed of feed m/s =>  $t=d/v \Rightarrow$

(2\*elsize)/feed = timestep

\*ENDDO

save

finish

/POST1  
/EFACET,4  
set,last  
/WINDOW,1,top,  
/WINDOW,2,bottom,  
/EXPAND,2,RECT,HALF,0,1E-12,0,  
/CVAL,1,40,60,80,100,120,140,160,  
/CVAL,2,  
/FOCUS,1,0.025,0,0,0  
/DIST,1,0.0020,0  
/EDGE,1,1,  
PLNSOL,TEMP, ,0,

### 0.91 mm hot-wire code for a straight cut

! This log file is modified by Hadley Brooks in 2008.

! Test in ANSYS 11.0 = ok

! units: SI, mm - degree C - W - kg -sec - J

! In this analysis a temperature of temp (degC) is assumed with a feedrate of feed (m/s).

! The wire is approximated by moving a temperature BC each time step.

! The time step is such that the 'wire' moves at the correct speed.

finish

/clear



```

/title,AWG 19 wire (%temperature%degC %feed%m/s)
/filnam,bigwire_xps_213degC_0.0133ms

/TRIAD, RBOT

/PREP7

!***** Cutting Parameters *****

! Choose foam material (XPS = 1, EPS = 1)
material = 1

! Choose wire temperature (deg C)
temperature = 213

! Choose feedrate (m/s)
feed = 0.0133

! choose element size (m)
elsize = 0.228e-3

! Choose wire radius (m)
wirerad = 1.02e-3/2

BLC4,0,3.876E-3,39.9E-3,-3.876E-3      !half of 9.6*30mm (because of symmetry)
aplot

ET,1,PLANE55
KEYOPT,1,1,0
KEYOPT,1,3,0      !2D plane problem
KEYOPT,1,4,0
KEYOPT,1,8,0
KEYOPT,1,9,0

*if,material,eq,1, then
!***** XPS foam *****
MP,DENS,1,30, , ,      !kg/m3
MPTEMP,1,20,110,160,400
MPDATA,KXX,1,1,0.0316,0.0316,0.16,0.16,      !W/m-C\
MPTEMP,1,20,110,160,400
MPDATA,C,1,1,1200,1550,2020,2560      !W-s / kg-C

*endif

*if,material,eq,2, then
!***** EPS foam *****
MP,DENS,1,26, , ,      !kg/m3
MPTEMP,1,20,110,160,400
MPDATA,KXX,1,1,0.0327,0.0327,0.16,0.16,      !W/m-C\
MPTEMP,1,20,110,160,400
MPDATA,C,1,1,1200,1550,2020,2560      !W-s / kg-C

*endif

type,1
mat,1
ESIZE,elsize,      !element size

```

```

MSHKEY,1
amesh,1                                !Create area mesh

FINISH

/CONFIG,NRES,2000

/SOLU
ANTYPE,trans
TRNOPT,FULL
NROPT,FULL, ,
EQSLV,
SOLCONTROL,ON
AUTOTS,off
KBC,0                                  !step
OUTRES,ALL,LAST,
DSYM,SYMM,Y,0                          !Set symmetry plane
                                !load step 1, initial conditions 25 C
TIME,0.001
DELTIM,0.001,,
TUNIF,25,                               !boundary conditions
solve
                                !load step 2..... , apply moving temp

timestep = (2*elsize)/feed

j=timestep

*DO,i,3,35.568e-3/elsize,2

    TIME,j
    DELTIM,0.01,,

    x0 = elsize*(i-2)
    y0 = 0
    local,11,1,x0,y0                    !Set old local coords
    nsel,s,loc,x,0,wirerad              !select old wire position
    DDELE,all,temp                      !Delete old temp bc
    allsel

    x1 = elsize*i
    y1 = 0
    local,11,1,x1,y1                    !Set new local coords
    nsel,s,loc,x,0,wirerad              !Select new wire nodes
    D,all,temp,temperature              !set temp bc
    allsel
    solve
    j=j+timestep
    (2*elsize)/feed = timestep

    !time needed for a cutting speed of feed m/s => t=d/v =>

*ENDDO
save

finish

/POST1
/EFACET,4
set,last
/WINDOW,1,top,
/WINDOW,2,bot,

```

```

/EXPAND,2,RECT,HALF,0,1E-12,0,
/CVAL,1,40,60,80,100,120,140,160,
/CVAL,2,
/FOCUS,1,0.030,0,0,0
/DIST,1,0.0035,0
/EDGE,1,1,
PLNSOL,TEMP, ,0,

```

### Hot-ribbon code for a straight cut

! This log file is modified by Hadley Brooks in 2008.

! Test in ANSYS 11.0 = ok

! units: SI, mm - degree C - W - kg -sec - J

! In this analysis a temperature of temp (degC) is assumed with a feedrate of feed (m/s).

! The ribbon is approximated by moving a temperature BC each time step.

! The time step is such that the 'ribbon' moves at the correct speed.

finish

/clear

/title,Constant ribbon temperature (%temperature%degC %feed%m/s)

/filnam,ribbon\_298degC\_0.028ms

/TRIAD, RBOT

/PREP7

!\*\*\*\*\* Cutting Parameters \*\*\*\*\*

! Choose foam material (XPS = 1, EPS = 2)

material = 2

! Choose ribbon temperature (deg C)

temperature = 298

! Choose feedrate (m/s)

feed = 0.028

! Element size

elsize = 0.2268E-3

length = 39.9168e-3

BLC4,0,4.7628E-3,length,-4.7628E-3 !half of 9.6012\*40.005mm (because of symmetry)  
aplot

ET,1,PLANE55

KEYOPT,1,1,0

KEYOPT,1,3,0 !2D plane problem

KEYOPT,1,4,0

KEYOPT,1,8,0

KEYOPT,1,9,0

\*if,material,eq,1, then

!\*\*\*\*\* XPS foam \*\*\*\*\*

MP,DENS,1,30, , , !kg/m3

MPTEMP,1,20,110,160,400

MPDATA,KXX,1,1,0.0316,0.0316,0.16,0.16, !W/m-C\

```

MPTEMP,1,20,110,160,400
MPDATA,C,1,1,1200,1550,2020,2560          !W-s / kg-C

*endif

*if,material,eq,2, then
|***** EPS foam *****
MP,DENS,1,26,, ,                          !kg/m3
MPTEMP,1,20,110,160,400
MPDATA,KXX,1,1,0.0327,0.0327,0.08,0.16,   !W/m-C\
MPTEMP,1,20,110,160,400
MPDATA,C,1,1,1200,1550,2020,2560          !W-s / kg-C

*endif

type,1
mat,1
ESIZE,elsize,      !element size
MSHKEY,1
amesh,1              !Create area mesh

FINISH

/CONFIG,NRES,2000

/SOLU
ANTYPE,trans
TRNOPT,FULL
NROPT,FULL, ,
EQSLV,
SOLCONTROL,ON
AUTOTS,on
KBC,0                !step
OUTRES,ALL,LAST,
DSYM,SYMM,Y,0       !Set symmetry plane
                        !load step 1, initial conditions 25 C
TIME,0.001
DELTIM,0.001,,
TUNIF,25,           !boundary conditions
solve
                        !load step 2..... , apply moving temp

timestep = (2*elsize)/feed

j=timestep

*DO,i,3,34.9272e-3/elsize,2

    TIME,j
    DELTIM,0.01,,

    x0 = elsize*(i-2)
    y0 = 0
    local,11,0,x0,y0          !Set old local coords
    nsel,s,loc,x,0,14*elsize !select old wire position
    nsel,r,loc,y,0,elsize
    DDELE,all,temp          !Delete old temp bc
    allsel

```

```

x1 = elsize*i
y1 = 0
local,11,0,x1,y1          !Set new local coords
nselect,s,loc,x,0,14*elsize !select new wire position
nselect,r,loc,y,0,elsize
D,all,temp,temperature    !set temp bc
allsel

solve
j=j+timestep              !time needed for a cutting speed of feed m/s => t=d/v =>
(2*0.16E-3)/feed = timestep

*ENDDO
save
finish

/POST1
/EFACET,4
set,last
/WINDOW,1,top,
/WINDOW,2,bot,
/EXPAND,2,RECT,HALF,0,1E-12,0,
/CVAL,1,40,60,80,100,120,140,160,
/CVAL,2,
/FOCUS,1,0.030,0,0,0
/DIST,1,0.0045,0
/EDGE,1,1,
PLNSOL,TEMP, ,0,

```

### Hot-ribbon code for a curved cut

```

! This log file is modified by Hadley Brooks in 2008.
! Test in ANSYS 11.0 = ok
! units: SI, mm - degree C - W - kg -sec - J

```

```

! In this analysis a temperature (degC) is assumed with a feedrate (m/s).
! The ribbon is approximated by moving a temperature BC each time step along an arced path.
! The time step is such that the 'ribbon' moves at the correct speed.

```

```

finish
/clear

```

```

/title,Arc (%radius%m %temperature%degC %feed%m/s)
/filnam,Arc_eps_0.000m_315degC_0.050ms

```

```

/TRIAD,RBOT

```

```

/PREP7

```

```

!***** Cutting Parameters *****

```

```

! Choose foam material (XPS = 1, EPS = 2)
material = 2

```

```

! Choose ribbon temperature (deg C)
temperature = 315

```

```

! Choose feedrate (m/s)

```

feed = 0.050

! Choose radius (m)

radius = 0

ribbonx = 3.175e-3

ribbony = 0.4572e-3

esize = 0.16e-3

pi = acos(-1)

BLC4,-10E-3,-10E-3,20E-3,20E-3 ! 20\*20mm

ET,1,PLANE55

KEYOPT,1,1,0

KEYOPT,1,3,0 !2D plane problem

KEYOPT,1,4,0

KEYOPT,1,8,0

KEYOPT,1,9,0

\*if,material,eq,1, then

!\*\*\*\*\* XPS foam \*\*\*\*\*

MP,DENS,1,36, , , !kg/m3

MPTEMP,1,20,110,160,400

MPDATA,KXX,1,1,0.0316,0.0316,0.16,0.16, !W/m-C\

MPTEMP,1,20,110,160,400

MPDATA,C,1,1,1200,1550,2020,2560 !W-s / kg-C

\*endif

\*if,material,eq,2, then

!\*\*\*\*\* EPS foam \*\*\*\*\*

MP,DENS,1,26, , , !kg/m3

MPTEMP,1,20,110,160,400

MPDATA,KXX,1,1,0.0327,0.0327,0.16,0.16, !W/m-C\

MPTEMP,1,20,110,160,400

MPDATA,C,1,1,1200,1550,2020,2560 !W-s / kg-C

\*endif

type,1

mat,1

lsel,all

LESIZE,1,0.16e-3, !element size = 0.16mm

LESIZE,2,0.16e-3,

MSHKEY,1

amesh,1, !Create area mesh

FINISH

/CONFIG,NRES,2000

/SOLU

ANTYPE,trans

TRNOPT,FULL

NROPT,FULL, ,

EQSLV,

SOLCONTROL,ON

```

AUTOTS,on
KBC,0                !step
OUTRES,ALL,LAST,
DSYM,SYMM,Y,0       !Set symmetry plane
                    !load step 1, initial conditions 25 C
TIME,0.001
DELTIM,0.001,,
TUNIF,25,           !boundary conditions
solve
                    !load step 2..... , apply moving temp

timestep = (2*esize)/feed
dangle = 180*2*esize/(PI*radius)
j=timestep

*DO,i,5,359,dangle

    TIME,j
    DELTIM,0.01,,,
    x0 = -radius*cos((i-dangle)*pi/180)
    y0 = -radius*sin((i-dangle)*pi/180)
    xy0 = -90+(i-dangle)
    local,11,0,x0,y0,,xy0,,, !Set old local coords
    nsel,s,loc,x,-ribbonx/2,ribbonx/2,
    nsel,r,loc,y,-ribbony/2,ribbony/2, !select old wire position

    DDELE,all,temp           !Delete old temp bc
    allsel

    x1 = -radius*cos(i*pi/180)
    y1 = -radius*sin(i*pi/180)
    xy1 = -90+i
    local,11,0,x1,y1,,xy1,,, !Set new local coords
    nsel,s,loc,x,-ribbonx/2,ribbonx/2,!Select new wire nodes
    nsel,r,loc,y,-ribbony/2,ribbony/2,
    D,all,temp,temperature   !set temp bc
    allsel

    solve
    j=j+timestep           !time needed for a cutting speed of feed m/s => t=d/v => (2*0.16E-
3)/feed = timestep

*ENDDO

DDELE,all,temp           !Delete old temp bc
allsel
time,0.25
deltim,0.01
solve

save

finish

/POST1
/EFACET,4
set,last
wpstyl,1e-6,,,,,0,2,1,

```

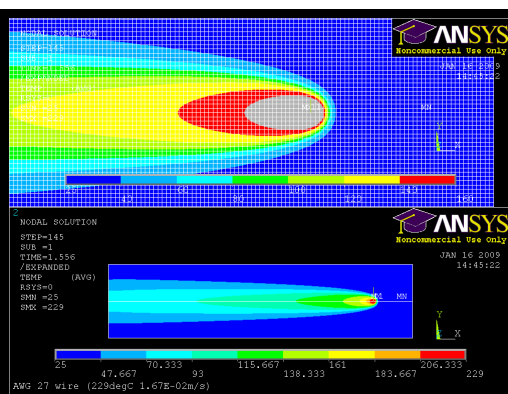
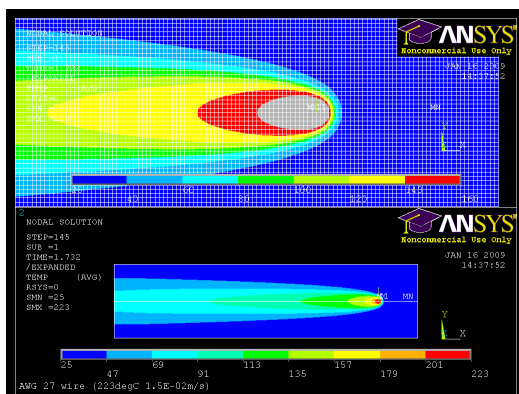
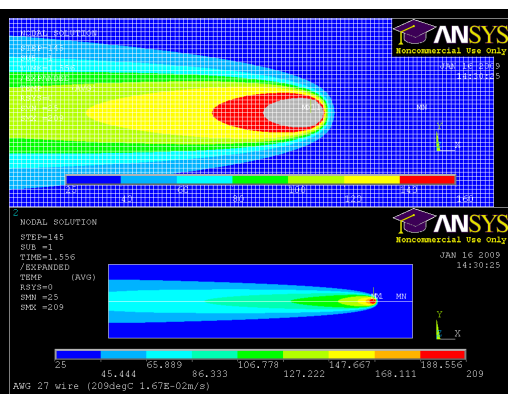
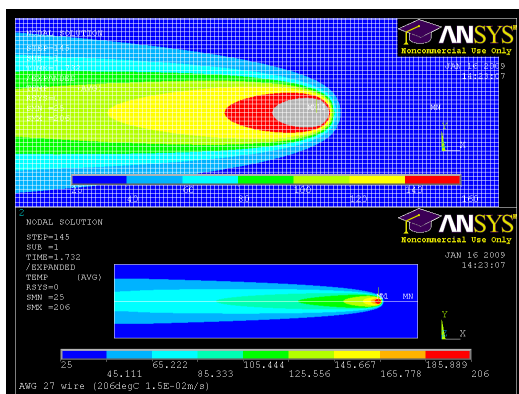
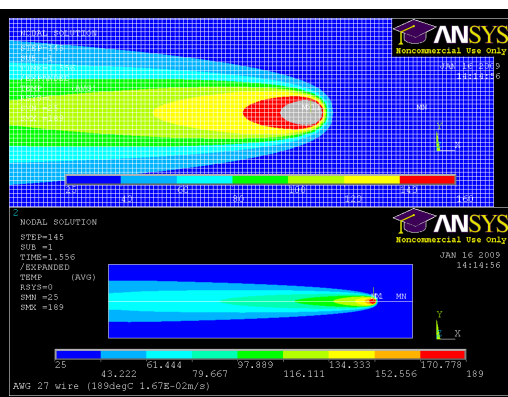
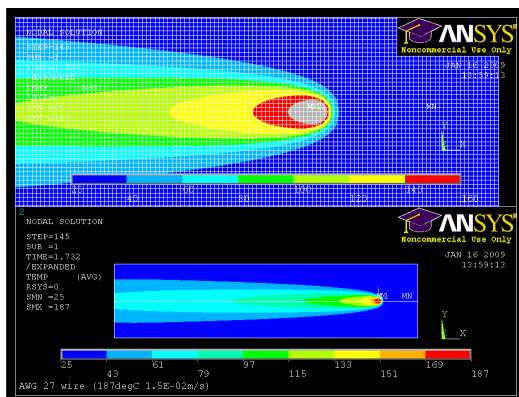
```
!/WINDOW,1,top,  
!/WINDOW,2,bot,  
/CVAL,1,40,60,80,100,120,140,160,  
!/CVAL,2,  
!/FOCUS,1,-0.001,-0.0075,0,0  
!/DIST,1,0.005,0  
/EDGE,1,1,  
PLNSOL,TEMP, ,0
```

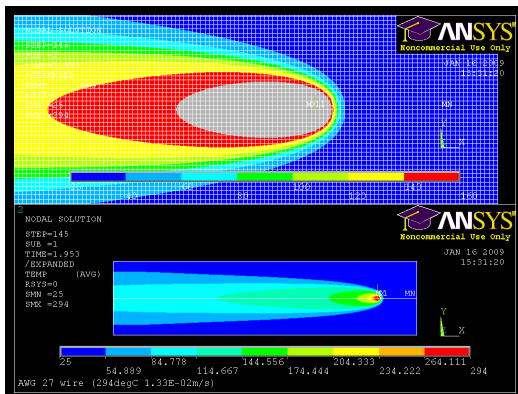
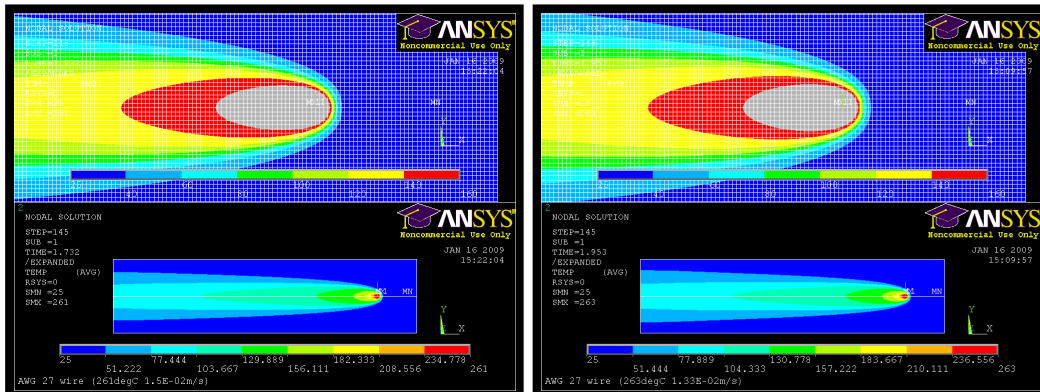
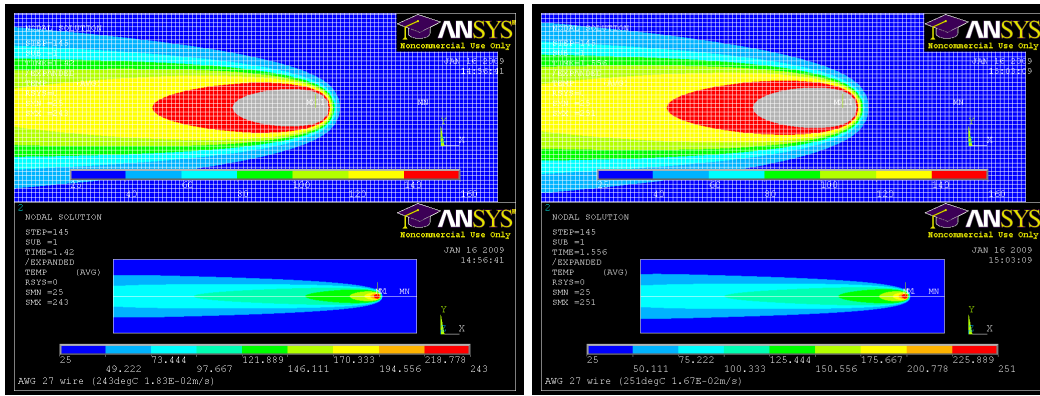


# Appendix I

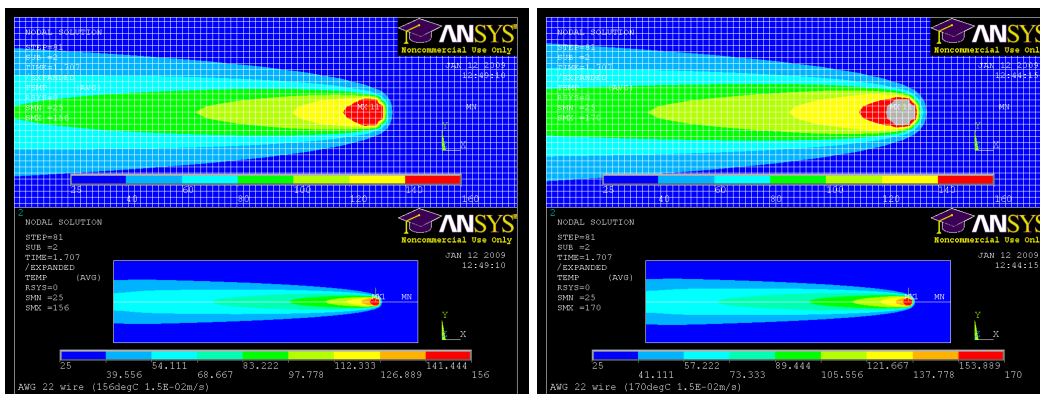
## Finite Element Simulation Screenshots

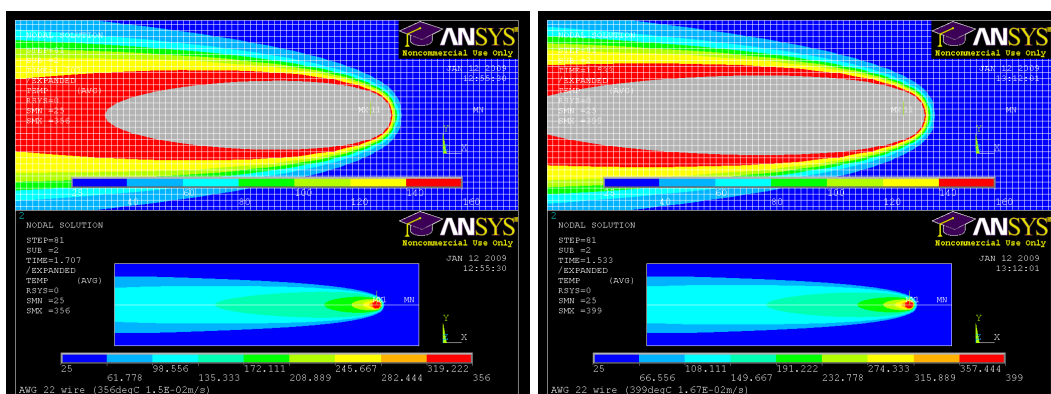
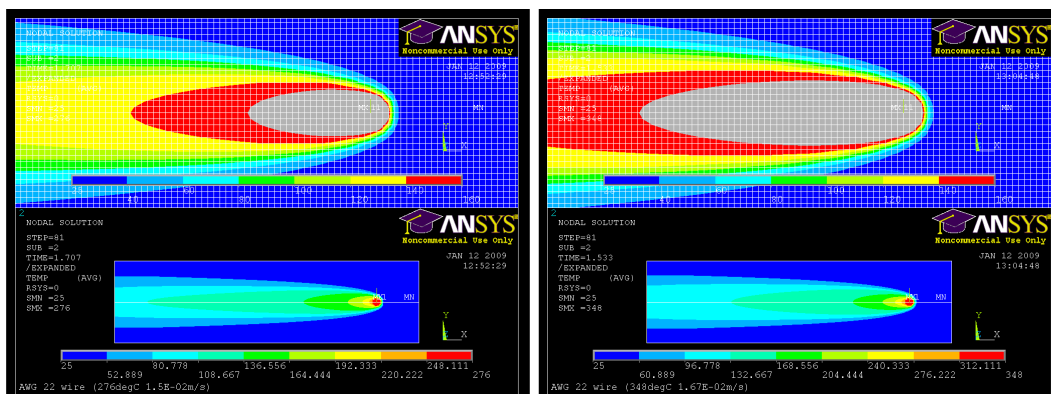
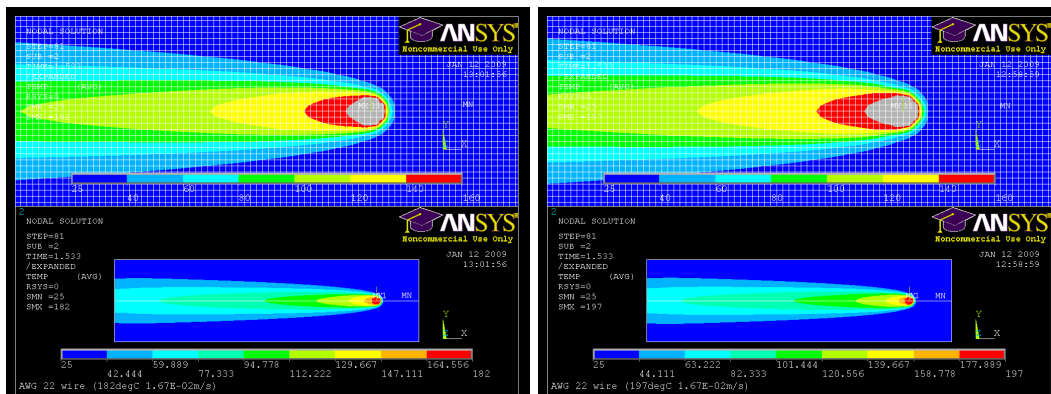
XPS 0.36 mm hot-wire simulations.



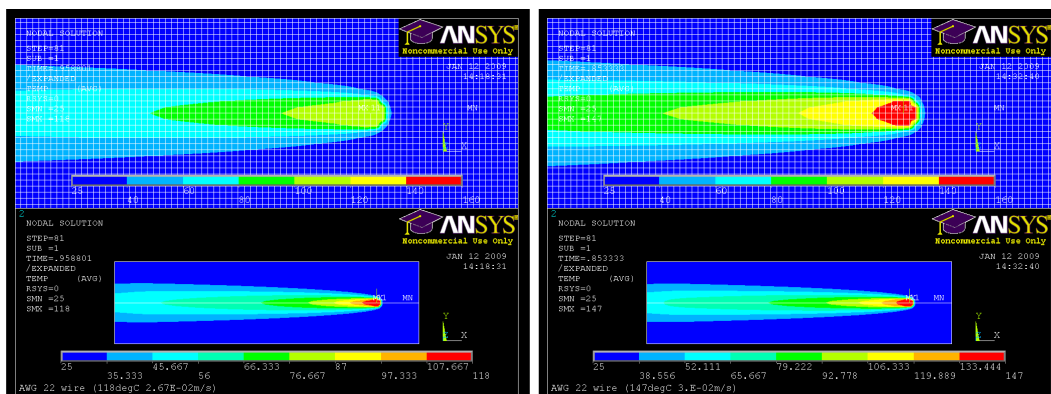


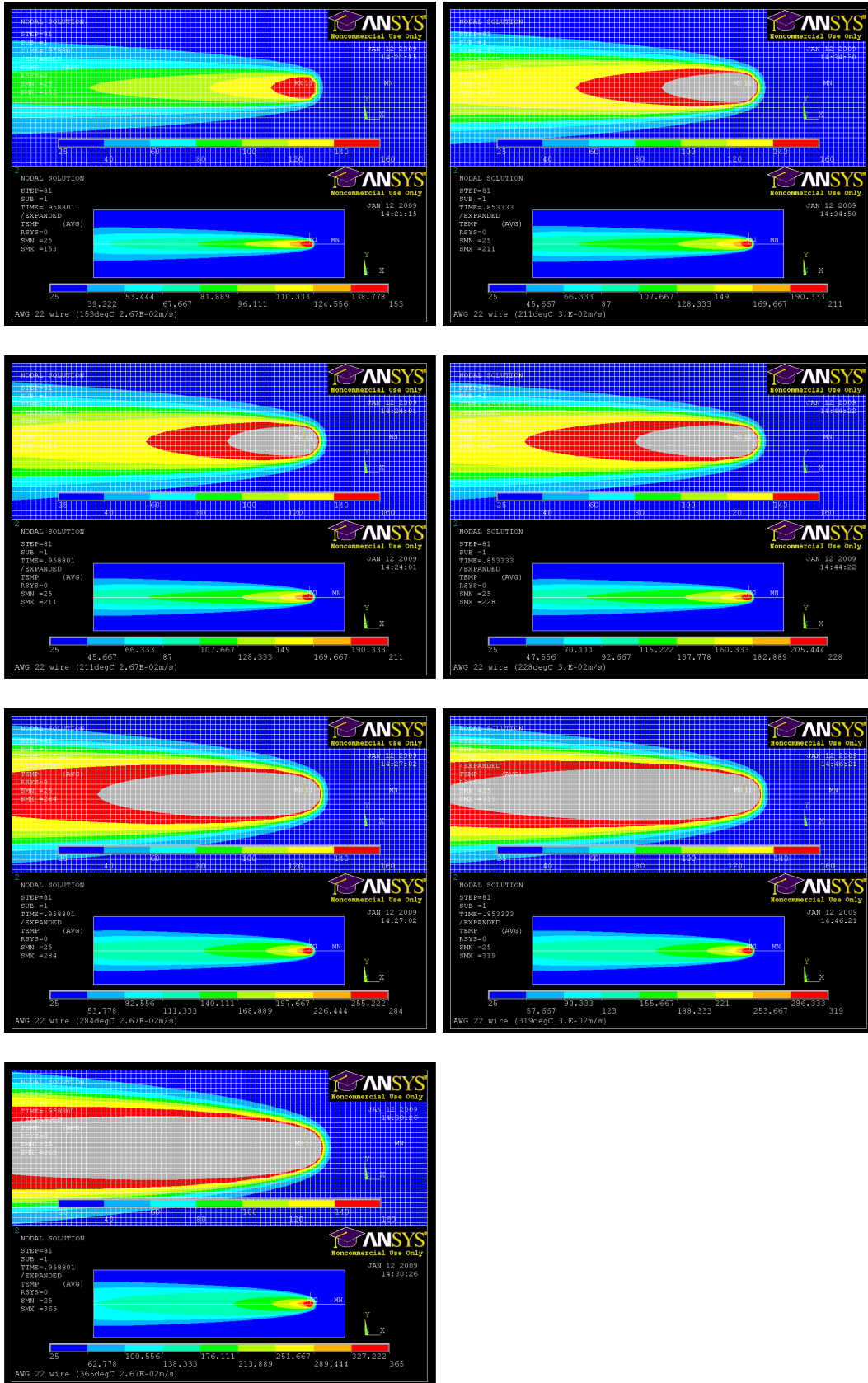
XPS 0.36 mm hot-wire simulations.



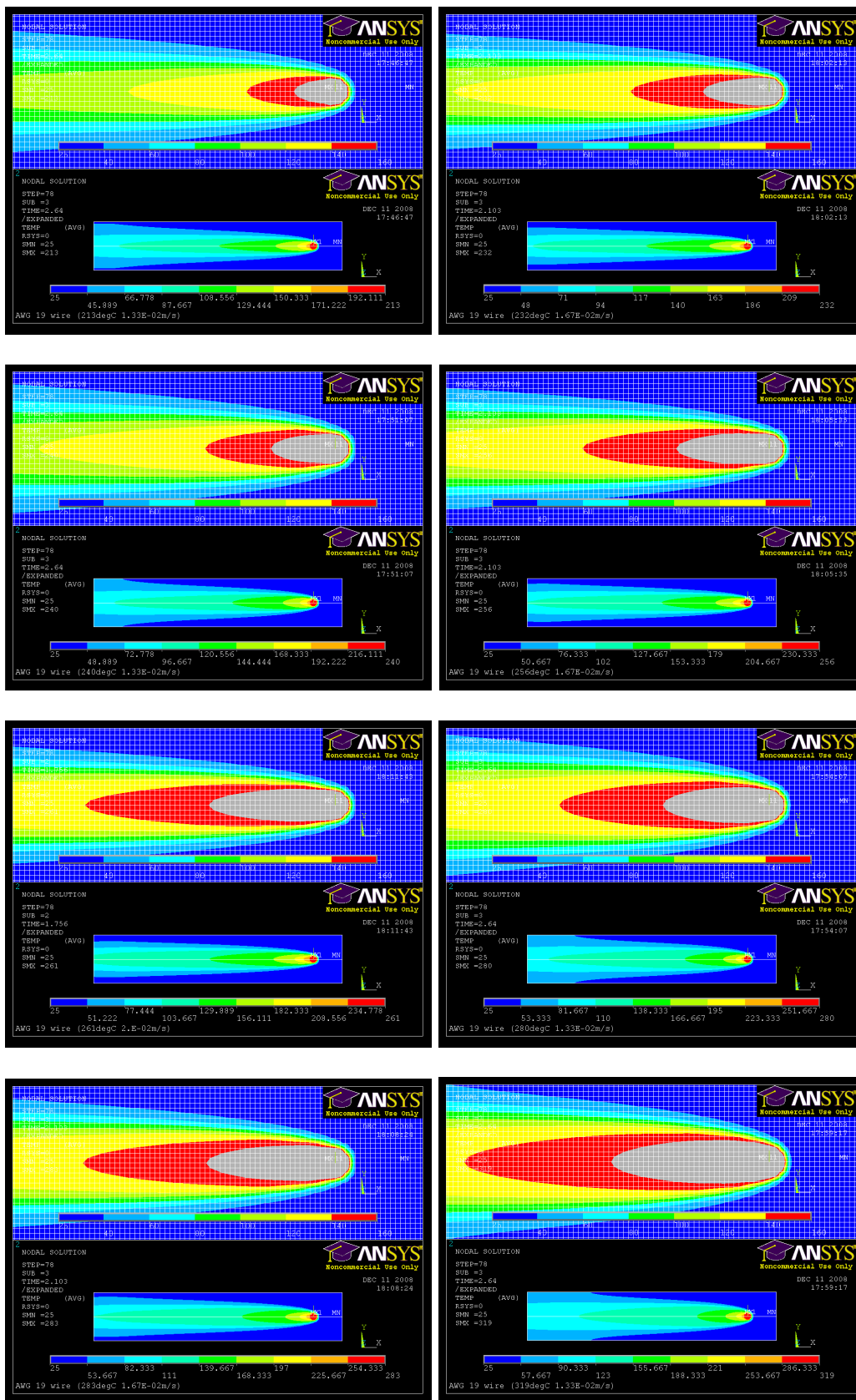


EPS 0.64 mm hot-wire simulations

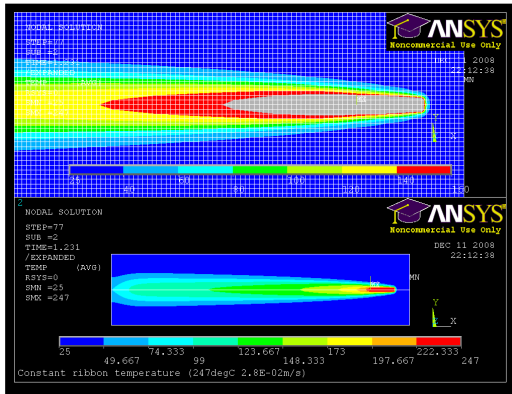
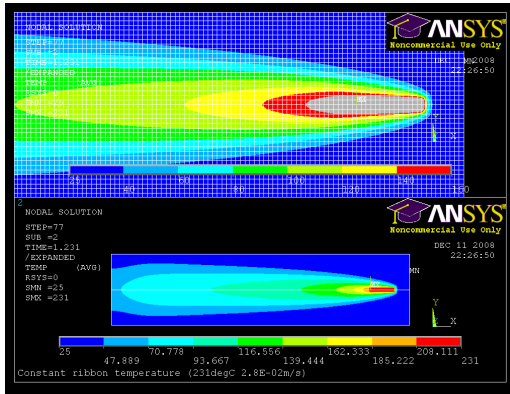
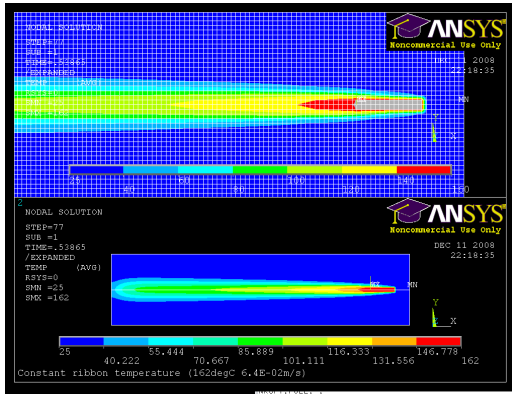




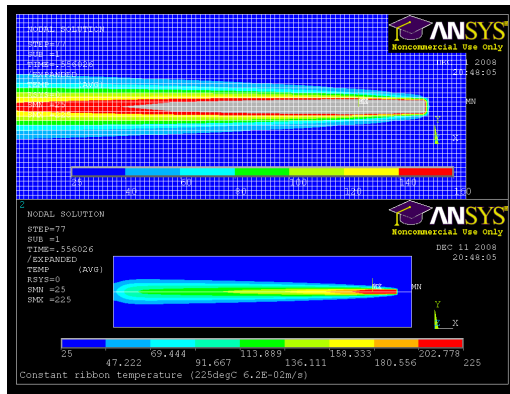
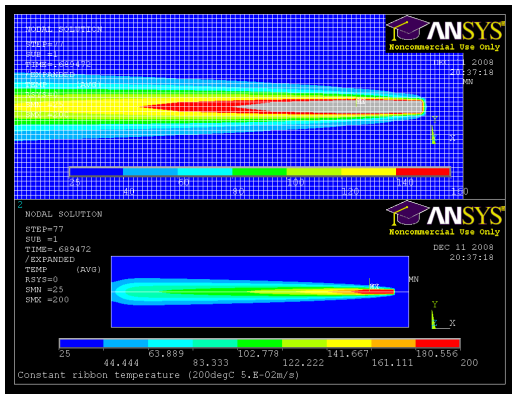
### XPS 0.91 mm hot-wire simulations

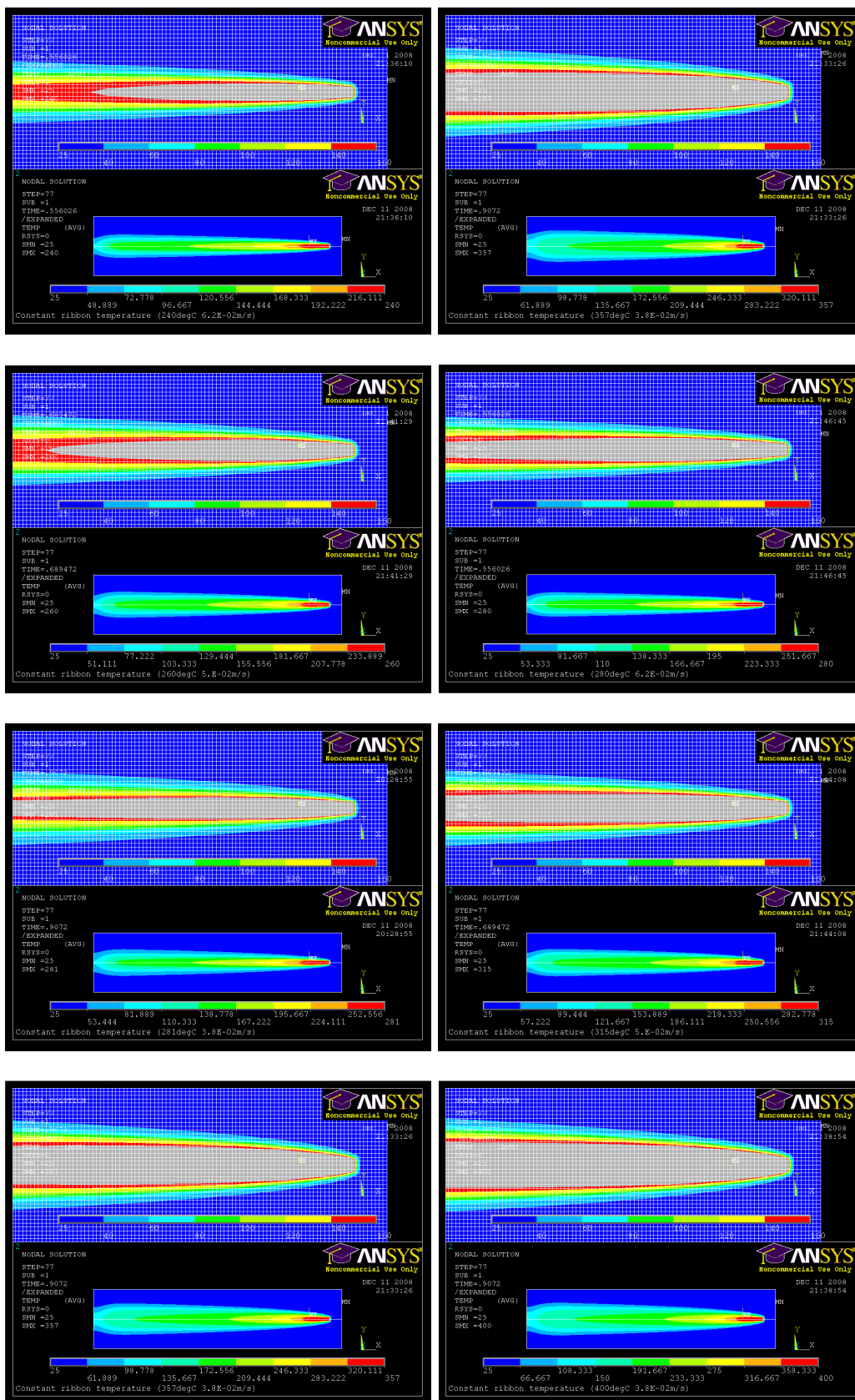


### XPS hot-ribbon simulations



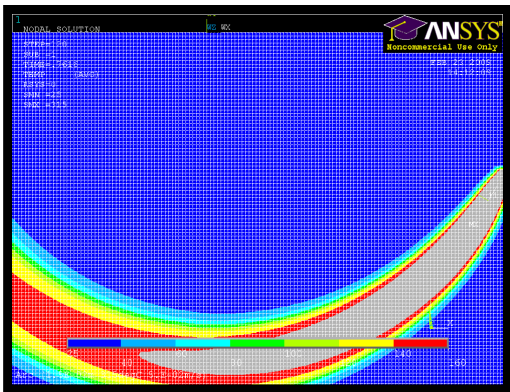
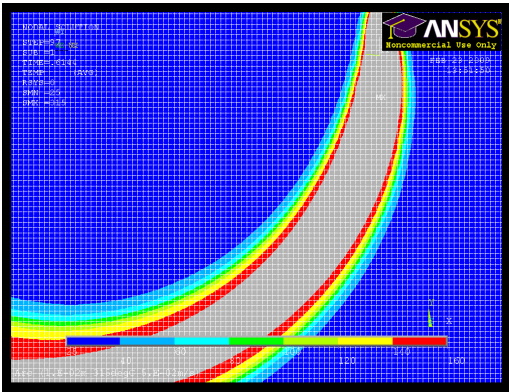
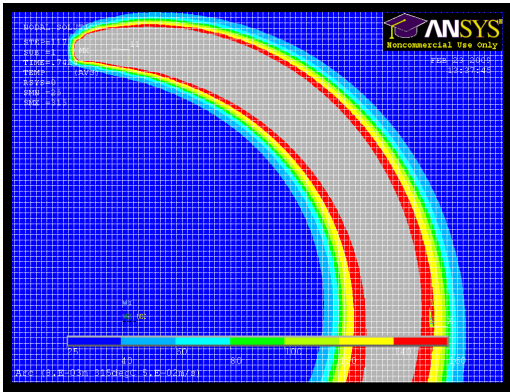
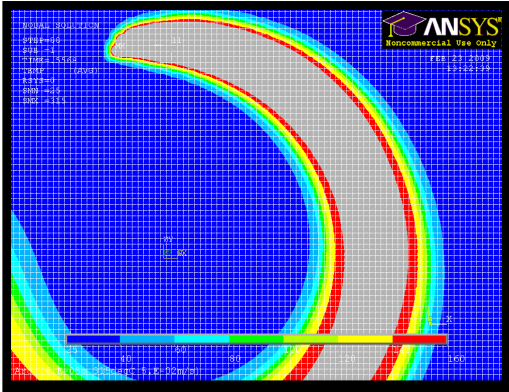
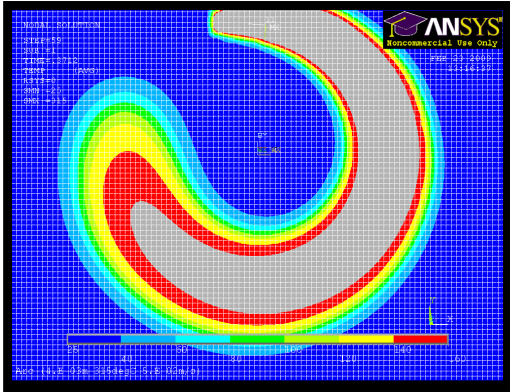
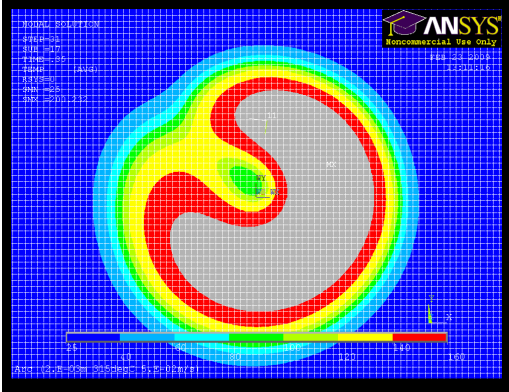
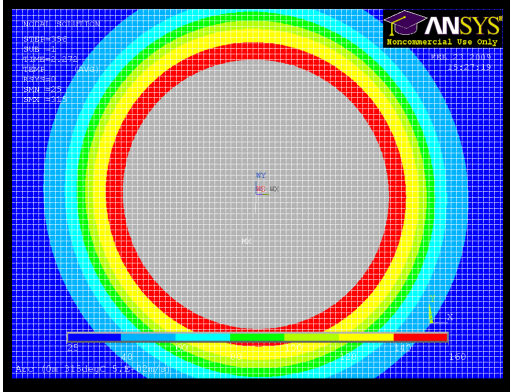
### EPS hot-ribbon simulations





EPS hot-ribbon curved cut simulations (315°C ribbon temperature, 0.050m/s, varying radii)







# Appendix J

## Associated Work

Attached are papers that were written as a result of the work in this thesis.

### Published Papers

1. H. Brooks, D. Aitchison, “*A Review of State-of-the-Art Large Sized Foam Cutting Rapid Prototyping and Manufacturing Technologies.*” 2009. (Lead author).
2. H. Brooks, D. Aitchison, “*Foam Cutting Mechanics for Rapid Prototyping and Manufacturing Purposes,*” 9<sup>th</sup> National Conference on Rapid Design, Prototyping & Manufacturing, Lancaster University, 13/06/2008. (Lead author).
3. D. Aitchison, J. Bain, H. Brooks, A. Posthuma, M. Taylor, “*Transient Temperature Effects in Hot-wire Plastic Foam Cutting,*” 4th International Conference and Exhibition on Design and Production of MACHINES and DIES/MOLDS, Cesme, TURKEY, 21-23/6/2007. (Co-author).
4. D. Aitchison, H. Brooks, R. Kandula, B. Kraus, and M. Taylor, “*Feed-rate, Temperature and Feed-force Relationships for Foam Plastics Cut by a Taut Hot-wire,*” in International Conference on Manufacturing Science and Technology Melaka, Malaysia: Proceedings of ICOMAST2006, 2006. (Co-author).

# Appendix K

## DVD contents page

### 1. Thesis

- Plastic foam cutting for rapid prototyping and manufacturing purposes
- Appendices

### 2. Cutting data and graphs

- Hot-ribbon cutting trials
  - Hot-ribbon cutting test 1
  - Hot-ribbon cutting test 2
- Hot-wire cutting trials
  - EPS
  - Force feedback temperature control
  - Vertical wire cuts
  - Wire temperature inside the cut
  - XPS
  - Kerf width tests

### 3. Graphs and tables

- Material properties data
- S-Grade EPS graphs and photos
- XPS graphs and photos
- Comparison of experimental and FEA kerf
- Force-feedrate graphs
- Hot-wire cutting calculator (HCC)
- Hot-wire cutting tables
- Normalised force-feedrate graphs
- Polystyrene thermal properties
- Ribbon Vol.Qeff for EPS and XPS
- S-Grade EPS Vol.Qeff calculations for HCC trial
- Vol.Qeff for EPS medium wire
- Vol.Qeff for XPS small, medium and big wires

### 4. Finite Element Analysis

- Hot-ribbon
  - EPS
  - XPS

- Experimental vs FEA kerf ribbon

- Hot-wire

## **5. Photos**

- S-Grade EPS

- XPS

- Wire cutting

## **6. Videos**

## **7. Solidworks**

- Blade jig

- Cutting head 3.0

## **8. Papers in order**